NASA CR71309

Final Report
F-B2280-1

Technical Report

ANALYSIS OF DYNAMICS OF A TYPICAL LARGE SURFACE STRUCTURE DEPLOYMENT IN ORBIT AND ON THE TEST STAND

GPO PRICE $ ____

CFSTI PRICE(S) $ ____

Hard copy (HC) #3.00

Microfiche (MF) .75

ff 653 July 65

by

Z. Zudans

June 1965

Prepared for

NATIONAL AERONAUTICS & SPACE ADMINISTRATION
George C. Marshall Space Flight Center
Huntsville, Alabama

Contract No. NAS8-11487

FACILITY FORM 602

N66 23771
(ACCESSION NUMBER) (THRU)
15
(PAGES) (CODE)
CR 71309 32
(NASA CR OR TMX OR AD NUMBER) (CATEGORY)

THE FRANKLIN INSTITUTE RESEARCH LABORATORIES

BENJAMIN FRANKLIN PARKWAY AT 20TH STREET, PHILA. 3, PA.

Final Report
F-B2280-1

Technical Report

ANALYSIS OF DYNAMICS OF A TYPICAL
LARGE SURFACE STRUCTURE
DEPLOYMENT IN ORBIT AND ON THE
TEST STAND

by

Z. Zudans

June 1965

Prepared for

NATIONAL AERONAUTICS & SPACE ADMINISTRATION
George C. Marshall Space Flight Center
Huntsville, Alabama

Contract No. NAS8-11487

THE FRANKLIN INSTITUTE RESEARCH LABORATORIES

BENJAMIN FRANKLIN PARKWAY AT 20TH STREET, PHILA. 3, PA.

Summary

23771

The method of analysis for the deployment dynamics of a large surface in orbit and on a test stand was developed and programmed for the IBM IBSYS system. Stiffness matrices were generated for forty-six (46) deployment stages of the large surface on a special plane structures program capable of accounting for scissor type joints.

Several deployment dynamics runs were performed. Results from these runs indicate fair correlation of the first panel rotation with the observed first panel rotation during the PEGASUS "A" flight.

The stress levels found in the scissor links in all runs performed up to this date are relatively low and indicate that the typical wing structure utilized for the analysis is adequate for the deployment during a 6°/sec rigid body rotation of the wing carrying vehicle.

Additional runs are suggested for further clarification of the effects of: a) motor torque characteristics, b) initial cinching strain energy, and c) friction.

TABLE OF CONTENTS

LIST OF FIGURES

LIST OF TABLES

Introduction

The method developed for the analysis of the deployment dynamics of a large surface in orbit and on the test stand is outlined in detail in Sections 1 and 2 of this report. The detailed derivation of the equations is given in Appendix A.

Section 3 gives a brief discussion of the input data. Section 4 is devoted to the discussion of the deployment analysis results based on the computer runs performed up to this date. Sections 5 of the basic report and the Appendix A indicate the modifications to the equations and input data required for the analysis of operation on the test stand.

The computer programs, compatible with the IBM 7094 II, IBSYS System, installed at the Computation Laboratory, NASA, George C. Marshall Space Flight Center, Huntsville, Alabama, have been delivered to the Electromechanical Engineering Branch, Astrionics Division. Mr. D. Counter, of R-ASTR-M, is familiar with the input format as well as the overall design and operation of the computer programs. There are three separate programs. The first program (MTEST) prepares the kinematic configuration data for the second program. The second program (STRUC) generates the structural stiffness matrix and punches it on cards. This is essentially a plane structures program suitably modified to account for scissor type joints. The third program (DYNA) performs the actual dynamic analysis of the deployment, produces printed output such as shown in Appendix B, and generates an input tape suitable for graphical output, such as given in Appendix C, on GD S-C4020 computer.

1. Mathematical Model

The dynamic analysis of the wing is based on the mathematical model consisting of the six (6) mass points representing the six panels and the three (3) mass points representing the rotatory inertia of the first half panel, mass point 7, Fig. 1, the scissor driving link at point A, mass point 8, Fig. 1, the rotating parts of the torque shaft including the gear box, and the electric motor and brake, mass point 9, Fig. 1. Each of the six mass points associated with the panels is allowed three elastic degrees of freedom: stretching along the wing axis in the direction of the unit vector $\vec{n}_2$, transverse deflection in the direction of the unit vector $\vec{n}_3$, and rotation about the axis parallel to the unit vector $\vec{n}_2$. An additional degree of freedom is that of the rigid body deployment and is incorporated in the mathematical model by allowing free variation of the angle of rotation, θ, of the first panel, Fig. 1.

The vehicle carrying the wing is allowed any prescribed combination of linear and angular rigid body motion. It is assumed, however, that the deployment of the wing does not affect the prescribed rigid body motion, i.e. the rigid body motion of the vehicle is a known function of time.

The stiffness of the wing is derived from the plane structure formed by the scissor links and the side members of the panels. This model was adopted after thorough examination of the wing structure from the point of view of its stiffness as related to the degrees of elastic freedom considered in the mathematical model. Another consideration weighing heavily on the selection of the plane structural mathematical model was the relative complexity of a true three-dimensional model. For the plane structure, an existing computer program could be used with relatively minor changes. In order to account for the flexibility of the torque shaft and the chain of driving elements up to and including the brakes, an elastic foundation with respect to rotation was introduced at point B, Fig. 1. The capability to include scissor type joints with common degrees of freedom for linear motion, but independent rotations, was incorporated in the mathematical model by rep-

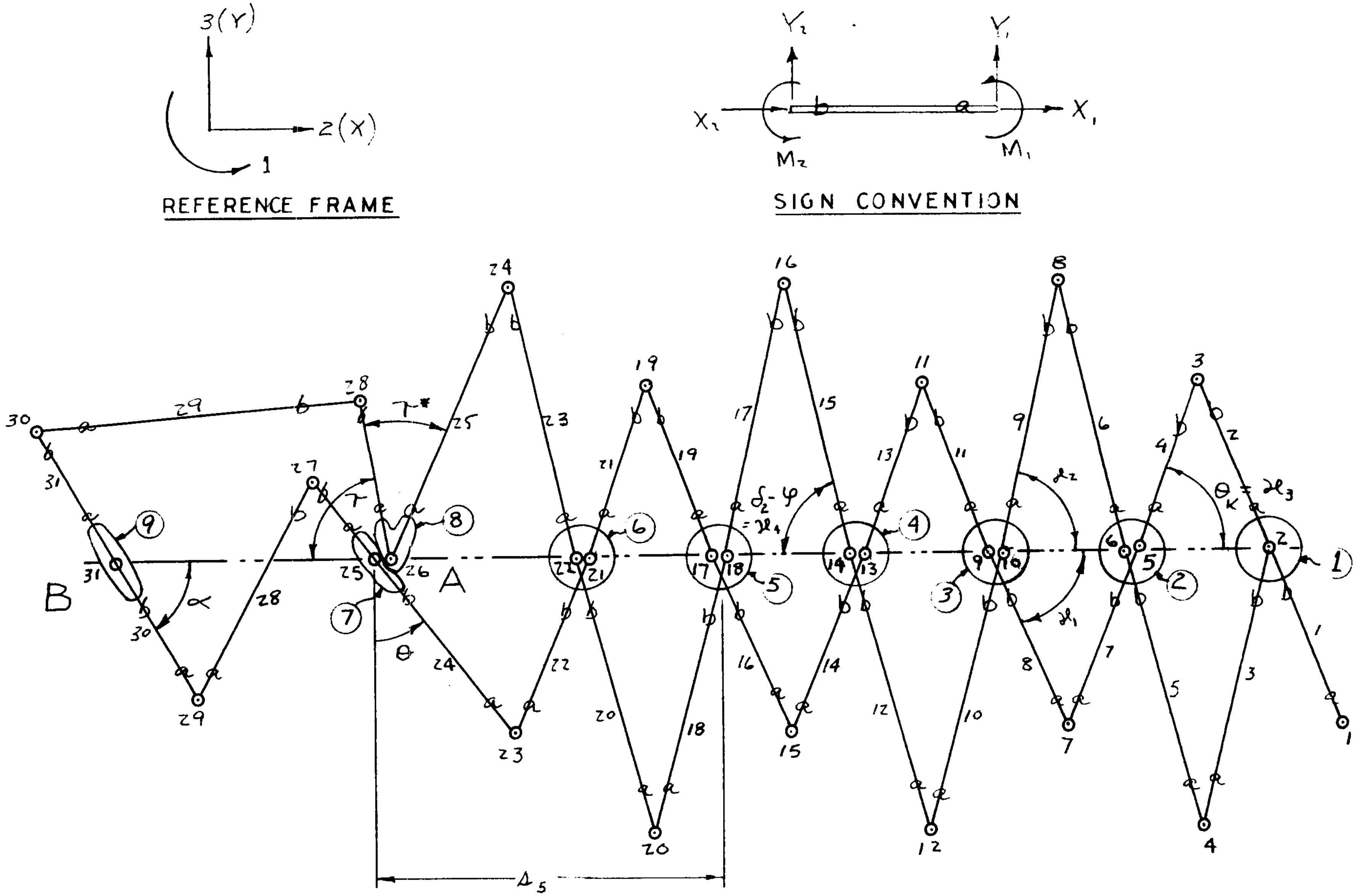

Fig. 1 - Schematic of the Mathematical Model of the Wing Structure

resenting each of the scissor-panel joints with two joints. During the process of the analysis, the stiffness matrix was formed for all joints (31 joints) and then modified to force these joints to perform common linear motion, but to allow independent rotation. Note further that the mathematical model for the dynamic analysis calls for variable stiffness coefficients, corresponding to various degrees of the deployment. This is accomplished by assuming that the structural stiffness is governed only by the rigid configuration as dictated by the kinematics of the mechanism for a given angle Θ .

2. Method of Analysis

The method of analysis is based on the direct numerical integration of the equations of motion. The equations of motion are derived by use of Lagrange's equations. The dependent variables are the nineteen (19) degrees of freedom considered in the mathematical model: eighteen (18) elastic and one rigid body deployment degree of freedom. The driving forces considered in the system are those due to the panel springs, initial cinching of the wing structure, and the torque developed by the electric motor. Other forces acting on the structure are those due to the friction in the panel joints, brake torque, and for the configuration on the test stand, the integrated friction force obtained by actual measurements of a typical real wing structure (see Section 5, Appendix A).

The detailed derivation of the governing equations is given in the Appendix A. Equation A.44 gives the final form of the system of first-order non-linear simultaneous differential equations to be solved.

$$\begin{aligned}
&\dot{Y}_i = F_i - B_i C && (i=1,12)\\
&\dot{Y}_{13} = C && \\
&\dot{Y}_j = F_j && (j=14,19)\\
&\dot{Y}_{k+19} = Y_k && (k=1,19)\\
&\dot{Y}_{39} = 1 &&
\end{aligned} \qquad (1)$$

coefficients at various degrees of deployment, motor torque data as a function of the torque shaft angular velocity, and other pertinent information required for the integration. All of this information is printed on the first three pages of the typical output, Appendix B. Note that the motor and brake torque were supplied as a defined function. During the course of the analysis the motor and brake torque function proved to be the major factor determining the behavior of the structure during the deployment. Torque functions corresponding to Figures 2, 3, and 4 were used for different runs.

3. Results of the Deployment Analysis

The deployment analysis results available at this time are those for the deployment in space only. The mathematical model and, consequently, the computer program are designed to perform the analysis of the deployment on the test stand (see Section 5, Appendix A) also; but, due to the lack of basic input data, no computer runs have been performed up to the present time. It is expected that such runs can be performed in the near future. A number of runs were performed before the capability of plotting the results had been incorporated. These runs generally served the purpose of establishing the effect of each of the individual driving forces on the dynamics of the deployment.

Series of runs listed in Table 1 were performed after the plotting capability had been incorporated in the program. Typical plots of displacements and velocities of mass points, first panel and torque shaft rotation, motor torque, structure induced torque on the torque shaft, strain energy in structure, and total energy in system are included in Appendix C.

The strain energy in structure plot was utilized to determine the time at which maximum stresses occurred. The resultant schemes in scissor bars are summarized in Table 2. The stresses in the panel frame side members were found to be considerably lower and are not recorded here.

As it is seen from Table 2, the highest stressed scissor link is bar 25, Figure 1. The high stress occurs during the 6°/sec roll (rigid body rotation of the vehicle about axis parallel to axis 1, Fig. 1), before the impact which occurs at the end of the rigid deployment motion. Stresses after the impact were not evaluated for this run. Similar stresses, however, were evaluated for runs 5021 and 5022. The strain energy levels in the structure are shown on pages 5020-14, 5021-24, and 5022-34, Appendix C. As it is noted from these pages, the strain energy in the structure was considerably higher during the initial phase of the deployment. The integration was monitored by comparing the strain energy in the structure at each integration step to a specified value (500 in-lb during these runs). When the specified value was exceeded, the integration was stopped and the results plotted. This occurred, for example, during run 6739, before the completion of the deployment. Additional monitoring of the integration was a check of the positive definiteness of the stiffness matrix at each step of the integration. The loss of the positive definite character of the stiffness matrix brought a breakdown of the integration stability with it. The initial stiffness matrix was derived from only four data points by polynomial interpolation. While at each of these four data points the stiffness matrix had been evaluated using the modified computer program and was positive definite, the interpolated matrices at the beginning of the deployment range were in general not positive definite. This caused the structure to act as a negative spring and the integration diverged very rapidly.

After examining the character of the variation of the stiffness properties of the wing structure, it was found necessary to increase the number of data points to forty-six (46). Using these data points and a Lagrangean three point interpolation, it was found that the interpolated stiffness matrices maintained their positive definite character. The structural stiffness matrices were plotted, and a typical set (corresponding to the first three rows of the stiffness matrix) is shown in pages 56 to 84 of Appendix C. Note from these plots that the elastic behavior of the wing structure can be subdivided into three distinctly different regions: a) fully retracted, b) intermediate, and c) fully deployed. The variation of the stiffness within the ranges (a) and (c) above is very large and, in order to retain the positive definite character, many data points were required in these ranges.

Table 1

LIST OF COMPLETE COMPUTER RUNS FOR DEPLOYMENT DYNAMICS

Run No.	Rigid Body Rotation of the Vehicle Degrees/Sec Axis 1	Axis 2	Axis 3	Torque Curve Figure No.	Prepack	Deployment Time Sec.
4560	0	0	0	2	zero	35.8
5020	6	0	0	2	zero	32.0
5021	0	0	6	2	zero	33.2
5022	0	6	0	2	zero	36.2
6739	0	0	6	3	zero	-
6740	0	0	0	3	zero	21.0
9828	0	0	0	4	zero	23.4

Table 2

STRESSES IN SCISSOR BARS, PSI

Scissor No. Fig. 1	Run No. 5020 Before Impact	Run No. 5020 After Impact	Run No. 5022 Before Impact	Run No. 5022 After Impact	Run No. 5021 Before Impact	Run No. 5021 After Impact
6	405		1,070	750	1,840	1,840
9	5,015		2,770	2,645	4,220	7,530
15	3,440		5,030	1,525	7,600	4,820
17	15,450		7,220	6,710	10,780	10,410
23	9,160		9,490	7,630	15,190	9,800
25	18,045		7,310	3,050	12,430	1,400

The deployment time indicated by the runs listed in Table 1 is in the range of 21 to 36 seconds. These runs differ from each other mainly with the type of motor and brake torque function employed. The variation of the vehicle rigid body motion from zero to 6°/sec in roll and yaw (axis 1 and 3) reduced the deployment time by approximately 3 to 4 seconds. Changes in the motor and brake torque characteristic, however, changed the deployment time by as much as 15 seconds.

During the initial deployment period, high oversynchronous speed was imposed by the driving forces of the system, causing (see Fig. 2) high braking torques to be introduced by the motor. This caused a considerable slow down of the motion. Because the resultant high braking torque seemed physically unrealizable, the motor and brake torque characteristic was changed to that shown in Figure 2. This limited asymptotically the torque at oversynchronous speeds to the nominal torque of the motor and brake. Runs 6739 and 6740 were performed using the torque characteristics of Figure 3. Since the braking torque was reduced considerably, the deployment was very fast. In the case of the vehicle rigid body motion (run 6739), the strain energy in structure exceeded the limit specified (500 in-lb) for automatic discontinuation of integration. In run 6740, with no rigid body motion, deployment proceeded very fast (torque function curve of Figure 3 was used) to completion in 21 seconds. At certain times of the deployment, the direction of rotation of the motor was reversed, and, following the straight line branch of the torque function, Figure 3, driving torque in excess of the locked-in torque of the motor was applied to the structure. This condition was rectified for run 9828, where the negative velocity branch of the torque curve was bounded by a straight line as shown in Figure 4. The deployment time was increased by about 2.4 seconds.

The experimentation with various torque functions was necessary inasmuch as no actual data from a typical drive unit could be obtained experimentally. In the normal speed range, the straight line characteristic of the motor and brake is satisfactory, but the behavior during the oversynchronous and reversed speed operations indicated by Figures 2 to 4 represent only rough estimates.

All of the runs listed in Table 1 were performed with no prepack strain energy in the structure. This condition was generated by an error

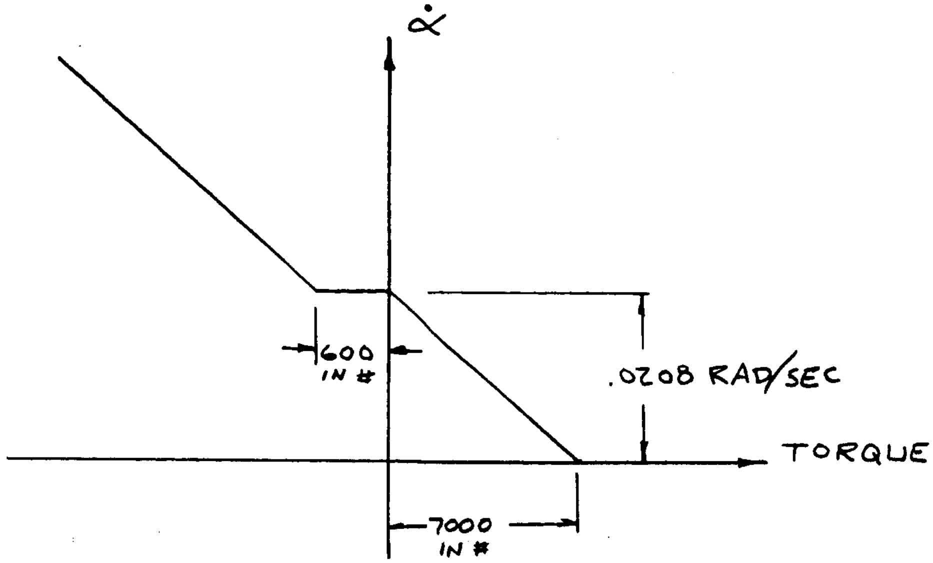

Fig. 2 - Torque Function

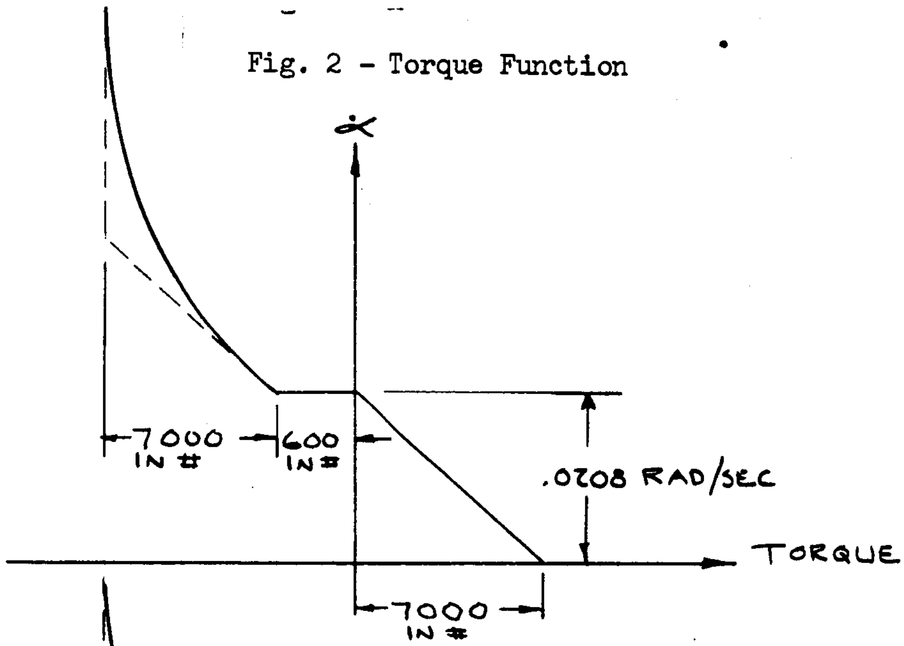

Fig. 3 - Torque Function

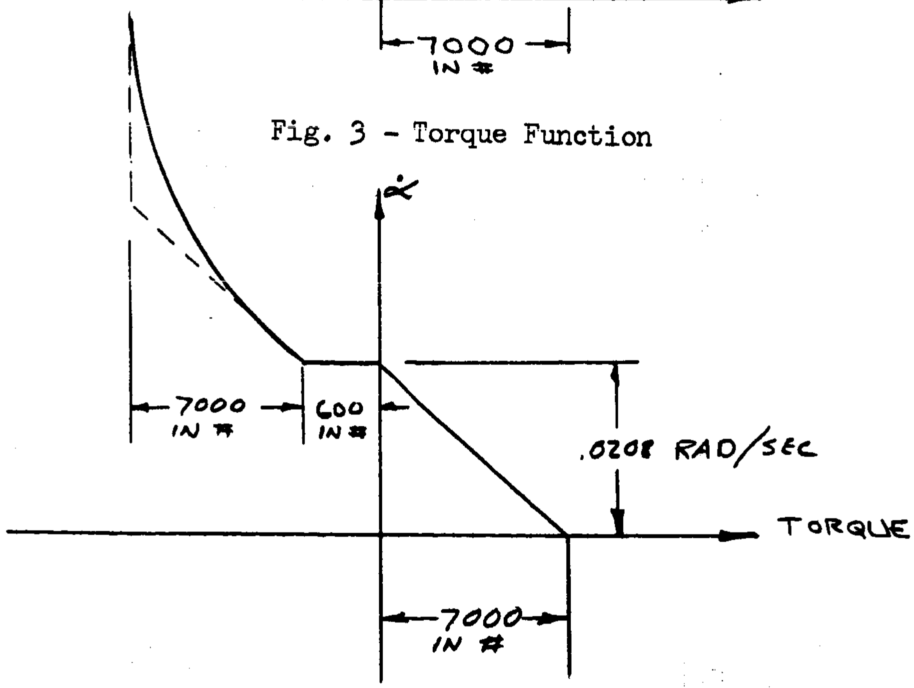

Fig. 4 - Torque Function

in the input data and was discovered only during the final evaluation. Runs with prepack active, however, were performed before the plotting capability was incorporated in the computer program. The results from these runs indicated very large braking torques generated during the first few seconds of the wing deployment. Total strain energy in the structure, however, did not differ significantly from that recorded during the runs listed in Table 1.

The degree of correlation of the analysis results for run 4560 with the data collected during the PEGASUS "A" launching is shown in Figure 5. The plotted curves represent the rigid and the elastic rotations of the first half panel (mass point 7) versus time. Circles represent the data collected from the PEGASUS "A" flight as reduced from the film. Triangles represent the telemetry data. Slower calculated deployment can be accounted for by the absence of the prepack strain energy in this run. In general, however, the agreement between this run and the observed behaviour is fair.

In view of the importance of the torque function on the deployment process, it appears that for a better correlation of the analysis results with the actual flight data, input quantities representing the actual conditions more accurately are required.

A more complex mathematical model may be suggested, such as, for example, that which could be obtained by adding the elastic torque shaft rotation as a degree of elastic freedom. This, however, would not necessarily yield better correlation if the basic input quantities were not improved.

Examination of the results plotted in Appendix C indicates that the dynamic behaviour of the wing is consistent with its stiffness properties. Thus, from page 56, Appendix C, increase of the stiffness coefficient $k_{1,1}$ (typical for all mass points) is noted as the deployment angle increases from 1.1 to 1.55. Corresponding to this, the curves on pages 4560-1, 5020-7, 5021-16 and 5022-26 indicate the increase of the frequency of the elastic oscillations along the axis 2. This is observed from the intersection of the elastic deformation and rigid deployment curves. Similar observations can be made from curves 5020-12, 5021-21, 5022-31, and 6739-41.

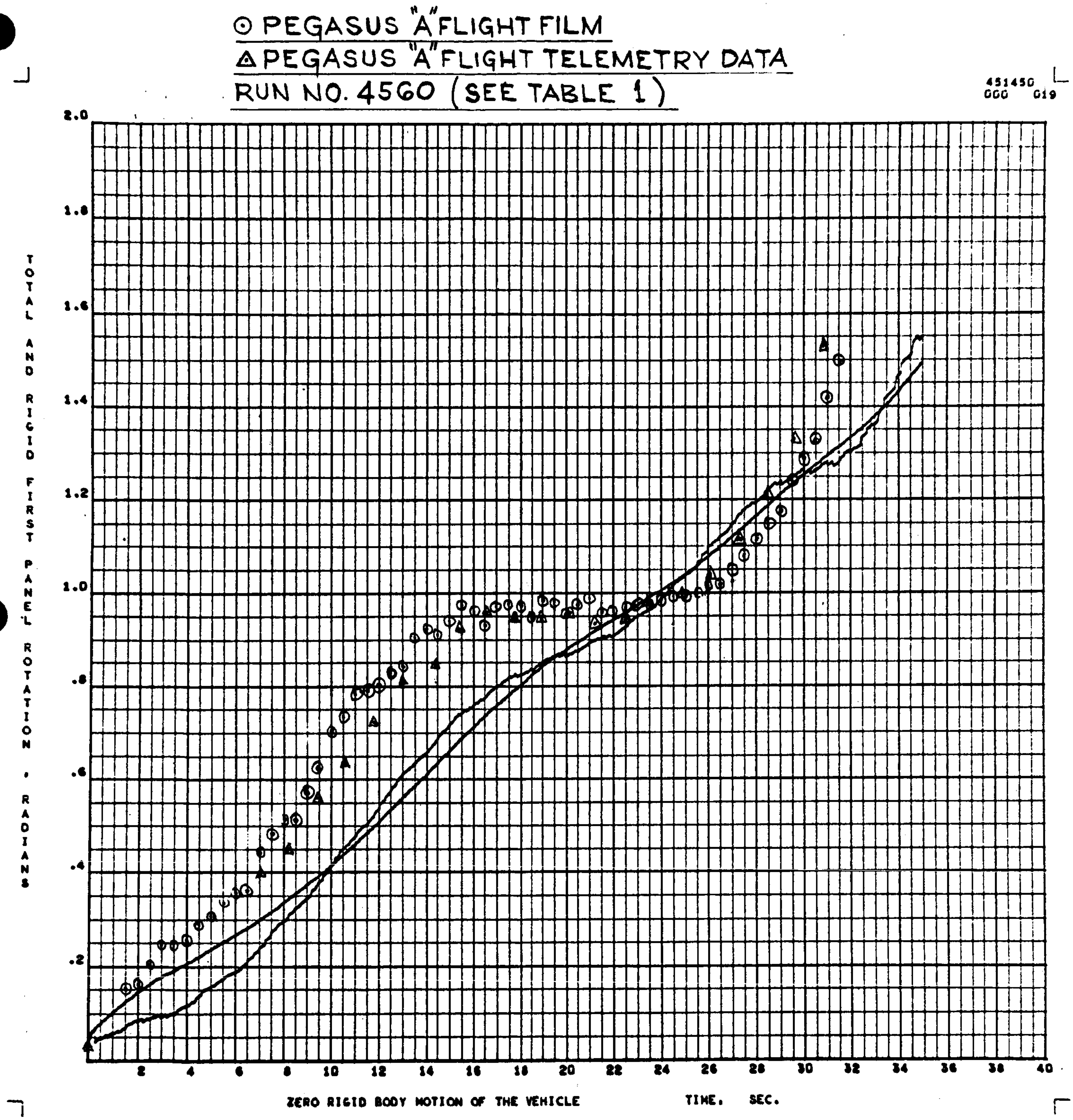

Fig. 5 - Correlation with Flight Results

The quantities forming Equation 1 are defined in Appendix A (see Eqs. A.45 to A.49, for the deployment in space, and in Section 5, Appendix A, for the deployment on test stand). These equations were derived by solving the coupled system for the second derivatives of the dependent variables and introducing additional dependent variables to reduce the system of second-order differential equations to a system of first-order differential equations.

Y_{39} represents the time and was integrated simultaneously using the same numerical scheme. Numerical integration was performed using the Runge-Kutta fourth-order method. Runs performed with different time step sizes indicated that an initial time step equal to .001 seconds was satisfactory for the integration during the action of the cinching preload. After the cinching strain energy was released, the time step could be raised to .003 seconds. Reduction of the time step by a factor of 10 was introduced from the time that full deployment impact took place. The above numbers were established by performing several runs with different time steps and comparing the results.

The results of the analysis were arranged to be presented in both tabular and graphical forms. The typical tabular form is given in Appendix B. Graphical representation was achieved by utilizing the plotting facility of the Computation Laboratory at NASA, MSFC, Huntsville. Typical plots are shown in Appendix C. The computer time required for one integration step ranged from 0.35 to 0.38 seconds on the IBM 7094, Model II, (Computation Laboratory, NASA, MSFC, Huntsville, Alabama) depending on the frequency of printing results. On the average, a complete deployment, with every 100th step printed and approximately 800 points plotted on thirty-eight (38) separate graphs, required about 72 minutes on the IBM 7094 II computer.

4. Input Data

The input data consist of the dimensions of various structural members, mass distribution relative to the degrees of freedom considered, various spring constants, cinching strain energy (expressed by the prepack stiffness coefficient), friction data, structural stiffness

The frequencies observed in actual flight and those found on page 5020-12 are of the same order of magnitude.

Similarly, page 68, Appendix C, indicates a decreasing value of $k_{2,2}$ (stiffness coefficient for elastic deformation transverse to the wing plane). This represents a case for which the frequency of vibration is expected to decrease and the amplitude is expected to increase with the deployment of the wing. Behaviour of this type is clearly indicated in the corresponding elastic motion shown on pages 4560-2, 5020-8, 5021-17, and 5022-27, Appendix C.

A condition identical to that above exists for the twisting stiffness $k'_{3,3}$, page 79, Appendix C. Decreasing frequency and increasing amplitude are clearly indicated on page 6739-39, Appendix C.

The properties of the solution indicated above are typical for a nonlinear system. These and the fact that the test runs performed with different step sizes produced identical results, indicate that the computer program is generating a valid solution. Only a fair correlation with the actual flight test is attributed to the approximate knowledge of the actual input quantities. In particular, the input quantities describing the actual torque characteristics are not known for the complete range of operation, and the total strain energy due to the initial cinching can only be bounded approximately. Since, however, the solution offered by the computer program is exact for the mathematical model described in Section 1, it appears that by performing few additional runs, more useful information can be gathered.

5. Analysis of the Dynamics of the Deployment of Large Surface on the Test Stand

The modifications to the mathematical model required for the analysis of the configuration on the test stand are given in detail in Section 5, Appendix A. No computer runs have been performed up to the present time. Proper input data, however, are expected shortly, and it is anticipated that the run will be performed within the next two months.

6. Additional Computer Runs

There is no limit to the number of the desired computer runs from the academic point of view. The problem is very complicated and each solution brings out some features of the behaviour of the nonlinear system whose configuration is changed in the process. From the practical point of view, the purpose of the present solution is only to predict the reliability of the deployment of the wing in orbit. Presently available analytical results indicate, that the structure is adequate from the point of view of the stresses for the specified rigid body motion of the vehicle during the deployment. Furthermore, actual films and telemetry data obtained from the successful flights of PEGASUS "A" and "B" confirm these findings. Accordingly, only a few additional computer runs, listed in Table 3 are suggested.

Table 3

ADDITIONAL RUNS SUGGESTED

Run No.	Rigid Body Rotation of the Vehicle Degrees/Sec: Axis 1	Axis 2	Axis 3	Torque Curve Fig. No.	Prepack Data: θ_p	k_p	Friction
1	0	0	0	Special	.034416	$.8833 \times 10^8$	Special Included
2	6	0	0	1	.034416	$.8833 \times 10^8$	Included
3	6	0	0	A	.034416	$.8833 \times 10^8$	Included

Run 1 represents the configuration on test stand, run 2 is essentially equivalent to run 5020 except for the prepack conditions, and, finally, run 3 is suggested for a torque function to be derived from the results obtained during the previous runs.

7. Acknowledgements

The mathematical description of the deployment dynamics of a large surface in space and on the test stand required the effort of many people. In particular, credit is due to Dr. M. Brull, Professor, University of Pennsylvania, who, acting as a consultant to The Franklin Institute Research Laboratories, critically reviewed and supplemented the basic analysis approach. During the final detail checking of the equations and the programming and debugging phases of work, Mr. H. Fishman and Mrs. M. Alexander contributed greatly.

The complete understanding and constructive suggestions received from Mr. J. Boehm, NASA, MSFC, R-ASTR-M, Huntsville, Alabama, sponsor of the project, provided the shortcuts leading to a better analysis.

Mr. D. Counter, NASA, MSFC, R-ASTR-M, Huntsville, Alabama performed the computer runs listed in Table 1. His quick orientation in the rather complex computer program made these runs possible at the Computation Laboratory of NASA, MSFC, Huntsville, Alabama.

APPENDIX A

EQUATIONS OF MOTION OF THE DEPLOYMENT OF LARGE SURFACES IN ORBIT

1. EQUATIONS OF MOTION OF THE DEPLOYMENT OF LARGE SURFACES IN ORBIT

1.1 Introduction

The large surface, called a wing in the following, will be represented by nine (9) mass points. Six of these mass points will be allowed three elastic degrees of freedom, in addition to the rigid body degrees of freedom. Thus, Figure A-1 the mass points 1 through 6, representing the lumped masses of the panels and scissor links will be allowed to deform elastically along the directions indicated by the unit vectors $\vec{n}_2$ and $\vec{n}_3$ as well as subjected to twisting around the axis parallel to the unit vector $\vec{n}_2$. Mass points 7 through 9 will only participate in the rigid body motion of the deployment and of the vehicle. Backlash in the scissor and panel hinges will be assumed equal to zero. Rotating inertia of the masses associated with the drive motor, gear box, brakes, and other rotating parts will be reduced to the torque shaft, point B, Figure A-1.

The stiffness matrix associated with allowed elastic degrees of freedom will be evaluated under the consideration of the scissors and the side bars of the panel framing. Rigid body deployment motion will be described by considering the angle θ as a generalized coordinate, Figures A-1. Governing differential equations will be derived by using Lagrangian equations

$$\frac{d}{dt}\frac{\partial T}{\partial g_i} - \frac{\partial T}{\partial g_i} + \frac{\partial V}{\partial g_i} = G_i \qquad (i = 1,N) \qquad \text{A.1}$$

where

T - kinetic energy

V - strain energy

g_i - generalized coordinate

F_i - generalized force associated with the generalized coordinate q_i.

In the following, various terms forming Equation 1 are evaluated.

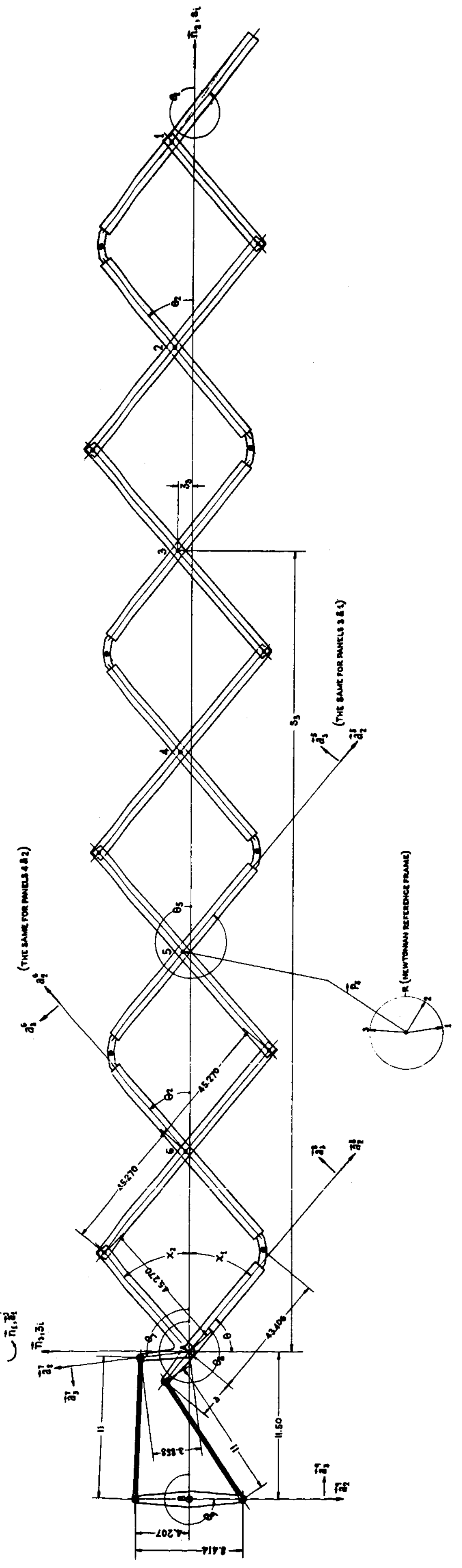

Fig. A.1 - General Configuration of Large Surface

1.2 Kinetic Energy

Kinetic energy of the wing is computed considering the translatory and rotatory kinetic energies associated with the deployment motion

$$T = \frac{1}{2} \sum_{i=1}^{9} (M_i \, {}^R\vec{V}_i \cdot {}^R\vec{V}_i + {}^R\omega_i \cdot \vec{\psi}_i \cdot {}^R\vec{\omega}_i) \qquad A.2$$

where

M_i - mass associated with the mass point i.

${}^R\vec{V}_i$ - velocity of mass point i in the Newtonian reference frame R.

${}^R\omega_i$ - angular velocity of the mass i in the Newtonian reference frame R.

$\vec{\psi}_i$ - dyadic form of the second order inertia tensor for the mass i.

Denoting the mass point position in the Newtonian reference frame by $\vec{p}_i$, we have

$$\vec{p}_i = \vec{p}_o + s_i \, \vec{n}_2 + z_i \, \vec{n}_3 + \vec{q}_i \qquad A.3$$

where

$s_i = s_i\,(\theta)$ indicates the displacement of the mass point i in the direction parallel to the unit vector $\vec{n}_2$, Fig.A.1, caused by the rigid body deployment of the wing.

$z_i = z_i\,(\theta)$ ibid., in the direction parallel to the unit vector $\vec{n}_3$ Fig. A.1.

$\vec{q}_i = \vec{q}_i\,(t)$ elastic deformation with respect to the reference frame fixed in vehicle, as identified by the unit vectors $\vec{n}_i$ $(i = 1,2,3)$.

Velocity of the mass point i is

$${}^R\vec{V}_i = \frac{{}^R d\vec{p}_i}{dt} = \frac{{}^R d\vec{p}_o}{dt} + {}^R\omega^V \times [s_i \, \vec{n}_2 + z_i \, \vec{n}_3 + \vec{q}_i] + \left(\frac{\partial s_i}{\partial \theta} \vec{n}_2 + \frac{\partial z_i}{\partial \theta} \vec{n}_3\right) \dot{\theta} + \frac{{}^V d\vec{q}_i}{dt} \qquad A.4$$

where the left superscript denotes the reference frame in which the differentiation has to be performed and the dot over a quantity denotes the time derivative.

Consistent with the assumption outlined in the Introduction, the angular velocity of the mass point i is found from the equation

$$ {}^{R}\omega_i = ({}^{R}\omega_1^{V} + \dot{\theta}_i)\,\vec{n}_1 + ({}^{R}\omega_2^{V} + \dot{\phi}_{2i})\,\vec{n}_2 + {}^{R}\omega_3^{V}\,\vec{n}_3 \qquad \text{A.5} $$

Writing

$$ \frac{{}^{R}d\vec{p}_o}{dt} = V_{10}\,\vec{n}_1 + V_{20}\,\vec{n}_2 + V_{30}\,\vec{n}_3 \qquad \text{A.6} $$

and utilizing Equations 5 and 6, the final expression for the velocity of the mass i is found to be

$$ \begin{aligned} {}^{R}\vec{V}_i = {} & [V_{10} + {}^{R}\omega_2^{V}(z_i + q_{3i}) - {}^{R}\omega_3^{V}(s_i + q_{2i})]\,\vec{n}_1 \\ & + [V_{20} - {}^{R}\omega_1^{V}(z_i + q_{3i}) + s_i'\,\dot{\theta} + \dot{q}_{2i}]\,\vec{n}_2 \\ & + [V_{30} + {}^{R}\omega_1^{V}(s_i + q_{2i}) + z_i'\,\dot{\theta} + \dot{q}_{3i}]\,\vec{n}_3 \end{aligned} \qquad \text{A.7} $$

where the prime over the quantity denotes the partial derivative with respect to the rigid deployment angle θ. q_{2i} and q_{3i} are the elastic displacements of the mass point i in the directions parallel to the unit vectors $\vec{n}_2$ and $\vec{n}_3$, respectively.

Considering the body axes parallel to the unit vectors $\vec{a}_i$, Fig. A.1, the diadic form of the inertia tensor can be written as the summation

$$ \vec{\Psi}_i^{*} = \sum_{k=1}^{3} \sum_{\ell=1}^{3} \bar{\Psi}_{k\ell}^{i}\,\vec{a}_{ik}\,\vec{a}_{i\ell} \qquad \text{A.8} $$

where

$\bar{\Psi}_{k\ell}^{i}$ are the components of the inertia tensor of the mass i referred to the body axes $\vec{a}_i$ $(i = 1,2,3)$, Fig. A.1.

The inertia tensor components $\bar{\psi}^i_{k\ell}$ are transformed to the reference frame $\bar{n}_i$ $(i = 1,2,3)$ by the following expressions

$$\psi^i_{11} = \bar{\psi}^i_{11}$$

$$\psi^i_{12} = \bar{\psi}^i_{12} \cos \theta_i - \bar{\psi}^i_{13} \sin \theta_i$$

$$\psi^i_{13} = \bar{\psi}^i_{12} \sin \theta_i + \bar{\psi}^i_{13} \cos \theta_i$$

$$\psi^i_{22} = \bar{\psi}^i_{22} \cos^2 \theta_i - \bar{\psi}^i_{23} \sin 2\theta_i + \bar{\psi}^i_{33} \sin^2 \theta_i$$

$$\psi^i_{23} = (\bar{\psi}^i_{22} - \bar{\psi}^i_{33}) \tfrac{1}{2} \sin 2\theta_i + \bar{\psi}^i_{23} \cos 2\theta_i$$

$$\psi^i_{33} = \bar{\psi}^i_{22} \sin^2 \theta_i + \bar{\psi}^i_{23} \sin 2\theta_i + \bar{\psi}^i_{33} \cos^2 \theta_i \qquad \text{A.9}$$

where $\psi^i_{k\ell}$ are the components of the inertia tensor in the reference frame defined by the unit vector $\vec{n}_i$ $(i = 1,2,3)$, fixed in the vehicle V.

Inertia tensor in dyadic form in this reference frame is simply

$$\psi_j = \psi^j_{11} \vec{n}_1\vec{n}_1 + \psi^j_{12} (\vec{n}_1\vec{n}_2 + \vec{n}_1\vec{n}_1) + \psi^j_{13} (\vec{n}_1\vec{n}_3 + \vec{n}_3\vec{n}_1)$$
$$+ \psi^j_{22} \vec{n}_2\vec{n}_2 + \psi^j_{23} (\vec{n}_2\vec{n}_3 + \vec{n}_3\vec{n}_2) \qquad \text{A.10}$$

Substituting Equations A.5 and A.7 into A.2 we obtain the kinetic energy in the wing and linkages

$$T = \tfrac{1}{2} \sum_{i=1}^{6} M_i \{[V_{10} + {}^R\omega^V_2 (z_i + q_{3i}) - {}^R\omega^V_3 (s_i + q_{2i})]^2$$
$$+ [V_{20} - {}^R\omega^V_1 (z_i + q_{3i}) + s'_i \dot{\theta} + \dot{q}_{2i}]^2$$
$$+ [V_{30} + {}^R\omega^V_1 (s_i + q_{2i}) + z'_i \dot{\theta} + \dot{q}_{3i}]^2\}$$
$$+ \tfrac{1}{2} \sum_{j=1}^{9} \sum_{k=1}^{3} \sum_{\ell=1}^{3} \psi^j_{k\ell} \, {}^R\omega^j_k \, {}^R\omega^j_\ell \qquad \text{A.11}$$

Note that the angular velocities ${}^{R}\omega_k^j$ are evaluated from Equation A.5 only for $j = 1,2,\ldots 6$. For the remaining three mass points we obtain from Fig. A.1

$$
\begin{aligned}
{}^{R}\omega_1^7 &= {}^{R}\omega_1^V + \dot{\theta} \\
{}^{R}\omega_1^8 &= {}^{R}\omega_1^V - \tau' \dot{\theta} \\
{}^{R}\omega_1^9 &= {}^{R}\omega_1^V - \alpha' \dot{\theta}
\end{aligned}
\qquad \text{A.12}
$$

and

$$
{}^{R}\omega_k^j = {}^{R}\omega_k^V \qquad \text{for} \qquad k = 2,3 \qquad \text{and} \qquad j = 7,8,9 \qquad \text{A.13}
$$

1.3 Strain Energy

Strain energy stored in the deformed wing consists of the elastic strain energy of the wing relative to the eighteen degrees of elastic freedom, strain energy of the panel springs, and strain energy due to elastic prepacking.

Strain energy stored in the deformed structure is computed from the following equation

$$
U_e = \frac{1}{2}\left[\sum_{i=1}^{6} \vec{q}_i \cdot \vec{F}_i + \sum_{i=1}^{6} \vec{\phi}_i \cdot \vec{M}_i\right] \qquad \text{A.14}
$$

where $\vec{F}_i$ and $\vec{M}_i$ are the force and moment vectors acting at the mass point i, and $\vec{q}_i$ and $\bar{\phi}_i$ are the elastic displacement and elastic rotation vectors of the mass point i, respectively. In order to evaluate Equation A.14, we will relate the $\vec{F}_i$ and $\vec{M}_i$ to the elastic displacements $\vec{q}_i$ and $\bar{\phi}_i$ by means of stiffness matrix k_{ij}. For that purpose, we define a displacement vector Q_i and a force vector, P_i related to $\vec{q}_i$, $\bar{\phi}_i$ and $\vec{F}_i$, $\vec{M}_i$ as indicated in Tables A1 and A2, respectively.

Table A1

$\vec{q}_j$, $\vec{\phi}_j$ RELATIONSHIP TO Q_j

	$j = 1$	$j = 2$	$j = 3$	$j = 4$	$j = 5$	$j = 6$
q_{2j}	Q_1	Q_4	Q_7	Q_{10}	Q_{13}	Q_{16}
q_{3j}	Q_2	Q_5	Q_8	Q_{11}	Q_{14}	Q_{17}
ϕ_{2j}	Q_3	Q_6	Q_9	Q_{12}	Q_{15}	Q_{18}

Table A2

$\vec{F}_j$, $\vec{M}_j$ RELATIONSHIP TO P_j MASS POINT

	$j = 1$	$j = 2$	$j = 3$	$j = 4$	$j = 5$	$j = 6$
F_{2j}	P_1	P_4	P_7	P_{10}	P_{13}	P_{16}
F_{3j}	P_2	P_5	P_8	P_{11}	P_{14}	P_{17}
M_{2j}	P_3	P_6	P_9	P_{12}	P_{15}	P_{18}

Based on Table A1, the following identities are written:

$$q_{2j} = Q_{3j-2} \quad q_{3j} = Q_{3j-1} \quad Q_{2j} = Q_{3j} \qquad \text{A.15}$$

Using this new notation the elastic strain energy stored in structures is found to be

$$U_e = \tfrac{1}{2} \sum_{i=1}^{18} Q_i \, P_i \qquad \text{A.16}$$

Defining the stiffness matrix k_{ij}

$$P_i = \sum_{j=1}^{18} k_{ij} \, Q_j, \qquad \text{A.17}$$

Equation A.17 reduces to

$$U_e = \frac{1}{2} \sum_{i=1}^{18} \sum_{j=1}^{18} k_{ij} Q_i Q_j \qquad \text{A.18}$$

Note that due to the rigid body deployment, the stiffness matrix coefficients are functions of the angle θ

$$k_{ij} = k_{ij} (\theta) \qquad (i,j = 1,18) \qquad \text{A.19}$$

Next we consider the strain energy stored in the spring. Assuming that there are m springs per panel hinge, we compute the strain energy stored in springs, Fig. A.2.

$$U_{sp} = \frac{1}{2} \sum_{i=1}^{6} m\, k_i (\beta_{oi} - \beta_i)^2 \qquad \text{A.20}$$

where β_{oi} is the angle between the panels when the springs are unstressed, β_i is the angle between the panels corresponding to the deployment position θ, and k_i is the spring constant.

After the wing is folded, it is cinched in the launching position. This introduces the elastic strain energy corresponding to the structural prestressing associated with the cinching operation. For the purpose of present analysis we assume that linear relationship exists between the change of the angle θ and the applied cinching load. With this, the prepack strain energy is evaluated from

$$U_{pr} = \frac{1}{2} k_p (\theta_p - \theta)^2 \qquad \text{A.21}$$

where k_p is the spring constant of the structure, and θ_p is the change of the angle θ during the cinching operation.

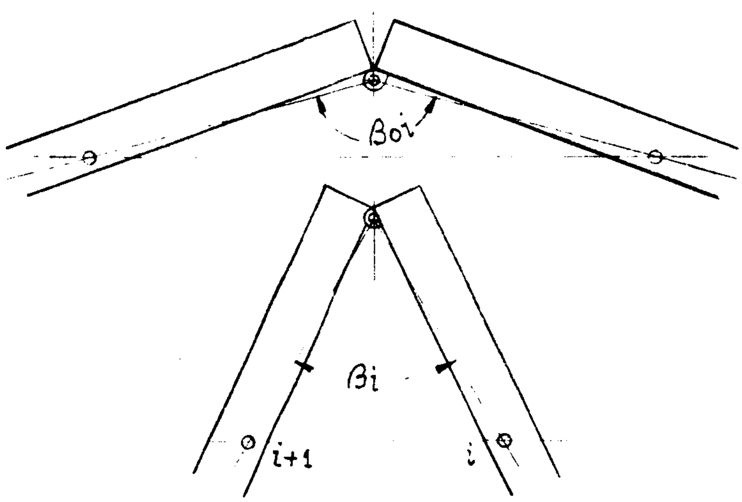

Fig. A.2 - Springs in Panel Hinge

Total strain energy is found by adding the above three contributions and is computed from the following equation

$$V = \frac{1}{2} \sum_{i=1}^{18} \sum_{j=1}^{18} k_{ij} Q_i Q_j + \frac{1}{2} \sum_{i=1}^{6} m (\beta_{oi} - \beta_i^2) k_i + \frac{1}{2} k_p (\theta_p - \theta)^2 \qquad \text{A.22}$$

Note that in Equation A.22, k_{ij} and β_i are functions of the angle θ.

1.4 Generalized Forces

Generalized forces associated with Q_i are zero. Neglecting small elastic relative angular displacements compared to θ, the friction forces will contribute only to the generalized force G_θ. Similarly, the torque on the torque shaft will contribute to the generalized force G_θ.

Virtual work due to friction forces at a joint i is defined by

$$W_\theta^1 = - \sum_{i=1}^{I} Y_i \, \delta\beta_i \qquad \text{A.23}$$

where Y_i is the friction torque at the joint i and $\delta\beta_i$ is the virtual angular displacement of the joint i. Since

$$\delta\beta_i = \frac{\partial\beta_i}{\partial\theta} \, \delta\theta = \beta_i' \, \delta\theta$$

we have

$$\omega_\theta' = - \sum_{i=1}^{I} Y_i \, \beta_i' \, \delta\theta$$

and

$$G_\theta' = - \sum_{i=1}^{I} Y_i \, \beta_i' \qquad \text{A.24}$$

where I is the total number of friction joints and Y_i is the friction torque at the joint i.

Similarly, if the torque of the drive unit is given as a function of the angular velocity $\dot{\alpha}$ of the torque shaft

$$\vec{R} = R\ (\dot{\alpha})\ \vec{n}_1 \qquad \text{A.25}$$

the virtual work due to this torque is

$$w_\theta'' = R\ (\alpha)\ \vec{n}_1 \cdot (-\ \delta\ \alpha\ \vec{n}_1) = -\ R\ (\dot{\alpha})\ \delta\alpha$$

Since the angular displacement of the torque shaft is a function of the angle θ, we have

$$\delta\alpha = \frac{\partial\alpha(\theta)}{\partial\theta}\ \delta\theta = \alpha'\delta\theta$$

$$W_\theta'' = -\ R\ (\dot{\alpha})\ \alpha'\delta\theta$$

and

$$G_\theta^{11} = -\ R\ (\dot{\alpha})\ \alpha' \qquad \text{A.26}$$

Total generalized force for the generalized coordinate θ is

$$G_\theta = -\sum_{i=1}^{I} Y_i\beta_i' - R\ (\dot{\alpha})\ \alpha' \qquad \text{A.27}$$

1.5 Equation of Motion for the Generalized Coordinate θ

Performing the differentiations indicated by Equation A.1 on the quantities T and V, we obtain the following equation of motion for the generalized coordinate θ:

$$\sum_{i=1}^{6} M_i \{[V_{20} - {}^R\omega_1^V (z_i + Q_{3i-1}) + s_i' \dot\theta + \dot Q_{3i-2}]\, s_i'' \dot\theta + [- {}^R\dot\omega_1^V (z_i + q_{3i}) +$$

$$+ \dot V_{20} - {}^R\omega_1^V (z_i' \dot\theta + \dot Q_{3i-1}) + s_i'' \dot\theta^2 + s_i' \ddot\theta + \ddot Q_{3i-2}]\, s_i' + [V_{30} + {}^R\omega_1^V (s_i +$$

$$+ Q_{3i-2}) + z_i' \dot\theta + \dot Q_{3i-1})\Big] + \; z_i'' \dot\theta + [{}^R\dot\omega_1^V (s_i + q_{2i}) +$$

$$\dot V_{30} + {}^R\omega_1^V (s_i' \dot\theta + \dot Q_{3i-2}) + z_i'' \dot\theta^2 + z_i' \ddot\theta + \ddot Q_{3i-1}\, z_i]\} + \sum_{k=1}^{3} \sum_{j=1}^{9} \{[(\psi_{1k}^j)^{\bullet}\, {}^R\omega_k^j +$$

$$+ \psi_{1k}^j ({}^R\omega_k^j)^{\bullet}]\, {}^R\omega_{1,\theta}^j + \psi_{1k}^j\, {}^R\omega_k^j ({}^R\omega_{1,\dot\theta}^j)^{\bullet}\} - \sum_{i=1}^{6} M_i \{[V_{10} + {}^R\omega_2^V (z_i + Q_{3i-1}) -$$

$${}^R\omega_3^V (s_i + Q_{3i-2})]\, ({}^R\omega_2^V z_i' - {}^R\omega_3^V s_i') + [V_{20} - {}^R\omega_1^V (z_i + Q_{3i-1}) + s_i' \dot\theta +$$

$$+ \dot Q_{3i-2}]\, (- {}^R\omega_1^V z_i' + s_i'' \dot\theta) + [V_{30} + {}^R\omega_1^V (s_i + Q_{3i-2}) + \dot z_i \dot\theta + \dot Q_{3i-1}]\, ({}^R\omega_1^V s_i'$$

$$+ z_i'' \dot\theta)\} - \tfrac{1}{2} \sum_{k=1}^{3} \sum_{\ell=1}^{3} \sum_{j=1}^{9} (\psi_{k\ell,\theta}^j\, {}^R\omega_k^j\, {}^R\omega_\ell^j + 2\, \psi_{k\ell}^j\, {}^R\omega_k^j\, {}^R\omega_{\ell,\theta}^j)] +$$

$$+ \tfrac{1}{2} \sum_{i=1}^{18} \sum_{j=1}^{18} k_{ij,\theta}\, Q_i Q_j - \sum_{i=1}^{6} m\, (\beta_{oi} - \beta_i)\, k_i\, \beta_{i,\theta} - k_p\, (\theta_p - \theta)$$

$$= -\sum_{i=1}^{I} Y_i\, \beta_i' - R\, (\dot\alpha)\, \alpha' \qquad \text{A.28}$$

In Equation A.28, primes over the quantities denote partial differentiation with respect to the angle θ. Similarly, a subscript following a comma at a quantity indicates partial derivative of this quantity with respect to the variable following the comma. A dot over a quantity indicates the time derivative of that quantity. Other quantities required in Equation A.28 are defined by the following equations:

$$(\psi^j_{11})_{,\theta} = 0$$

$$(\psi^j_{12})_{,\theta} = -(\bar{\Psi}^j_{12} \sin\theta_j + \bar{\Psi}^j_{13} \cos\theta_j)\,\theta'_j = (\psi^j_{21})_{,\theta}$$

$$(\psi^j_{13})_{,\theta} = (\bar{\Psi}^j_{12} \cos\theta_j - \bar{\Psi}^j_{13} \sin\theta_j)\,\theta'_j = (\psi^j_{31})_{,\theta}$$

$$(\psi^j_{22})_{,\theta} = [(\bar{\Psi}^j_{33} - \bar{\Psi}^j_{22}) \sin 2\theta_j - 2\,\bar{\Psi}^j_{23} \cos 2\theta_j]\,\theta'_j$$

$$(\psi^j_{23})_{,\theta} = [(\bar{\Psi}^j_{22} - \bar{\Psi}^j_{33}) \cos 2\theta_j - 2\,\bar{\Psi}^j_{23} \sin 2\theta_j]\,\theta'_j = (\psi^j_{32})_{,\theta}$$

$$(\psi^j_{33})_{,\theta} = [(\bar{\Psi}^j_{22} - \bar{\Psi}^j_{33}) \sin 2\theta_j + 2\,\bar{\Psi}^j_{23} \cos 2\theta_j]\,\theta'_j$$

$$(\psi^j_{k\ell}) = (\psi^j_{k\ell,\theta})\,\dot{\theta} \qquad \text{A.29}$$

$${}^R\omega^j_{1,\theta} = \theta''_j\,\dot{\theta}$$

$${}^R\omega^j_{2,\theta} = {}^R\omega^j_{3,\theta} = 0 \qquad (j = 1,6)$$

$${}^R\omega^7_{1,\theta} = {}^R\omega^7_{2,\theta} = {}^R\omega^7_{3,\theta} = 0$$

$${}^R\omega^8_{1,\theta} = -\,\tau''\,\dot{\theta}$$

$${}^R\omega^8_{2,\theta} = {}^R\omega^8_{3,\theta} = 0$$

$${}^R\omega^9_{1,\theta} = -\,\alpha''\,\dot{\theta}$$

$${}^R\omega^9_{2,\theta} = {}^R\omega^9_{3,\theta} = 0 \qquad \text{A.30}$$

$$({}^R\omega_1^j)^{\bullet} = \gamma_1^j + \kappa_1^j\,\ddot{\theta}$$

$$\gamma_1^j = {}^R\dot{\omega}_1^V + \theta_j''\,\dot{\theta}^2 \qquad \kappa_1^j = \theta_j'$$

$$({}^R\omega_2^j)^{\bullet} = \gamma_2^j + \ddot{Q}_{3j} \qquad ({}^R\omega_3^j)^{\bullet} = \gamma_3^j$$

$$\gamma_2^j = {}^R\dot{\omega}_2^V \qquad \gamma_3^j = {}^R\dot{\omega}_3^j$$

$$(j = 1,6) \tag{A.31}$$

$$({}^R\omega_1^7)^{\bullet} = {}^R\gamma_1^7 + {}^R\kappa_1^7\,\ddot{\theta}$$

$${}^R\gamma_1^7 = {}^R\dot{\omega}_1^V \qquad {}^R\kappa_1^7 = 1$$

$$({}^R\omega_1^8)^{\bullet} = {}^R\gamma_1^8 + {}^R\kappa_1^8\,\ddot{\theta}$$

$${}^R\gamma_1^8 = {}^R\dot{\omega}_1^V - \tau''\,\dot{\theta}^2 \qquad {}^R\kappa_1^8 = -\tau'$$

$$({}^R\omega_1^9)^{\bullet} = {}^R\gamma_1^9 + {}^R\kappa_1^9\,\ddot{\theta}$$

$${}^R\gamma_1^9 = {}^R\dot{\omega}_1^V - \alpha''\,\dot{\theta}^2 \qquad {}^R\kappa_1^9 = -\alpha' \tag{A.32}$$

$$({}^R\omega_k^j)^{\bullet} = {}^R\gamma_k^j$$

$${}^R\gamma_k^j = {}^R\dot{\omega}_k^j \qquad (j = 7,\ 8,\ 9;\ k = 2,\ 3) \tag{A.33}$$

$$({}^R\omega_1^j)_{,\dot{\theta}} = \theta_j'$$

$$({}^R\omega_2^j)_{,\dot{\theta}} = ({}^R\omega_3^j)_{,\dot{\theta}} = 0 \qquad (j = 1,6) \tag{A.34}$$

$$({}^R\omega_1^7)_{,\dot{\theta}} = 1$$

$$({}^R\omega_1^8)_{,\dot{\theta}} = -\tau'$$

$$({}^R\omega_1^9)_{,\dot\theta} = -\alpha'$$

$$({}^R\omega_k^j)_{,\dot\theta} = 0 \qquad (j = 7, 8, 9;\ k = 2, 3) \qquad \text{A.35}$$

$$({}^R\omega^j_{1,\dot\theta})^{\cdot} = \theta_j''\,\dot\theta \qquad (j = 1, 6)$$

$$({}^R\omega^7_{1,\dot\theta})^{\cdot} = 0$$

$$({}^R\omega^8_{1,\dot\theta})^{\cdot} = -\tau''\,\dot\theta$$

$$({}^R\omega^9_{1,\dot\theta})^{\cdot} = -\alpha''\,\dot\theta$$

$$({}^R\omega^j_{k,\dot\theta})^{\cdot} = 0 \qquad (j = k, 9;\ k = 2, 3) \qquad \text{A.36}$$

1.6 Equations of Motion for the Generalized Coordinates Q_n

Performing the differentiations indicated by Equation A.1 we obtain the following equations of motion for the generalized coordinates Q_n

$$\sum_{i=1}^{6} M_i \{[-{}^R\dot\omega_1^V (z_i + Q_{3i-1}) + \dot V_{20} - {}^R\omega_1^V (z_i'\,\dot\theta + \dot Q_{3i-1}) + s_i''\,\dot\theta^2 + s_i'\,\ddot\theta + \ddot Q_{3i-2}]\,\delta_n^{3i-2} + [{}^R\dot\omega_1^V (s_i + Q_{3i-2}) + \dot V_{30} + {}^R\omega_1^V (s_i'\,\dot\theta + \dot Q_{3i-2}) + z_i''\,\dot\theta^2 + z_i'\,\ddot\theta + \ddot Q_{3i-1}]\,\delta_n^{3i-1}\} + \sum_{k=1}^{3}\sum_{j=1}^{6} [(\psi_{k2}^j)^{\cdot}\,{}^R\omega_k^j + \psi_{k2}^j\,({}^R\omega_k^j)^{\cdot}]\,{}^V\delta_n^{3j} -$$

$$\sum_{i=1}^{6} M_i \{[V_{10} + {}^R\omega_2^V (z_i + Q_{3i-1}) - {}^R\omega_3^V (s_i + Q_{3i-2})]\,({}^R\omega_2^V\,\delta_n^{3i-1} - {}^R\omega_3^V\,\delta_n^{3i-2}) + [V_{20} - {}^R\omega_1^V (z_i + Q_{3i-1}) + s_i'\,\dot\theta + \dot Q_{3i-2}]\,(-{}^R\omega_1^V\,\delta_n^{3i-1}) + [V_{30} + {}^R\omega_1^V (s_i + Q_{3i-2}) + z_i'\,\dot\theta + \dot Q_{3i-1}]\,({}^R\omega_1^V\,\delta_n^{3i-2})\} + \sum_{i=1}^{18} k_{in}\,Q_i = 0$$

$$(n = 1, 18) \qquad \text{A.37}$$

In Equation A.37 δ_i^j denotes the Kronecker delta which is equal to unity if $i = j$ and zero if $i \neq j$. All other quantities have been defined previously.

Equations A.28 and A. 37 define the problem of the deployment dynamics of the wing. There are nineteen equations in terms of eighteen generalized coordinates corresponding to the elastic degrees of freedom, Table A1, and one equation corresponding to the rigid body deployment angle θ.

2. TRANSFORMATION OF THE EQUATIONS OF MOTION

Equations A.28 and A.37 form a system of nineteen coupled, second order, non-linear, ordinary differential equations. Dependent variables are θ and Q_i ($i = 1, 19$). If no further simplifications are introduced, the solution of this system is only possible by numerical methods. Accordingly we will transform this system into a form convenient for the numerical integration by use of the Runge-Kutta-Gill[1] direct integration method.

For that purpose, we collect the terms containing the second derivatives of the dependent variables on the left hand side of the equations. This results in the following system of non-linear coupled, second order, differential equations.

[1]Ralston, A., and Wilf, H. S., Mathematical Methods for Digital Computers, J. Wiley and Sons, Inc., 1960.

$$\sum_{i=1}^{6} \{M_i \, [(\ddot{Q}_{3i-2} + s_i' \ddot{Q}_{19}) \, \delta_n^{3i-2} + (\ddot{Q}_{3i-1} + z_i' \ddot{Q}_{19}) \, \delta_n^{3i-1}] + \Gamma\psi_{22}^{i} \, \ddot{Q}_{3i} +$$

$$\psi_{12}^{i} \, \kappa_1^{i} \, \ddot{Q}_{19}] \, \delta_n^{3i}\} = -\sum_{i=1}^{6} \{[-{}^R\dot{\omega}_1^V \, (z_i + Q_{3i-1}) + \dot{V}_{20} - {}^R\omega_1^V \, (z_i' \, \dot{Q}_{19} + \dot{Q}_{3i-1}) +$$

$$s_i'' \, \dot{Q}_{19}^2] \, \delta_n^{3i-2} + [{}^R\dot{\omega}_1^V \, (s_i + Q_{3i-2}) + \dot{V}_{30} + {}^R\omega_1^V \, (s_i' \, \dot{Q}_{19} + \dot{Q}_{3i-2}) +$$

$$z_i'' \, \dot{Q}_{19}^2] \, \delta_n^{3i-1}\} - \sum_{j=1}^{6} \sum_{k=1}^{3} \left[(\psi_{k2}^{j})^{\cdot} \, {}^R\omega_k^j + \psi_{k2}^{j} \, \gamma_k^j\right] \delta_n^{3j} + \sum_{i=1}^{6} M_i \, \{[V_{10} +$$

$${}^R\omega_2^V \, (z_i + Q_{3i-1}) - {}^R\omega_3^V \, (s_i + Q_{3i-2})] \, ({}^R\omega_2^V \, \delta_n^{3i-1} - {}^R\omega_3^V \, \delta_n^{3i-2}) + \Gamma V_{20} -$$

$${}^R\omega_1^V \, (z_i + Q_{3i-1}) + s_1' \, \dot{Q}_{19} + \dot{Q}_{3i-2}] \, (-{}^R\omega_1^V \, \delta_n^{3i-1}) + [V_{30} + {}^R\omega_1^V \, (s_i + Q_{3i-2}) +$$

$$z_i' \, \dot{Q}_{19} + \dot{Q}_{3i-1}] \, ({}^R\omega_1^V \, \delta_n^{3i-2})\} - \sum_{i=1}^{18} k_{in} \, Q_i \qquad (n = 1, 18) \qquad \text{A.38}$$

$$\sum_{i=1}^{6} [M_i \, (s_i' \, \ddot{Q}_{3i-2} + z_i' \, \ddot{Q}_{3i-1}) + \psi_{12}^{i} \, {}^R\omega_{1,\dot{\theta}}^{i} \, \ddot{Q}_{3i}] + \Bigg[\sum_{i=1}^{6} M_i \, (s_i'^2 +$$

$$z_i^2) + \sum_{i=1}^{9} \psi_{11}^{i} \, \kappa_1^{i} \, {}^R\omega_{1,\dot{\theta}}^{i}\Bigg] \ddot{Q}_{19} = \sum_{i=1}^{6} M_i \, \{\Gamma V_{10} + {}^R\omega_2^V \, (z_i + Q_{3i-1}) -$$

$${}^R\omega_3^V \, (s_i + Q_{3i-2})] \, ({}^R\omega_2^V \, z_i' - {}^R\omega_3^V \, s_i') + [V_{20} - {}^R\omega_1^V \, (z_i + Q_{3i-1}) + s_i' \, \dot{Q}_{19} +$$

$$\dot{Q}_{3i-2}] \, (-{}^R\omega_1^V \, z_i') + \Gamma V_{30} + {}^R\omega_1^V \, (s_i + Q_{3i-2}) + z_i' \, \dot{Q}_{19} + \dot{Q}_{3i-1}] \, {}^R\omega_1^V \, s_i' +$$

$$\Gamma-{}^R\dot{\omega}_1^V \, (z_i + Q_{3i-1}) + \dot{V}_{20} - {}^R\omega_1^V \, (z_i' \, \dot{Q}_{19} + \dot{Q}_{3i-1}) + s_i'' \, \dot{Q}_{19}^2] \, (-s_i') +$$

$$\Gamma{}^R\dot{\omega}_1^V \, (s_i + Q_{3i-2}) + \dot{V}_{30} + {}^R\omega_1^V \, (s_i' \, \dot{Q}_{19} + \dot{Q}_{3i-2}) + z_i'' \, \dot{Q}_{19}^2] \, (-z_i')\} +$$

$$\sum_{j=1}^{9} \left\{ \sum_{k=1}^{3} \left(-\left[(\psi_{1k}^{j})^{\cdot}\, {}^{R}\omega_{k}^{j} + \psi_{1k}^{j}\, \gamma_{k}^{j} \right] {}^{R}\omega_{1,\dot{\theta}}^{j} - \psi_{1k}^{j}\, {}^{R}\omega_{k}^{j} \left({}^{R}\omega_{1,\dot{\theta}}^{j}\right)^{\cdot} \right) \right.$$

$$\left. + \frac{1}{2} \sum_{k=1}^{3} \left[\sum_{\ell=1}^{3} \psi_{k\ell,\theta}^{j}\, {}^{R}\omega_{k}^{j}\, {}^{R}\omega_{\ell}^{j} + 2\, \psi_{k1}^{j}\, {}^{R}\omega_{k}^{j}\, {}^{R}\omega_{1,\theta}^{j} \right] \right\} - \frac{1}{2} \sum_{i=1}^{18} \sum_{j=1}^{18} k_{ij,\theta}\, Q_i Q_j +$$

$$\sum_{i=1}^{6} m\,(\beta_{oi} - \beta_i)\, k_i\, \beta_{i,\theta} + k_p\,(\theta_p - Q_{19}) - \sum_{i=1}^{I} Y_i\, \beta_i' - R\,(\alpha')\, \alpha' \qquad \text{A.39}$$

where for the sake of the uniformity the notation

$$Q_{19} = \theta \qquad \text{A.40}$$

was introduced.

Equations A.38 and A.39 can be written in the following form:

$$A_{ij}\, \ddot{Q}_j = F_i \qquad (i,\ j = 1,\ 19) \qquad \text{A.41}$$

where A_{ij} and F_i can be found by comparing Equations A.41 to Equations A.38 and A.39. Prior to the evaluation of A_{ij} and F_i we introduce additional information which will reduce the coupling of Equations A.41 considerably. This additional information consists in the recognition of the fact that the six panels of the wing are symmetric with respect to the reference frame fixed in panel with the axes parallel to the unit vectors $\vec{a}_i^{\,j}$ ($i = 1, 2, 3,$ $j = 1, 6$). This results in

$$\bar{\psi}_{k\ell}^{j} = 0 \quad \text{for} \quad k \neq \ell \quad \text{and} \quad j = 1,\ 6$$

and, in virtue of Equation A.9, also

$$\psi_{12}^{j} = \psi_{13}^{j} = 0 \qquad (j = 1,\ 6) \qquad \text{A.42}$$

Substituting Equation A.42 into Equations A.38 and A.39, we note that the coupling in Equation A.38 exists only through Q_{19} for the elastic displacement degrees of freedom, Q_{3i-1}, Q_{3i-2}, and that there is no coupling at all for the elastic twisting of the wing, Q_{3i}. Accordingly, the problem reduces to solving thirteen coupled and six uncoupled differential equations.

Introducing new symbols for the dependent variables

$$Y_{2i+19} = Q_{3i-1} \qquad Y_{32} = Q_{19}$$

$$Y_{2i+18} = Q_{3i-2}$$

$$Y_{i+32} = Q_{3i}$$

$$Y_{2i} = \dot{Q}_{3i-1}$$

$$Y_{2i-1} = \dot{Q}_{3i-2}$$

$$Y_{i+13} = \dot{Q}_{3i}$$

$$Y_{13} = \dot{Q}_{19} \qquad (i - 1, 6) \qquad \text{A.43}$$

$$Y_{39} = \text{time}$$

the final system of the differential equations can be solved for the highest derivatives of the dependent variables and written in the following form, convenient for the numerical integration.

$$\dot{Y}_i = F_i - B_i\, C \qquad (i = 1, 12)$$

$$\dot{Y}_{13} = C$$

$$\dot{Y}_j = F_j \qquad (j = 14, 19)$$

$$\dot{Y}_{k+19} = Y_k \qquad (k = 1, 19)$$

$$\dot{Y}_{39} = 1 \qquad \text{A.44}$$

where

$$C = \left(F_{13} - \sum_{i=1}^{12} F_i\ A_i\right) \Big/ \left(A_{13} - \sum_{i=1}^{12} B_i\ A_i\right) \qquad \text{A.45}$$

and the other quantities are defined by the following equations.

$$B_{2i-1} = s_i' \qquad B_{2i} - z_i'$$

$$A_{2i-1} = M_i\ s_i' \quad A_{2i} = M_i\ z_i' \qquad (i = 1,\ 6)$$

$$A_{13} = \sum_{i=1}^{6} M_i\ (s_i'^2 + z_i'^2) + \sum_{i=1}^{9} \psi_{11}^i\ \kappa_1^i\ {}^R\omega_{1,\theta}^i\ . \qquad \text{A.46}$$

$$V1_i = V_{10} + {}^R\omega_2^V\ (z_i + Q_{3i-1}) - {}^R\omega_3^V\ (s_i + Q_{3i-2})$$

$$V2_i = V_{20} - {}^R\omega_1^V\ (z_i + Q_{3i-1}) + s_i'\ \dot{Q}_{19} + \dot{Q}_{3i-2}$$

$$V3_i = V_{30} + {}^R\omega_1^V\ (s_i + Q_{3i-2}) + z_i'\ \dot{Q}_{19} + \dot{Q}_{3i-1}$$

$$V4_i = \dot{V}_{20} - {}^R\omega_1^V\ (3_i'\ \dot{Q}_{19} + \dot{Q}_{3i-1}) - {}^R\dot{\omega}_1^V\ (z_i + Q_{3i-1}) + s_i''\ \dot{Q}_{19}^2$$

$$V5_i = \dot{V}_{30} + {}^R\omega_1^V\ (s_i'\ \dot{Q}_{19} + \dot{Q}_{3i-2}) + {}^R\dot{\omega}_1^V\ (s_i + Q_{3i-2}) + z_i''\ \dot{Q}_{19}^2$$

$$(i = 1,\ 6) \qquad \text{A.47}$$

$$F_{2i-1} = -\ V4_i + V1_i\ (-{}^R\omega_3^V) + V3_i\ {}^R\omega_1^V - \frac{1}{M_i} \sum_{j=1}^{18} k_{j,3i-2}\ Q_j$$

$$F_{2i} = -\ V5_i + V1_i\ {}^R\omega_2^V + V2_i\ (-{}^R\omega_1^V\ ) - \frac{1}{M_i} \sum_{j=1}^{18} k_{j,3i-1}\ Q_j$$

$$F_{i+13} = -\frac{1}{\psi_{22}^i} \sum_{k=1}^{3} (\psi_{k2}^i)^{\cdot}\ {}^R\omega_k^i + \sum_{k=1}^{18} K_{k,3i}\ Q_k + \sum_{k=1}^{3} \psi_{k2}^i\ \gamma_k^i\ ]$$

$$(i = 1,6) \qquad \text{A.48}$$

$$
\begin{aligned}
F_{13} = \sum_{i=1}^{6} M_i \{ & V1_i \, ({}^R\omega_2^V \, z_i' - {}^R\omega_3^V \, s_i') + V2_i \, (-{}^R\omega_1^V \, z_i') + V3_i \, {}^R\omega_1^V \, s_i' \\
& + V4_i \, (-s_i') + V5_i \, (-z_i')\} + \sum_{j=1}^{9} \left\{ \sum_{k=1}^{3} \left(-[(\psi_{1k}^j)^{\cdot} \, {}^R\omega_k^j + \psi_{1k}^j \, \gamma_k^j] \, {}^R\omega_{1,\dot{\theta}}^j \right.\right. \\
& \left.\left. - \psi_k^j \, {}^R\omega_k^j \, (\omega_{1,\dot{\theta}}^j)^{\cdot}\right) + \tfrac{1}{2} \sum_{k=1}^{3} \left[\sum_{\ell=1}^{3} \psi_{k\ell,\theta}^j \, {}^R\omega_k^j \, {}^R\omega_\ell^j + 2 \, \psi_{k1}^j \, {}^R\omega_k^j \, {}^R\omega_{1,\theta}^j \right] \right\} \\
& - \tfrac{1}{2} \sum_{i=1}^{18} \sum_{j=1}^{18} k_{ij,\theta} \, Q_i Q_j + \sum_{i=1}^{6} m \, (\beta_{oi} - \beta_i) \, k_i \, \beta_{i,\theta} + k_p \, (\theta_p - Q_{19}) \\
& - \sum_{i=1}^{I} Y_i \, \beta_i' - R \, (\dot{\alpha}) \, \alpha' \qquad \text{A.49}
\end{aligned}
$$

3. EVALUATION OF RIGID BODY DEPLOYMENT INERTIA FORCE AND INERTIA TORQUE

If the elastic degrees of freedom are neglected, rigid body deployment motion of the wing results. To obtain some information of the loading on the structure for this condition, the inertia forces and inertia torque will be evaluated for the panels and linkages.

Differentiating the velocity $\vec{v}_i$, Equation A.4, with respect to time in reference frame R, we obtain the acceleration

$$
\begin{aligned}
\frac{{}^R d \, {}^R\vec{v}_i}{dt} = & \, (\dot{V}_{10} + {}^R\dot{\omega}_2^V \, z_i + {}^R\omega_2^V \, z_i' \, \dot{\theta} - {}^R\dot{\omega}_3^V \, s_i - {}^R\omega_3^V \, s_i' \, \dot{\theta} + W_{30i} \, {}^R\omega_2^V - W_{20i} \, {}^R\omega_3^V) \, \vec{n}_1 \\
& + [\dot{V}_{20} - {}^R\dot{\omega}_1^V \, z_i - {}^R\omega_1^V \, z_i' \, \dot{\theta} + s_i'' \, \dot{\theta}^2 + s_i' \, \ddot{\theta} + W_{10i} \, {}^R\omega_3^V - ({}^R\omega_1^V + \theta_j' \, \dot{\theta}) \, W_{30i}] \, \vec{n}_2 \\
& + [\dot{V}_{30} + {}^R\dot{\omega}_1^V \, s_i + {}^R\omega_1^V \, s_i' \, \dot{\theta} + z_i'' \, \dot{\theta}^2 + z_i' \, \ddot{\theta} - W_{10i} \, {}^R\omega_3^V + ({}^R\omega_1^V + \theta_j' \, \dot{\theta}) \, W_{30i}] \, \vec{n}_3
\end{aligned}
$$

$$(i = 1, 6) \qquad \text{A.50}$$

where

$$W_{10i} = V_{10} + {}^R\omega_2^V z_i - {}^R\omega_3^V s_i$$

$$W_{20i} = V_{20} - {}^R\omega_1^V z_i + s_i' \dot{\theta}$$

$$W_{30i} = V_{30} + {}^R\omega_1^V s_i + z_i' \dot{\theta} \qquad (i = 1, 6) \qquad \text{A.51}$$

Inertia force follows

$$\vec{F}_i = - M_i \{(\dot{V}_{10} + {}^R\dot{\omega}_2^V z_i + {}^R\omega_2^V z_i' \dot{\theta} - {}^R\dot{\omega}_3^V s_i - {}^R\omega_3^V s_i' \dot{\theta} + W_{30i} \, {}^R\omega_2^V - W_{20i} \, {}^R\omega_3^V) \vec{n}_2 + [\dot{V}_{20} - {}^R\dot{\omega}_1^V z_i - {}^R\omega_1^V z_i' \dot{\theta} + s_i'' \dot{\theta}^2 + s_i' \ddot{\theta} + W_{10i} \, {}^R\omega_3^V - ({}^R\omega_1^V + \theta_i' \dot{\theta}) W_{30i}] \vec{n}_2 + [\dot{V}_{30} + {}^R\dot{\omega}_1^V s_i + {}^R\omega_1^V s_i' \dot{\theta} + z_i'' \dot{\theta}^2 + z_i' \ddot{\theta} - W_{10i} \, {}^R\omega_2^V + ({}^R\omega_1^V + \theta_j' \dot{\theta}) W_{30i}] \vec{n}_3$$

$$(i = 1, 6) \qquad \text{A.52}$$

Inertia couple is evaluated from

$${}^R\vec{T}^i = - \sum_{k=1}^{3} \sum_{\ell=1}^{3} \psi_{k\ell}^i \left({}^R\alpha_k^i \, \vec{n}_\ell + {}^R\omega_k^i \, {}^R\vec{\omega}^i \times \vec{n}_\ell\right) \qquad \text{A.53}$$

where ${}^R\alpha_k^i$ is the angular acceleration of the element i in the reference frame R

$${}^R\vec{\alpha}^i = ({}^R\dot{\omega}_1^V + \theta_j'' \dot{\theta}^2 + \theta_j' \ddot{\theta}) \vec{n}_1 + {}^R\dot{\omega}_2^V \vec{n}_2 + {}^R\dot{\omega}_3^V \vec{n}_3 \qquad \text{A.54}$$

Substituting Equation A.54 into Equation A.53 we obtain the inertia torque

$$
{}^{R}\vec{T}^{i} = -\sum_{k=1}^{3} \{[\psi^{i}_{k1}\, {}^{R}\alpha^{i}_{k} - {}^{R}\omega^{i}_{k}\, {}^{R}\omega^{V}_{3}\, \psi^{i}_{k2} + {}^{R}\omega^{i}_{k}\, {}^{R}\omega^{V}_{2}\, \psi^{i}_{k3}]\vec{n}_{1}
$$

$$
+ [\psi^{i}_{k1}\, {}^{R}\omega^{i}_{k}\, {}^{R}\omega^{V}_{3} + \psi^{i}_{k2}\, {}^{R}\alpha^{i}_{k} - ({}^{R}\omega^{V}_{1} + \dot{\theta}_{i})\, {}^{R}\omega^{i}_{k}\, \psi^{i}_{k3}]\, \vec{n}_{2}
$$

$$
+ [-\psi^{i}_{k1}\, {}^{R}\omega^{i}_{k}\, {}^{R}\omega^{V}_{2} + ({}^{R}\omega^{V}_{1} + \dot{\theta}_{i})\, {}^{R}\omega^{i}_{k}\, \psi^{i}_{k2} + \psi^{i}_{k3}\, {}^{R}\alpha^{i}_{k}]\, \vec{n}_{3} \qquad \text{A.55}
$$

4. RIGID BODY DEPLOYMENT KINEMATICS

In order to perform the integration of Equation A.44, the quantities depending on θ determined by the kinematics of the ring mechanism will be evaluated as outlined below.

Expression for the angle α is determined from Figure A.3

$$
\sin\alpha = \left(-B_1 + \sqrt{B_1^2 - 4A_1C_1}\right)\Big/(2A_1)
$$

$$
\cos\alpha = \pm\sqrt{1 - \sin^2\alpha} \qquad \text{A.56}
$$

where

$$
A_1 = 4b_1^2(d^2 + a_1^2 - 2a_1 d\sin\theta)
$$

$$
B_1 = 4a_1 b_1 \cos\theta\, [(d^2 + a_1^2 + b_1^2 - \ell_1^2) - 2a_1 d\sin\theta]
$$

$$
C_1 = (d^2 + a_1^2 + b_1^2 - \ell_1^2)^2 - 4(d^2 + a_1^2 + b_1^2 - \ell_1^2)\, a_1 d\sin\theta
$$

$$
+ 4a_1^2 d^2 \sin^2\theta - 4b_1^2(d - a_1\sin\theta)^2 \qquad \text{A.57}
$$

In the second of Equations A.56 plus sign is used for $\theta \le \theta^*$, where

$$
\theta^* = \arcsin\left[\left(-b + \sqrt{b^2 - 4ac}\right)\Big/(2a)\right]
$$

and

$$
A = (d^2 + a_1^2 + b_1^2 - \ell_1^2)/(2a_1)
$$

$$
a = d^2 + b_1^2
$$

$$
b = -2Ad \qquad \text{A.58}
$$

$$
c = A^2 - b^2
$$

If $\theta > \theta^*$ minus sign in Equation A.56_2 is used.

From Figure A.3 we obtain also the angle τ.

$$\sin \tau = \left(- B_2 + \sqrt{B_2^2 - 4 A_2 C_2}\right) \Big/ (2A_2)$$

$$\cos \tau = \pm \sqrt{1 - \sin^2 \tau} \qquad \text{A.59}$$

where

$$A_2 = 4 a_2^2 (b_2^2 + d^2 + 2 b_2 d \cos \alpha)$$

$$B_2 = - 4 a_2^2 b_2 \sin \alpha [(d^2 + a_2^2 + b_2^2 - \ell_2^2) + 2 b_2 d \cos \alpha]$$

$$C_2 = (d^2 + a_2^2 + b_2^2 - \ell_2^2)^2 + 4 (a_2^2 + d^2 + b_2^2 - \ell_2^2) d b_2 \cos \alpha$$

$$+ 4 d^2 b_2^2 \cos^2 \alpha - 4 a_2^2 (d + b_2 \cos \alpha)^2 \qquad \text{A.60}$$

In the second of Equations A.59 the plus sign is used for $\alpha \leq \alpha^*$, where

$$\alpha^* = \text{arc } \sin \left[\left(- b + \sqrt{b^2 - 4ac}\right) \Big/ (2a)\right] \qquad \text{A.61}$$

and

$$a = a_2^2 + d^2$$

$$b = - 2 T a_2$$

$$c = T^2 - d^2$$

$$T = (d^2 + a_2^2 + b_2^2 - \ell_2^2)/(2 b_2) \qquad \text{A.62}$$

From Figure A.3 we find

$$s_i = 2 (7 - i) \bar{c}_1 \cos (\delta_1 - \gamma) \cos \varphi$$

$$z_i = 2 (7 - i) \bar{c}_1 \cos (\delta_1 - \gamma) \sin \varphi \qquad \text{A.63}$$

where

$$\varphi = \text{arc } \tan [(\bar{c}_1 \sin (\theta + \gamma) + c_2 \cos (\tau + \tau^*))/(\bar{c}_1 \cos (\theta + \gamma) + c_2 \sin (\tau + \tau^*))]$$

$$\bar{c}_1 = c_1/\cos\gamma$$

$$\delta_1 = \pi/2 + \varphi - \theta$$

$$\delta_2 = \pi - (\tau + \tau^* + \varphi) \tag{A.64}$$

From Figure A.4

$$\kappa = \delta_1 - \gamma + \varphi$$

$$\theta_2 = \theta_4 = \theta_6 = \delta_1 + \varphi$$

$$\theta_1 = \theta_3 = \theta_5 = 3\pi/2 + \theta$$

$$\beta_i = \pi - 2\,(\delta_1 - \gamma) \qquad (i = 1,\ 6) \tag{A.65}$$

Partial derivatives with respect to θ are found from the following equations

$$\alpha' = \frac{a_1\, D_1}{b_1\, D_2} \qquad \alpha'' = \frac{a_1\,(D_2 D_1' - D_2' D_1)}{b_1\, D_2^2} \tag{A.66}$$

where

$$D_1 = \cos\theta\,(d - b_1\cos\alpha) + \sin\theta\; b_1\sin\alpha$$

$$D_2 = \sin\alpha\,(d - a_1\sin\theta) + \cos\alpha\; a_1\cos\theta$$

$$D_1' = b_1\,\alpha'\,(\cos\theta\sin\alpha + \sin\theta\cos\alpha) - (d - b_1\cos\alpha)\sin\theta + b_1\sin\alpha\cos\theta$$

$$D_2' = \alpha'\,[\,(d - a_1\sin\theta)\cos\alpha - a_1\cos\theta\sin\alpha] - a_1\sin\alpha\cos\theta -$$

$$a_1\cos\alpha\sin\theta \tag{A.67}$$

$$\tau' = \frac{\alpha'\, b_2\, z_1}{a_2\, z_2}$$

$$\tau'' = \frac{\alpha''\, b_2\, z_1}{a_2\, z_2} + \frac{b_2\,\alpha'}{a_2}\,\frac{z_2 z_1' - z_1 z_2'}{z_2^2} \tag{A.68}$$

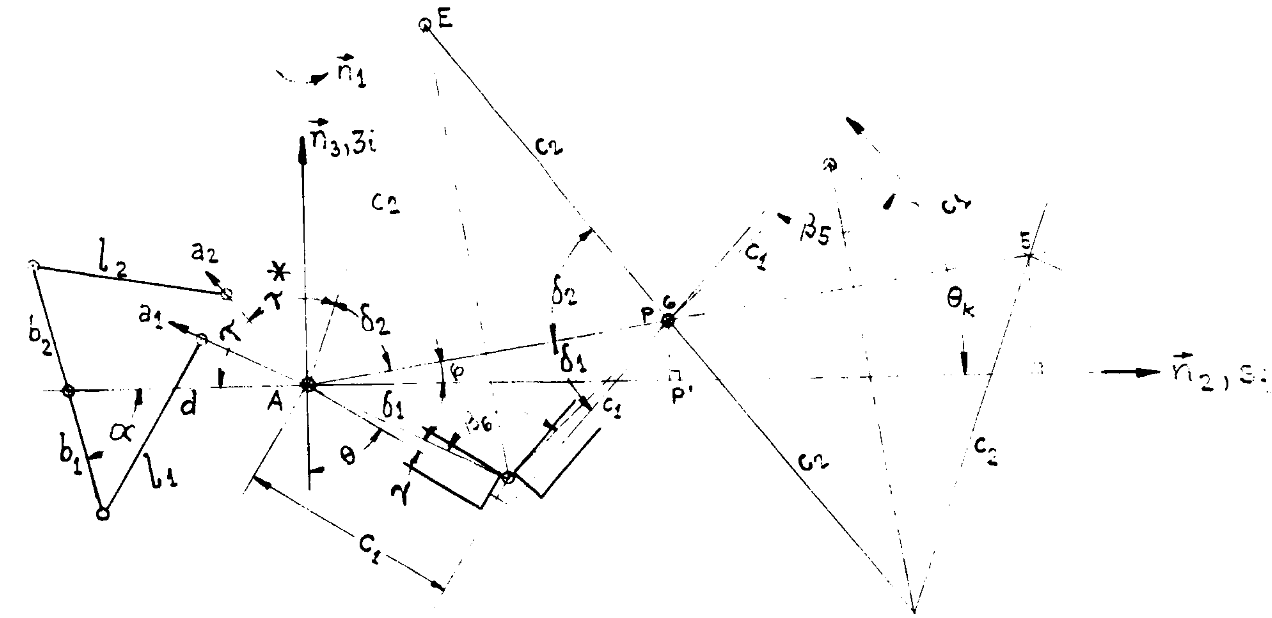

Fig. A.3 - Arrangement of Linkages

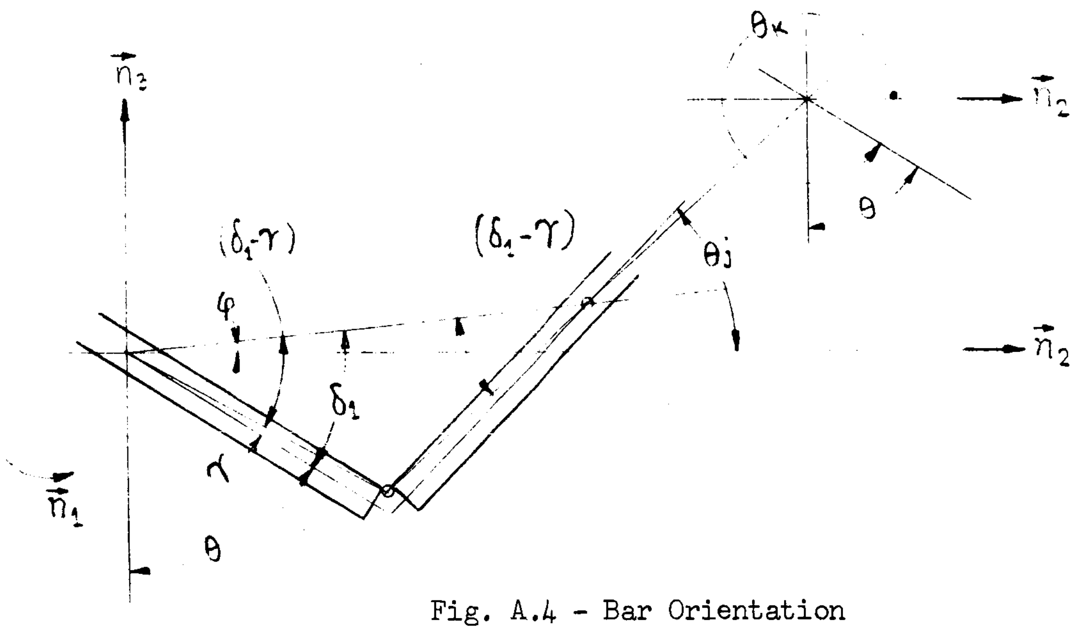

Fig. A.4 - Bar Orientation

where:

$$z_1 = \sin\alpha\,(d - a_2 \cos\tau) + \cos\alpha\, a_2 \sin\tau$$

$$z_2 = \sin\tau\,(d + b_2 \cos\alpha) - \cos\tau\, b_2 \sin\alpha$$

$$z_1' = \cos\alpha\,(d - a_2\cos\tau)\,\alpha' + \tau' \sin\alpha\, a_2 \sin\tau$$

$$+ \tau' a_2 \cos\tau \cos\alpha - \alpha' a_2 \sin\tau \sin\alpha$$

$$z_2' = \tau' \cos\tau\,(d + b_2\cos\alpha) - \alpha' b_2 \sin\tau \sin\alpha$$

$$+ \tau' b_2 \sin\tau \sin\alpha - \alpha' b_2 \cos\tau \cos\alpha \qquad \text{A.69}$$

$$\varphi' = \omega V$$

$$\varphi'' = \omega' V + \omega V' \qquad \text{A.70}$$

where

$$s_1 = \bar{c}_1 \sin(\theta + \gamma) + c_2 \cos(\tau + \tau^*)$$

$$s_2 = \bar{c}_1 \cos(\theta + \gamma) + c_2 \sin(\tau + \tau^*)$$

$$s_1' = \bar{c}_1 \cos(\theta + \gamma) - c_2 \tau' \sin(\tau + \tau^*)$$

$$s_2' = -\bar{c}_1 \sin(\theta + \gamma) + c_2 \tau' \cos(\tau + \tau^*)$$

$$V = [1 + (s_1/s_2)^2]^{-1}$$

$$\omega = (s_2 s_1' - s_1 s_2')/s_2^2$$

$$V' = -2 V^2 \omega\, s_1/s_2$$

$$s_3 = -\bar{c}_1 \sin(\theta + \gamma) - c_2 \cos(\tau + \tau^*)\,\tau'^2 - c_2 \sin(\tau + \tau^*)\,\tau''$$

$$s_4 = -\bar{c}_1 \cos(\theta + \gamma) - c_2 \sin(\tau + \tau^*)\,\tau'^2 + c_2 \cos(\tau + \tau^*)\,\tau''$$

$$s_5 = s_2 s_3 + s_2' s_1' - (s_1 s_4 + s_2' s_1')$$

$$\omega' = [s_2^2 s_5 - (s_2 s_1' - s_1 s_2')\, 2 s_2 s_2']/s_2^4 \qquad \text{A.71}$$

$$\delta_1' = -1 + \varphi'$$

$$\delta_1'' = \varphi'' \qquad \text{A.72}$$

$$s_i' = -2\,(7-i)\,\bar{c}_1\,[\sin(\delta_1-\gamma)\cos\varphi\,\delta_1' + \cos(\delta_1-\gamma)\sin\varphi\,\varphi']$$

$$s_i'' = -2\,(7-i)\,[(\delta_1'^2+\varphi'^2)\cos(\delta_1-\gamma)\cos\varphi - 2\,\delta_1'\,\varphi'\sin(\delta_1-\gamma)\sin\varphi$$
$$+\,\delta_1''\sin(\delta_1-\gamma)\cos\varphi + \varphi''\cos(\delta_1-\gamma)\sin\varphi]\,\bar{c}_1$$

$$z_i' = 2\,(7-i)\,[\varphi'\cos(\delta_1-\gamma)\cos\varphi - \delta_1'\sin(\delta_1-\gamma)\sin\varphi]\,\bar{c}_1$$

$$z_i'' = 2\,(7-i)\,[-(\varphi'^2+\delta_1'^2)\cos(\delta_1-\gamma)\sin\varphi - 2\,\delta_1'\,\varphi_1'\sin(\delta_1-\gamma)\cos\varphi$$
$$+\,\varphi''\cos(\delta_1-\gamma)\cos\varphi - \delta_1''\sin(\delta_1-\gamma)\sin\varphi]\,\bar{c}_1$$

$$\theta_2' = \theta_4' = \theta_6' = \delta_1' + \varphi'$$

$$\theta_2'' = \theta_4'' = \theta_6'' = \delta_1'' + \varphi''$$

$$\theta_1' = \theta_3' = \theta_5' = 1$$

$$\theta_1'' = \theta_3'' = \theta_5'' = 0$$

$$\beta_i' = -2\,\delta_1'$$

$$\beta_i'' = -2\,\delta_1'' \qquad \text{A.73}$$

5. MODIFICATIONS TO THE MATHEMATICAL MODEL FOR WING DEPLOYMENT TEST

Basic test set up is shown in Fig. A.5. Panels 1,3, and 5 are suspended from a test fixture by means of hangers, capable of pivoting about their center collars. The collar in turn can move in the $\pm \vec{n}_3$ direction along the trolley. The latter in turn moves along a track in the direction of $\pm \vec{n}_2$. The resultant effects of this test arrangement on the mathematical model can be summarized as follows:

a) Zero "g" condition is simulated
b) Motion is restricted to $\vec{n}_2$, $\vec{n}_3$ plane.
c) Effective mass of the panels 1,3 and 5 is increased
d) Friction is introduced in the structural joints and auxiliary equipment.

The mass and inertia of panels 2,4,6 remain unchanged. The masses of panels 1,3,5 changes as follows:

a) Increase of mass by the weight of the hanger and the pivot collar, M_h, for all motions.
b) Increase of mass by the effective weight of the counterbalance M_b, and the weight of the trolley, M_t, for the motion in $\pm \vec{n}_2$ direction only.
c) The inertia moment Φ^j_{11} is increased by the inertia of the hanger. Note that this is an idealization, since the adjustable rods, Fig. A.5, do not actually form a rigid body.

According to the presently available information, only the M_b is known:

$$M_b^1 \cong .0 \ (16\text{-sec}^2/\text{in})$$

$$M_b^2 \cong .00939 \ (16\text{-sec}^2/\text{in})$$

$$M_b^3 \simeq .00582 \ (16\text{-sec}^2/\text{in})$$

The remaining information has been requested and is expected in the near future.

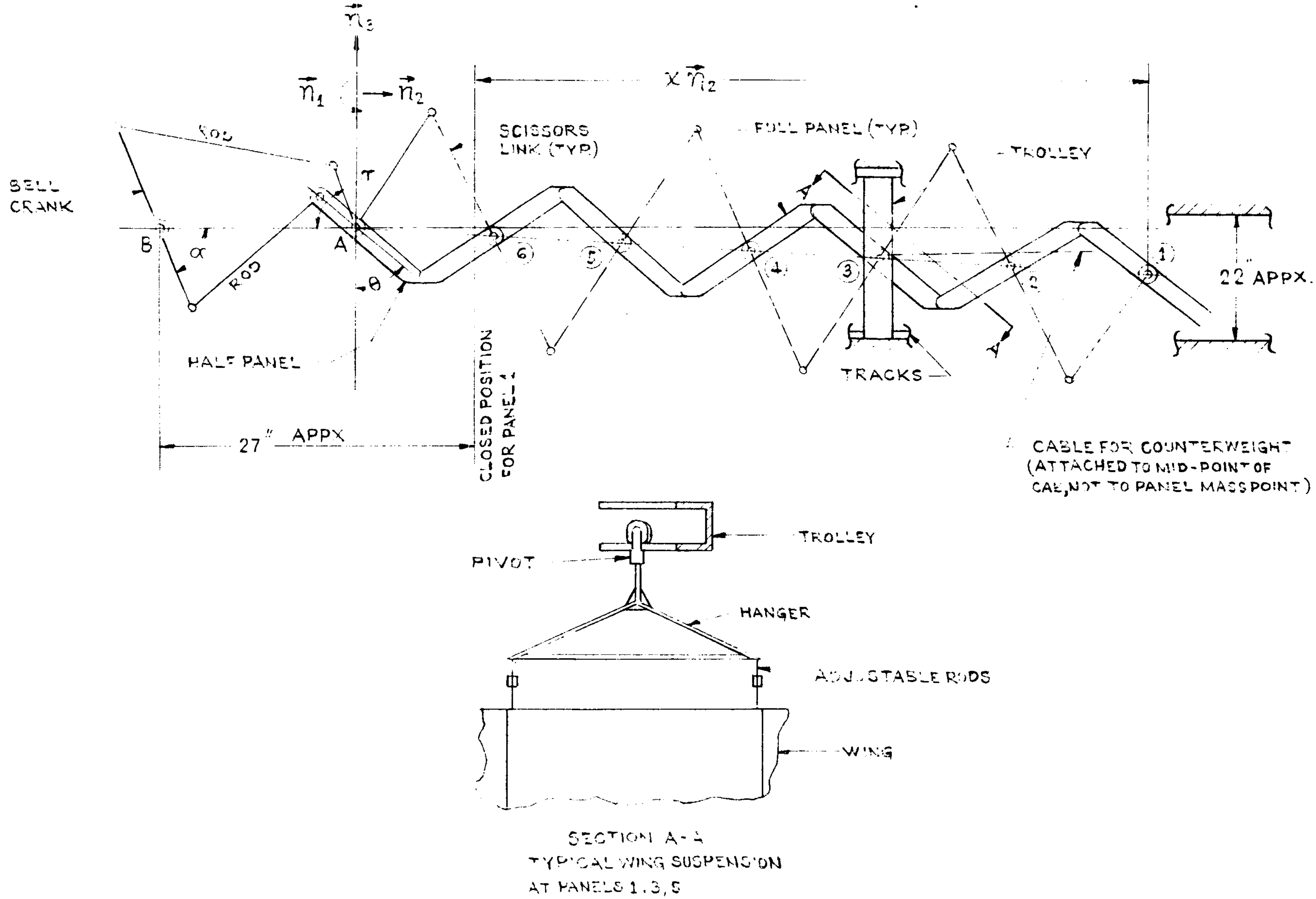

Fig. A.5 - Wing Deployment Test

Friction of the wing suspension system has been determined experimentally on a fully balanced configuration. After closing the wing panels against the center structure, Fig. A.5, the trolley attached to the first panel was pulled by means of a temporary line and pulley arrangement with a 10 lb. spring scale. The friction in the entire wing structure was then recorded at different distances x, Fig. A.5. The data summarized below represent averages over a number of individual readings.

x in	f lb
.0	1.7
28.	1.5
108.	1.4
188.	.71
268.	.54
348.	.50
428.	.46

Changes to the mathematical model due to this friction will appear only as an additional generalized force associated with the generalized coordinates Q_1 and θ.

Virtual work due to this friction, referred to the motion of the mass point 1 is

$$W = -f\ \delta(s_1 + Q_1) \qquad \text{A.75}$$

since

$$\delta(s_1 + Q_1) = s_{1,\theta}\ \delta\theta + \delta Q_1$$

$$W = -f\ s_{1,\theta}\ \delta\theta - f\ \delta Q_1$$

and the generalized forces to be added are

$$G_\theta''' = -f\ s_{1,\theta}$$

$$G_{Q_1} = -f \qquad \text{A.76}$$

Total generalized force for the generalized coordinate θ is

$$G_\theta = - \sum_{i=1}^{I} Y_i \beta_i' - R(\alpha') \alpha' - fs_1' \qquad \text{A.77}$$

and for the generalized coordinate Q_1

$$G_{Q_1} = - f \qquad \text{A.78}$$

Eq. A.77 modifies the right hand side of the Eq. A.39, Eq. A.78 replaces the zero right side of Eq. A.37 with -f. Similarly the expression, Eq. A.48, for F_1 is changed to

$$F_1 = - V4_1 + V1_i \left(\frac{R\,V}{-\omega_3} \right) + V3_1 \frac{R\,V}{\omega_1} - \frac{1}{M_1} \sum_{j=1}^{18} K_{j,1} Q_j - f/M_1$$

and in the expression for F_{13}, Eq. A.49 the term $- fs_1'$ is added on the right hand side.

APPENDIX B

INPUT DATA AND SAMPLE PRINTOUTS OF THE WING DEPLOYMENT MOTION, RUN 5020, TABLE 1, SECTION 4

WINC CEFLØYMENT MØTIØN

INPUT CATA

GEØMETRIC CATA

D =	11.5CCC (IN)	EL1 =	11.00CC (IN)	B2 =	4.2070 (IN)	C2 =	45.27CC (IN)
A1 =	3.0C0C (IN)	EL2 =	11.00CC (IN)	TST =	0.94247796 (RAC)	GAM3 =	C.C2733963 (RAC)
A2 =	3.858C (IN)	B1 =	4.20699996 (IN)	C1 =	43.4060 (IN)	W =	163.23CC (IN)

MASSES AND MASS MØMENTS ØF INERTIA

B1

PØINT NØ.	MASS (LB-SEC**2/IN)	I	J = 1	J = 2	J = 3
1	0.47126999E-00	1	C.42411000E 03	-0.	-C.
		2	-C.	0.13181999E 04	-C.
		3	-C.	-0.	C.173121C0E 04
2	0.31962000E-00	1	C.22671000E 03	-0.	-0.
		2	-C.	0.75043000E 03	-0.
		3	-C.	-0.	C.581C6CC0E 03
3	0.31728999E-00	1	C.2352C999E 03	-0.	-C.
		2	-C.	0.71128000E 03	-C.
		3	-C.	-0.	C.960C7CC0E C3
4	0.35636599E-00	1	C.28852999E 03	-0.	-C.
		2	-C.	0.79029999E 03	-C.
		3	-C.	-0.	C.109C29C0E 04
5	0.37526C00E-00	1	C.28817999E 03	-0.	-C.
		2	-C.	0.89420000E 03	-C.
		3	-C.	-0.	C.118466C0E 04
6	0.37369999E-00	1	C.287C5999E 03	-0.	-0.
		2	-C.	0.82827000E 03	-C.
		3	-C.	-0.	C.11035799E 04
7	-0.	1	C.1246C399E 03	-0.	-C.
		2	-C.	0.47542000E 03	-0.
		3	-C.	-0.	C.599342CCE C3
8	-0.	1	C.25179999E 01	-0.	-C.
		2	-C.	0.38850000E C2	C.120C0000E C1
		3	-C.	0.1200C000E 01	C.38010CC0E 02
9	-0.	1	C.46820C0E 04	-0.	-C.
		2	-C.	0.1825C0C0E C3	-C.
		3	-C.	-0.	C.18250CC0E C3

SPRING AND PREPACK DATA

NUMBER SPRINGS IN PANEL	SPRING ANGLE STRESS LESS STATE (RAD)	SPRING CØNSTANTS IN-LB/RAD PANEL NØ. 1	2	3	4	5	6	ZERØ PREPACK ANGLE RAD	PREPACK STIFFNESS CØEFFICIENT LB/RAD
5.	3.0869887	0.61192E 01	0.61192E 01	0.61192E 01	0.61192E 01	0.61192E 01	0.61192E 01	0.31416E-01	0.16667E 09

RIGID BØDY MØTIØN ØF THE VEHICLE

(REFERENCE FRAME FIXED IN VEHICLE)

	ANGULAR MØTIØN AXIS 1	AXIS 2	AXIS 3	DIM.	LINEAR MØTIØN	AXIS 1	AXIS 3	DIM.
VELØCITY	0.1047E-00	0.	0.	RAD/SEC	0.	0.	0.1204E 01	IN/SEC
ACCELERATIØN	-0.	-0.	-0.	RAD/SEC**2	-0.	-0.	-0.	IN/SEC**2

2

INITIAL CATA FØR INTEGRATIØN

INITIAL TIME = C. SEC

INITIAL TIME STEP = 0.0C10CCC SEC TRUNCATIØN ERRØR = 0.000C100C RAC FINAL TIME = 45.C000 SEC

INITIAL ELASTIC ANC RIGIC BØCY MØTIØN CATA

DEPLØYMENT ANGLE (RIGIC)	REFERENCE AXIS		ELASTIC CISPLACEMENTS AND VELØCITIES ØF MASS PØINTS 1	2	3	4	5	6
ANGLE,RAC	CISPL. AXIS 2	IN	-0.	-C.	-0.	-0.	-C.	-0.
	CISPL. AXIS 3	IN	-0.	-C.	-0.	-0.	-C.	-0.
0.03141592	RØTAT. AXIS 2	RAD	-0.	-C.	-0.	-0.	-C.	-0.
ANG.VEL.,RAD/SEC	LIN.VEL.AXIS 2	IN/SEC	-C.	-C.	-0.	-0.	-C.	-0.
	LIN.VEL.AXIS 3	IN/SEC	-C.	-C.	-0.	-0.	-C.	-C.
-0.	ANC.VEL.AXIS 2	RAC/SEC	-C.	-C.	-0.	-0.	-0.	-0.

INITIAL KINETIC AND STRAIN ENERGIES

TØTAL KINETIC ENERGY = 0.46529445E 02 (IN-LB)
TØTAL STRAIN ENERGY = 0.11754366E 04 (IN-LB)
TØRQUE SHAFT CØUPLE = -0.69999999E 04 (IN-LB)

BREAKDØWN ØF KINETIC AND STRAIN ENERGIES

PANEL ØR PØINT	TRANS.KINETIC ENERGY ØF PANELS	RØTATØRY KINETIC ENERGIES ØF PANELS ANC LINKS	TØTAL PER PØINT
1	0.408C99C2E 01	0.23254541E 01	0.64064442E C1
2	0.215C9779E 01	0.12540486E 01	0.34050266E C1
3	0.160CC871E 01	0.12896891E 01	0.28897762E C1
4	0.12826133E 01	0.15842433E 01	0.28668566E C1
5	0.89993892E 0C	0.15801310E 01	0.248C0698E C1
6	0.53819764E 0C	0.15739898E 01	0.21121874E C1
7	0.	0.68322105E 00	0.68322105E CC
8	0.	0.13806543E-01	0.138C6543E-C1
9	0.	0.25672057E 02	0.25672C57E C2

STRAIN ENERGY IN STRUCTURE 0. (IN-LB)
STRAIN ENERGY IN SPRINGS C.11754366E C4 (IN-LB)
STRAIN ENERGY IN PREPACK 0.35417270E-C8 (IN-LB)

B3

DYNAMIC LØADING ØN MASS PØINTS AT TIME = 0.00099999 SEC

MASS PØINT NØ.	FØRCE LB AXIS 2	FØRCE LB AXIS 3	MØMENT IN-LB AXIS 2	EQUIVALENT FØRCE ALØNG AXIS 3 ØN SIDE 1 LB	SIDE 2 LB
1	0.43496726E-07	-0.11950742E-05	0.	-0.	0.
2	-0.23155200E-06	-0.48936227E-05	0.	-0.	0.
3	0.15844050E-05	-0.23887740E-04	0.	-0.	0.
4	-0.68665624E-05	-0.12141550E-03	0.	-0.	0.
5	0.41909263E-04	-0.57805050E-03	-0.	0.	-0.
6	-0.25250085E-03	-0.18573678E-02	0.	-0.	0.

TØRQUE ØN SHAFT FRØM STRUCTURE

PØSITIVE N1 SIDE = 0.14215800E-01 (IN-LB)
NEGATIVE N1 SIDE = 0.14215800E-01 (IN-LB)

MØTØR WØRK = 0.32432253E-02 (IN-LB)

TØTAL ENERGY IN THE WING

0.12215671E 04(IN-LB)

B5

RIGID BØDY DYNAMIC LØADING

MASS PØINT NØ.	FØRCE 1	FØRCE 2	FØRCE 3	TØRQUE 1	TØRQUE 2	TØRQUE 3
1	0.	-0.35603245E 03	-0.24842294E 01	-0.64145464E 03	-0.	0.
2	0.	-0.20121732E 03	-0.14034141E 01	0.31865763E 03	0.	-0.
3	0.	-0.15978946E 03	-0.11150312E 01	-0.35574862E 03	-0.	0.
4	0.	-0.13459428E 03	-0.93586747E 00	0.40256110E 03	0.	-0.
5	0.	-0.94467766E 02	-0.65537569E 00	-0.43586427E 03	-0.	0.
6	0.	-0.47015511E 02	-0.32817463E-00	0.30995566E 03	0.	-0.
7	0.	0.	0.	-0.18846010E 03	-0.	0.
8	0.	0.	0.	0.33585501E 01	0.	-0.
9	0.	0.	0.	0.41948799E 04	-0.	0.

INTERPØLATED STIFFNESS CØEFFICIENTS

FK(2,1)	FK(2,2)	FK(2,3)	FK(2,4)	FK(2,5)	FK(2,6)
-0.30308679E 03	0.12864316E 05	-0.	0.65555152E 03	-0.23352419E 05	-0.

CURRENT INTEGRATIØN CATA

CURRENT TIME = C.CC2CCCO SEC CURRENT TIME STEP = 0.0030000 SEC FINAL TIME = 45.0CCCCCC SEC

CURRENT ELASTIC AND RIGID BØDY MØTIØN CATA

DEPLØYMENT ANGLE (RIGID)	REFERENCE AXIS		ELASTIC DISPLACEMENTS AND VELØCITIES ØF MASS PØINTS 1	2	3	4	5	6
ANGLE,RAD	DISPL. AXIS 2	IN	-0.15514E-C2	-C.12928E-02	-0.10342E-C2	-0.77560E-C3	-0.51698E-03	-0.25836E-03
	DISPL. AXIS 3	IN	-0.10488E-C4	-C.87398E-05	-0.69017E-05	-0.52434E-05	-C.34930E-05	-0.17414E-05
0.03141902	RØTAT. AXIS 2	RAD	0.	C.	0.	0.	C.	0.
ANG.VEL.,RAD/SEC	LIN.VEL.AXIS 2	IN/SEC	-0.15398E C1	-C.12831E 01	-0.10264E 01	-0.76976E CC	-C.51309E 00	-0.25642E-00
	LIN.VEL.AXIS 3	IN/SEC	-0.10409E-C1	-C.86742E-02	-0.69392E-02	-0.52037E-02	-0.34656E-02	-0.17219E-02
0.30825832E-C2	ANG.VEL.AXIS 2	RAD/SEC	0.	C.	0.	0.	C.	0.

CURRENT RIGID DEPLØYMENT INFØRMATIØN FØR MASS PØINTS

		1	2	3	4	5	6
DISPL. AXIS 2	IN	0.28242E C2	C.23535E 02	0.18828E 02	0.14121E C2	0.94140E C1	0.47C70E 01
DISPL. AXIS 3	IN	0.12798E-CC	C.10665E-00	0.85318E-01	0.63988E-01	0.42659E-C1	0.21329E-01
LIN.VEL.AXIS 2	IN/SEC	0.15406E C1	C.12839E 01	0.10271E 01	0.77032E 0C	C.51355E CC	0.25677E-0C
LIN.VEL.AXIS 3	IN/SEC	0.10412E-C1	C.86764E-02	0.69412E-02	0.52050E-02	0.34706E-02	0.17353E-02

CURRENT KINETIC AND STRAIN ENERGIES

TØTAL KINETIC ENERGY = 0.45756368E 02 (IN-LB)	STRAIN ENERGY IN STRUCTURE	C.10594834E-C6	(IN-LB)
TØTAL STRAIN ENERGY = 0.11754327E C4 (IN-LB)	STRAIN ENERGY IN SPRINGS	C.11754327E 04	(IN-LB)
TØRQUE SHAFT CØUPLE = -0.65434843E 04 (IN-LB)	STRAIN ENERGY IN PREPACK	C.	(IN-LB)

BREAKDØWN ØF KINETIC AND STRAIN ENERGIES

PANEL ØR PØINT	TRANS.KINETIC ENERGY ØF PANELS	RØTATØRY KINETIC ENERGIES ØF PANELS AND LINKS	TØTAL PER PØINT
1	0.408C9899E 01	0.24643752E 01	0.65453651E C1
2	0.215C9779E 01	0.11869594E 01	0.33379374E C1
3	0.160CC873E 01	0.13667343E 01	0.29668216E C1
4	0.12826140E 01	0.14994893E 01	0.27821C33E C1
5	0.89994231E 0C	0.16745270E 01	0.25744693E C1
6	0.5382C585E 0C	0.14897844E 01	0.20279502E 01
7	0.	0.72403625E 00	0.72403625E CC
8	0.	0.13099030E-01	0.13099C30E-C1
9	0.	0.24784546E 02	0.24784546E C2

FIRST PANEL RØTATIØN, RADIANS		TØRQUE SHAFT RØTATIØN, RADIANS	
ELASTIC	TØTAL	ELASTIC	TØTAL
-0.28796437E-C5	C.31416144E-01	0.16463882E-05	0.94481628E CC

6

DYNAMIC LØADING ØN MASS PØINTS AT TIME = 0.C020CCCO SEC

MASS PØINT NØ.	FØRCE LB AXIS 2	FØRCE LB AXIS 3	MØMENT IN-LB AXIS 2	EQUIVALENT FØRCE ALØNG AXIS 3 ØN SIDE 1 LB	SIDE 2 LB
1	0.12651395E-06	-C.3C998153E-05	0.	-0.	0.
2	-0.72272746E-06	-C.16972670E-04	C.	-0.	0.
3	0.5643C399E-05	-C.88913628F-04	0.	-0.	0.
4	-0.26174333E-04	-C.49061491E-03	0.	-0.	0.
5	0.167C7257E-03	-C.23871567E-02	-0.	0.	-0.
6	-0.10025495E-02	-C.7C8C1564E-02	C.	-0.	0.

TØRQUE ØN SHAFT FRØM STRUCTURE

PØSITIVE N1 SIDE = C.56199391E-01 (IN-LB)
NEGATIVE N1 SIDE = C.56199391E-01 (IN-LB)

MØTØR WØRK = C.124CC381E-01 (IN-LB)

TØTAL ENERGY IN THE WING

0.12211766E 04(IN-LB)

B7

RIGID BØDY DYNAMIC LØADING

MASS PØINT NØ.	FØRCE 1	FØRCE 2	FØRCE 3	TØRQUE 1	TØRQUE 2	TØRQUE 3
1	0.	-C.35574652E 03	-C.25594042E 01	-0.64094700E 03	-0.	C.
2	0.	-C.20105906E 03	-C.14441021E 01	0.31840476E 03	0.	-C.
3	0.	-C.15966092E 03	-C.11487729E 01	-0.35546708E 03	-0.	C.
4	0.	-C.13448864E 03	-C.96608724E 00	0.40224165E 03	0.	-C.
5	0.	-0.94391409E 02	-C.67932893E 00	-0.43551934E 03	-0.	C.
6	0.	-C.46979009E 02	-C.33768910E-00	0.39963828E 03	0.	-C.
7	0.	C.	C.	-0.18831095E 03	-0.	C.
8	0.	C.	C.	0.33558847E 01	0.	-C.
9	0.	C.	C.	0.41915767E 04	-0.	C.

INTERPØLATED STIFFNESS CØEFFICIENTS

FK(2,1)	FK(2,2)	FK(2,3)	FK(2,4)	FK(2,5)	FK(2,6)
-0.30307713E 03	C.12863025E C5	-0.	0.65552221E 03	-0.23350286E 05	-C.

7

CURRENT INTEGRATIØN CATA

CURRENT TIME = 5.4229230 SEC CURRENT TIME STEP = 0.003000C SEC FINAL TIME = 45.00C0C00 SEC

CURRENT ELASTIC AND RIGID BØDY MØTIØN CATA

DEPLØYMENT ANGLE (RIGID)	REFERENCE AXIS		ELASTIC CISPLACEMENTS AND VELØCITIES ØF MASS PØINTS 1	2	3	4	5	6
ANGLE,RAD	CISPL. AXIS 2	IN	-0.59649E C2	-C.47570E 02	-0.35854E 02	-0.24849E 02	-C.15C19E C2	-0.652C4E 01
	CISPL. AXIS 3	IN	-0.24351E C1	-C.19241E 01	-0.14647E 01	-0.94322E 0C	-C.59632E CC	-0.14533E-00
0.23921092	RØTAT. AXIS 2	RAD	C.	C.	0.	0.	C.	0.
ANG.VEL.,RAD/SEC	LIN.VEL.AXIS 2	IN/SEC	0.73923E C1	C.50843E 01	0.32893E 01	0.21585E 01	0.1224CE 01	0.47764E-00
	LIN.VEL.AXIS 3	IN/SEC	-0.58407E C0	-C.47972E-00	-0.32152E-0C	-0.20984E-0C	-0.128C6E-CC	-0.35805E-01
0.31684740E-C1	ANG.VEL.AXIS 2	RAD/SEC	C.	C.	0.	0.	C.	0.

CURRENT RIGID DEPLØYMENT INFØRMATIØN FØR MASS PØINTS

		1	2	3	4	5	6
CISPL. AXIS 2	IN	0.13008E C3	C.10840E 03	0.86722E 02	0.65041E C2	C.43361E C2	C.21680E 02
CISPL. AXIS 3	IN	0.18485E C1	C.15404E 01	0.12323E 01	0.92423E 0C	C.61615E C0	0.3C808E-0C
LIN.VEL.AXIS 2	IN/SEC	C.15214E C2	C.12679E 02	0.10143E 02	0.76072E 01	0.5C715E C1	0.25357E 01
LIN.VEL.AXIS 3	IN/SEC	0.41428E-C0	C.34523E-00	0.27619E-00	0.20714E-0C	C.138C9E-C0	0.69C47E-01

CURRENT KINETIC AND STRAIN ENERGIES

TØTAL KINETIC ENERGY = 0.29746857E 03 (IN-LB) STRAIN ENERGY IN STRUCTURE C.13482051E 03 (IN-LB)
TØTAL STRAIN ENERGY = 0.10643670E 04 (IN-LB) STRAIN ENERGY IN SPRINGS 0.92954649E 03 (IN-LB)
TØRQUE SHAFT CØUPLE = -0.1752C534E 04 (IN-LB) STRAIN ENERGY IN PREPACK C. (IN-LB)

BREAKDØWN ØF KINETIC AND STRAIN ENERGIES

PANEL ØR PØINT	TRANS.KINETIC ENERGY ØF PANELS	RØTATØRY KINETIC ENERGIES ØF PANELS AND LINKS	TØTAL PER PØINT
1	0.13774784E 03	0.39455489E 01	0.14169338E C3
2	0.59499145E 02	0.66190910E 00	0.6C161054E C2
3	0.354C1C95E 02	0.21881883E 01	0.37589283E C2
4	0.22216715E 02	0.83619165E 0C	0.23052907E C2
5	0.10713241E 02	0.26809749E 01	0.13394216E C2
6	0.31688213E 01	0.83077970E 00	0.39996010E C1
7	0.	0.11592067E 01	0.11592C67E C1
8	0.	0.75400116E-02	0.754C0116E-C2
9	0.	0.16411377E 02	0.16411377E C2

FIRST PANEL RØTATIØN, RADIANS		TØRQUE SHAFT RØTATIØN, RADIANS	
ELASTIC	TØTAL	ELASTIC	TØTAL
-0.74336509E-C1	C.16487440E-0C	0.47581849E-01	C.11227614E 01

DYNAMIC LØADING ØN MASS PØINTS AT TIME = 5.42292303 SEC

MASS PØINT NØ.	FØRCE LB AXIS 2	FØRCE LB AXIS 3	MØMENT IN-LB AXIS 2	EQUIVALENT FØRCE ALØNG AXIS 3 ØN SIDE 1 LB	SIDE 2 LB
1	-0.41871218E 01	-0.10901800E 01	0.	-0.	0.
2	-0.62395205E 00	-0.11362037E 01	0.	-0.	0.
3	0.62631849E 00	-0.10977691E 01	0.	-0.	0.
4	0.30374527E-02	-0.10112738E 01	0.	-0.	0.
5	-0.14498144E-01	-0.83908844E 00	-0.	0.	-0.
6	-0.40157962E-00	-0.31398773E-00	0.	-0.	0.

TØRQUE ØN SHAFT FRØM STRUCTURE

POSITIVE N1 SIDE = 0.16242058E 04 (IN-LB)
NEGATIVE N1 SIDE = 0.16242058E 04 (IN-LB)
MØTØR WØRK = 0.83892203E 02 (IN-LB)

TØTAL ENERGY IN THE WING

0.12779433E 04(IN-LB)

B9

RIGID BØDY DYNAMIC LØADING

MASS PØINT NØ.	FØRCE 1	FØRCE 2	FØRCE 3	TØRQUE 1	TØRQUE 2	TØRQUE 3
1	0.	0.88117518E 00	-0.17405144E 01	-0.31625462E-00	-0.	0.
2	0.	0.25801780E-00	-0.74234770E 00	0.16657996E-00	0.	-0.
3	0.	0.41288374E-00	-0.78121927E 00	-0.17539376E-00	-0.	0.
4	0.	0.18567133E-00	-0.49662184E-00	0.21044094E-00	0.	-0.
5	0.	0.27498134E-00	-0.46197540E-00	-0.21489296E-00	-0.	0.
6	0.	0.87726130E-01	-0.17359072E-00	0.20907894E-00	0.	-0.
7	0.	0.	0.	-0.92915966E-01	-0.	0.
8	0.	0.	0.	0.17055795E-02	0.	-0.
9	0.	0.	0.	0.39021371E 01	-0.	0.

INTERPØLATED STIFFNESS CØEFFICIENTS

FK(2,1)	FK(2,2)	FK(2,3)	FK(2,4)	FK(2,5)	FK(2,6)
-0.51222380E 02	0.39523930E 03	0.	0.10277610E 03	-0.78783863E 03	-0.

CURRENT INTEGRATIØN DATA

CURRENT TIME = 9.7427124 SEC   CURRENT TIME STEP = 0.0030000 SEC   FINAL TIME = 45.0000000 SEC

CURRENT ELASTIC AND RIGID BØDY MØTIØN DATA

DEPLØYMENT ANGLE (RIGID)	REFERENCE AXIS		ELASTIC DISPLACEMENTS AND VELØCITIES ØF MASS PØINTS 1	2	3	4	5	6
ANGLE,RAD	DISPL. AXIS 2	IN	0.47642E 01	0.35610E 01	0.23832E 01	0.15639E 01	0.68283E 00	0.54230E 00
	DISPL. AXIS 3	IN	-0.57360E 01	-0.43772E 01	-0.30440E 01	-0.18647E 01	-0.85124E 00	-0.21510E-00
0.40195915	RØTAT. AXIS 2	RAD	0.	0.	0.	0.	0.	0.
ANG.VEL.,RAD/SEC	LIN.VEL.AXIS 2	IN/SEC	0.18095E 02	0.15747E 02	0.12971E 02	0.93962E 01	0.55836E 01	0.23826E 01
	LIN.VEL.AXIS 3	IN/SEC	-0.86461E-01	-0.31883E-01	-0.96990E-01	0.48813E-01	0.11727E-00	0.13196E-02
0.45464410E-01	ANG.VEL.AXIS 2	RAD/SEC	0.	0.	0.	0.	0.	0.

CURRENT RIGID DEPLØYMENT INFØRMATIØN FØR MASS PØINTS

		1	2	3	4	5	6
DISPL. AXIS 2	IN	0.20665E 03	0.17221E 03	0.13777E 03	0.10332E 03	0.68883E 02	0.34441E 02
DISPL. AXIS 3	IN	0.44238E 01	0.36865E 01	0.29492E 01	0.22119E 01	0.14746E 01	0.73731E 00
LIN.VEL.AXIS 2	IN/SEC	0.20885E 02	0.17404E 02	0.13923E 02	0.10442E 02	0.69616E 01	0.34808E 01
LIN.VEL.AXIS 3	IN/SEC	0.81404E 00	0.67837E 00	0.54270E 00	0.40702E-00	0.27135E-00	0.13567E-00

CURRENT KINETIC AND STRAIN ENERGIES

TØTAL KINETIC ENERGY =	0.10753950E 04 (IN-LB)	STRAIN ENERGY IN STRUCTURE	0.24125039E 02	(IN-LB)
TØTAL STRAIN ENERGY =	0.78080846E 03 (IN-LB)	STRAIN ENERGY IN SPRINGS	0.75668342E 03	(IN-LB)
TØRQUE SHAFT CØUPLE =	0.17450143E 04 (IN-LB)	STRAIN ENERGY IN PREPACK	0.	(IN-LB)

B10

BREAKDØWN ØF KINETIC AND STRAIN ENERGIES

PANEL ØR PØINT	TRANS.KINETIC ENERGY ØF PANELS	RØTATØRY KINETIC ENERGIES ØF PANELS AND LINKS	TØTAL PER PØINT
1	0.49708082E 03	0.47829761E 01	0.50186379E 03
2	0.24197927E 03	0.45107572E-00	0.24243034E 03
3	0.15711554E 03	0.26526227E 01	0.15976816E 03
4	0.98357642E 02	0.56984524E 00	0.98927487E 02
5	0.44011033E 02	0.32500013E 01	0.47261034E 02
6	0.10984632E 02	0.56615712E 00	0.11550790E 02
7	0.	0.14052438E 01	0.14052438E 01
8	0.	0.53026123E-02	0.53026123E-02
9	0.	0.12182964E 02	0.12182964E 02

FIRST PANEL ROTATIØN, RADIANS		TØRQUE SHAFT RØTATIØN, RADIANS	
ELASTIC	TØTAL	ELASTIC	TØTAL
0.30700058E-02	0.40502916E-00	-0.30773234E-02	.11843612E 01

DYNAMIC LØACING ØN MASS PØINTS AT TIME = 9.74271238 SEC

MASS PØINT NØ.	FØRCE LB AXIS 2	FØRCE LB AXIS 3	MØMENT IN-LB AXIS 2	EQUIVALENT FØRCE ALØNG AXIS 3 ØN SIDE 1 LB	SICE 2 LB
1	0.12874567E 01	-C.35428239E 01	0.	-0.	0.
2	0.1C3E31C5E-00	-C.25CC1473E 01	-0.	0.	-0.
3	-0.40816890E-00	-C.19553401E 01	0.	-0.	0.
4	-0.62361C08E 00	-C.18027975E 01	C.	-0.	0.
5	-0.15653094E-00	-C.11828365E 01	-0.	0.	-0.
6	-0.349545C0E-00	-C.51665878E 00	0.	-0.	0.

TØRQUE ØN SHAFT FRØM STRUCTURE

PØSITIVE N1 SIDE = -C.1C5C4469E 03 (IN-LB)
NEGATIVE N1 SIDE = -C.1C5C4469E 03 (IN-LB)

MØTØR WØRK = C.1CC89530E 03 (IN-LB)

TØTAL ENERGY IN THE WING

0.17553082E 04(IN-LB)

RIGID BØDY DYNAMIC LØACING

MASS PØINT NØ.	FØRCE 1	FØRCE 2	FØRCE 3	TØRQUE 1	TØRQUE 2	TØRQUE 3
1	0.	C.59627446E 00	-C.25418625E 01	-0.24866804E 01	-0.	C.
2	0.	-C.20958523E-00	-C.96131849E 00	0.13087184E 01	0.	-C.
3	0.	0.28676290E-00	-C.11408994E 01	-0.13791047E 01	-0.	C.
4	0.	-0.12942840E-00	-C.64311069E 00	0.16533077E 01	0.	-C.
5	0.	C.20351319E-00	-C.67467294E 00	-0.16896832E 01	-0.	C.
6	0.	-C.26397571E-01	-C.22479489E-00	0.16426072E 01	0.	-C.
7	0.	0.	C.	-0.73058954E 00	-0.	C.
8	0.	C.	C.	0.13524871E-01	0.	-C.
9	0.	C.	C.	0.22793267E 02	-0.	C.

INTERPØLATED STIFFNESS CØEFFICIENTS

FK(2,1)	FK(2,2)	FK(2,3)	FK(2,4)	FK(2,5)	FK(2,6)
-0.29771171E 02	C.12408856E 03	-0.	0.59588619E 02	-0.24799891E 03	-C.

11

CURRENT INTEGRATIØN CATA

CURRENT TIME = 16.0422556 SEC   CURRENT TIME STEP = C.0030000 SEC   FINAL TIME = 45.0000000 SEC

CURRENT ELASTIC AND RIGID BØDY MØTIØN CATA

DEPLØYMENT ANGLE (RIGID)	REFERENCE AXIS		ELASTIC CISPLACEMENTS AND VELØCITIES ØF MASS PØINTS 1	2	3	4	5	6
ANGLE,RAD	CISPL. AXIS 2	IN	0.72698E C2	C.57978E 02	0.43527E 02	0.3C090E 02	C.17731E C2	0.78032E 01
	CISPL. AXIS 3	IN	-0.56428E C1	-C.40201E 01	-0.23330E 01	-0.12948E 01	-C.35976E-C3	-0.25687E-00
0.75851078	RØTAT. AXIS 2	RAD	0.	C.	0.	0.	C.	0.
ANG.VEL.,RAD/SEC	LIN.VEL.AXIS 2	IN/SEC	-0.24077E C1	-C.3C616E 01	-0.32887E 01	-0.29376E 01	-C.19448E C1	-0.95040E 00
	LIN.VEL.AXIS 3	IN/SEC	0.24842E C1	C.17392E 01	0.12535E 01	0.46388E-0C	C.24130E-00	0.22203E-01
0.59636948E-01	ANG.VEL.AXIS 2	RAD/SEC	0.	C.	0.	0.	C.	0.

CURRENT RIGID DEPLØYMENT INFØRMATIØN FØR MASS PØINTS

		1	2	3	4	5	6
CISPL. AXIS 2	IN	0.35730E C3	C.29775E 03	0.23820E 03	0.17865E 03	C.11910E 03	0.59549E 02
CISPL. AXIS 3	IN	0.10673E C2	C.88942E 01	0.71154E 01	0.53365E C1	C.35577E C1	0.17788E 01
LIN.VEL.AXIS 2	IN/SEC	0.22393E C2	C.18661E 02	0.14929E 02	0.11197E 02	C.74644E C1	0.37322E 01
LIN.VEL.AXIS 3	IN/SEC	0.85867E CC	C.71556E 00	0.57245E 0C	0.42934E-0C	C.28622E-00	0.14311E-0C

CURRENT KINETIC AND STRAIN ENERGIES

TØTAL KINETIC ENERGY = 0.13637516E C4 (IN-LB)   STRAIN ENERGY IN STRUCTURE C.43102118E 03 (IN-LB)
TØTAL STRAIN ENERGY = 0.86524276E 03 (IN-LB)   STRAIN ENERGY IN SPRINGS 0.43422157E 03 (IN-LB)
TØRQUE SHAFT CØUPLE = 0.56365263E 04 (IN-LB)   STRAIN ENERGY IN PREPACK 0. (IN-LB)

B12

BREAKDØWN ØF KINETIC AND STRAIN ENERGIES

PANEL ØR PØINT	TRANS.KINETIC ENERGY ØF PANELS	RØTATØRY KINETIC ENERGIES ØF PANELS AND LINKS	TØTAL PER PØINT
1	0.66836271E 03	0.57282852E 01	0.674C91C0E C3
2	0.30385466E 03	0.24349517E-0C	0.30409815E C3
3	0.18758858E 03	0.31766880E 01	0.19076547E C3
4	0.1132C355E 03	0.3C760814E-0C	0.11351120E C3
5	0.53368495E 02	0.38923327E 01	0.57260828E C2
6	0.1454C626E 02	0.30561726E-00	0.14846243E C2
7	0.	0.16829767E 01	0.16829767E C1
8	0.	0.32070071E-02	0.32070071E-C2
9	0.	0.74926171E 01	0.74926171E C1

FIRST PANEL RØTATIØN, RADIANS		TØRQUE SHAFT RØTATIØN, RADIANS	
ELASTIC	TØTAL	ELASTIC	TØTAL
0.10406115E-CC	0.86257193E 0C	-0.82182761E-01	C.13788234E 01

DYNAMIC LOADING ON MASS POINTS AT TIME = 16.04225564 SEC

MASS POINT NO.	FORCE LB AXIS 2	FORCE LB AXIS 3	MOMENT IN-LB AXIS 2	EQUIVALENT FORCE ALONG AXIS 3 ON SIDE 1 LB	SIDE 2 LB
1	0.71790255E 01	-0.27266734E 01	-0.	0.	-0.
2	0.29700726E 01	-0.12181219E 01	0.	-0.	0.
3	0.12873246E 01	-0.37610940E-00	0.	-0.	0.
4	0.14431039E 01	-0.49976802E-00	0.	-0.	0.
5	0.20172895E 01	-0.73794603E 00	-0.	0.	-0.
6	0.13913124E 01	-0.17083836E-00	0.	-0.	0.

TORQUE ON SHAFT FROM STRUCTURE

POSITIVE N1 SIDE = -0.28053053E 04 (IN-LB)
NEGATIVE N1 SIDE = -0.28053053E 04 (IN-LB)

MOTOR WORK = -0.11552633E 04 (IN-LB)

TOTAL ENERGY IN THE WING

0.33842578E 04(IN-LB)

B13

RIGID BODY DYNAMIC LOADING

MASS POINT NO.	FORCE 1	FORCE 2	FORCE 3	TORQUE 1	TORQUE 2	TORQUE 3
1	0.	0.41967189E 01	-0.26856289E 01	0.13245910E 01	-0.	0.
2	0.	0.11318062E 01	-0.84797494E 00	-0.58980381E 00	0.	-0.
3	0.	0.19046055E 01	-0.12054282E 01	0.73461380E 00	-0.	0.
4	0.	0.76508646E 00	-0.56728520E 00	-0.74510085E 00	0.	-0.
5	0.	0.11634297E 01	-0.71283208E 00	0.90005103E 00	-0.	0.
6	0.	0.28127513E-00	-0.15829062E-00	-0.74027845E 00	0.	-0.
7	0.	0.	0.	0.38916635E-00	-0.	0.
8	0.	0.	0.	-0.70521254E-02	0.	-0.
9	0.	0.	0.	-0.94740645E 01	-0.	0.

INTERPOLATED STIFFNESS COEFFICIENTS

FK(2,1)	FK(2,2)	FK(2,3)	FK(2,4)	FK(2,5)	FK(2,6)
-0.19047222E 02	0.37080547E 02	0.	0.38097544E 02	-0.74157177E 02	0.

CURRENT INTEGRATIØN CATA

CURRENT TIME = 20.1619556 SEC   CURRENT TIME STEP = 0.0030000 SEC   FINAL TIME = 45.0CCCC00 SEC

CURRENT ELASTIC AND RIGID BØDY MØTIØN DATA

DEPLØYMENT ANGLE (RIGID)	REFERENCE AXIS		ELASTIC DISPLACEMENTS AND VELØCITIES ØF MASS PØINTS 1	2	3	4	5	6
ANGLE,RAD	DISPL. AXIS 2	IN	0.21835E C2	C.17240E 02	0.12781E 02	0.86312E 01	C.5C680E C1	0.20328E 01
	DISPL. AXIS 3	IN	0.86806E C1	C.67814E 01	0.49954E 01	0.30295E 01	0.17016E C1	0.24934E-00
0.98079344	RØTAT. AXIS 2	RAD	0.	C.	0.	0.	C.	0.
ANG.VEL.,RAD/SEC	LIN.VEL.AXIS 2	IN/SEC	-0.15267E C2	-C.11867E 02	-0.88147E 01	-0.59212E 01	-C.33105E C1	-0.14606E 01
	LIN.VEL.AXIS 3	IN/SEC	0.24303E C1	C.22569E 01	0.15442E 01	0.72884E 0C	-C.12378E-C0	-0.40238E-01
0.44133658E-01	ANG.VEL.AXIS 2	RAD/SEC	0.	C.	0.	0.	0.	0.

CURRENT RIGID DEPLØYMENT INFØRMATIØN FØR MASS PØINTS

		1	2	3	4	5	6
DISPL. AXIS 2	IN	0.43182E C3	C.35985E 03	0.28788E 03	0.21591E 03	0.14394E C3	0.71970E 02
DISPL. AXIS 3	IN	0.13225E C2	C.11021E 02	0.88170E 01	0.66127E 01	0.44085E C1	0.22042E 01
LIN.VEL.AXIS 2	IN/SEC	0.12847E C2	C.10706E 02	0.85649E 01	0.64237E 01	C.42825E C1	0.21412E 01
LIN.VEL.AXIS 3	IN/SEC	0.39864E-C0	C.33220E-00	0.26576E-0C	0.19932E-0C	0.13288E-00	0.66440E-01

CURRENT KINETIC AND STRAIN ENERGIES

TØTAL KINETIC ENERGY =	0.13312400E 04 (IN-LB)		STRAIN ENERGY IN STRUCTURE	0.6632366CE 02	(IN-LB)
TØTAL STRAIN ENERGY =	0.34165911E C3 (IN-LB)		STRAIN ENERGY IN SPRINGS	0.27533545E 03	(IN-LB)
TØRQUE SHAFT CØUPLE =	0.25196390E 04 (IN-LB)		STRAIN ENERGY IN PREPACK	C.	(IN-LB)

B14

BREAKDØWN ØF KINETIC AND STRAIN ENERGIES

PANEL ØR PØINT	TRANS.KINETIC ENERGY ØF PANELS	RØTATØRY KINETIC ENERGIES ØF PANELS AND LINKS	TØTAL PER PØINT
1	0.6311660CE 03	0.46985897E 01	0.63586466E C3
2	0.30084284E 03	0.42009426E-00	0.30126293E C3
3	0.1892777CE 03	0.26058223E 01	0.19188352E C3
4	0.11724456E 03	0.53070627E 0C	0.11777526E C3
5	0.53087596E 02	0.31926613E 01	0.56280259E C2
6	0.151C1364E 02	0.52727146E 0C	0.15628635E 02
7	0.	0.13804509E 01	0.13804509E C1
8	0.	0.54351307E-02	0.54351307E-C2
9	0.	0.11158893E 02	0.11158893E C2

FIRST PANEL RØTATIØN, RADIANS		TØRQUE SHAFT RØTATIØN, RADIANS	
ELASTIC	TØTAL	ELASTIC	TØTAL
0.30896794E-C1	C.10176902E 01	-0.28273673E-C1	0.16135398E 01

DYNAMIC LØACING ØN MASS PØINTS AT TIME = 20.18195558 SEC

MASS PØINT NØ.	FØRCE LB AXIS 2	FØRCE LB AXIS 3	MØMENT IN-LB AXIS 2	EQUIVALENT FØRCE ALØNG AXIS 3 ØN SIDE 1 LB	SIDE 2 LB
1	0.46747701E 01	C.14220034E-00	0.	-0.	0.
2	0.15752724E 01	C.12093890E 01	-C.	0.	-0.
3	-0.88369825E-01	C.15157122E 01	-C.	0.	-0.
4	-0.71876550E 00	C.28951842E-00	C.	-0.	0.
5	-0.98601189E 00	-C.43817449E-00	-C.	0.	-0.
6	-0.61876917E 00	-C.53484535E 00	0.	-0.	0.

TØRQUE ØN SHAFT FRØM STRUCTURE

PØSITIVE N1 SIDE = -C.96512122E 03 (IN-LB)
NEGATIVE N1 SIDE = -C.96512122E 03 (IN-LB)

MØTØR WØRK = -C.15852982E 04 (IN-LB)

TØTAL ENERGY IN THE WING

0.36581973E 04(IN-LB)

B15

RIGID BØDY DYNAMIC LØACING

MASS PØINT NØ.	FØRCE 1	FØRCE 2	FØRCE 3	TØRQUE 1	TØRQUE 2	TØRQUE 3
1	0.	0.44019293E 01	-C.14019357E 01	0.21737681E 01	-0.	C.
2	0.	C.13912360E 01	-C.52293088E 00	-0.11661454E 01	0.	-C.
3	0.	C.19947384E 01	-C.62925031E 00	0.12055645E 01	-0.	C.
4	C.	C.94112528E 00	-C.34983458E-00	-0.14791949E 01	0.	-C.
5	0.	C.12132268E 01	-C.37210828E-00	0.14770613E 01	-0.	C.
6	0.	0.34714844E-00	-C.12228225E-00	-0.14636601E 01	0.	-C.
7	C.	C.	C.	0.63865554E 00	-0.	C.
8	0.	C.	C.	-0.12751659E-01	0.	-C.
9	0.	C.	C.	-0.20855101E 02	-0.	C.

INTERPØLATEC STIFFNESS CØEFFICIENTS

FK(2,1)	FK(2,2)	FK(2,3)	FK(2,4)	FK(2,5)	FK(2,6)
-0.19189277E 02	C.24511258E 02	0.	0.38370957E 02	-0.49029911E 02	-0.

CURRENT INTEGRATIØN DATA

CURRENT TIME = 25.2215903 SEC   CURRENT TIME STEP = 0.0030000 SEC   FINAL TIME = 45.0000000 SEC

CURRENT ELASTIC AND RIGID BØDY MØTIØN DATA

DEPLØYMENT ANGLE (RIGID)	REFERENCE AXIS		ELASTIC DISPLACEMENTS AND VELØCITIES ØF MASS PØINTS 1	2	3	4	5	6
ANGLE,RAD	DISPL. AXIS 2	IN	0.76664E 01	0.62749E 01	0.48553E 01	0.35265E 01	0.21027E 01	0.10635E 01
	DISPL. AXIS 3	IN	-0.13254E 02	-0.10054E 02	-0.69569E 01	-0.41501E 01	-0.18452E 01	-0.51095E 00
1.17569898	RØTAT. AXIS 2	RAD	0.	0.	0.	0.	0.	0.
ANG.VEL.,RAD/SEC	LIN.VEL.AXIS 2	IN/SEC	0.71843E 01	0.52894E 01	0.33160E 01	0.19387E 01	0.85111E 00	0.30542E-00
	LIN.VEL.AXIS 3	IN/SEC	-0.10857E 02	-0.74524E 01	-0.46161E 01	-0.29589E 01	-0.12787E 01	-0.58769E 00
0.44510212E-01	ANG.VEL.AXIS 2	RAD/SEC	0.	0.	0.	0.	0.	0.

CURRENT RIGID DEPLØYMENT INFØRMATIØN FØR MASS PØINTS

		1	2	3	4	5	6
DISPL. AXIS 2	IN	0.48001E 03	0.40001E 03	0.32000E 03	0.24000E 03	0.16000E 03	0.80001E 02
DISPL. AXIS 3	IN	0.14772E 02	0.12310E 02	0.98478E 01	0.73859E 01	0.49239E 01	0.24620E 01
LIN.VEL.AXIS 2	IN/SEC	0.89843E 01	0.74869E 01	0.59895E 01	0.44921E 01	0.29948E 01	0.14974E 01
LIN.VEL.AXIS 3	IN/SEC	0.30218E-00	0.25182E-00	0.20146E-00	0.15109E-00	0.10073E-00	0.50364E-01

CURRENT KINETIC AND STRAIN ENERGIES

TØTAL KINETIC ENERGY = 0.10791300E 04 (IN-LB)   STRAIN ENERGY IN STRUCTURE 0.34865449E 02 (IN-LB)
TØTAL STRAIN ENERGY = 0.20028136E 03 (IN-LB)   STRAIN ENERGY IN SPRINGS 0.16541591E 03 (IN-LB)
TØRQUE SHAFT CØUPLE = 0.18351243E 04 (IN-LB)   STRAIN ENERGY IN PREPACK 0. (IN-LB)

BREAKDØWN ØF KINETIC AND STRAIN ENERGIES

PANEL ØR PØINT	TRANS.KINETIC ENERGY ØF PANELS	RØTATØRY KINETIC ENERGIES ØF PANELS AND LINKS	TØTAL PER PØINT
1	0.47051191E 03	0.47223917E 01	0.47523429E 03
2	0.23861356E 03	0.41603644E-00	0.23902999E 03
3	0.16344240E 03	0.26190227E 01	0.16606142E 03
4	0.10838434E 03	0.52558002E 00	0.10890992E 03
5	0.56566813E 02	0.32088346E 01	0.59775648E 02
6	0.16141608E 02	0.52217839E 00	0.16663786E 02
7	0.	0.13874440E 01	0.13874440E 01
8	0.	0.60592806E-02	0.60592806E-02
9	0.	0.12061527E 02	0.12061527E 02

FIRST PANEL RØTATIØN, RADIANS ELASTIC	TØTAL	TØRQUE SHAFT RØTATIØN, RADIANS ELASTIC	TØTAL
0.23465186E-01	0.11991641E 01	-0.17690448E-01	0.17762980E 01

B16

DYNAMIC LØADING ØN MASS PØINTS AT TIME = 25.22159025 SEC

MASS PØINT NØ.	FØRCE LB AXIS 2	FØRCE LB AXIS 3	MØMENT IN-LB AXIS 2	EQUIVALENT FØRCE ALØNG AXIS 3 ØN SIDE 1 LB	SIDE 2 LB
1	-0.27239867E-00	-C.13953755E 01	C.	-0.	0.
2	0.80534168E 00	-C.13123287E 01	-C.	0.	-0.
3	0.19249306E 01	-C.80719328E 00	-C.	0.	-0.
4	0.31325055E 01	-C.53224921E-01	0.	-0.	0.
5	0.30941227E 01	-C.83420658E 00	-C.	0.	-0.
6	0.19451474E 01	-C.11501598E-00	0.	-0.	0.

TØRQUE ØN SHAFT FRØM STRUCTURE

PØSITIVE N1 SIDE = -C.60386342E 03 (IN-LB)
NEGATIVE N1 SIDE = -C.60386342E 03 (IN-LB)

MØTØR WØRK = -C.21628445E 04 (IN-LB)

TØTAL ENERGY IN THE WING

0.34422559E 04(IN-LB)

B17

RIGID BØDY DYNAMIC LØADING

MASS PØINT NØ.	FØRCE 1	FØRCE 2	FØRCE 3	TØRQUE 1	TØRQUE 2	TØRQUE 3
1	0.	C.36922147E 01	-C.96104377E 00	-0.18199220E 01	-0.	C.
2	0.	0.86453025E 00	-C.36702564E-00	0.99099029E 00	0.	-C.
3	0.	C.16762352E 01	-C.43135864E-00	-0.10093227E 01	-0.	C.
4	0.	0.58871493E 00	-C.24553581E-00	0.12519208E 01	0.	-C.
5	0.	0.10249645E 01	-C.25508469E-00	-0.12366252E 01	-0.	C.
6	0.	C.22387780E-00	-C.85825344E-01	0.12438182E 01	0.	-C.
7	0.	C.	C.	-0.53469516E 00	-0.	C.
8	0.	0.	C.	0.52540848E-02	0.	-C.
9	0.	C.	C.	0.96790258E 01	-0.	C.

INTERPØLATED STIFFNESS CØEFFICIENTS

FK(2,1)	FK(2,2)	FK(2,3)	FK(2,4)	FK(2,5)	FK(2,6)
-0.23447680E 02	C.19038041E 02	-C.	0.46664890E 02	-0.38094415E 02	C.

CURRENT INTEGRATIØN CATA

CURRENT TIME = 30.0812380 SEC   CURRENT TIME STEP = 0.0030000 SEC   FINAL TIME = 45.0000000 SEC

CURRENT ELASTIC AND RIGID BØDY MØTIØN DATA

DEPLØYMENT ANGLE (RIGID)	REFERENCE AXIS		ELASTIC DISPLACEMENTS AND VELØCITIES ØF MASS PØINTS 1	2	3	4	5	6
ANGLE,RAD	DISPL. AXIS 2	IN	0.15237E C1	C.11331E 01	0.74064E 00	0.47562E-0C	0.20262E-00	0.14541E-00
	DISPL. AXIS 3	IN	-0.16417E C2	-C.12310E 02	-0.83295E 01	-0.5C647E 01	-C.21670E C1	-0.53487E 00
1.44065163	RØTAT. AXIS 2	RAD	C.	C.	0.	0.	C.	0.
ANG.VEL.,RAD/SEC	LIN.VEL.AXIS 2	IN/SEC	-0.42121E-CO	-C.81247E 00	-0.11790E 01	-0.12157E 01	-C.85564E 00	-0.46356E-00
	LIN.VEL.AXIS 3	IN/SEC	0.12912E C2	C.1C626E 02	0.80564E 01	0.36023E 01	0.20766E C1	0.67430E 00
0.58699781E-C1	ANG.VEL.AXIS 2	RAD/SEC	0.	C.	0.	0.	C.	0.

CURRENT RIGID DEPLØYMENT INFØRMATIØN FØR MASS PØINTS

		1	2	3	4	5	6
DISPL. AXIS 2	IN	0.51672E C3	C.43060E 03	0.34448E 03	0.25836E 03	0.17224E C3	0.86119E 02
DISPL. AXIS 3	IN	0.12523E C2	C.1C436E 02	0.83485E C1	0.62614E 01	C.41742E C1	0.20871E 01
LIN.VEL.AXIS 2	IN/SEC	0.43545E C1	C.36288E 01	0.2903CE 01	0.21773E 01	0.14515E 01	0.72576E 00
LIN.VEL.AXIS 3	IN/SEC	-0.30587E C1	-C.25489E 01	-0.20391E 01	-0.15294E 01	-C.1C196E C1	-0.5C979E 00

CURRENT KINETIC AND STRAIN ENERGIES

TØTAL KINETIC ENERGY = 0.20751320E 04 (IN-LB)	STRAIN ENERGY IN STRUCTURE	C.19238276E 02	(IN-LB)
TØTAL STRAIN ENERGY = 0.77904555E 02 (IN-LB)	STRAIN ENERGY IN SPRINGS	0.58666279E 02	(IN-LB)
TØRQUE SHAFT CØUPLE = 0.11227736E 04 (IN-LB)	STRAIN ENERGY IN PREPACK	C.	(IN-LB)

B18

BREAKDØWN ØF KINETIC AND STRAIN ENERGIES

PANEL ØR PØINT	TRANS.KINETIC ENERGY ØF PANELS	RØTATØRY KINETIC ENERGIES ØF PANELS AND LINKS	TØTAL PER PØINT
1	0.101CC692E 04	0.56631458E 01	0.10157324E C4
2	0.47558155E 03	0.13048825E-00	0.47611207E C3
3	0.29894061E 03	0.31407619E 01	0.3C208136E C3
4	0.1646C375E 03	0.16484618E-0C	0.16476859E C3
5	0.77496178E 02	0.38480709E 01	0.81344248E C2
6	0.20221CC7E 02	0.16377927E-00	0.20384786E C2
7	0.	0.16638386E 01	0.16638386E C1
8	0.	0.67105794E-02	0.671C5794E-C2
9	0.	0.13038137E 02	0.13038137E C2

FIRST PANEL RØTATIØN, RADIANS		TØRQUE SHAFT RØTATIØN, RADIANS	
ELASTIC	TØTAL	ELASTIC	TØTAL
0.52723333E-C2	C.14459239E 01	-0.33934098E-02	C.19599529E 01

18

DYNAMIC LØADING ØN MASS PØINTS AT TIME = 30.C8123803 SEC

MASS PØINT NØ.	FØRCE LB AXIS 2	FØRCE LB AXIS 3	MØMENT IN-LB AXIS 2	EQUIVALENT FØRCE ALØNG AXIS 3 ØN SIDE 1 LB	SIDE 2 LB
1	0.61356872E 01	-C.16518690E 01	-0.	0.	-0.
2	0.22055674E-00	-C.87711602E 00	C.	-0.	0.
3	-0.22574019E 01	C.20040656E 01	-C.	0.	-0.
4	-0.41145548E 01	-C.29673042E 01	0.	-0.	0.
5	-0.45528282E 01	C.13460331E 01	-0.	0.	-0.
6	-0.19744405E 01	-C.71331358E 00	0.	-0.	0.

TØRQUE ØN SHAFT FRØM STRUCTURE			TØTAL ENERGY IN THE WING
PØSITIVE N1 SIDE	= -C.11583399E 03	(IN-LB)	0.47123428E 04(IN-LB)
NEGATIVE N1 SIDE	= -C.11583399E 03	(IN-LB)	
MØTØR WØRK	= -C.25593063E 04	(IN-LB)	

B19

RIGID BØDY DYNAMIC LØADING

MASS PØINT NØ.	FØRCE 1	FØRCE 2	FØRCE 3	TØRQUE 1	TØRQUE 2	TØRQUE 3
1	0.	C.49624328E 01	C.60948417E 00	0.28670127E 01	-0.	C.
2	0.	0.10024291E 01	C.44554443E-00	0.34563283E-00	0.	-C.
3	0.	C.22481722E 01	C.27356325E-00	0.15900357E 01	-0.	C.
4	0.	0.67641213E 00	C.30073991E-00	0.43663894E-00	0.	-C.
5	0.	0.13663866E 01	C.16177211E-00	0.19481166E 01	-0.	C.
6	0.	0.24657000E-00	C.10512155E-00	0.43381295E-00	0.	-C.
7	0.	C.	C.	0.84233160E 00	-0.	C.
8	0.	C.	C.	-0.19801745E-01	0.	-C.
9	0.	C.	C.	-0.34503201E 02	-0.	C.

INTERPØLATED STIFFNESS CØEFFICIENTS

FK(2,1)	FK(2,2)	FK(2,3)	FK(2,4)	FK(2,5)	FK(2,6)
-0.58085886E 02	C.14146563E C2	-0.	0.11554021E 03	-0.28415127E 02	0.

CURRENT INTEGRATIØN CATA

CURRENT TIME = 31.8811076 SEC   CURRENT TIME STEP = 0.0030000 SEC   FINAL TIME = 45.0000000 SEC

CURRENT ELASTIC AND RIGID BØDY MØTIØN CATA

DEPLØYMENT ANGLE (RIGID)	REFERENCE AXIS		ELASTIC DISPLACEMENTS AND VELØCITIES ØF MASS PØINTS 1	2	3	4	5	6
ANGLE,RAD	CISPL. AXIS 2	IN	0.18966E C1	C.15645E 01	0.12376E 01	0.89689E 0C	0.59841E CC	0.25309E-0C
	CISPL. AXIS 3	IN	0.13074E C2	C.91847E 01	0.54278E 01	0.20429E 01	-0.24970E-CC	-0.13046E 01
1.53359401	RØTAT. AXIS 2	RAD	0.	C.	0.	0.	C.	0.
ANG.VEL.,RAD/SEC	LIN.VEL.AXIS 2	IN/SEC	-0.10165E C2	-C.81096E 01	-0.62063E 01	-0.45741E 01	-0.29091E C1	-0.12831E 01
	LIN.VEL.AXIS 3	IN/SEC	0.18276E C2	C.13495E 02	0.45942E 01	0.17023E 01	0.20921E C1	0.40862E 01
0.38303768E-01	ANG.VEL.AXIS 2	RAD/SEC	0.	C.	0.	0.	0.	0.

CURRENT RIGID DEPLØYMENT INFØRMATIØN FØR MASS PØINTS

		1	2	3	4	5	6
CISPL. AXIS 2	IN	0.52100E C3	C.43417E 03	0.34733E 03	0.26050E 03	0.17367E C3	0.86833E 02
CISPL. AXIS 3	IN	0.27514E C1	C.22928E 01	0.18343E 01	0.13757E 01	C.91714E 00	0.45857E-00
LIN.VEL.AXIS 2	IN/SEC	0.44538E-C0	C.37115E-00	0.29692E-00	0.22269E-0C	0.14846E-00	0.74230E-01
LIN.VEL.AXIS 3	IN/SEC	-0.70058E C1	-C.58382E 01	-0.46705E 01	-0.35029E 01	-0.23353E C1	-0.11676E 01

CURRENT KINETIC AND STRAIN ENERGIES

TØTAL KINETIC ENERGY = 0.20803470E C4 (IN-LB)   STRAIN ENERGY IN STRUCTURE C.37713960E 02 (IN-LB)

TØTAL STRAIN ENERGY = 0.68133655E 02 (IN-LB)   STRAIN ENERGY IN SPRINGS C.30419689E 02 (IN-LB)

TØRQUE SHAFT CØUPLE = -0.31627674E C4 (IN-LB)   STRAIN ENERGY IN PREPACK 0. (IN-LB)

B20

BREAKDØWN ØF KINETIC AND STRAIN ENERGIES

PANEL ØR PØINT	TRANS.KINETIC ENERGY ØF PANELS	RØTATØRY KINETIC ENERGIES ØF PANELS AND LINKS	TØTAL PER PØINT
1	0.10955958E 04	0.43377541E 01	0.10999335E C4
2	0.48728558E 03	0.17855163E-00	0.48746414E C3
3	0.23170536E 03	0.24057040E 01	0.23411106E C3
4	0.13171311E 03	0.22556479E-00	0.13193868E C3
5	0.70744278E 02	0.29474758E 01	0.73691753E C2
6	0.33001522E 02	0.22410490E-0C	0.33225627E C2
7	0.	0.12744370E 01	0.12744370E C1
8	0.	0.98862680E-02	0.98862680E-02
9	0.	0.18698006E 02	0.18698006E C2

FIRST PANEL RØTATIØN, RADIANS		TØRQUE SHAFT RØTATIØN, RADIANS	
ELASTIC	TØTAL	ELASTIC	TØTAL
0.51100729E-01	0.15846947E 01	-0.19618578E-01	C.19862675E 01

DYNAMIC LØADING ØN MASS PØINTS AT TIME = 31.8811C757 SEC

MASS PØINT NØ.	FØRCE LB AXIS 2	FØRCE LB AXIS 3	MØMENT IN-LB AXIS 2	EQUIVALENT FØRCE ALØNG AXIS 3 ØN SIDE 1 LB	SIDE 2 LB
1	0.67134728E 01	C.45989530E-00	0.	-0.	0.
2	0.64057564E 01	C.15480509E 01	C.	-0.	0.
3	0.42845616E 01	-C.83137032E 00	-0.	0.	-0.
4	0.33098831E 01	C.31689646E 01	0.	-0.	0.
5	0.37333164E 01	-C.43473567E 01	-C.	0.	-0.
6	0.77363586E 00	-C.11513400E 02	0.	-0.	0.

TØRQUE ØN SHAFT FRØM STRUCTURE

PØSITIVE N1 SIDE = -C.66967922E 03 (IN-LB)
NEGATIVE N1 SIDE = -C.66967922E 03 (IN-LB)

MØTØR WØRK = -C.25627805E 04 (IN-LB)

TØTAL ENERGY IN THE WING

0.47112612E 04(IN-LB)

B21

RIGID BØDY DYNAMIC LØADING

MASS PØINT NØ.	FØRCE 1	FØRCE 2	FØRCE 3	TØRQUE 1	TØRQUE 2	TØRQUE 3
1	0.	0.23847608E 01	C.20885317E 02	-0.94740393E 02	-0.	C.
2	0.	0.61082029E-02	C.11808193E 02	0.90059881E 02	0.	-C.
3	0.	0.10886020E 01	C.93742473E 01	-0.52547698E 02	-0.	C.
4	0.	C.10869620E-01	C.78555419E 01	0.11377290E 03	0.	-C.
5	0.	0.67606420E 00	C.55434777E 01	-0.64381598E 02	-0.	C.
6	0.	C.15654702E-01	C.27612301E 01	0.11303654E 03	0.	-C.
7	0.	0.	C.	-0.27837479E 02	-0.	C.
8	0.	C.	C.	0.23156503E-00	0.	-C.
9	0.	C.	C.	0.41045359E 03	-0.	C.

INTERPØLATED STIFFNESS CØEFFICIENTS

FK(2,1)	FK(2,2)	FK(2,3)	FK(2,4)	FK(2,5)	FK(2,6)
-0.20478664E 03	C.12323544E C2	0.	0.38703533E 03	-0.25714707E 02	-C.

CURRENT INTEGRATIØN CATA

CURRENT TIME = 32.0C16670 SEC   CURRENT TIME STEP = 0.0003000 SEC   FINAL TIME = 45.0CCCCCC SEC

CURRENT ELASTIC AND RIGID BØCY MØTIØN CATA

DEPLØYMENT ANGLE (RIGID)	REFERENCE AXIS		ELASTIC CISPLACEMENTS AND VELØCITIES ØF MASS PØINTS 1	2	3	4	5	6
ANGLE,RAD	CISPL. AXIS 2	IN	0.63187E CC	C.53187E 00	0.42863E-00	0.29592E-0C	0.21425E-C0	0.85492E-01
	CISPL. AXIS 3	IN	0.15626E C2	C.11003E 02	0.62636E 01	0.23825E 01	C.19603E-C0	-0.58025E 00
1.53938030	RØTAT. AXIS 2	RAD	C.	C.	0.	0.	C.	C.
ANG.VEL.,RAD/SEC	LIN.VEL.AXIS 2	IN/SEC	-0.10585E C2	-C.87914E 01	-0.69717E 01	-0.52686E 01	-0.32866E 01	-0.14971E 01
	LIN.VEL.AXIS 3	IN/SEC	0.23902E C2	C.16238E 02	0.92171E 01	0.41895E 01	C.51475E C1	0.74493E 01
-0.	ANG.VEL.AXIS 2	RAD/SEC	0.	C.	0.	0.	C.	0.

CURRENT RIGID DEPLØYMENT INFØRMATIØN FØR MASS PØINTS

		1	2	3	4	5	6
CISPL. AXIS 2	IN	0.52105E C3	C.43421E 03	0.34737E 03	0.26053E 03	C.17368E C3	C.86842E 02
CISPL. AXIS 3	IN	0.16518E C1	C.13765E 01	0.11012E 01	0.82591E 0C	C.55061E CC	0.27530E-00
LIN.VEL.AXIS 2	IN/SEC	-0.	-C.	-0.	-0.	-C.	-0.
LIN.VEL.AXIS 3	IN/SEC	0.	C.	0.	0.	0.	0.

CURRENT KINETIC AND STRAIN ENERGIES

TØTAL KINETIC ENERGY =	0.29487272E 04 (IN-LB)	STRAIN ENERGY IN STRUCTURE	0.21096640E 02	(IN-LB)
TØTAL STRAIN ENERGY =	0.49870065E 02 (IN-LB)	STRAIN ENERGY IN SPRINGS	0.28773425E 02	(IN-LB)
TØRQUE SHAFT CØUPLE =	-0.69999999E C4 (IN-LB)	STRAIN ENERGY IN PREPACK	C.	(IN-LB)

B22

BREAKDØWN ØF KINETIC AND STRAIN ENERGIES

PANEL ØR PØINT	TRANS.KINETIC ENERGY ØF PANELS	RØTATØRY KINETIC ENERGIES ØF PANELS ANC LINKS	TØTAL PER PØINT
1	0.15343719E 04	0.23254541E 01	0.15366973E 04
2	0.64991722E 03	0.12540486E 01	0.65117127E C3
3	0.35761395E 03	0.12896891E 01	0.35890364E C3
4	0.19620984E 03	0.15842433E 01	0.19779408E C3
5	0.11532345E 03	0.15801310E 01	0.11690359E C3
6	0.59314400E 02	0.15739898E 01	0.60888389E C2
7	0.	0.68322105E 00	0.68322105E CC
8	0.	0.13806543E-01	0.138C6543E-C1
9	0.	0.25672057E 02	0.25672057E C2

FIRST PANEL RØTATIØN, RADIANS		TØRQUE SHAFT RØTATIØN, RADIANS	
ELASTIC	TØTAL	ELASTIC	TØTAL
0.20446451E-C1	C.15598267E 01	-0.77172501E-02	C.20004662E 01

DYNAMIC LØADING ØN MASS PØINTS AT TIME = 32.C0166702 SEC

MASS PØINT NØ.	FØRCE LB AXIS 2	FØRCE LB AXIS 3	MØMENT IN-LB AXIS 4	EQUIVALENT FØRCE ALØNG AXIS 3 ØN SIDE 1 LB	SIDE 2 LB
1	0.47367431E 01	-C.735528C6E 00	-C.	0.	-0.
2	0.79633808E 00	C.61423345E 01	C.	-0.	0.
3	0.26431486E 01	-C.21458717E 01	-0.	0.	-0.
4	0.26069469E 01	-C.3C776457E 01	0.	-0.	0.
5	-0.17072114E 01	-C.26491603E 01	-0.	0.	-0.
6	0.98896027E 00	-C.4C592145E 01	0.	-0.	0.

TØRQUE ØN SHAFT FRØM STRUCTURE

PØSITIVE N1 SIDE = -C.26342835E 03 (IN-LB)
NEGATIVE N1 SIDE = -C.26342835E 03 (IN-LB)

MØTØR WØRK = -C.25584075E 04 (IN-LB)

TØTAL ENERGY IN THE WING

0.55570048E 04(IN-LB)

B23

RIGID BØDY DYNAMIC LØADING

MASS PØINT NØ.	FØRCE 1	FØRCE 2	FØRCE 3	TØRQUE 1	TØRQUE 2	TØRQUE 3
1	0.	0.22291145E 01	C.17712220E 02	-0.80727884E 02	-0.	C.
2	0.	C.12665576E 01	C.1CC10502E 02	0.76515295E 02	0.	-C.
3	0.	0.10138624E 01	C.79500218E 01	-0.44771416E 02	-0.	C.
4	0.	C.86528912E 00	C.66569C80E 01	0.96661993E 02	0.	-C.
5	0.	C.62321175E 00	C.47C12594E 01	-0.54854075E 02	-0.	C.
6	0.	C.33387449E-00	C.234C8578E 01	0.96036381E 02	0.	-C.
7	0.	C.	C.	-0.23717944E 02	-0.	C.
8	0.	C.	C.	0.19779251E-00	0.	-C.
9	0.	C.	C.	0.35057715E 03	-0.	C.

INTERPØLATED STIFFNESS CØEFFICIENTS

FK(2,1)	FK(2,2)	FK(2,3)	FK(2,4)	FK(2,5)	FK(2,6)
-0.2408C881E 03	0.12140498E C2	-0.	0.44586033E 03	-0.25637349E 02	C.

APPENDIX C

PLOTTED RESULTS OF DEPLOYMENT DYNAMICS
ANALYSIS - LISTED IN TABLE 1 OF SECTION 4

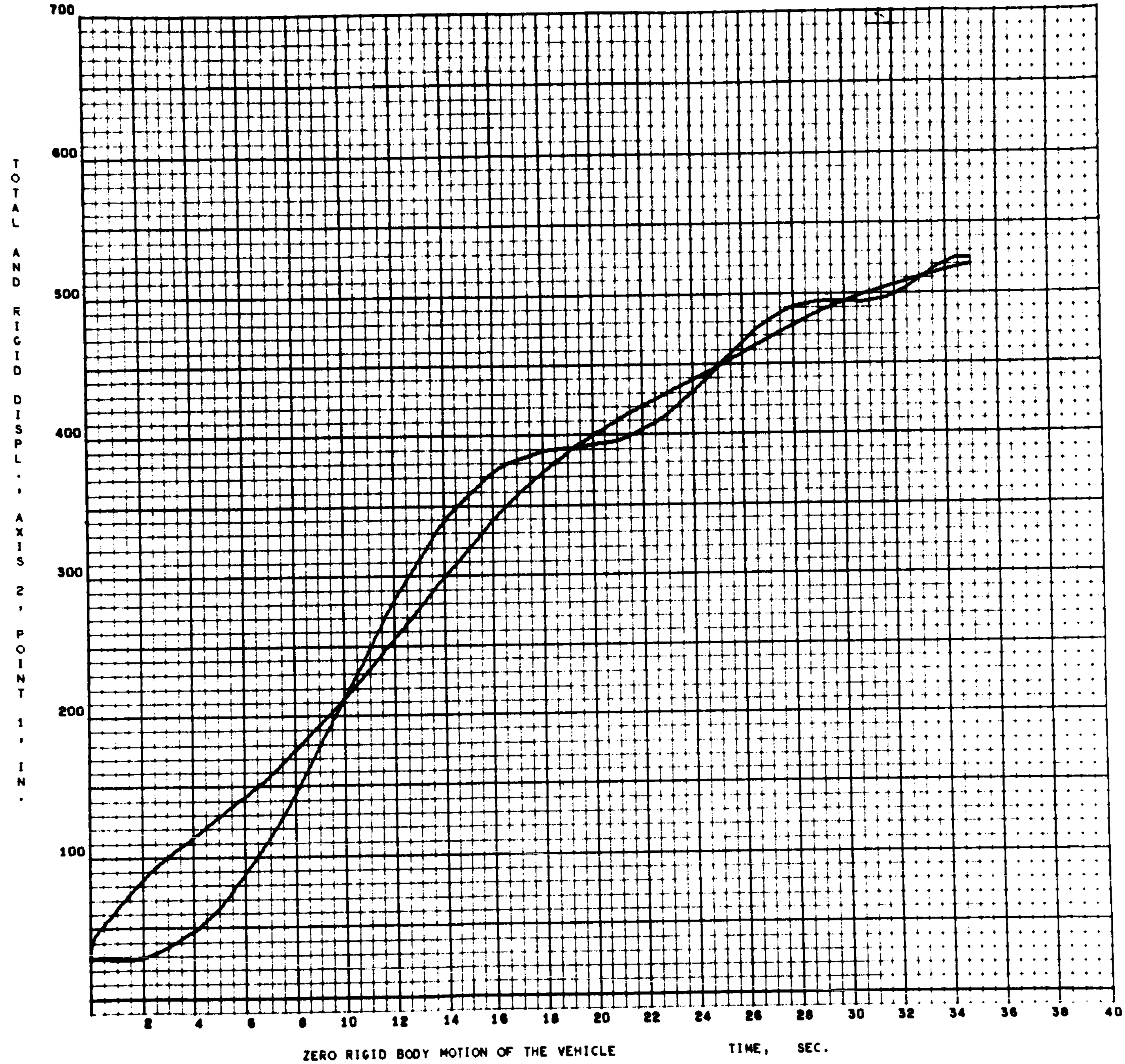
TOTAL AND RIGID DISPL., AXIS 2, POINT 1, IN.
700
600
500
400
300
200
100
2
4
6
8
10
12
14
16
18
20
22
24
26
28
30
32
34
36
38
40
ZERO RIGID BODY MOTION OF THE VEHICLE
TIME, SEC.

4560 1

451450
000 007

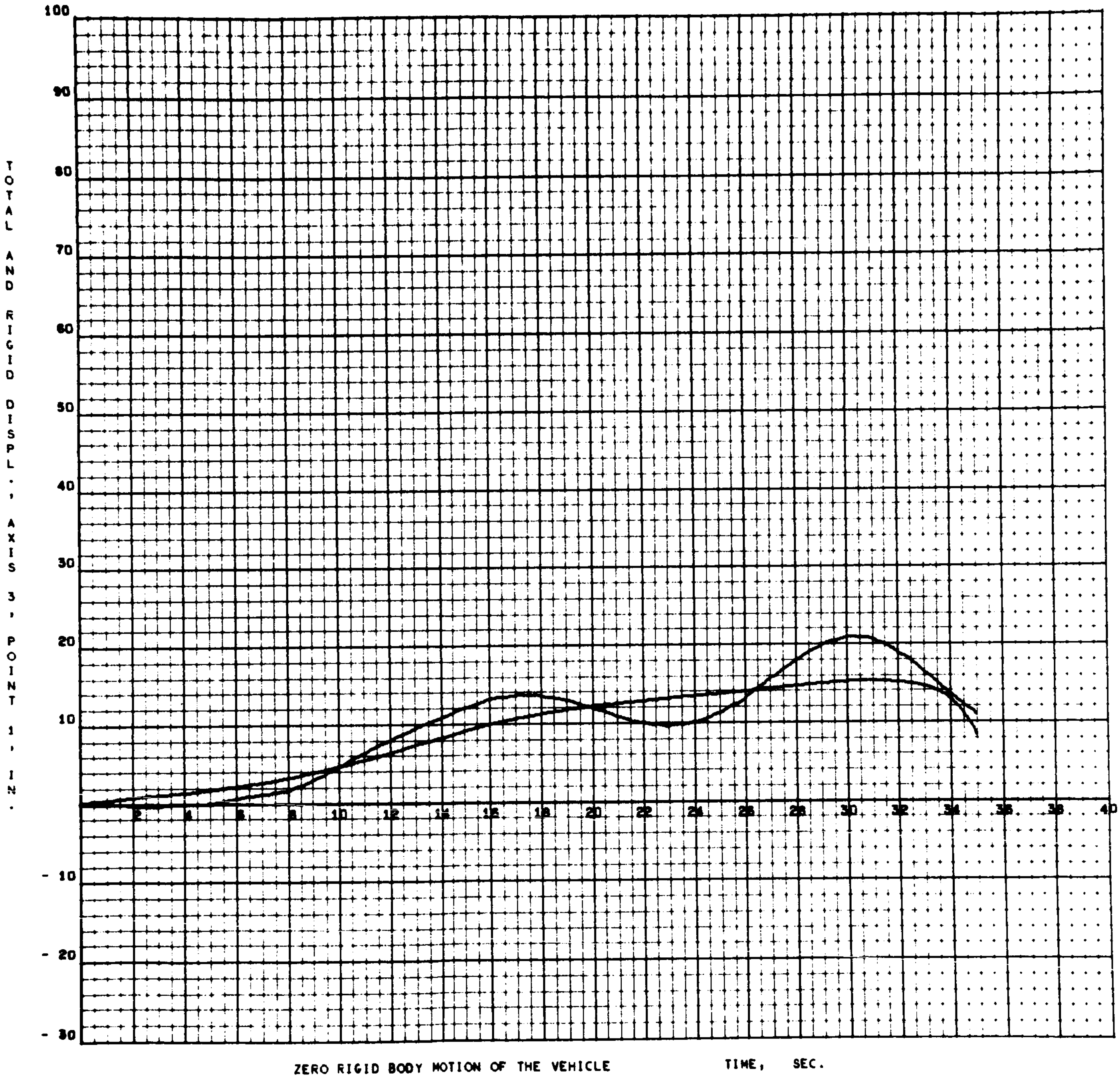

4560 2

451450
000 019

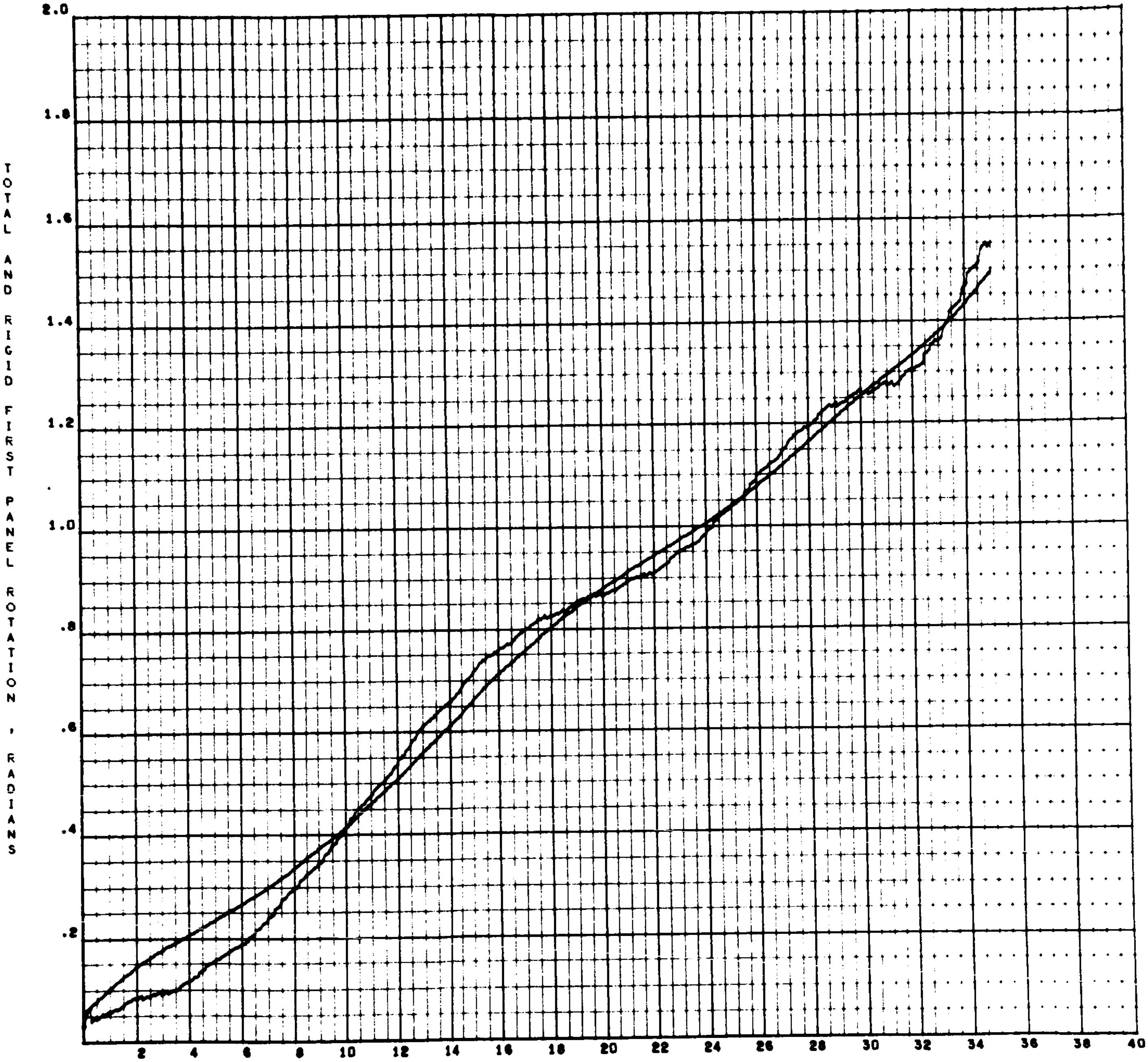

ZERO RIGID BODY MOTION OF THE VEHICLE

4560

451450
000 029

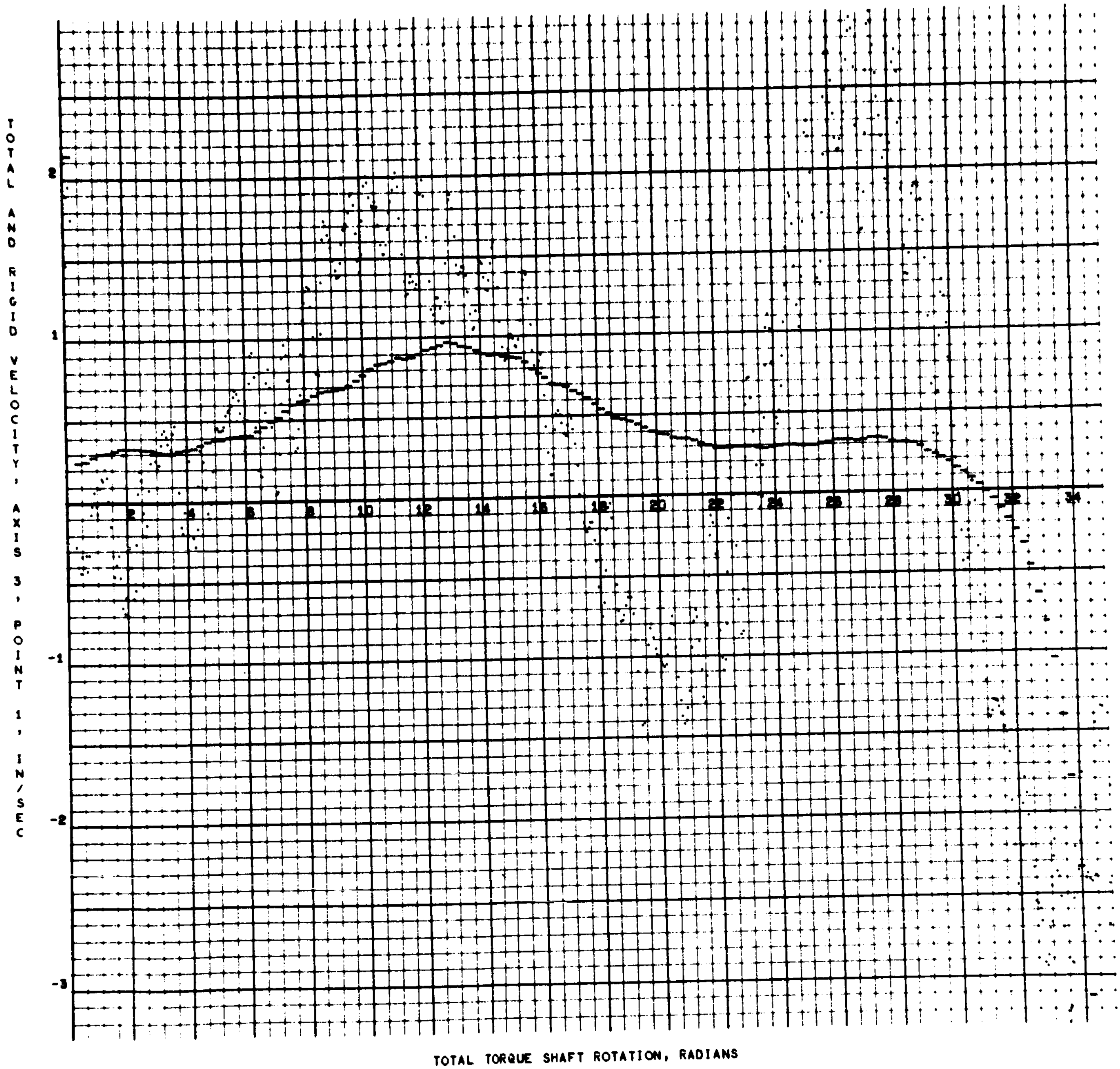

4560 4

451450
000 035

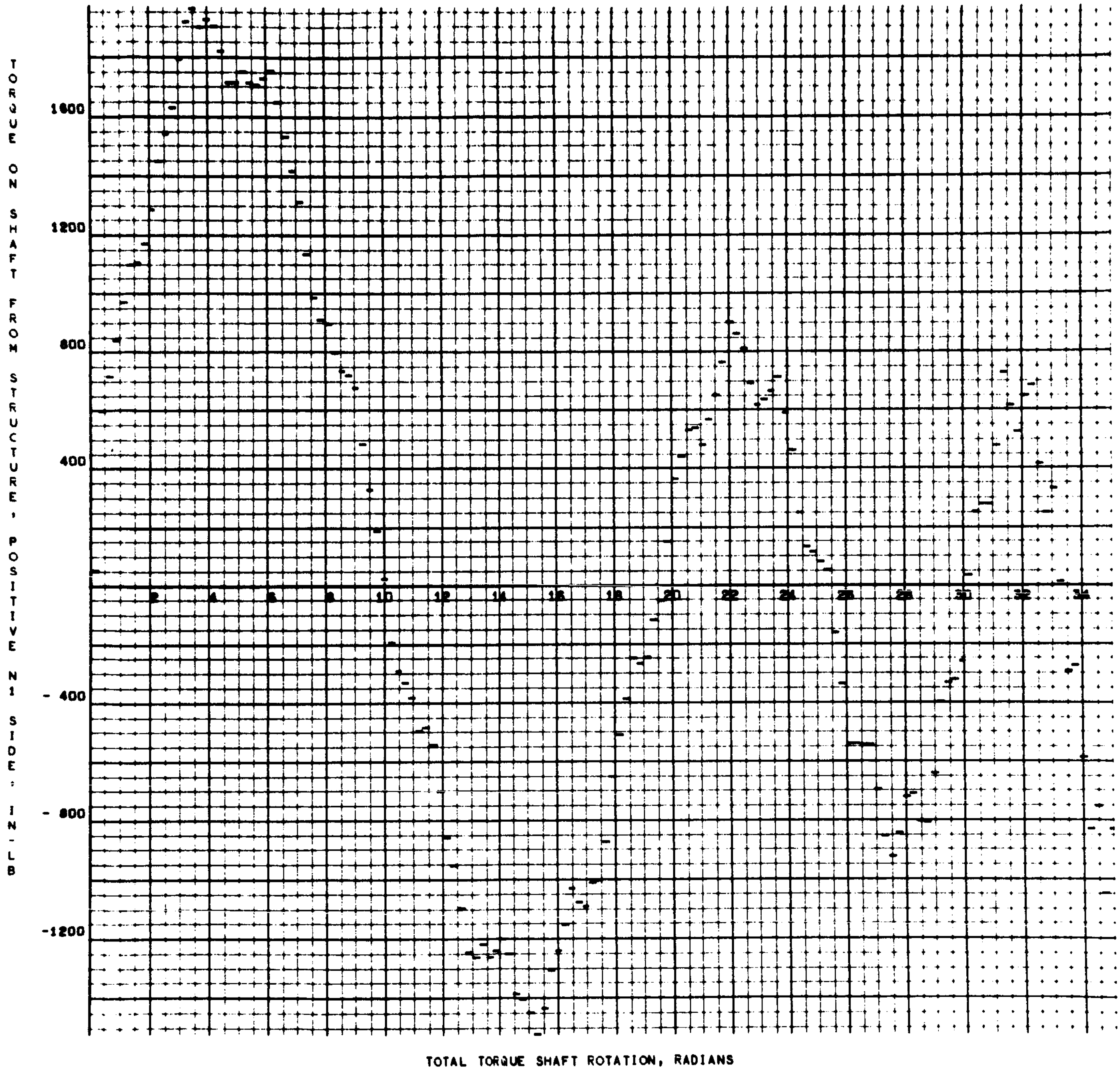

4560 5

451450
000 037

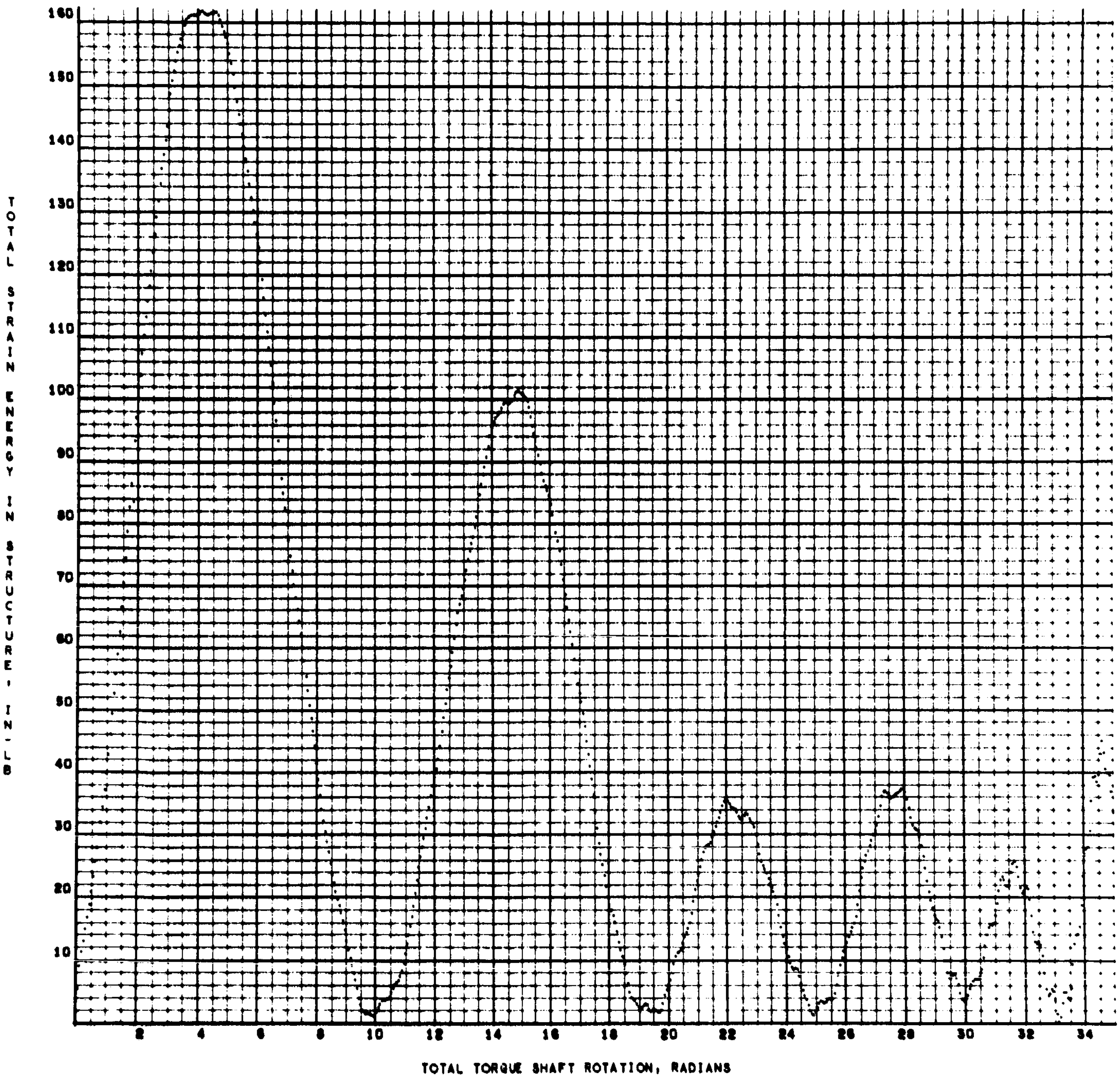

4560 6

45/250

006 001

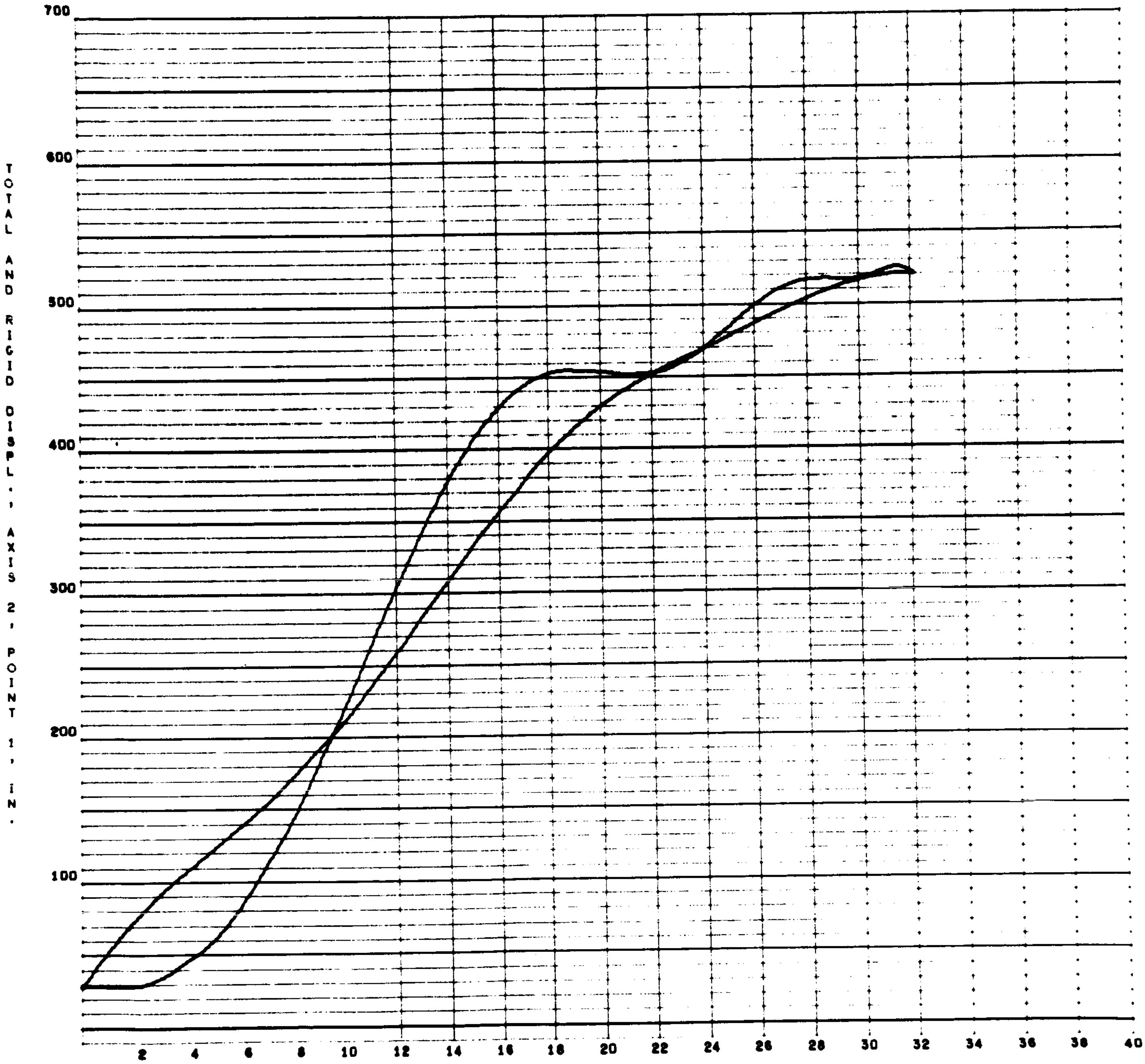

VEHICLE RIGID BODY MOTION-6 DEGR. PER SEC.-AXIS 1

5020 7

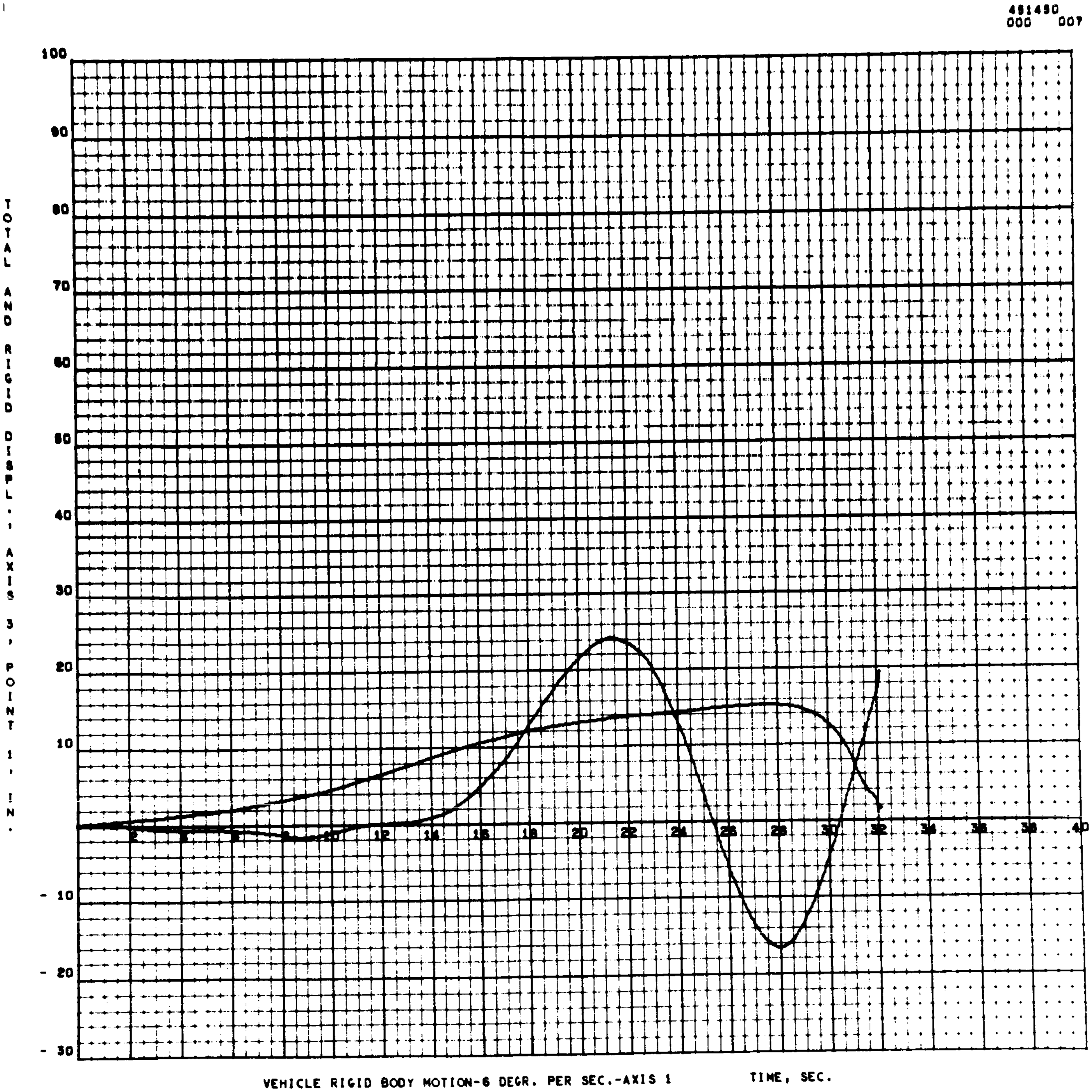
481450
000 007
100
90
80
70
60
50
40
30
20
10
- 10
- 20
- 30
TOTAL AND RIGID DISPL., AXIS 3, POINT 1, IN.
2
4
6
8
10
12
14
16
18
20
22
24
26
28
30
32
34
36
38
40
VEHICLE RIGID BODY MOTION-6 DEGR. PER SEC.-AXIS 1
TIME, SEC.

5020 8

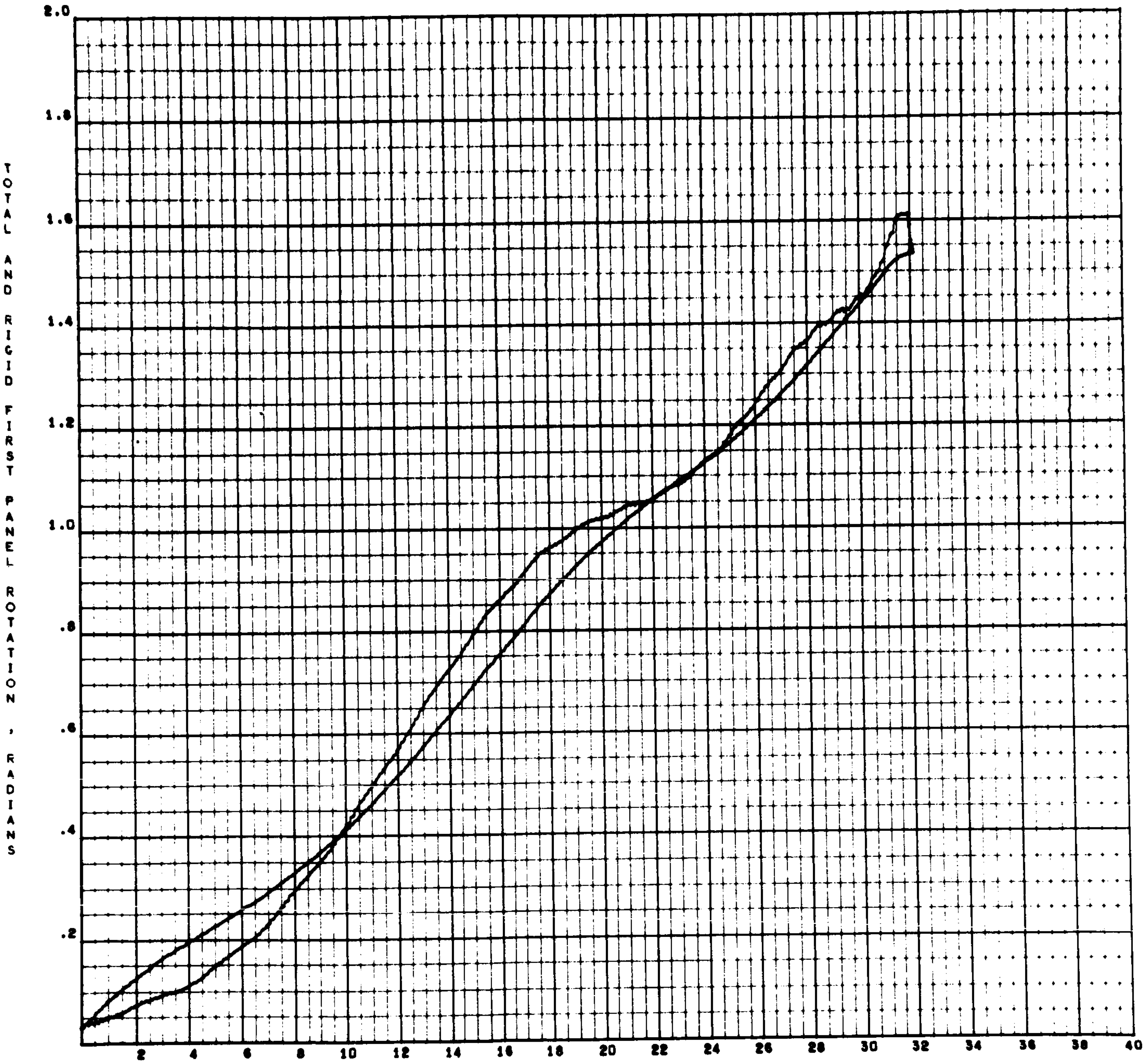

VEHICLE RIGID BODY MOTION-6 DEGR. PER SEC.-AXIS 1

5020

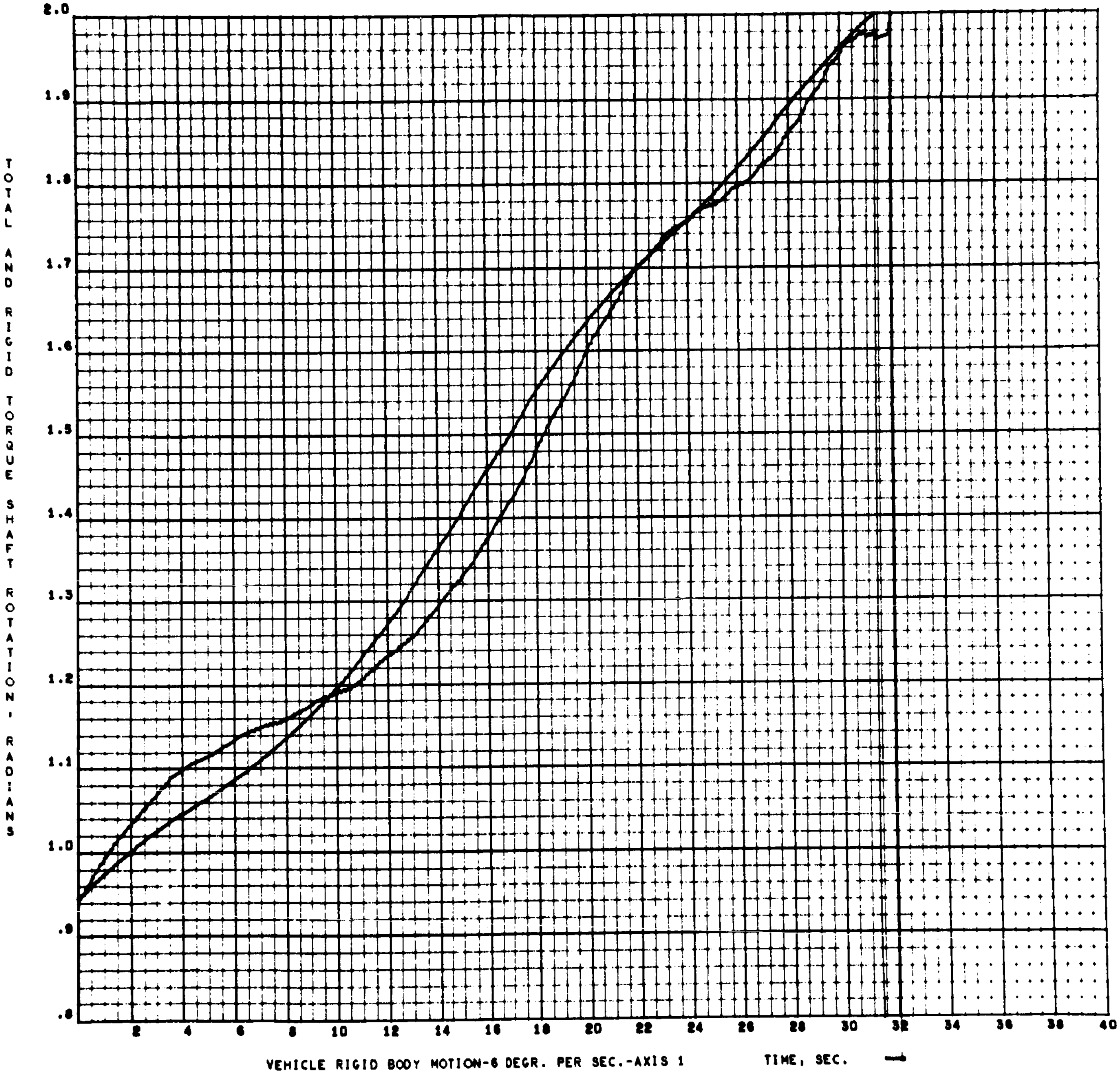
TOTAL AND RIGID TORQUE SHAFT ROTATION, RADIANS
2.0
1.9
1.8
1.7
1.6
1.5
1.4
1.3
1.2
1.1
1.0
.9
.8
2
4
6
8
10
12
14
16
18
20
22
24
26
28
30
32
34
36
38
40
VEHICLE RIGID BODY MOTION-6 DEGR. PER SEC.-AXIS 1
TIME, SEC.

451450
000 022

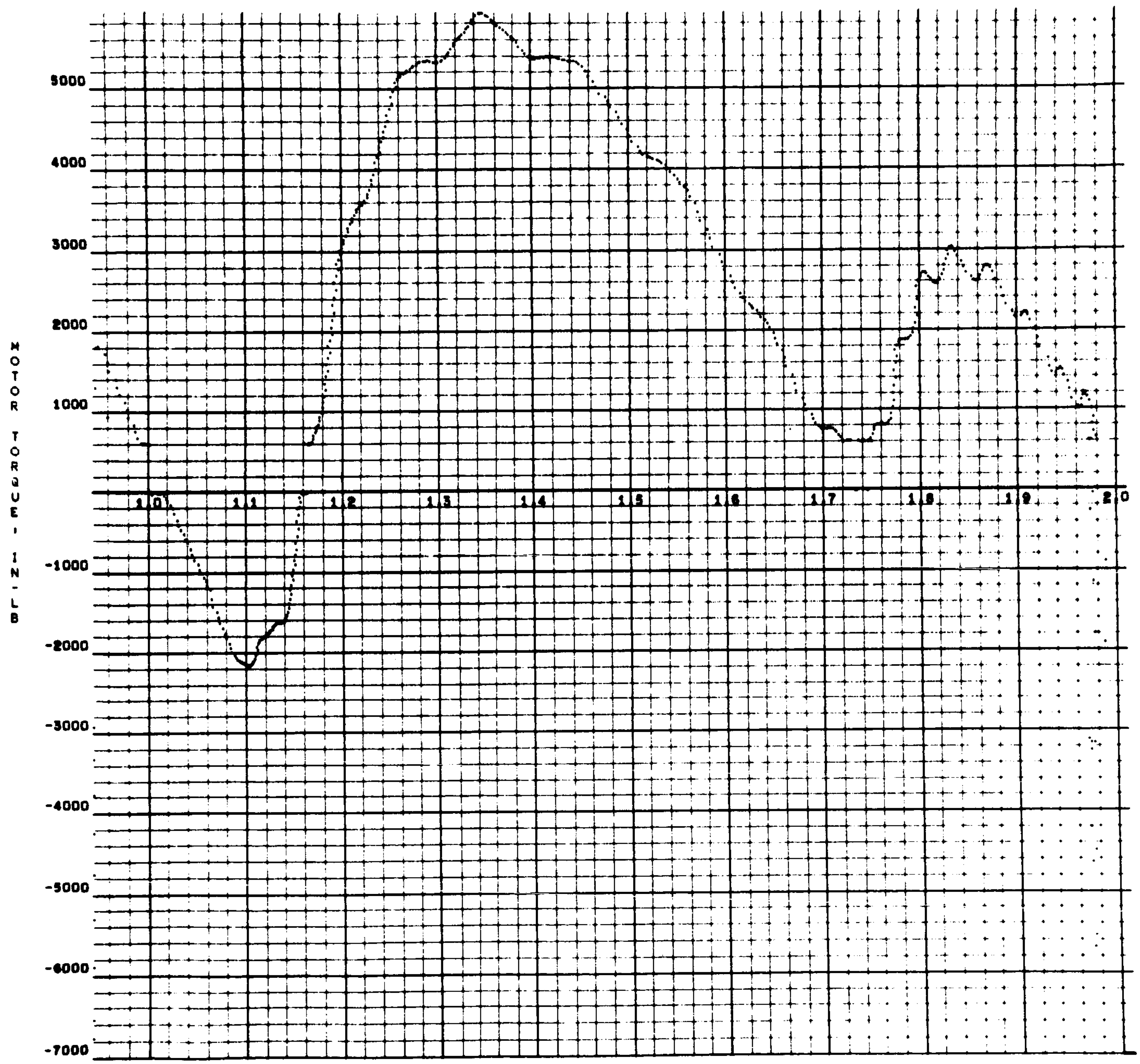

VEH. RIGID B. MOTION-6 DEGR.PER SEC.AXIS 1 -TOTAL T. SHAFT ROT., RAD.

5020 11

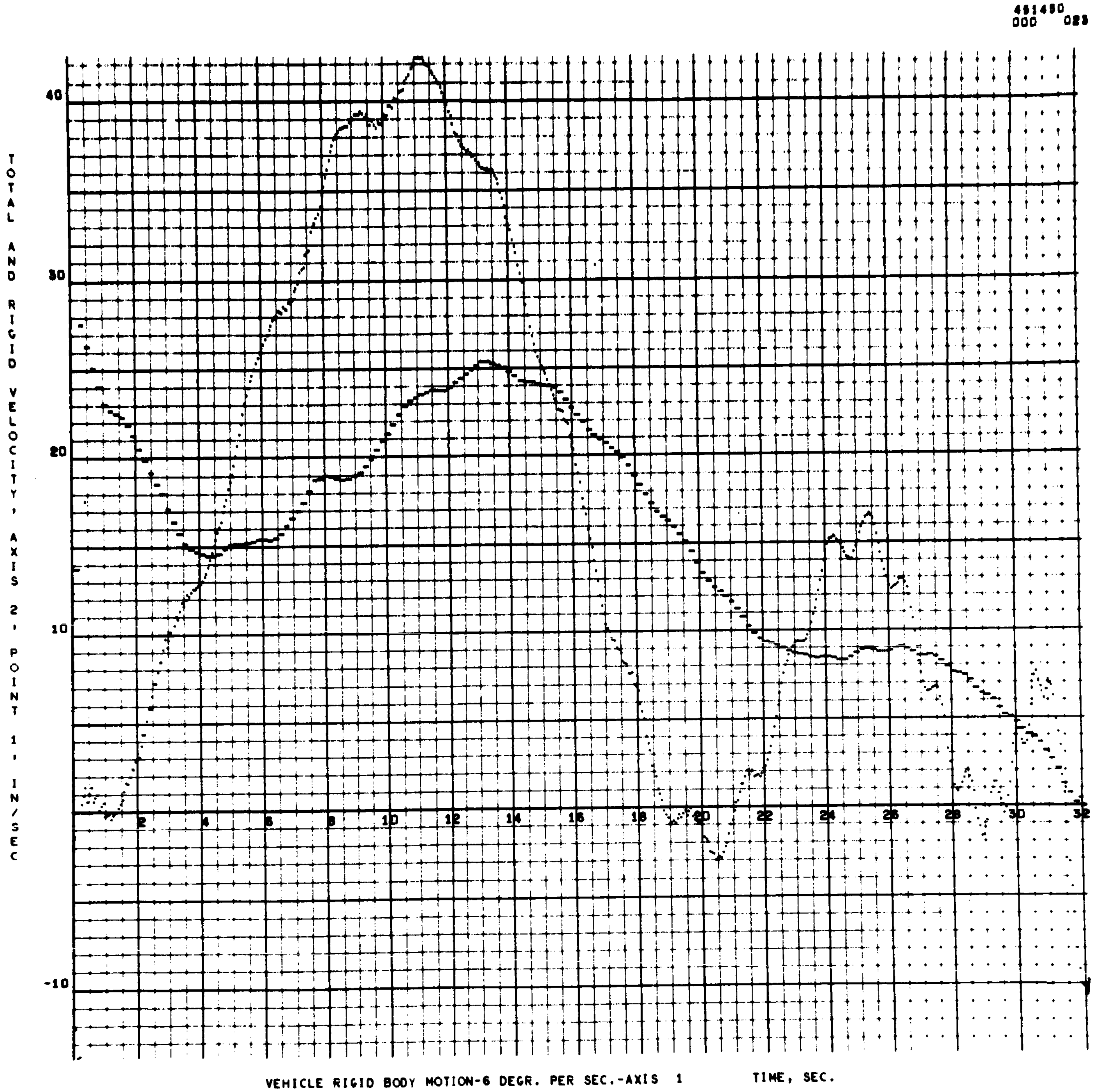
491450
000 023
TOTAL AND RIGID VELOCITY, AXIS 2, POINT 1, IN/SEC
40
30
20
10
-10
2
4
6
8
10
12
14
16
18
20
22
24
26
28
30
32
VEHICLE RIGID BODY MOTION-6 DEGR. PER SEC.-AXIS 1
TIME, SEC.

5020 12

451450
000 029

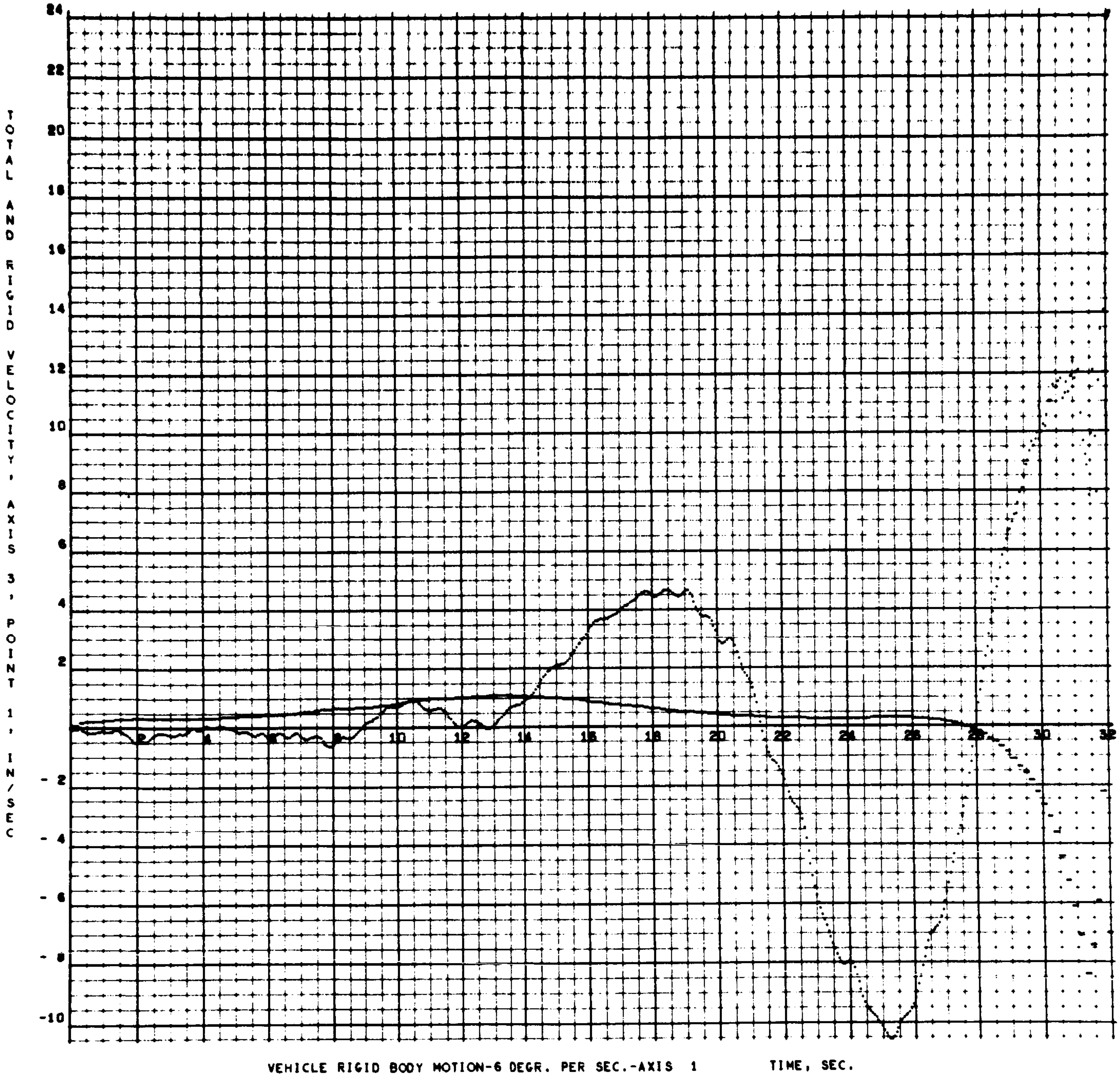

5020 13

451450
000 037

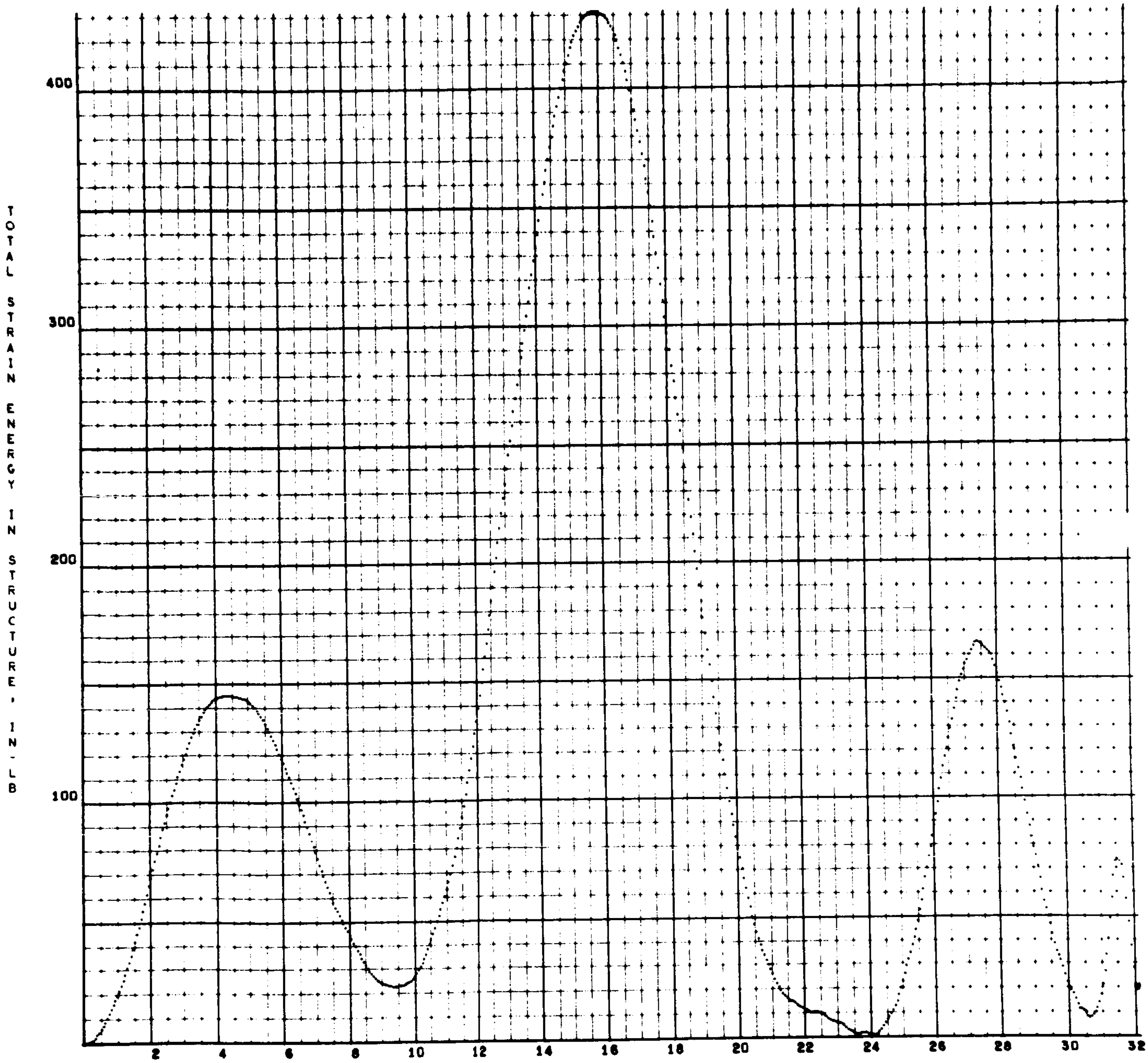

VEHICLE RIGID BODY MOTION-6 DEGR. PER SEC.-AXIS 1 TIME, SEC.

5020 14

451450
000 038

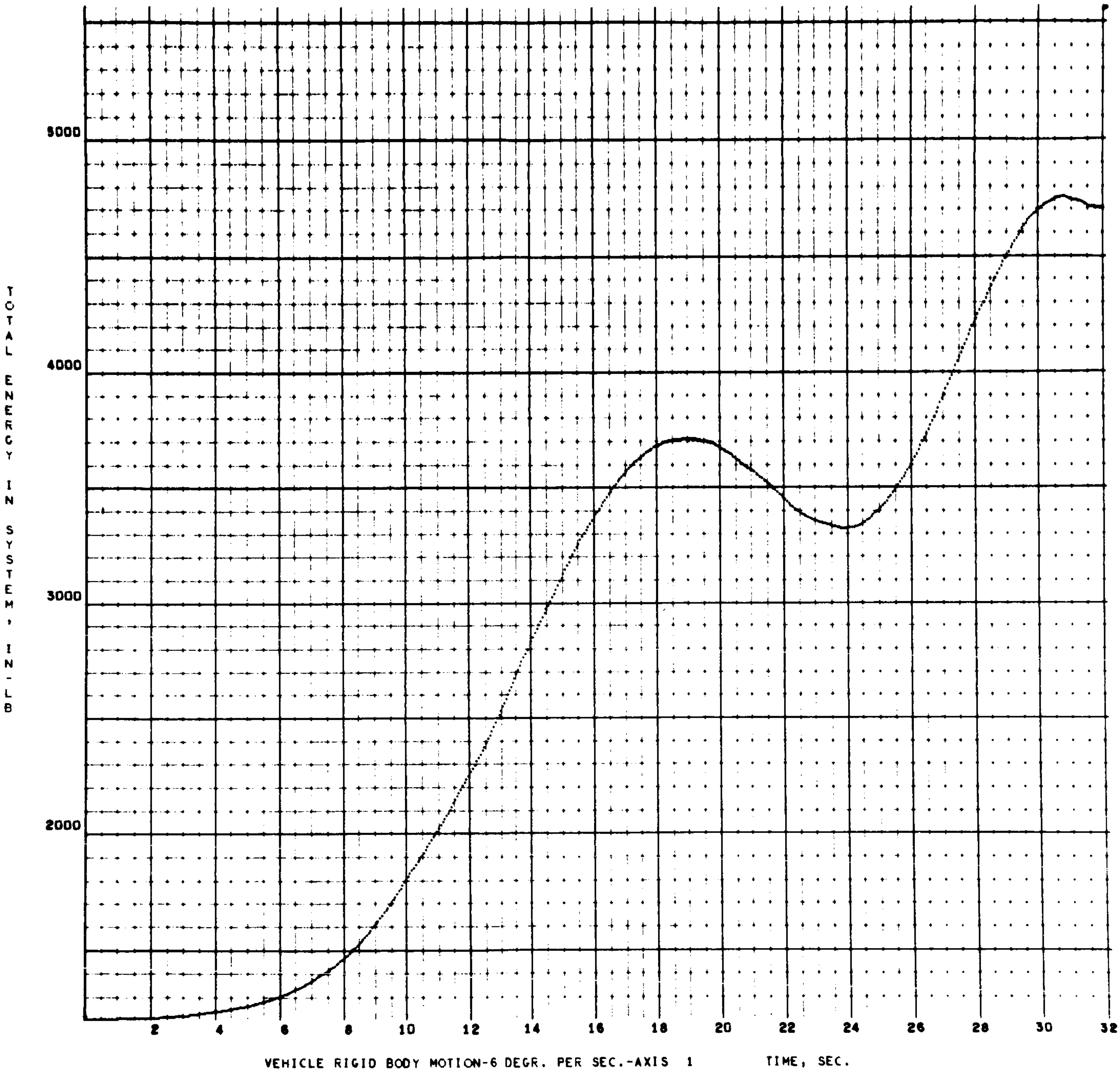

5020 15

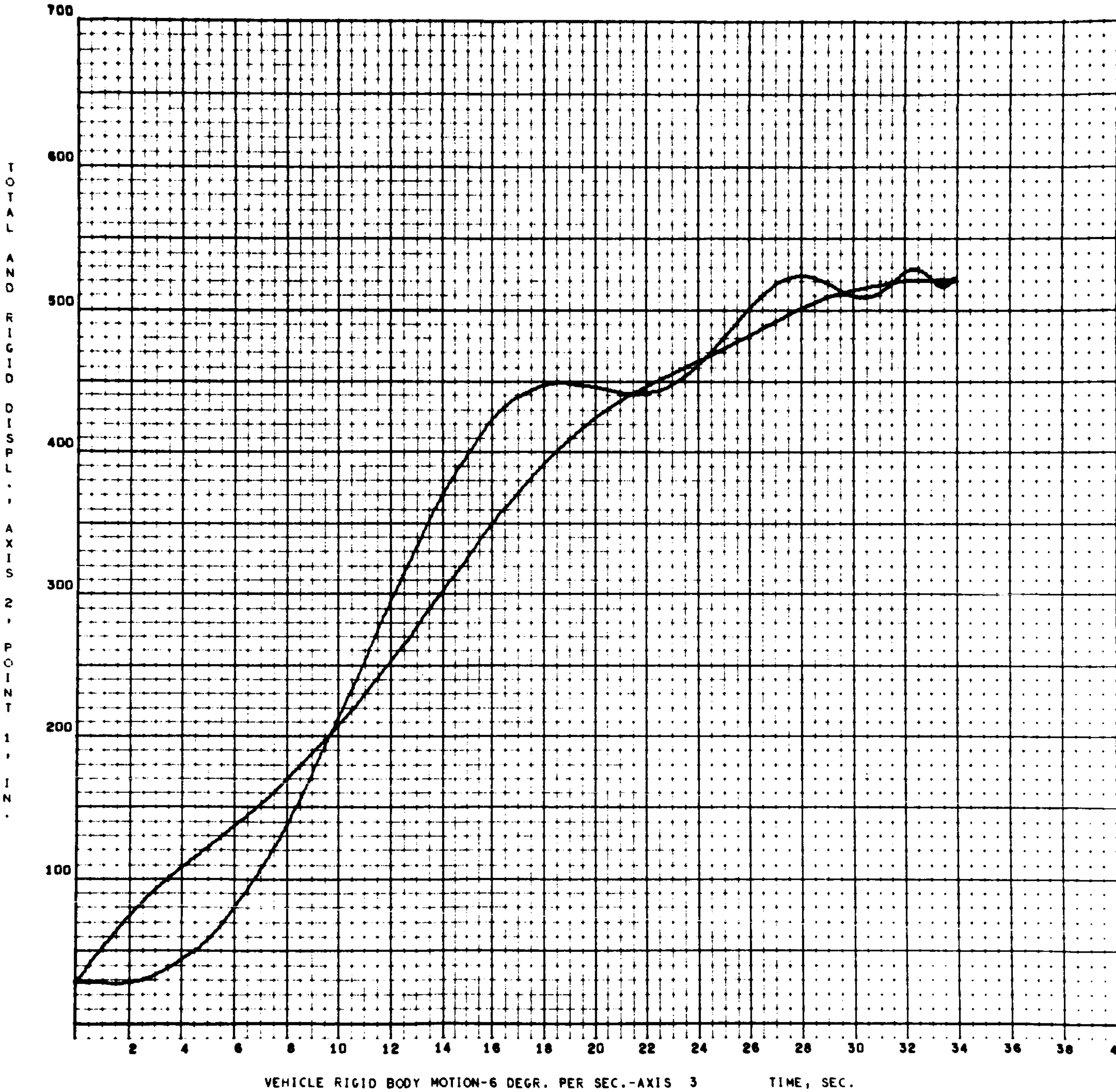
TOTAL AND RIGID DISPL., AXIS 2, POINT 1, IN.
700
600
500
400
300
200
100
2 4 6 8 10 12 14 16 18 20 22 24 26 28 30 32 34 36 38 40
VEHICLE RIGID BODY MOTION-6 DEGR. PER SEC.-AXIS 3
TIME, SEC.

451450
000 007

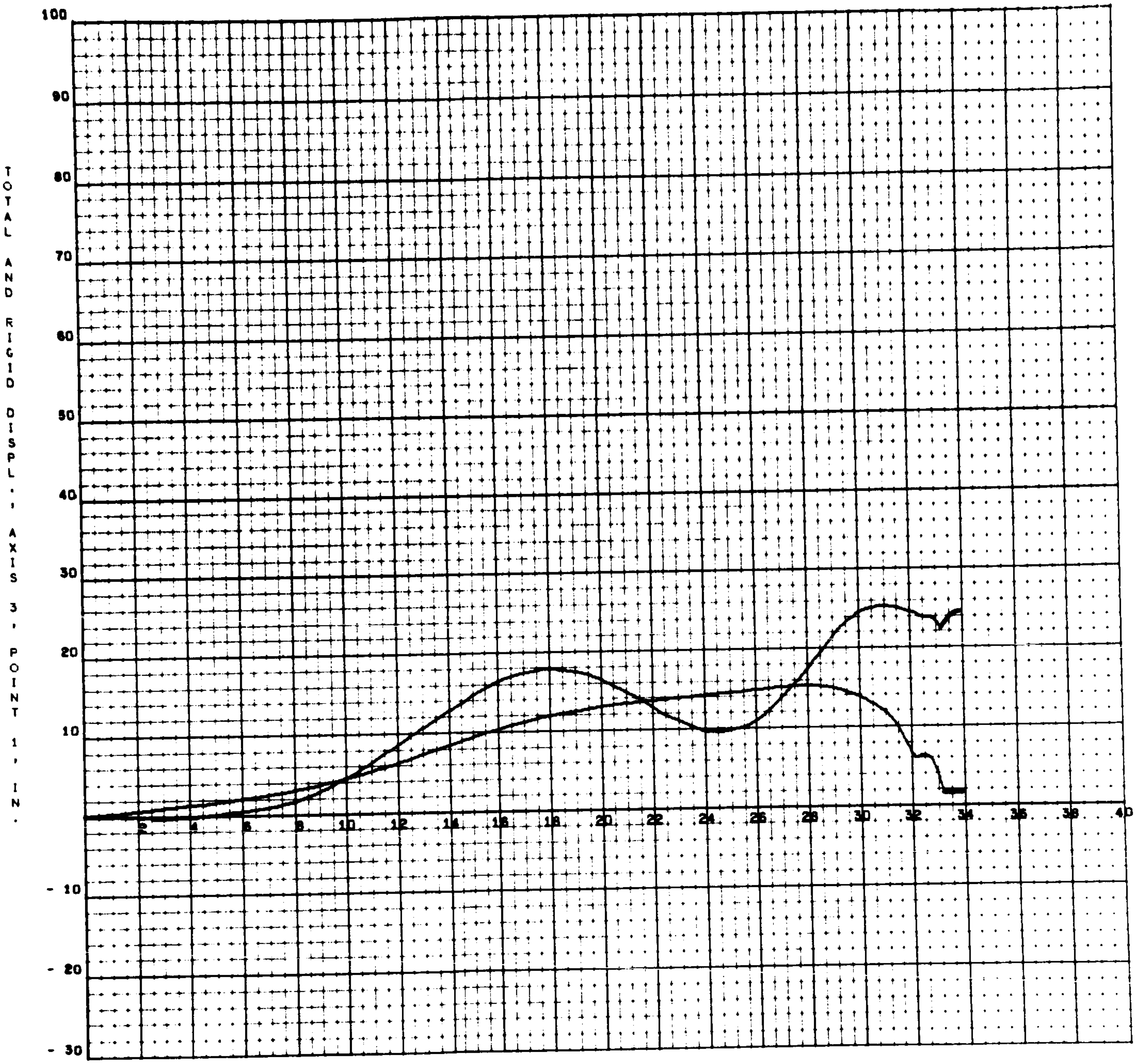

VEHICLE RIGID BODY MOTION-6 DEGR. PER SEC.-AXIS 3

5021 17

451450
000 019

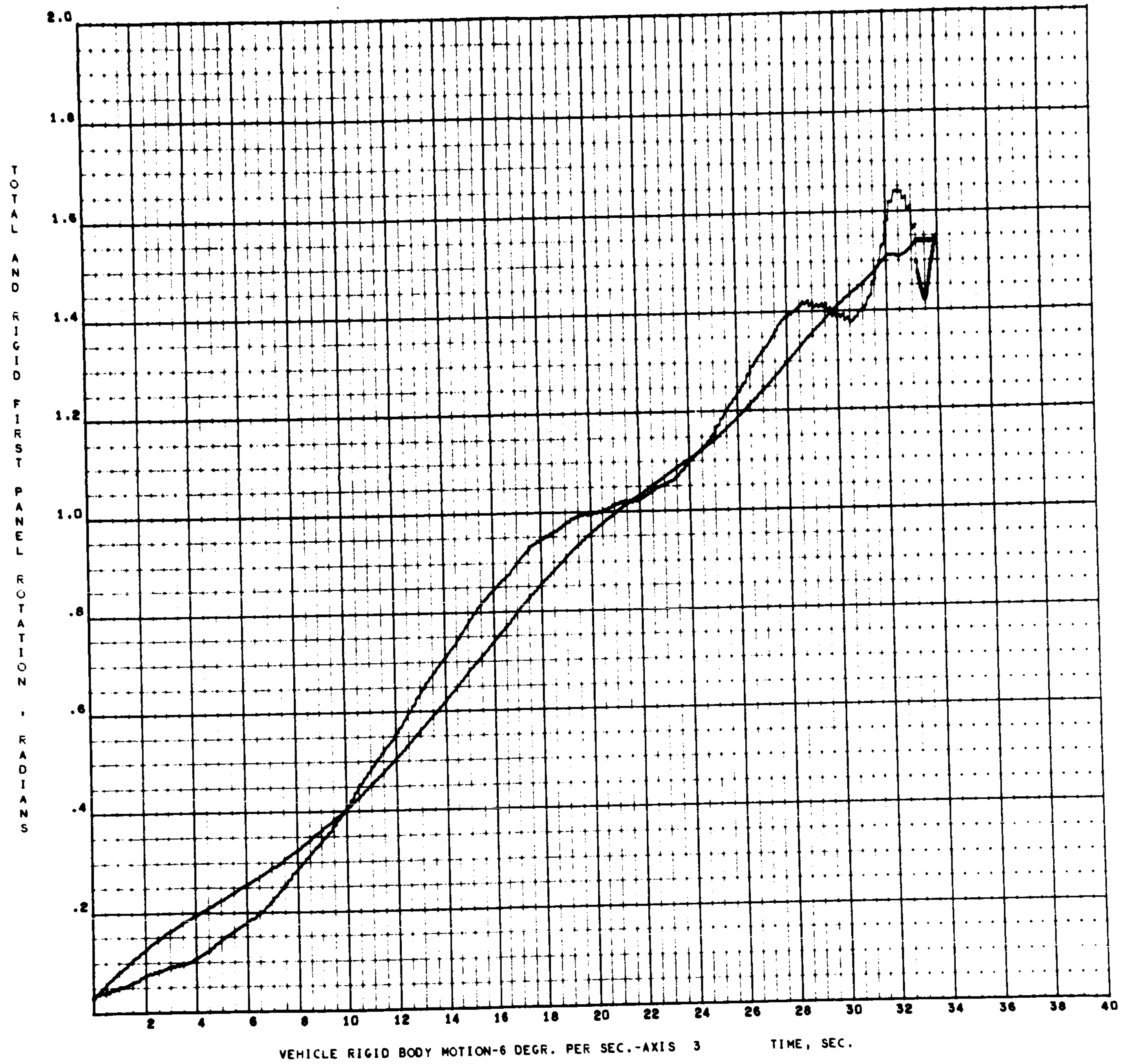

5021 18

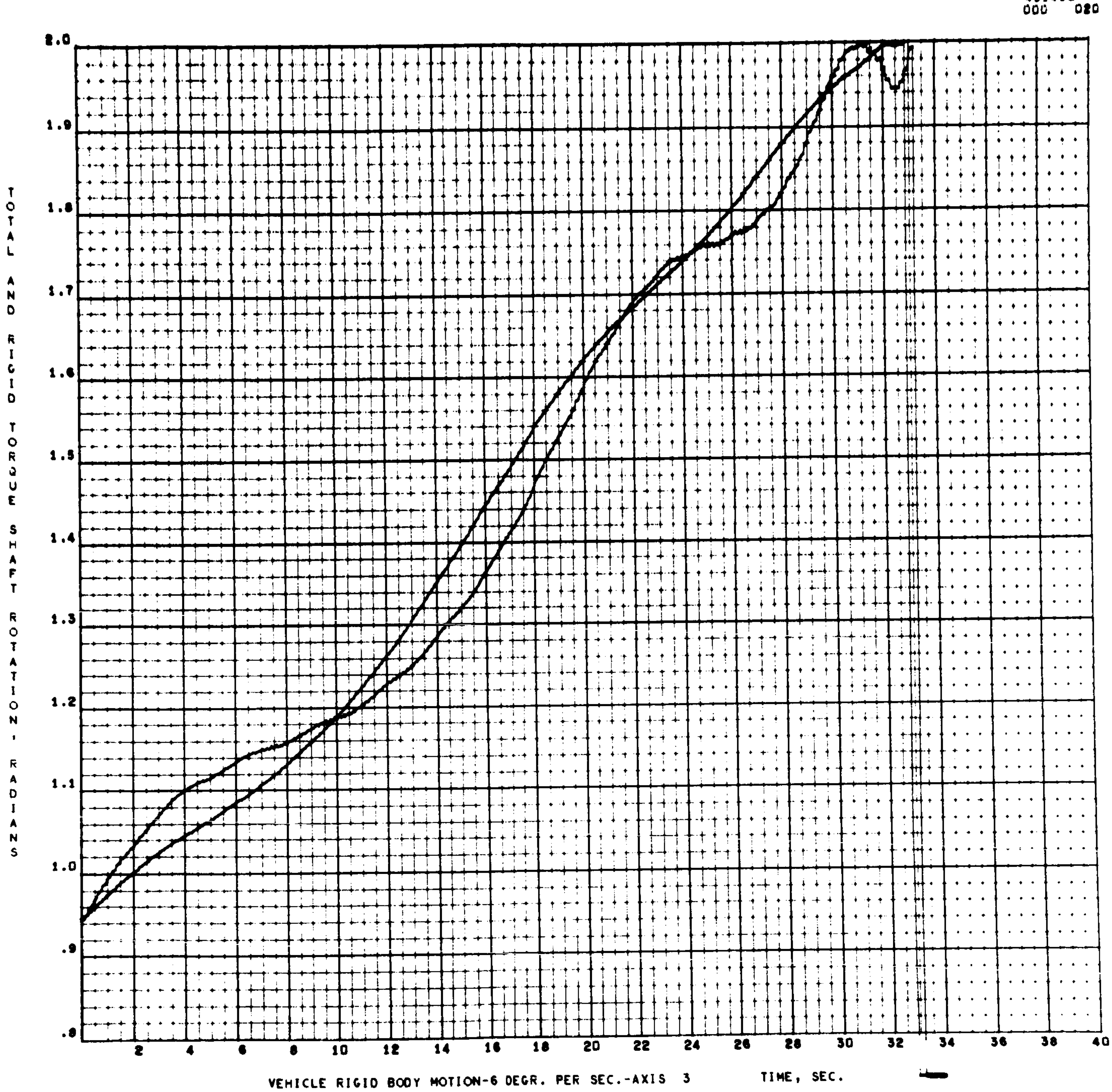
451490
000 020
2.0
1.9
1.8
1.7
1.6
1.5
1.4
1.3
1.2
1.1
1.0
.9
.8
TOTAL AND RIGID TORQUE SHAFT ROTATION, RADIANS
2
4
6
8
10
12
14
16
18
20
22
24
26
28
30
32
34
36
38
40
VEHICLE RIGID BODY MOTION-6 DEGR. PER SEC.-AXIS 3
TIME, SEC.

5021 19

451450
000 022

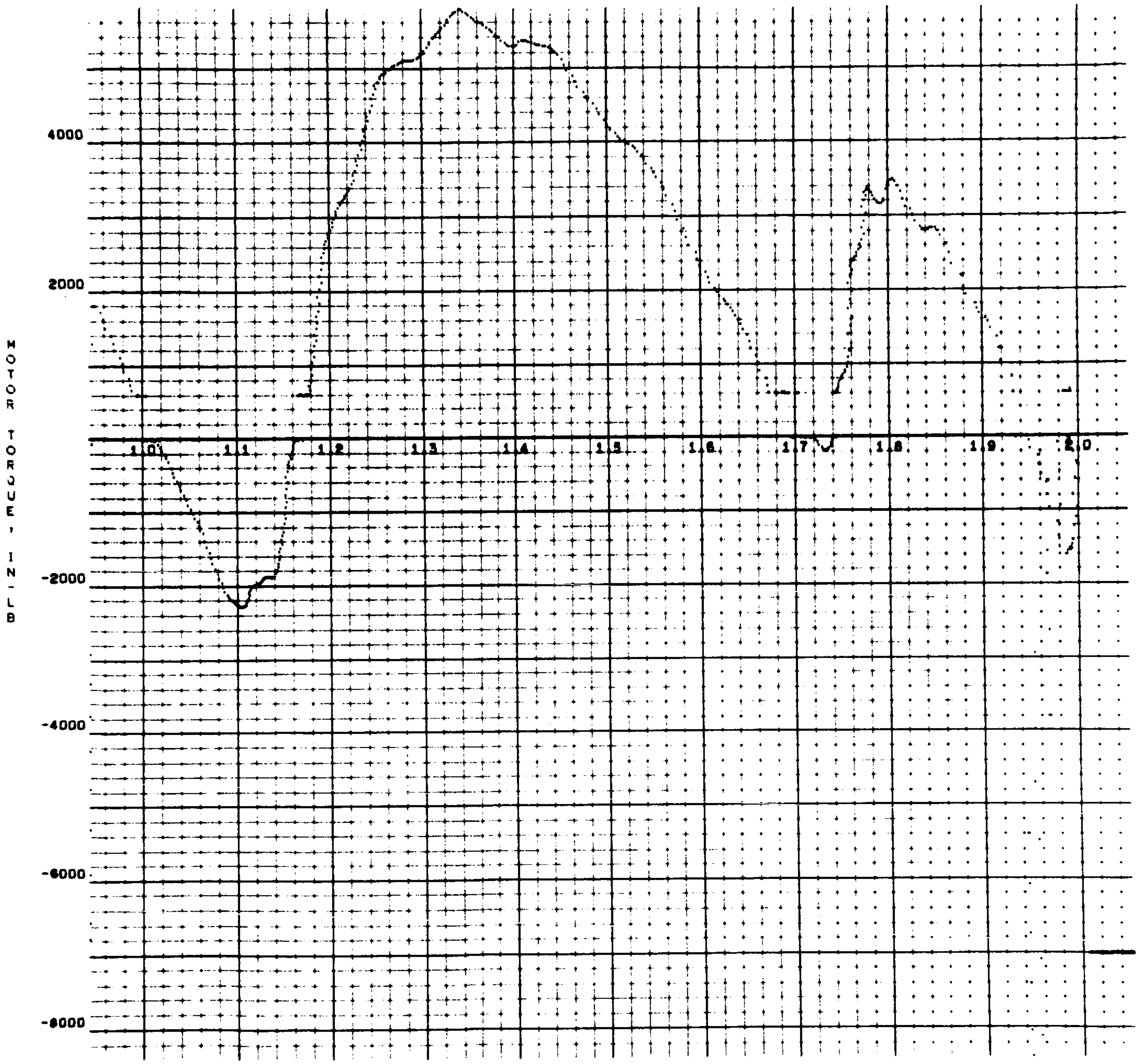

VEH. RIGID B. MOTION-6 DEGR.PER SEC.AXIS 3 -TOTAL T. SHAFT ROT., RAD.

5021 20

451450
000 023

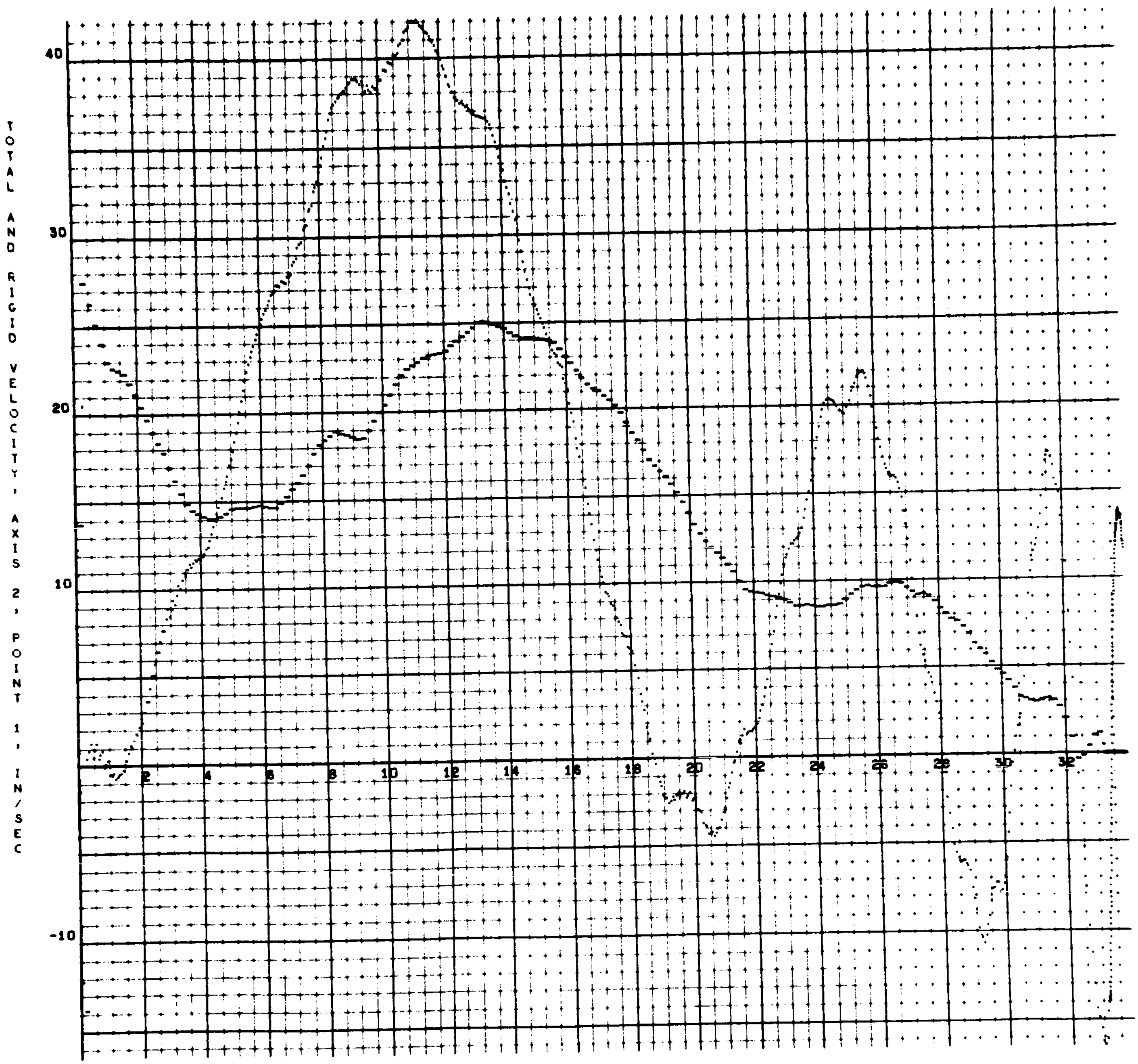

VEHICLE RIGID BODY MOTION-6 DEGR. PER SEC.-AXIS 3   TIME, SEC.

5021 21

451450
000 029

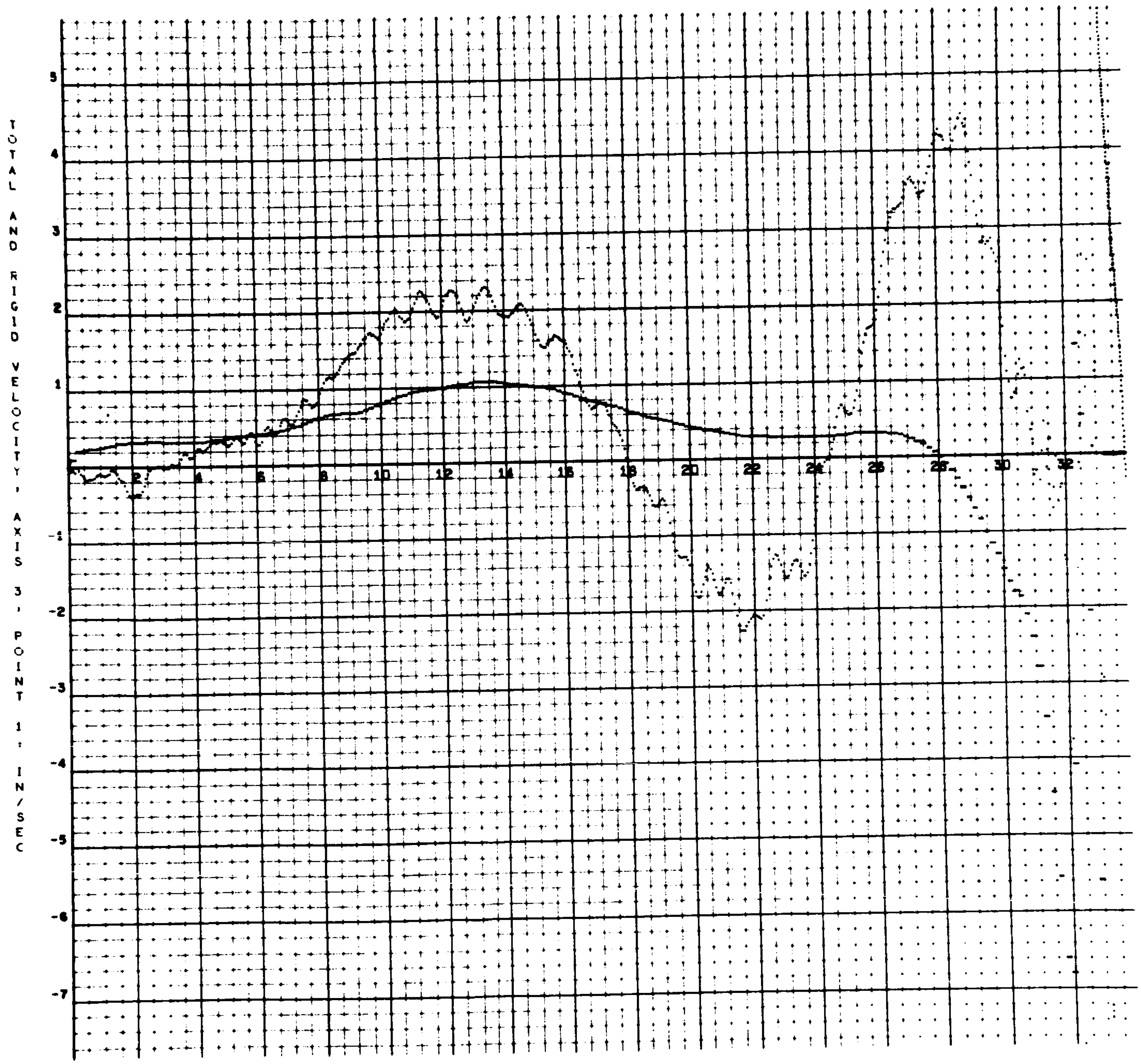

VEHICLE RIGID BODY MOTION-6 DEGR. PER SEC.-AXIS 3 TIME, SEC.

5021 22

451450
000 035

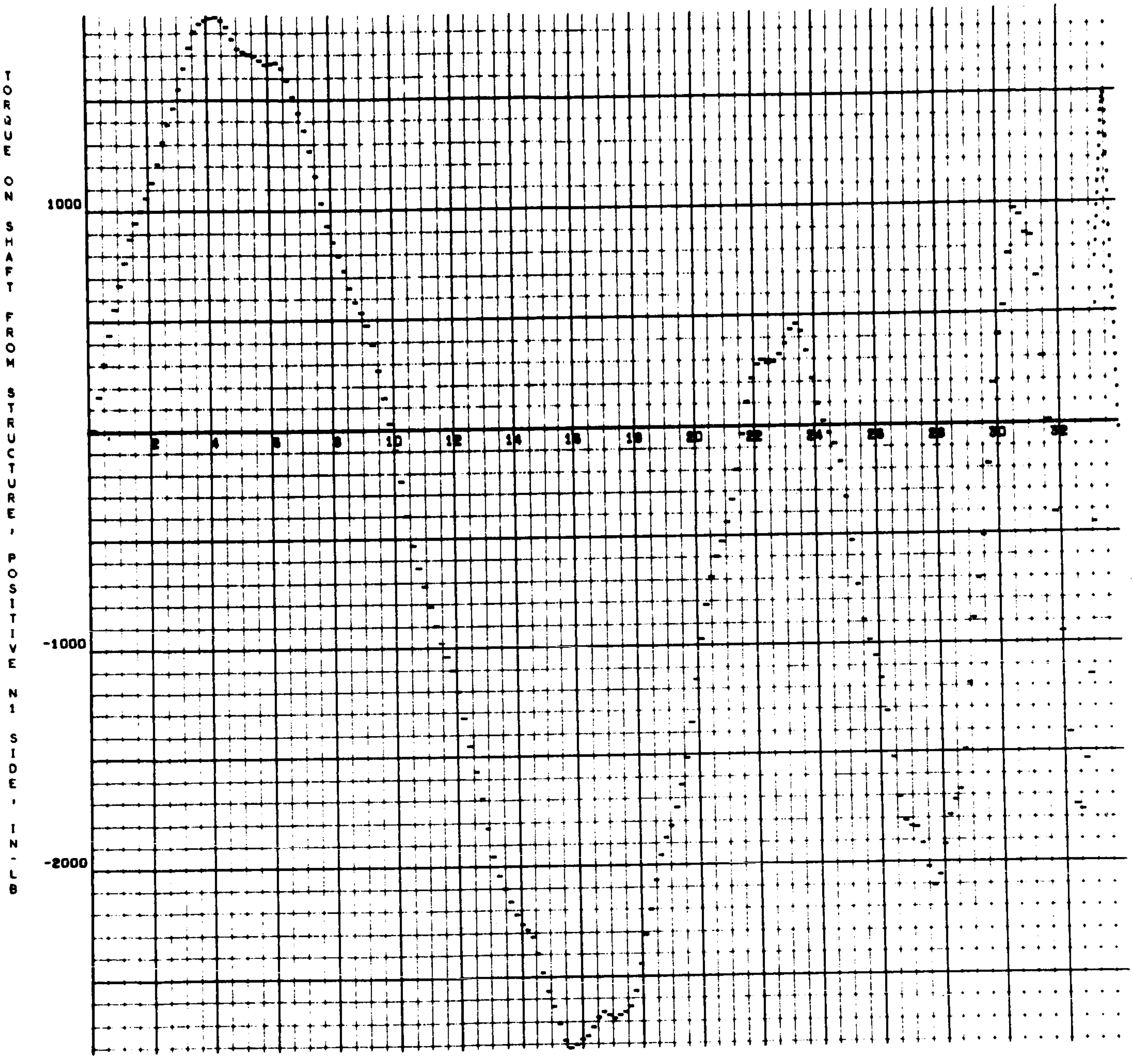

VEHICLE RIGID BODY MOTION-6 DEGR. PER SEC.-AXIS 3 TIME, SEC.

5021 23

451450
000 037

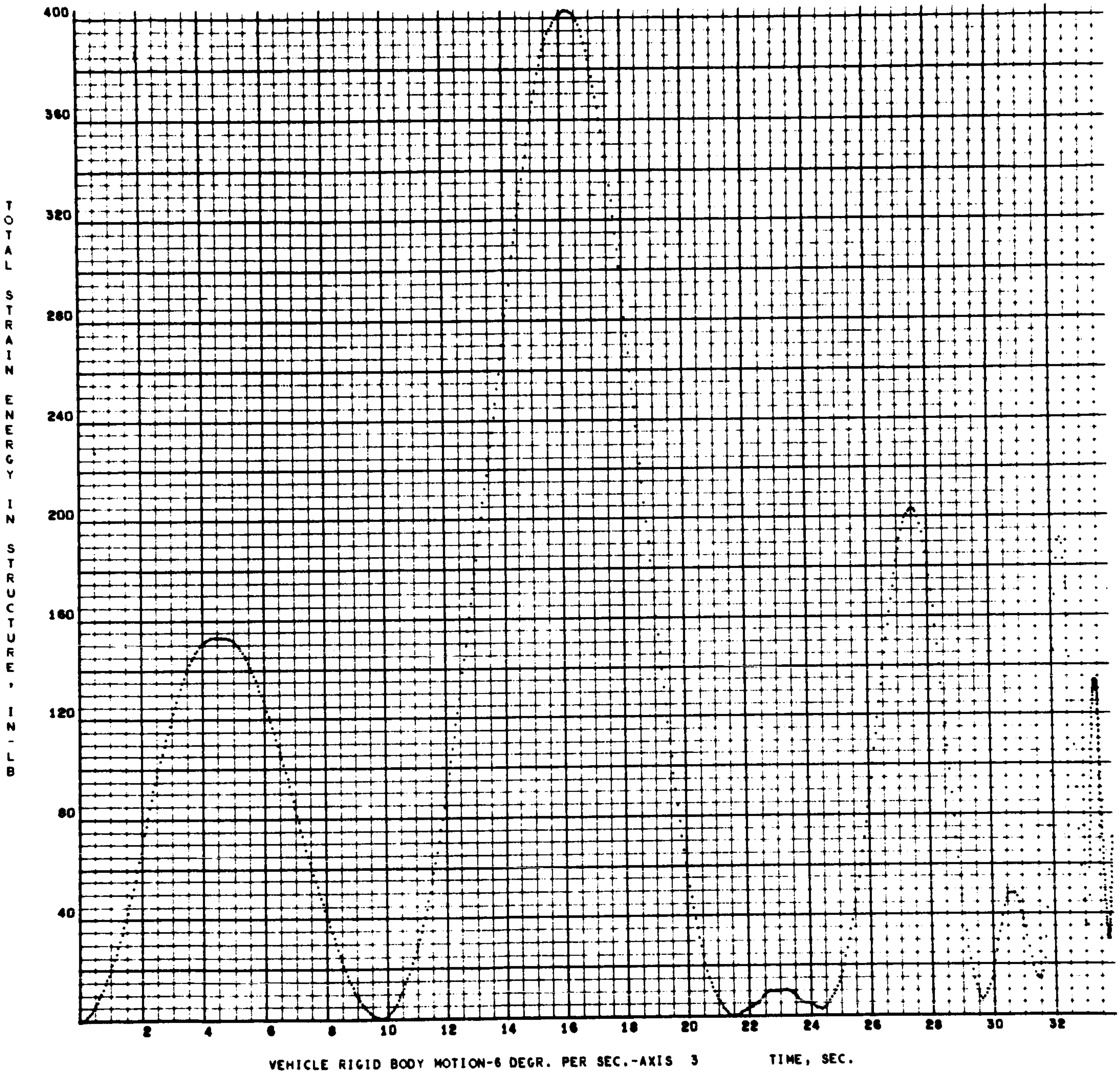

5021 24

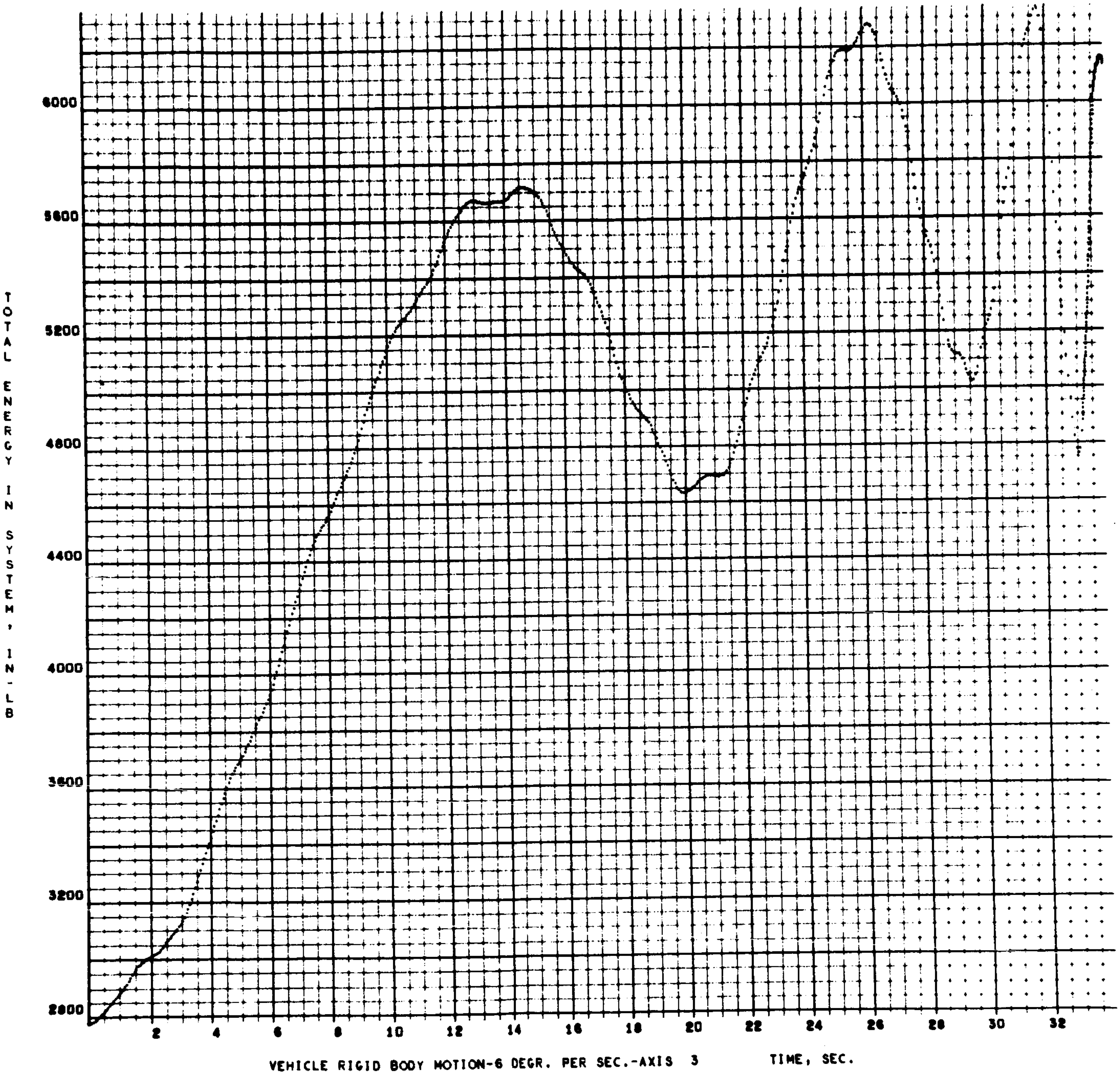
TOTAL ENERGY IN SYSTEM, IN-LB
6000
5600
5200
4800
4400
4000
3600
3200
2800
2
4
6
8
10
12
14
16
18
20
22
24
26
28
30
32
VEHICLE RIGID BODY MOTION-6 DEGR. PER SEC.-AXIS 3
TIME, SEC.

5021 25

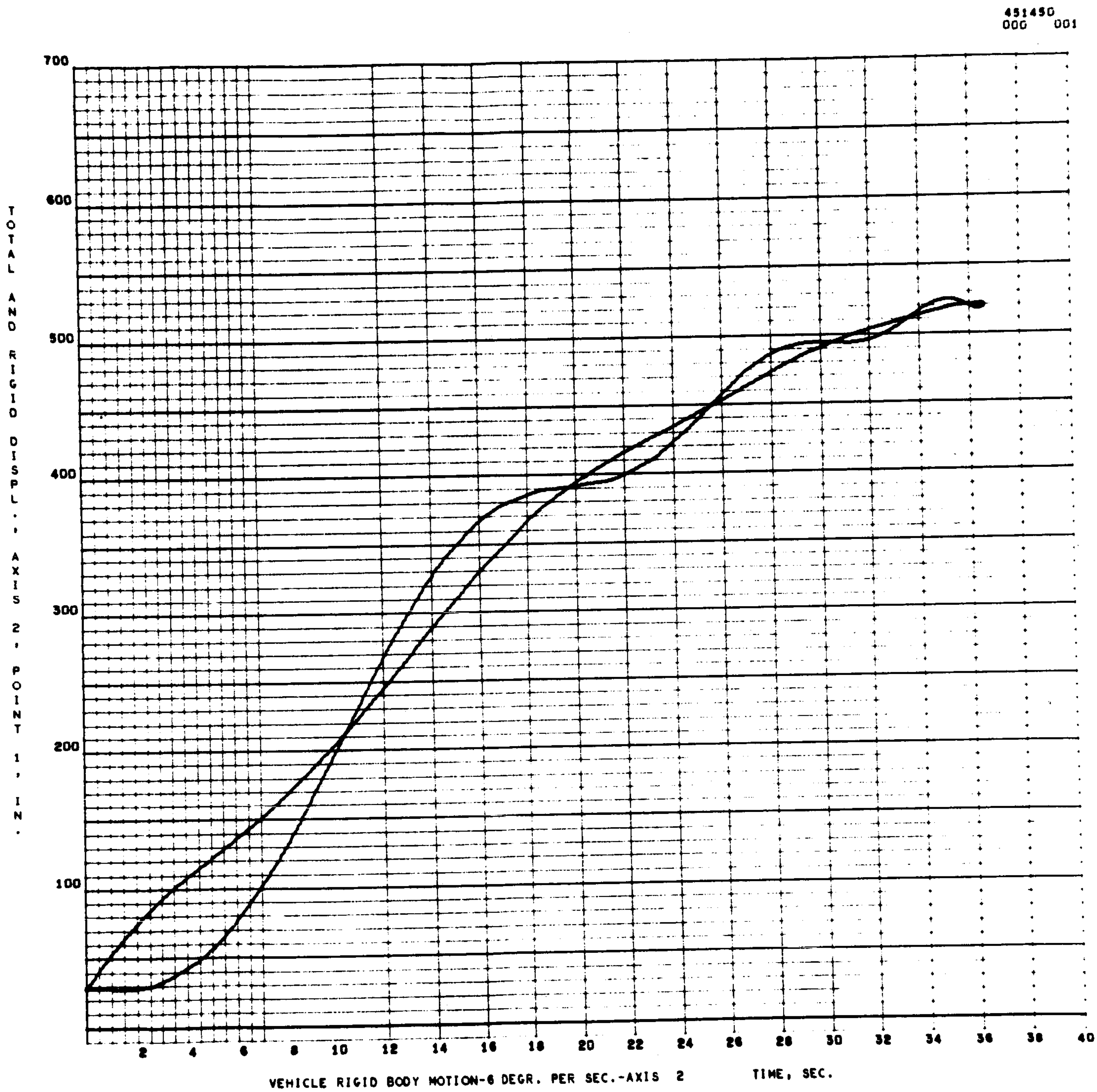
451450
000 001
TOTAL AND RIGID DISPL., AXIS 2, POINT 1, IN.
700
600
500
400
300
200
100
2
4
6
8
10
12
14
16
18
20
22
24
26
28
30
32
34
36
38
40
VEHICLE RIGID BODY MOTION-6 DEGR. PER SEC.-AXIS 2
TIME, SEC.

5022 26

451450
000 007

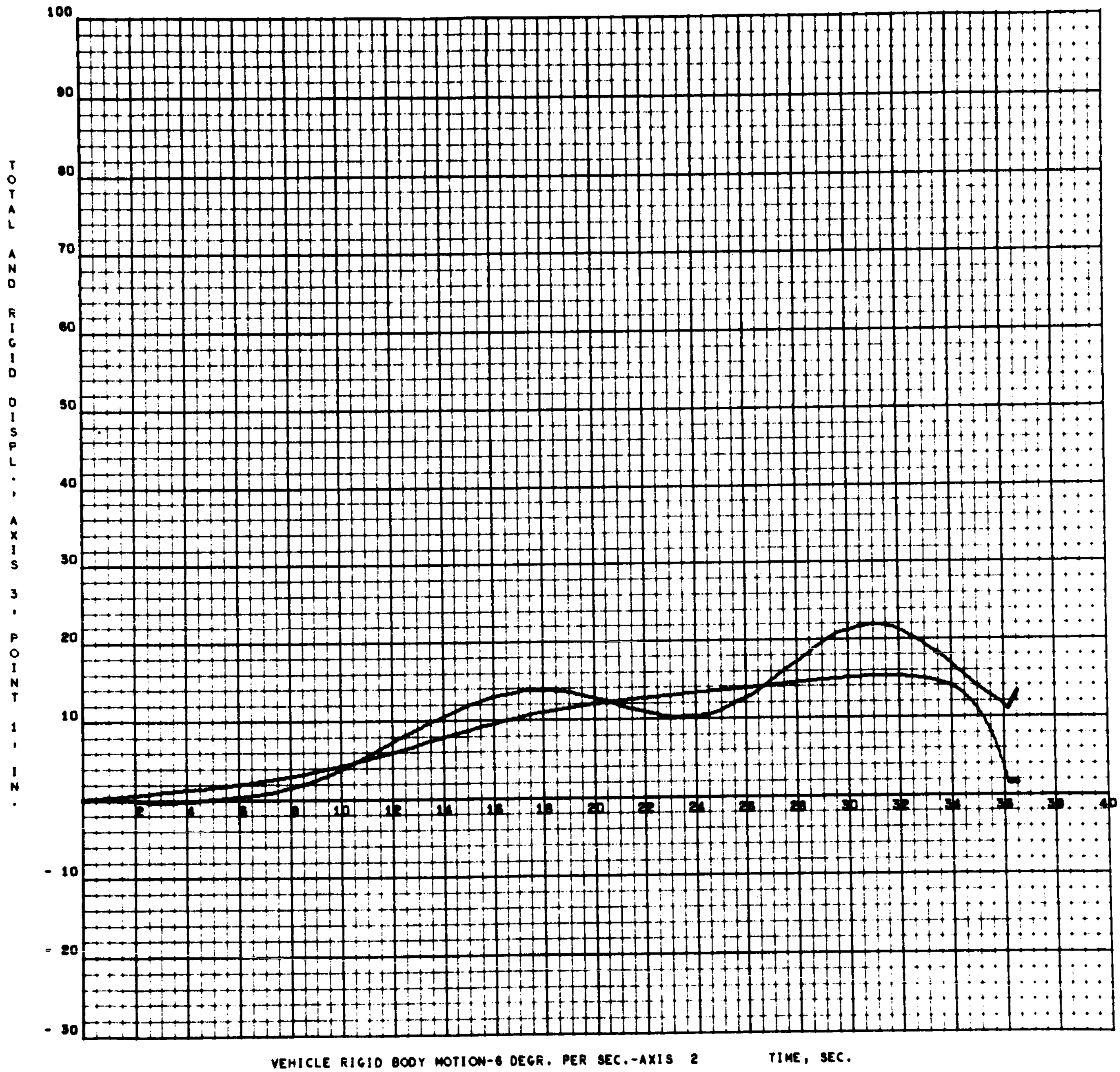

5022 27

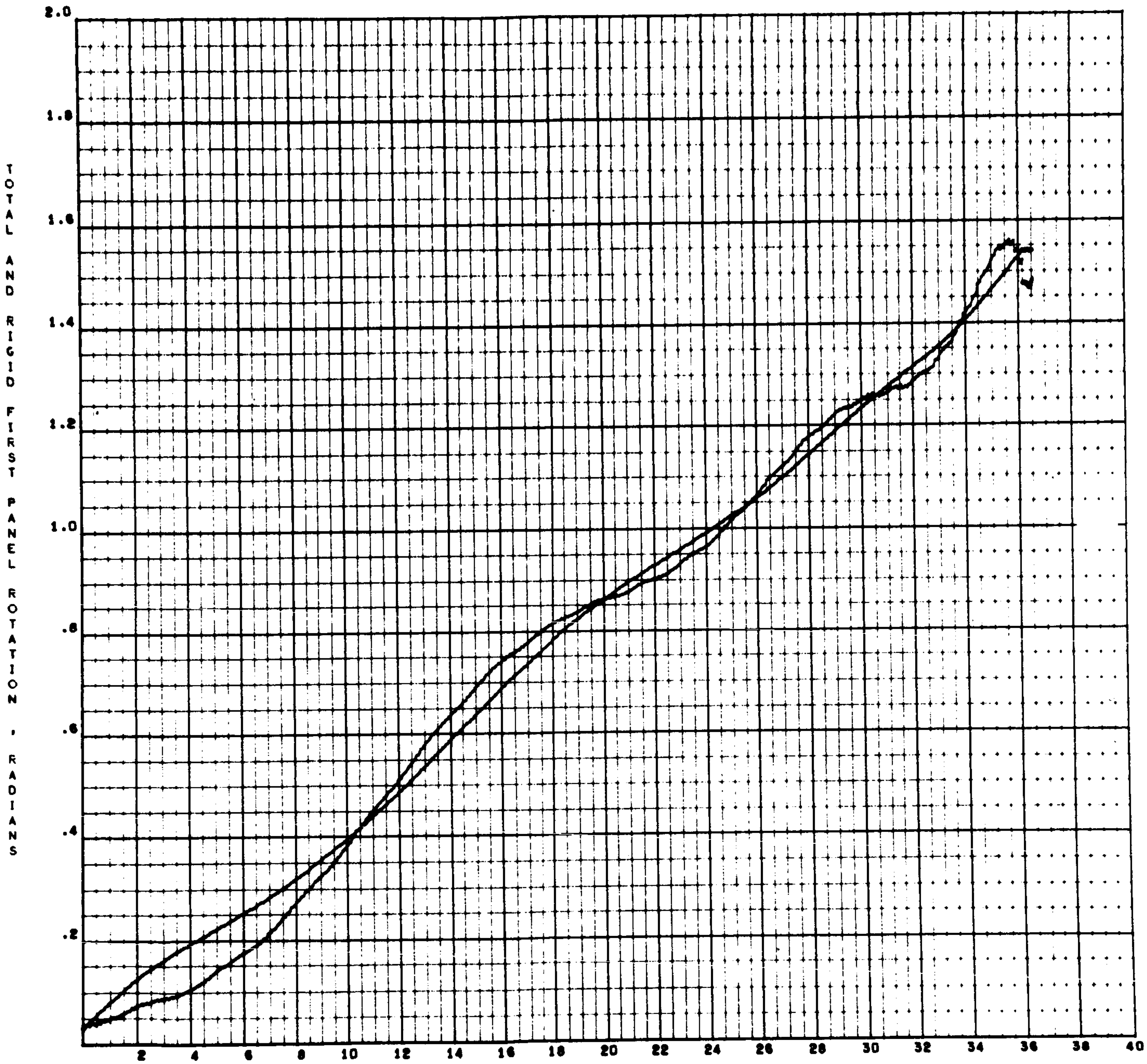

VEHICLE RIGID BODY MOTION-6 DEGR. PER SEC.-AXIS 2

5022 28

451450
000 020

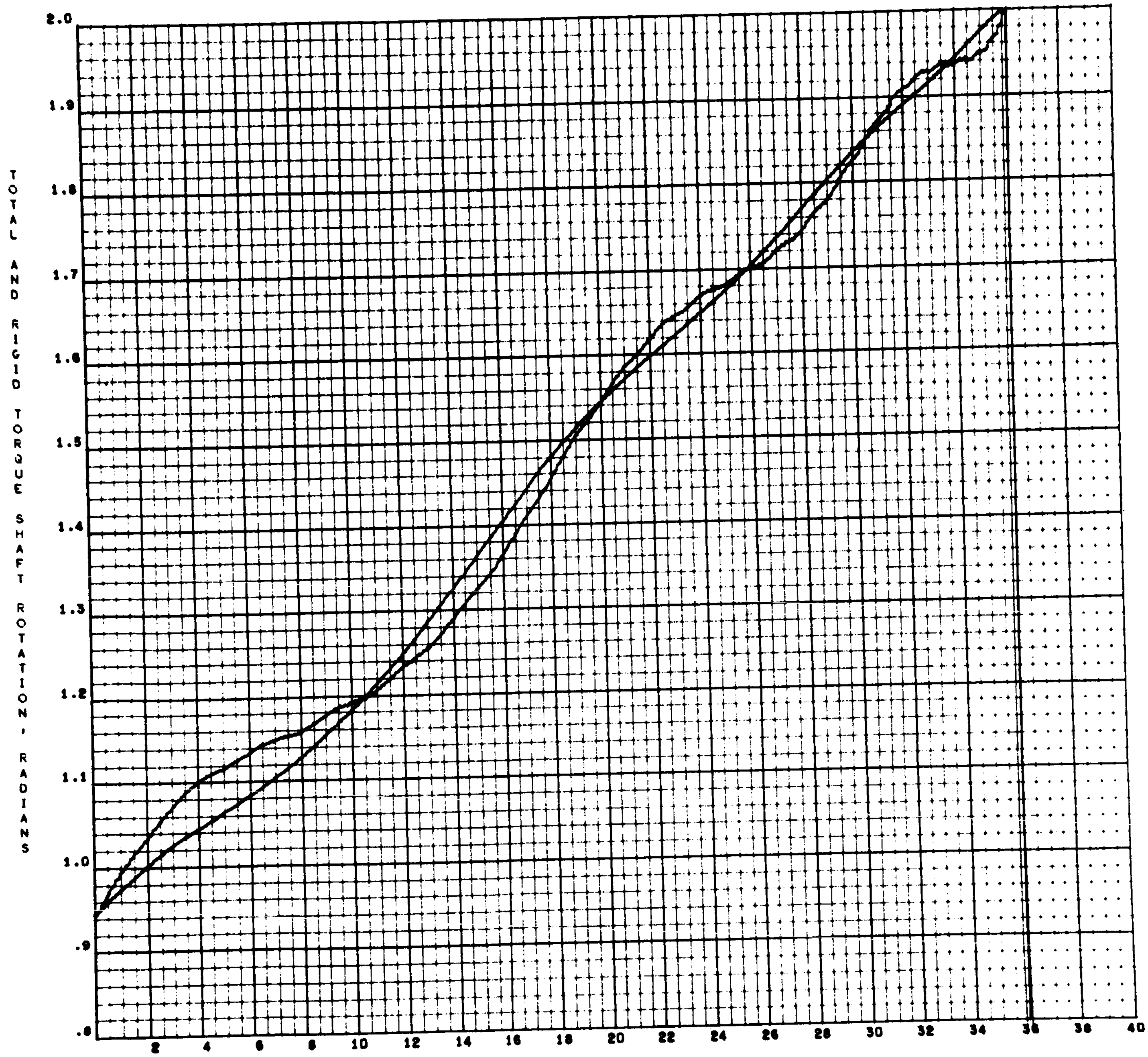

VEHICLE RIGID BODY MOTION-6 DEGR. PER SEC.-AXIS 2

5022 29

451450
000 022

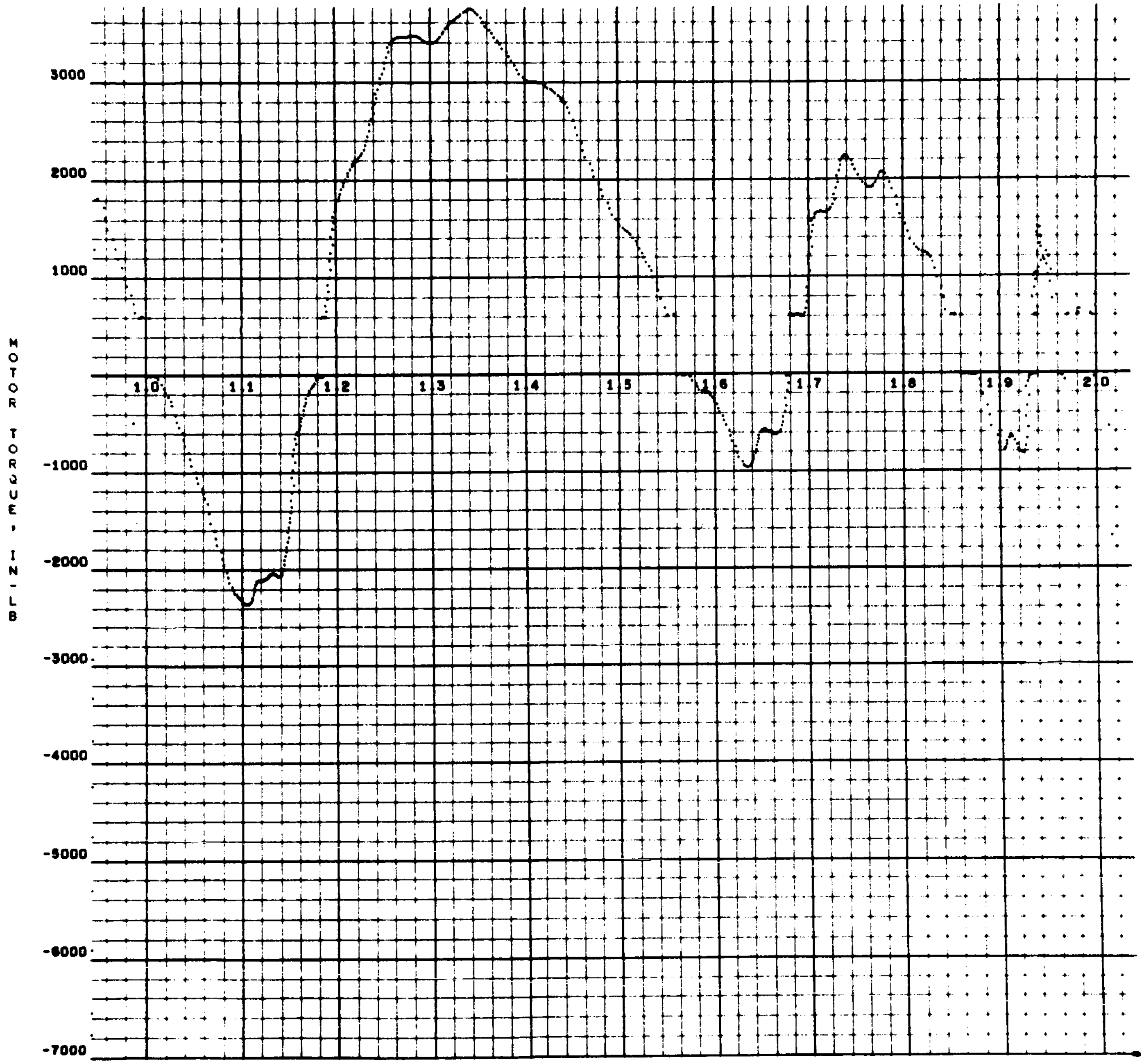

VEH. RIGID B. MOTION-6 DEGR.PER SEC.AXIS 2 -TOTAL T. SHAFT ROT., RAD.

5022 30

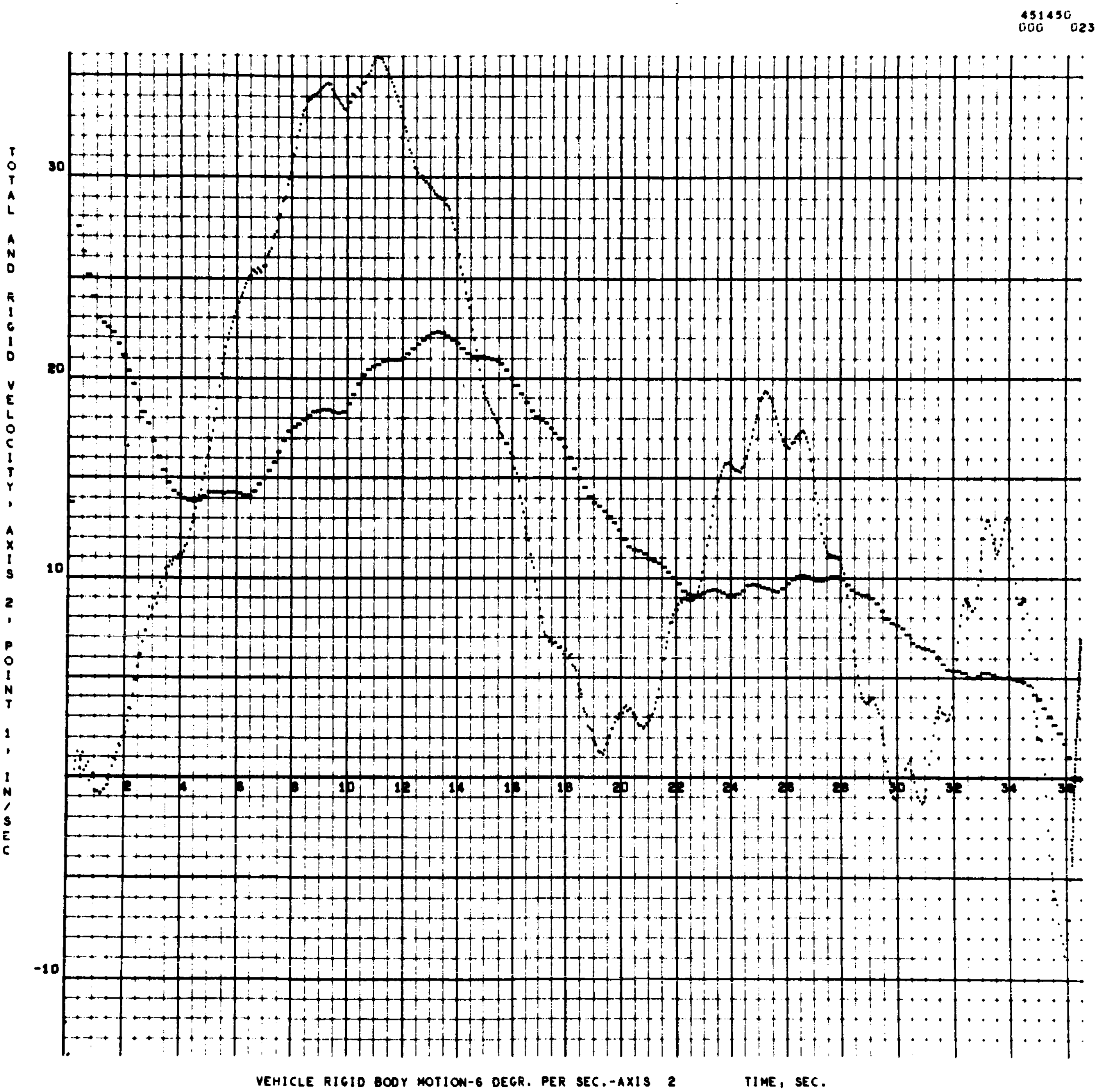
451450
000 023
TOTAL AND RIGID VELOCITY, AXIS 2, POINT 1, IN/SEC
30
20
10
-10
2
4
6
8
10
12
14
16
18
20
22
24
26
28
30
32
34
36
VEHICLE RIGID BODY MOTION-6 DEGR. PER SEC.-AXIS 2
TIME, SEC.

5022 31

451450
000 029

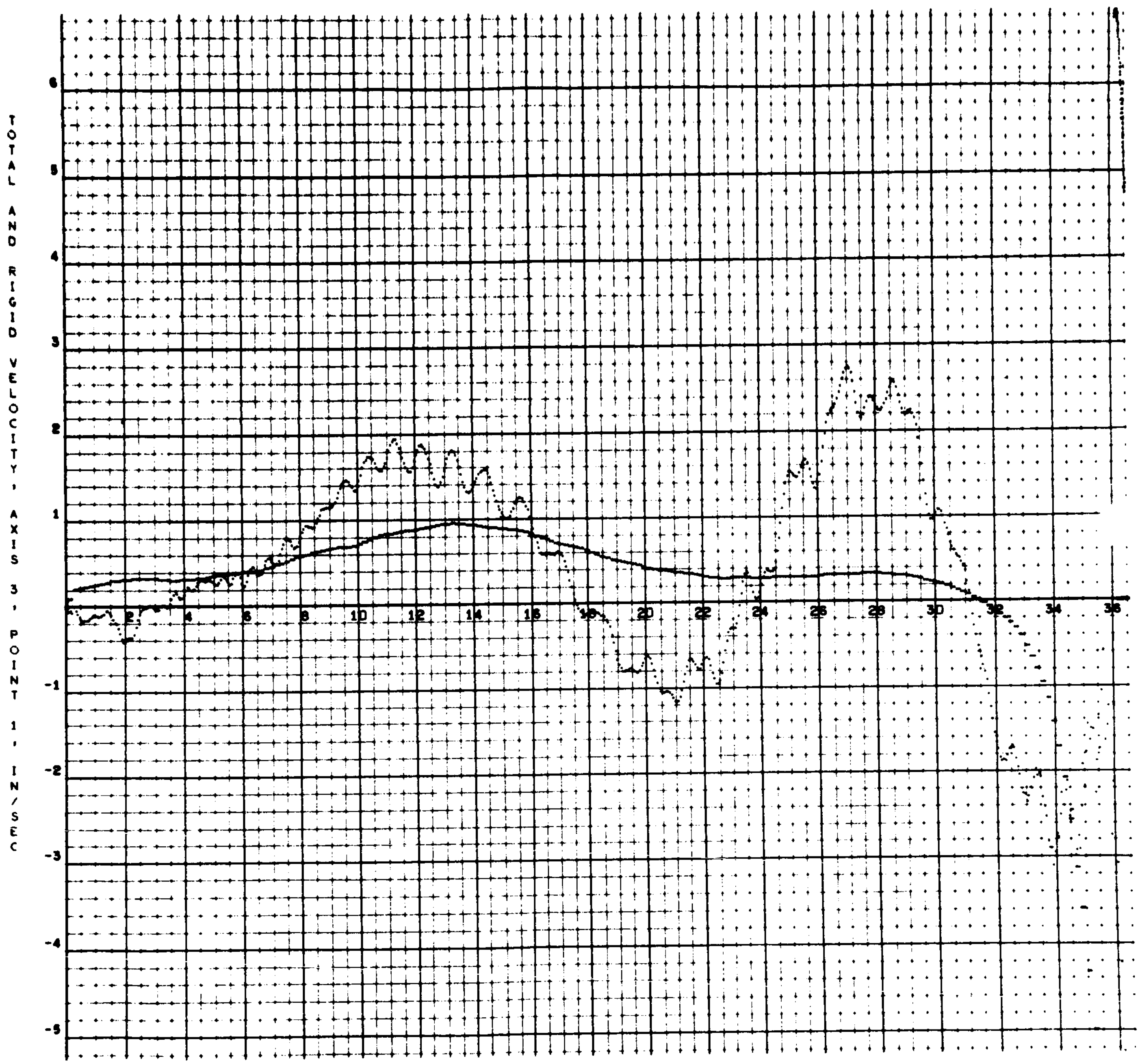

VEHICLE RIGID BODY MOTION-6 DEGR. PER SEC.-AXIS 2 TIME, SEC.

5022 32

451450
000 035

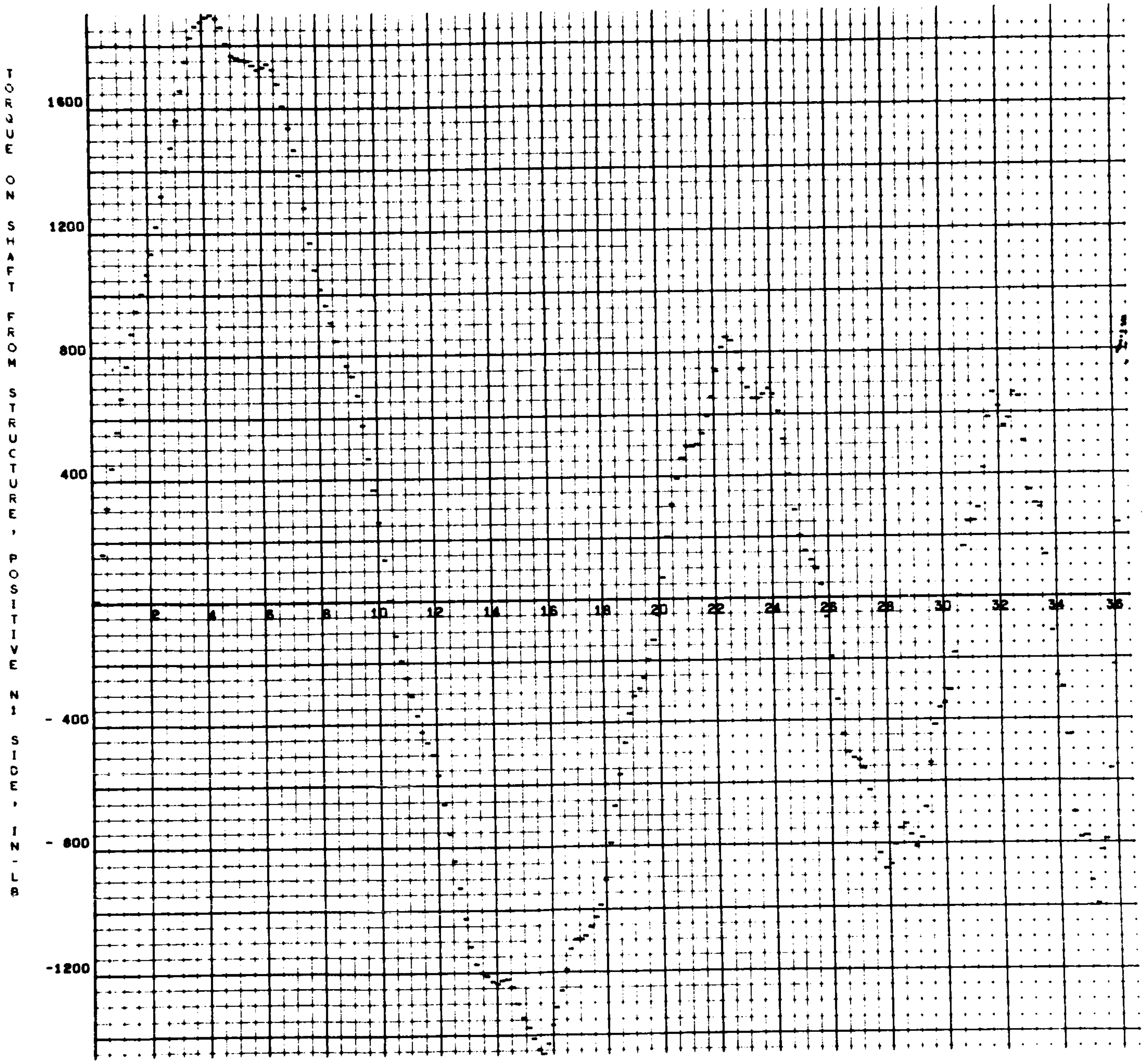

VEHICLE RIGID BODY MOTION-6 DEGR. PER SEC.-AXIS 2 TIME, SEC.

5022 33

451450
000 037

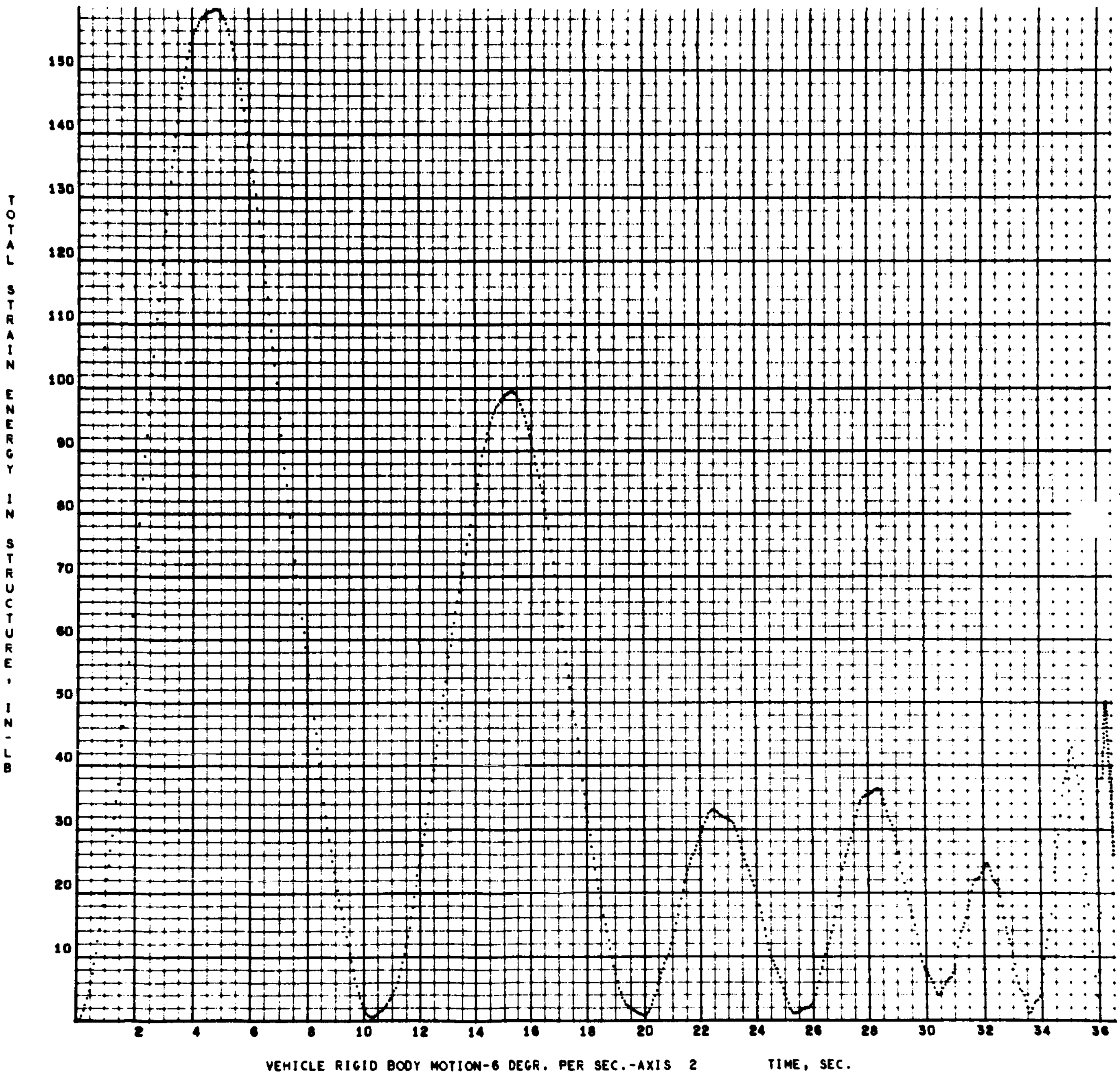

5022 34

451450
000 038

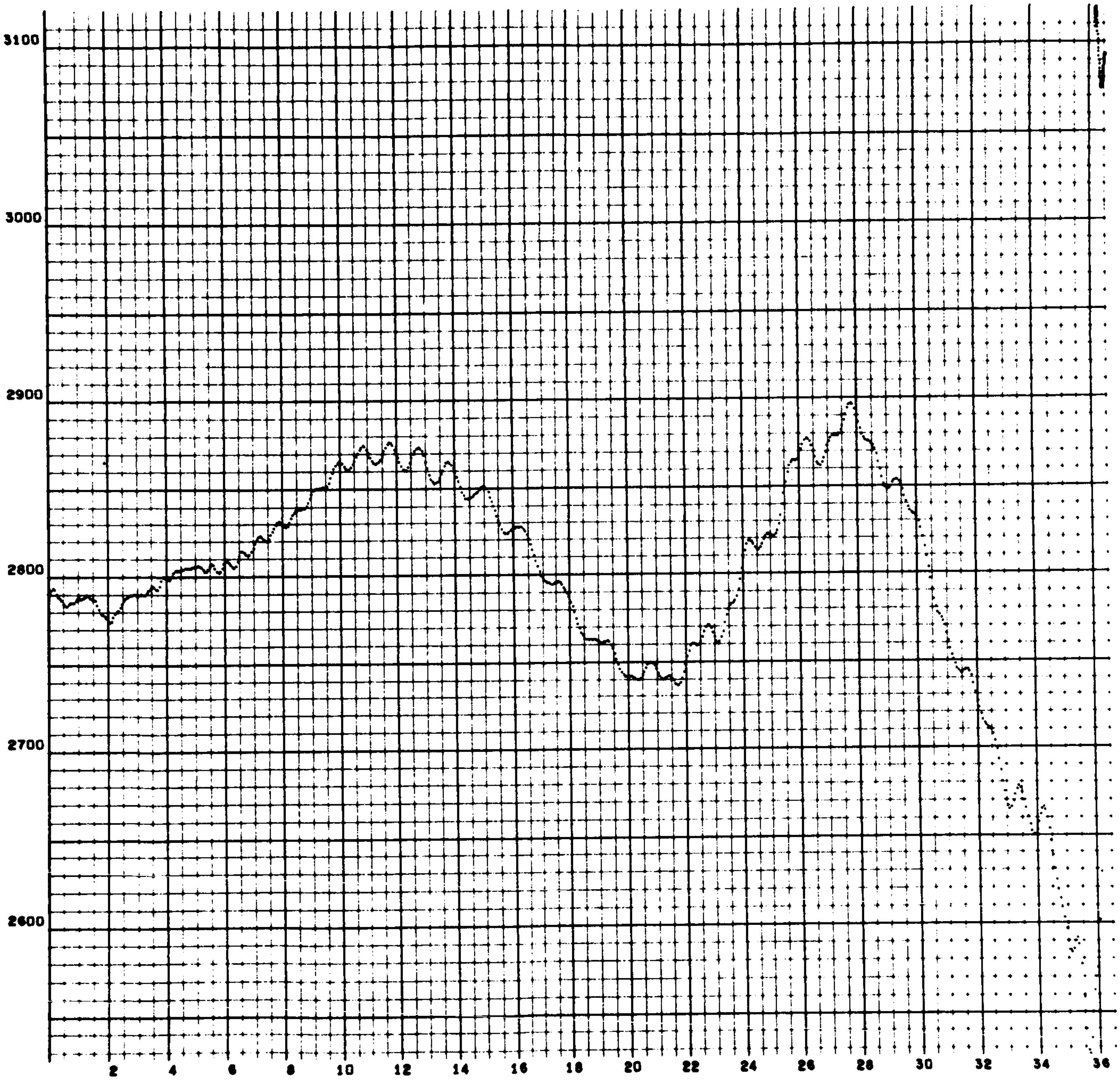

VEHICLE RIGID BODY MOTION-6 DEGR. PER SEC.-AXIS 2 TIME, SEC.

5022 35

451450
000 001

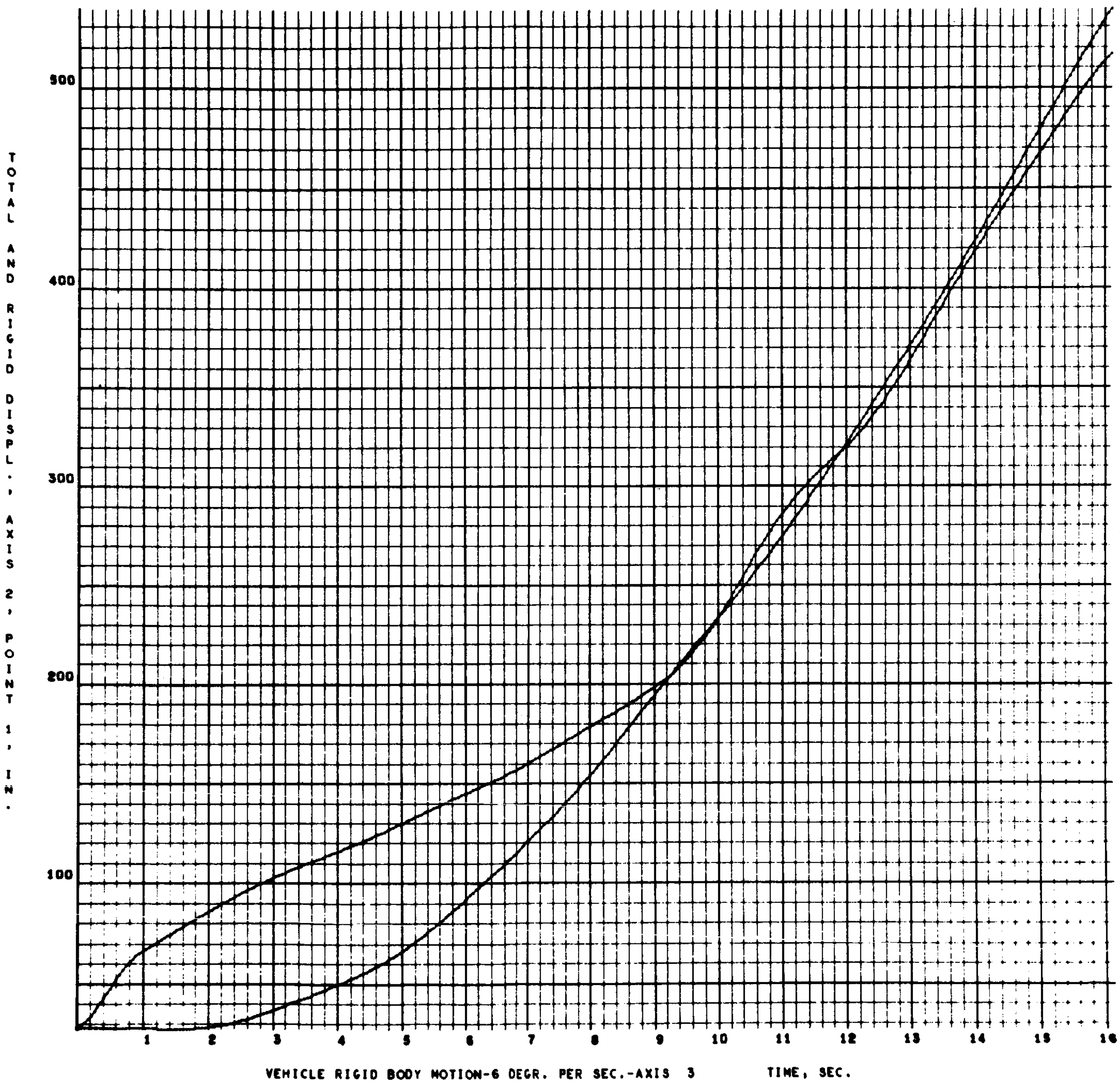

6739 36

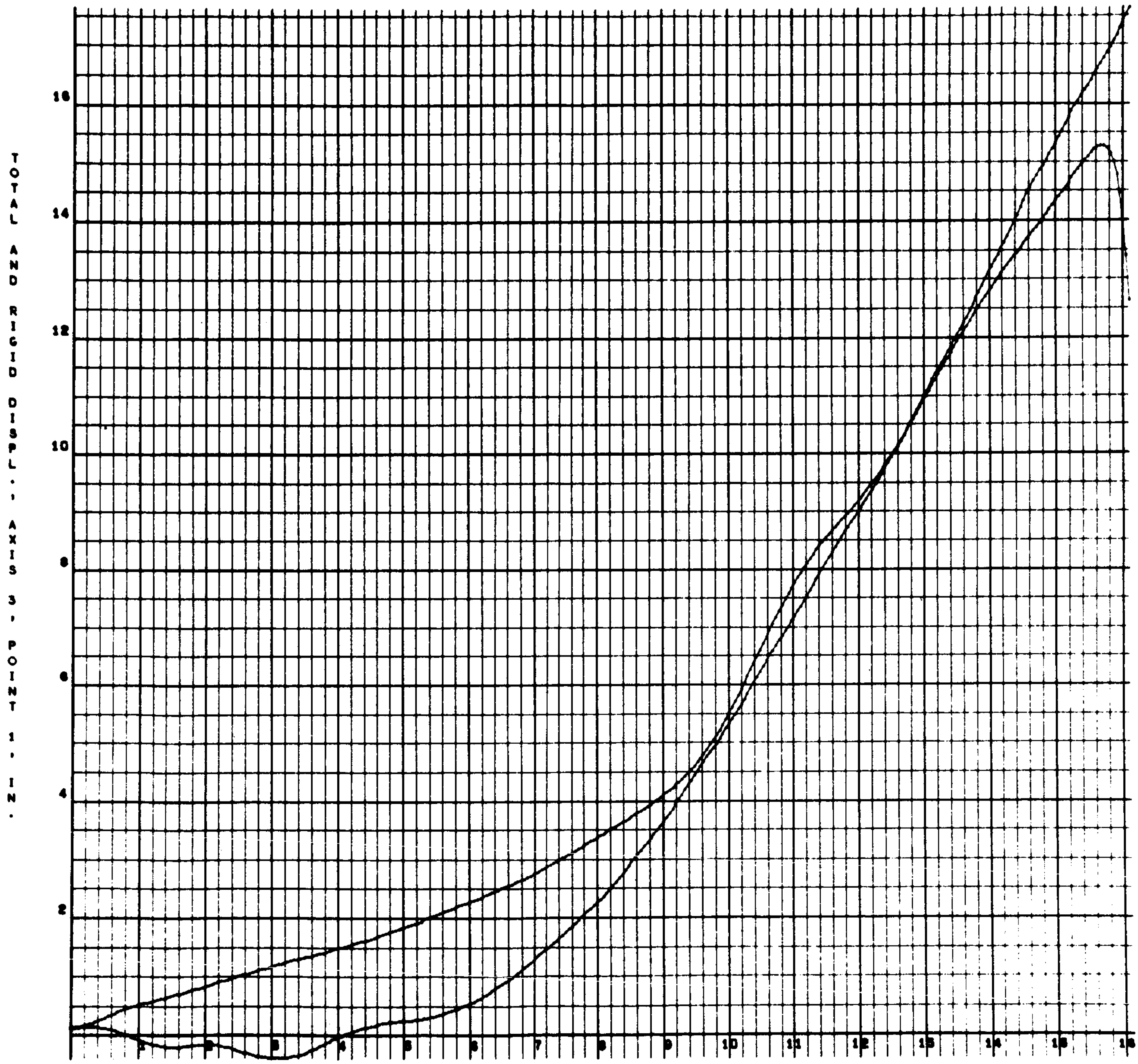

VEHICLE RIGID BODY MOTION-6 DEGR. PER SEC.-AXIS 3 TIME, SEC.

6739 37

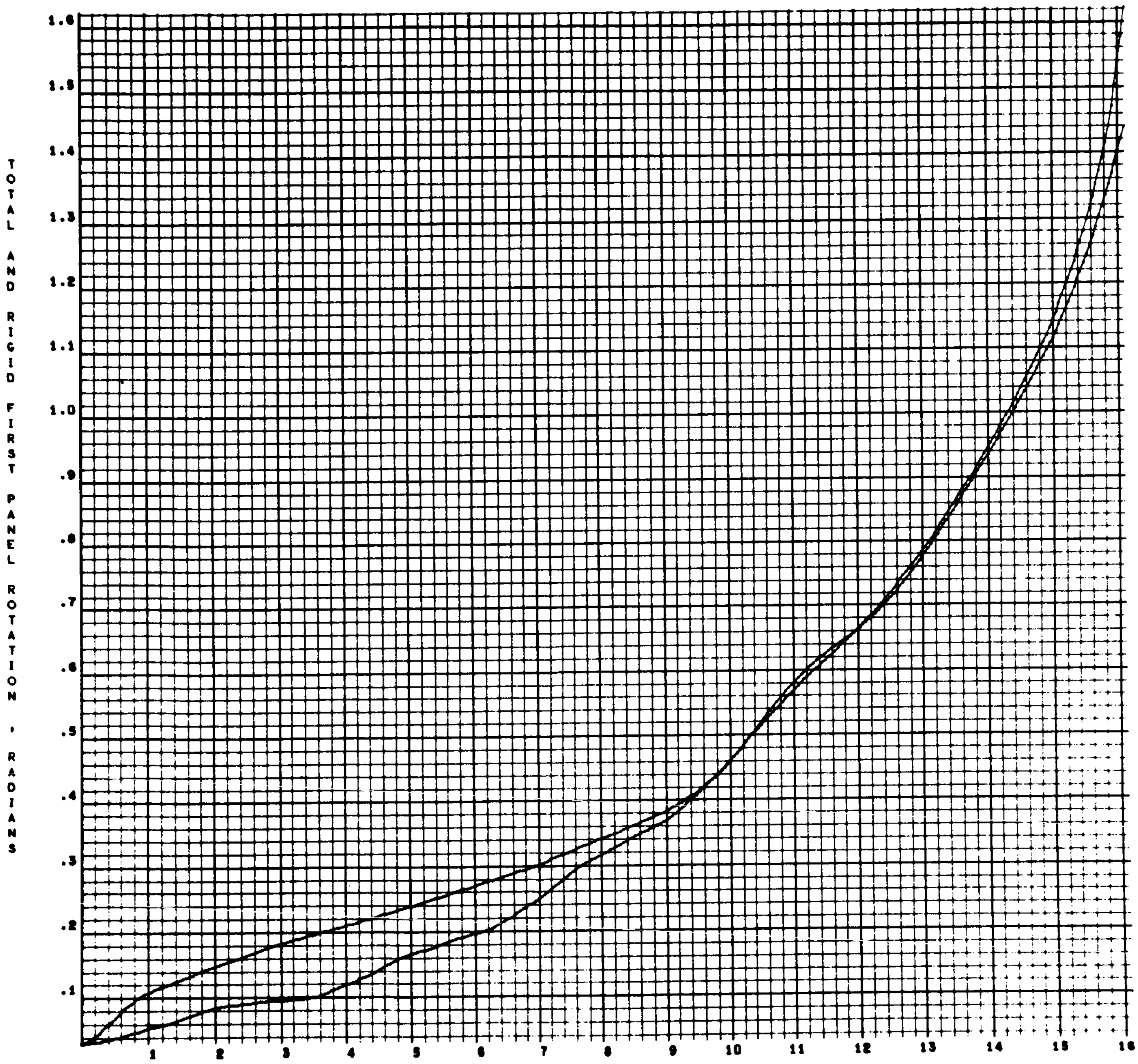

VEHICLE RIGID BODY MOTION-6 DEGR. PER SEC.-AXIS 3

6739 38

451450
000 013

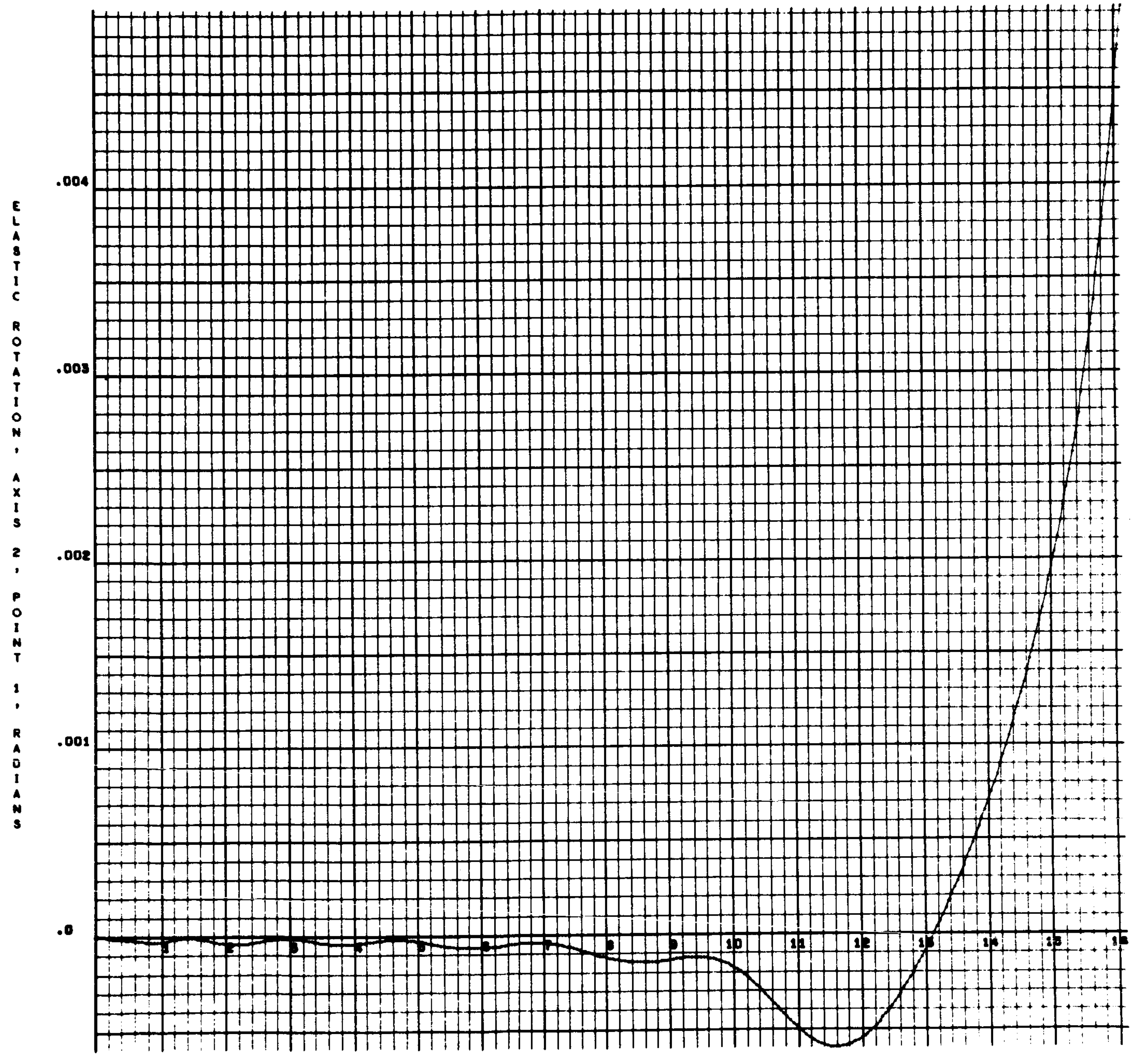

VEHICLE RIGID BODY MOTION-6 DEGR. PER SEC.-AXIS 3

6739 39

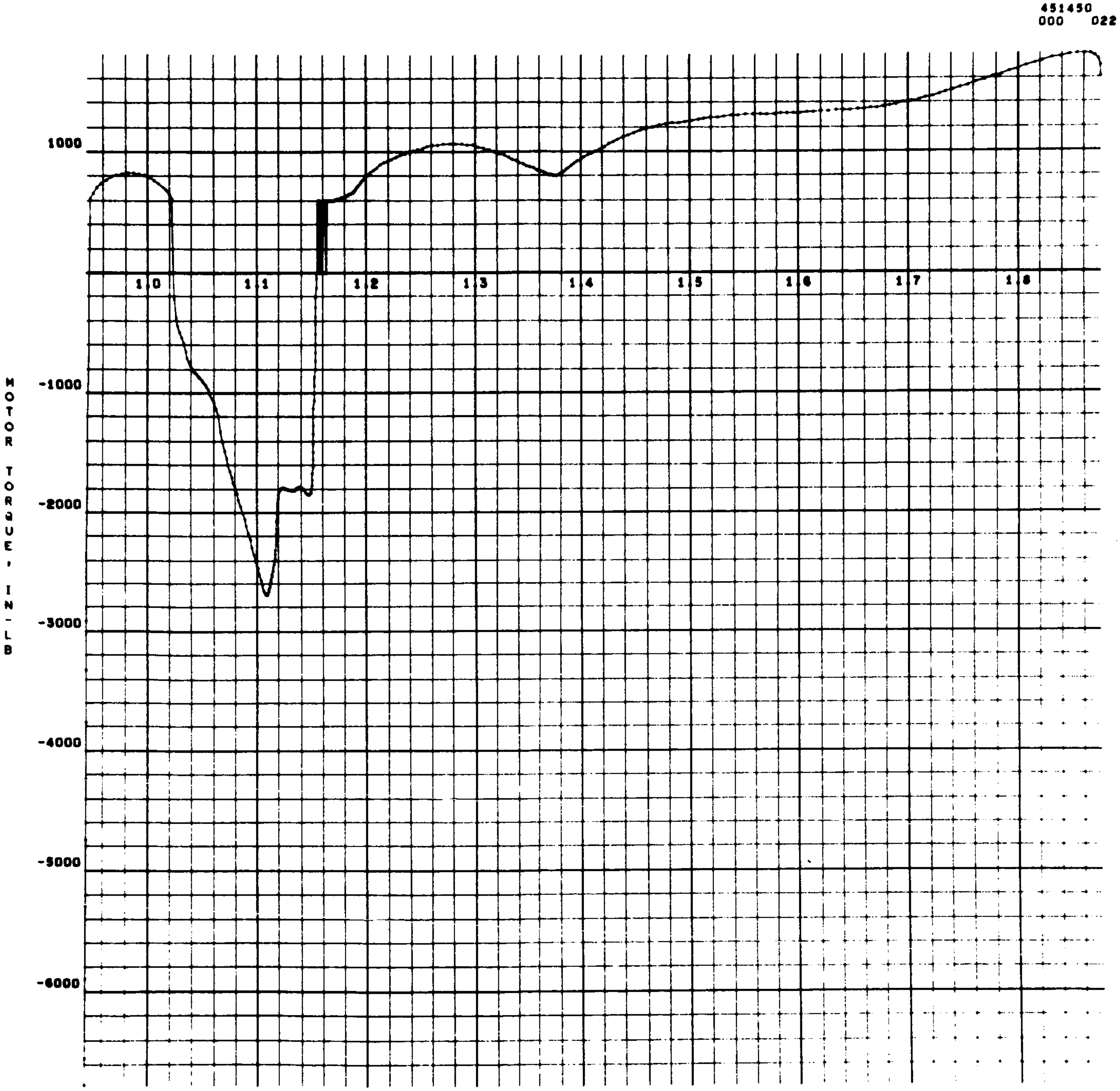

VEH. RIGID B. MOTION-6 DEGR.PER SEC.AXIS 3 -TOTAL T. SHAFT ROT., RAD.

6739 40

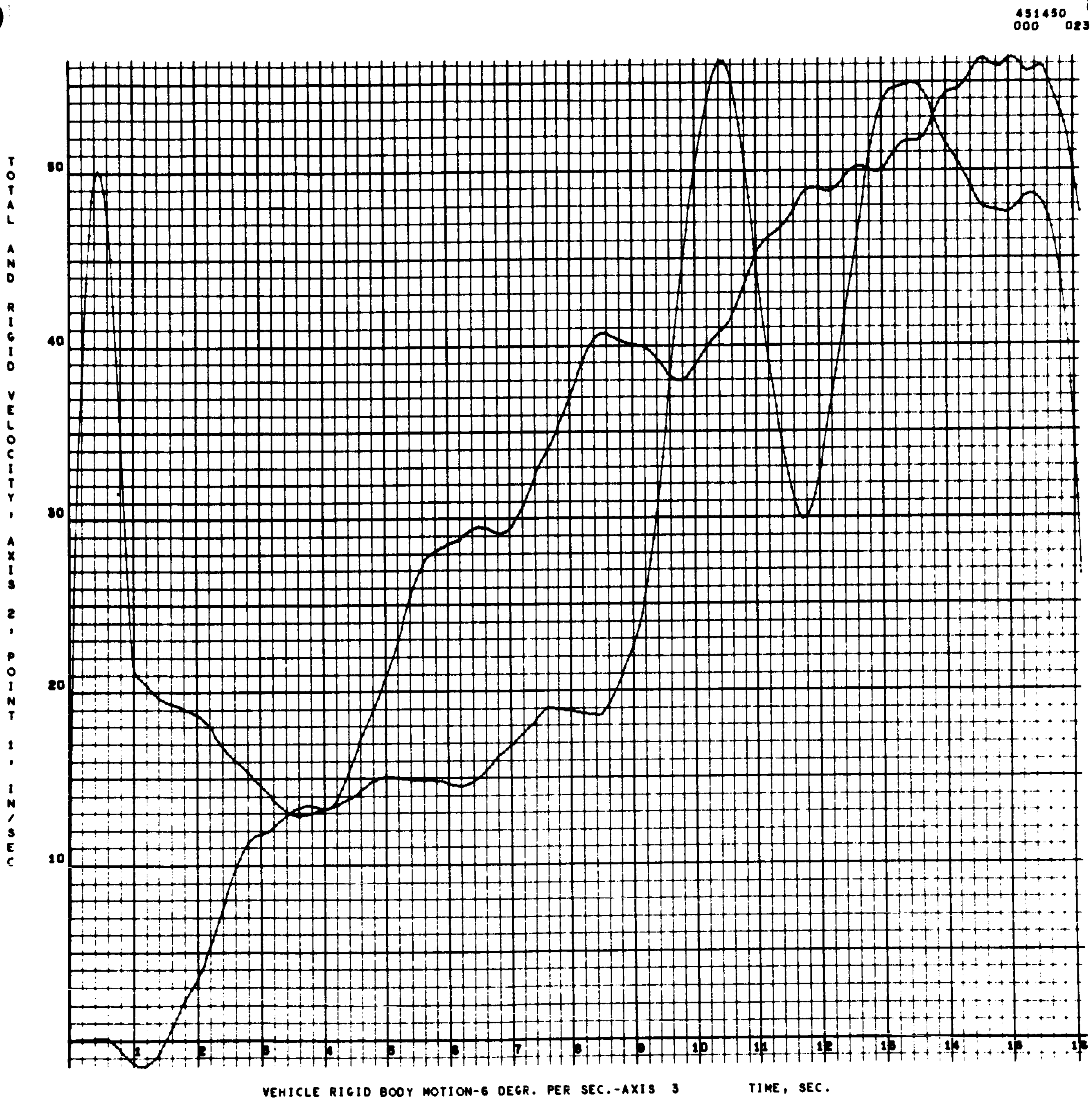
451450
000 023
TOTAL AND RIGID VELOCITY, AXIS 2, POINT 1, IN/SEC
50
40
30
20
10
1
2
3
4
5
6
7
8
9
10
11
12
13
14
15
16
VEHICLE RIGID BODY MOTION-6 DEGR. PER SEC.-AXIS 3
TIME, SEC.

6739 41

451450
000 029

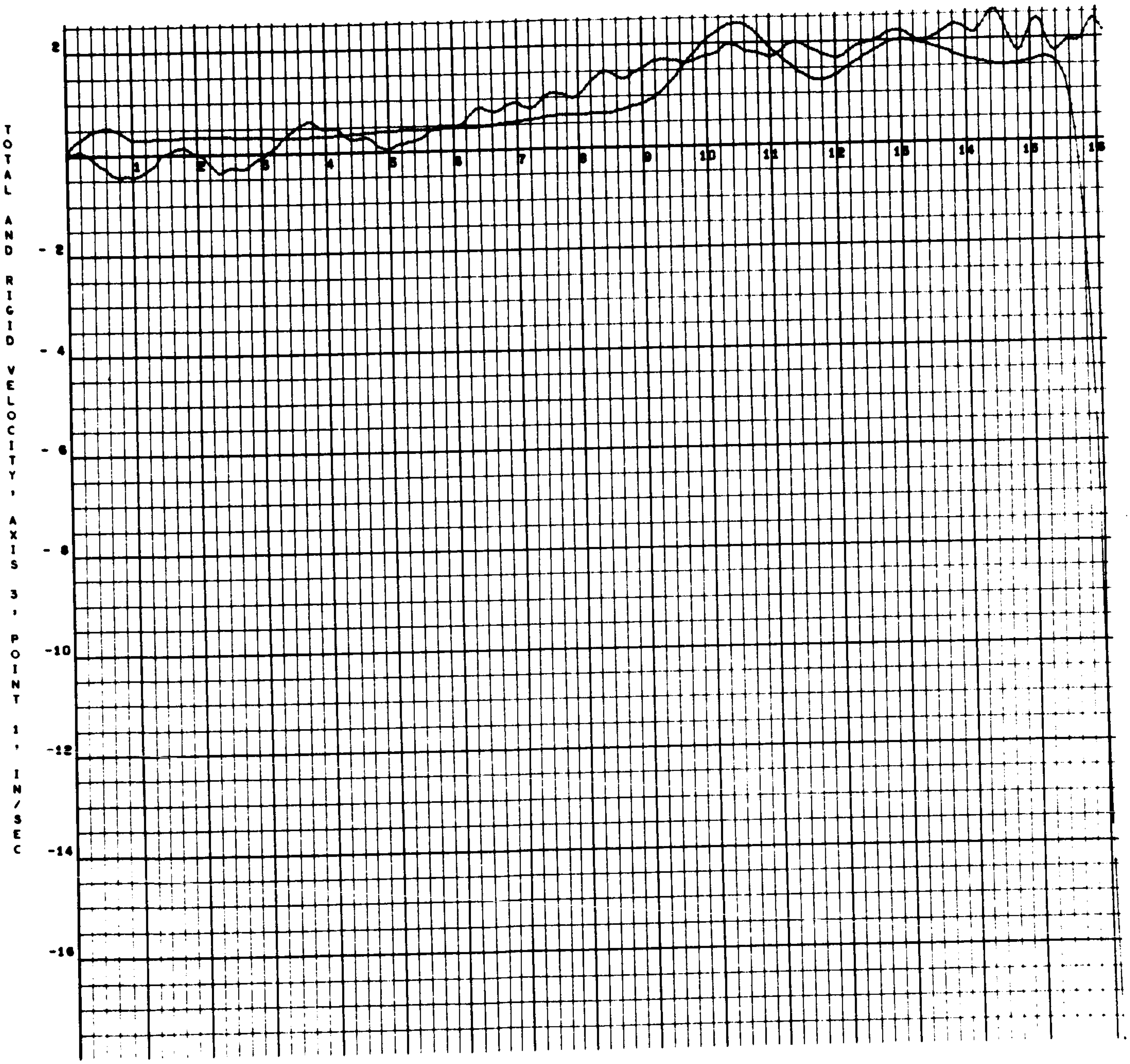

VEHICLE RIGID BODY MOTION-6 DEGR. PER SEC.-AXIS 3

6739

451450
000 035

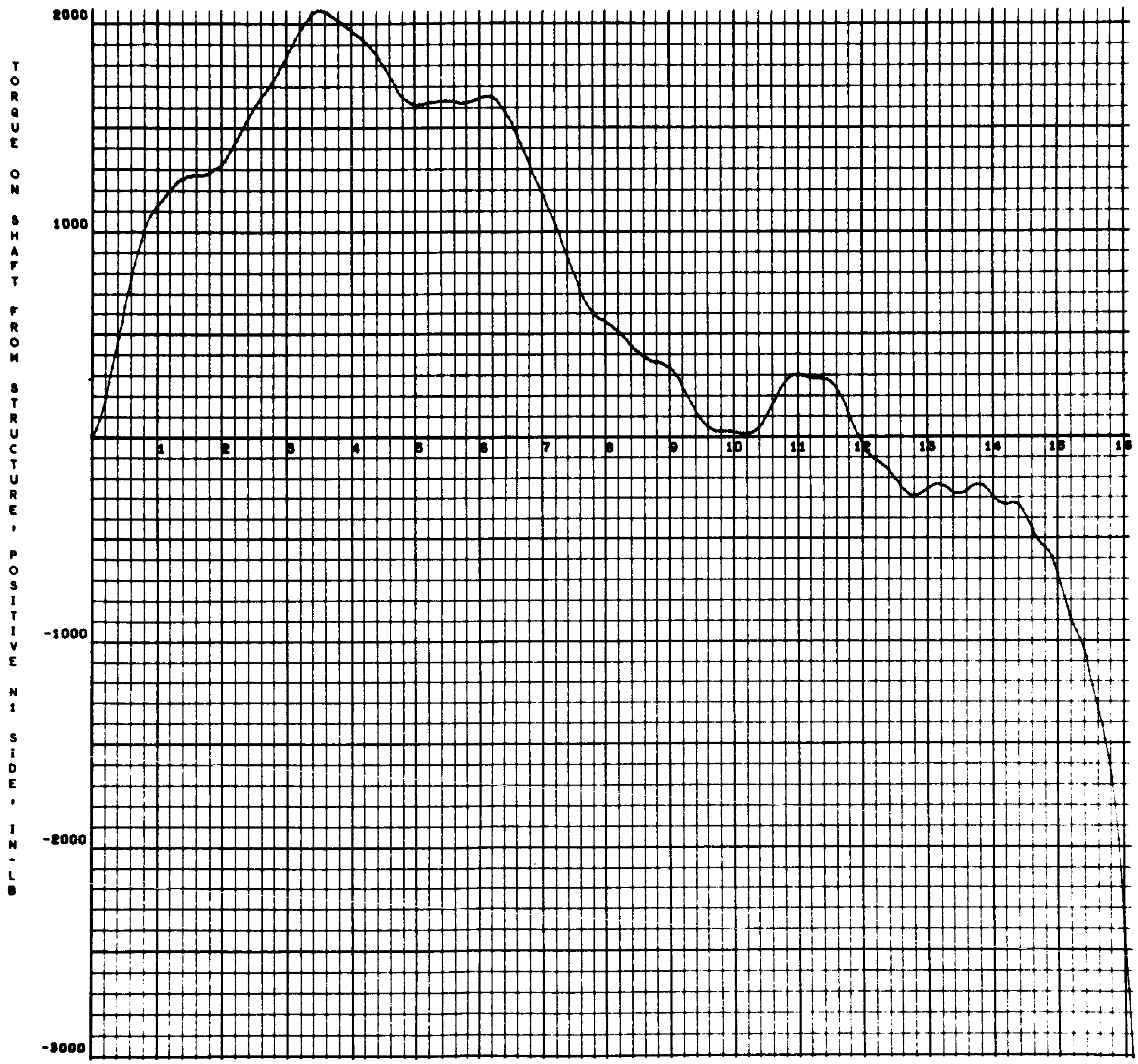

VEHICLE RIGID BODY MOTION-6 DEGR. PER SEC.-AXIS 3

6739 43

451450
000 037

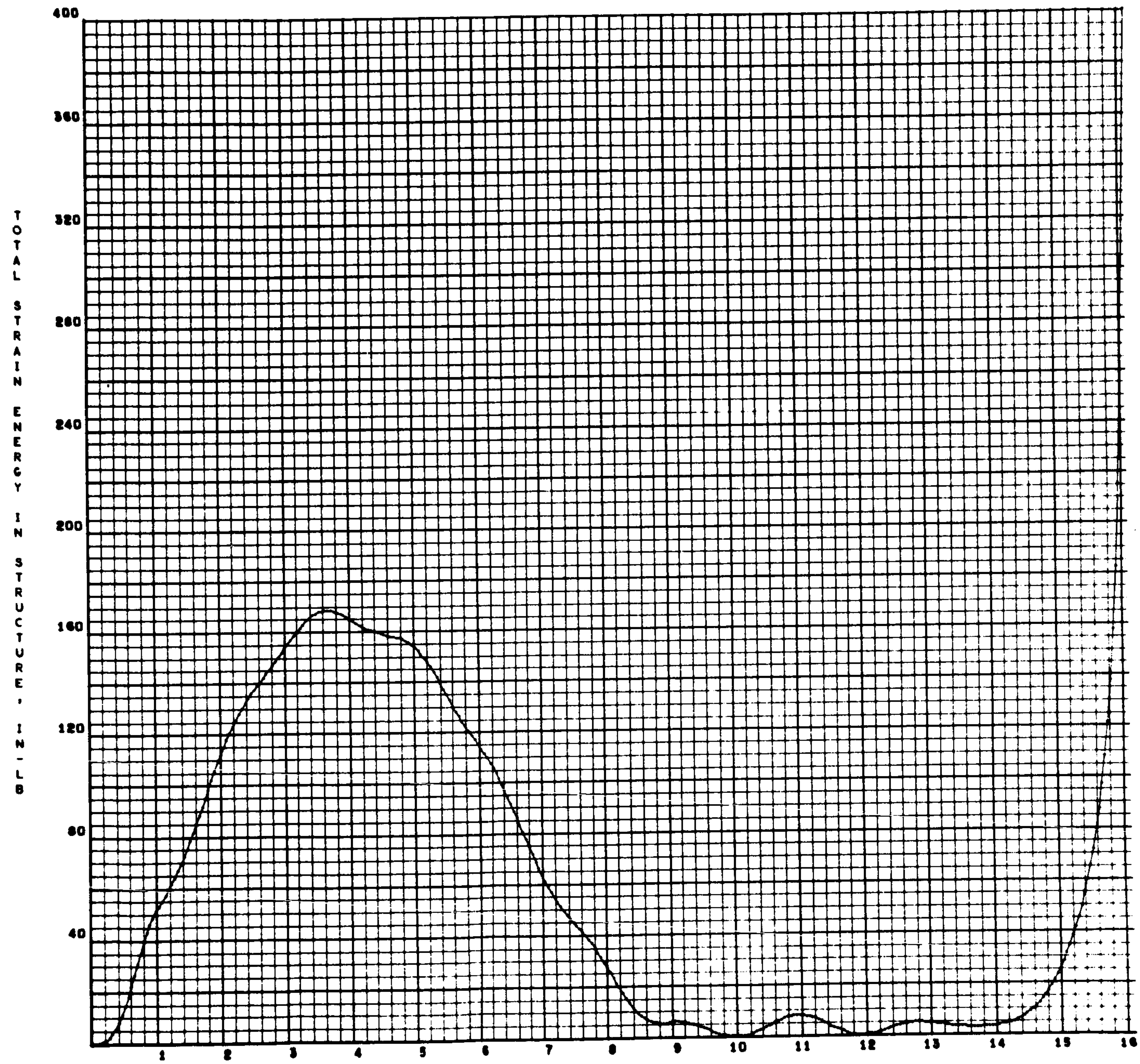

VEHICLE RIGID BODY MOTION-6 DEGR. PER SEC.-AXIS 3 TIME, SEC.

6739 44

451450
000 038

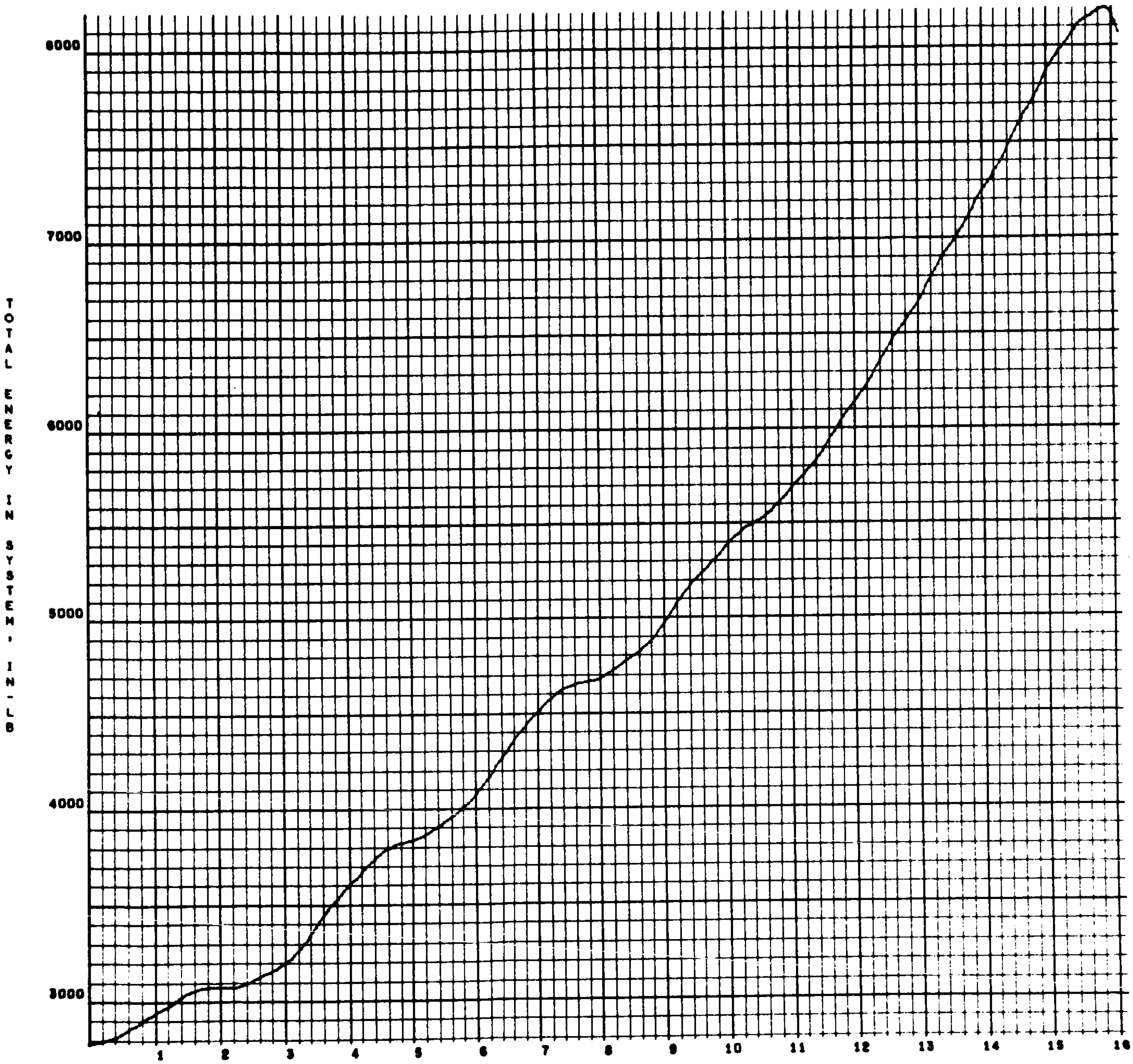

VEHICLE RIGID BODY MOTION-6 DEGR. PER SEC.-AXIS 3

6739 45

451450
000 001

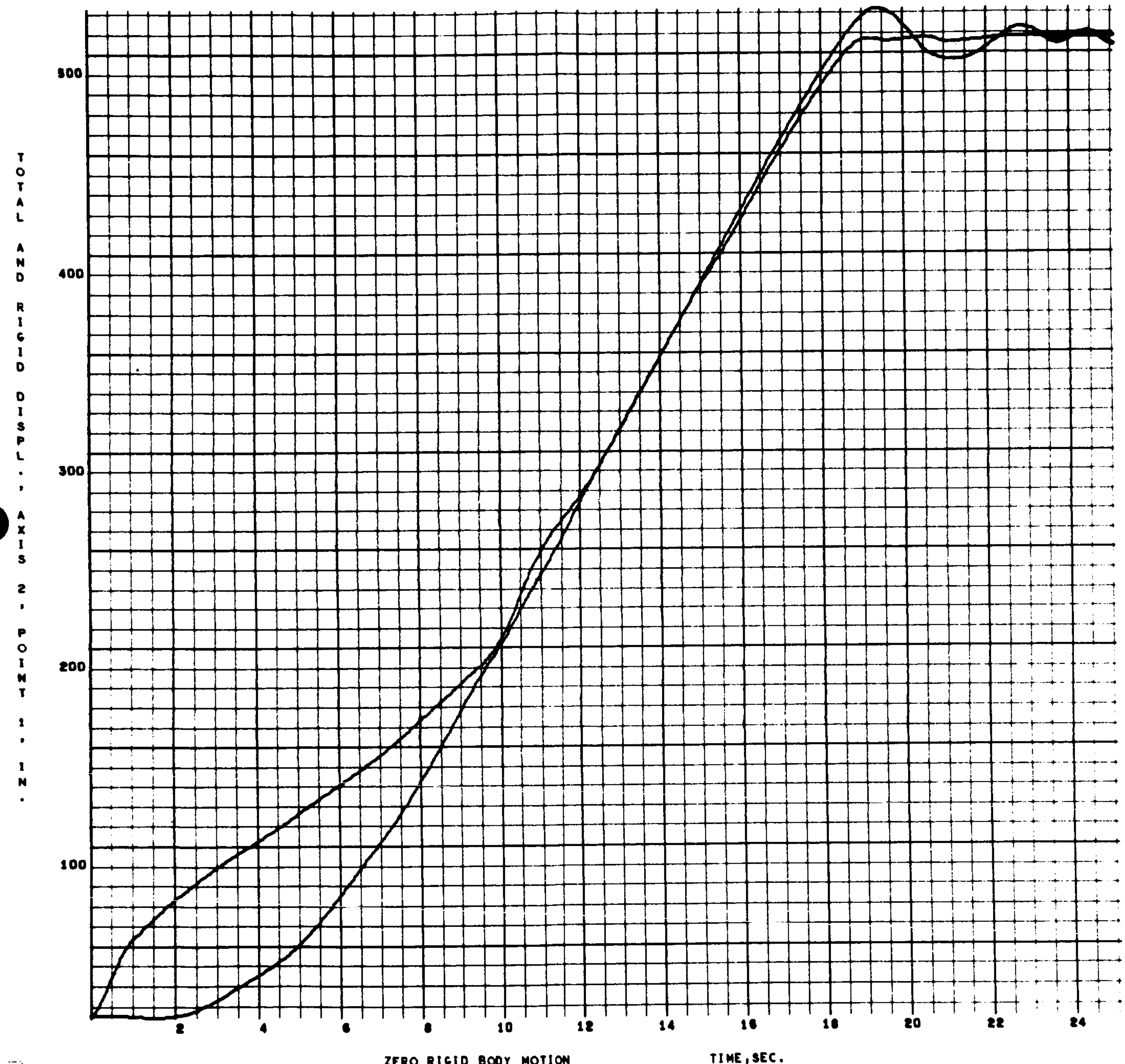

9828 46

451450
000 007

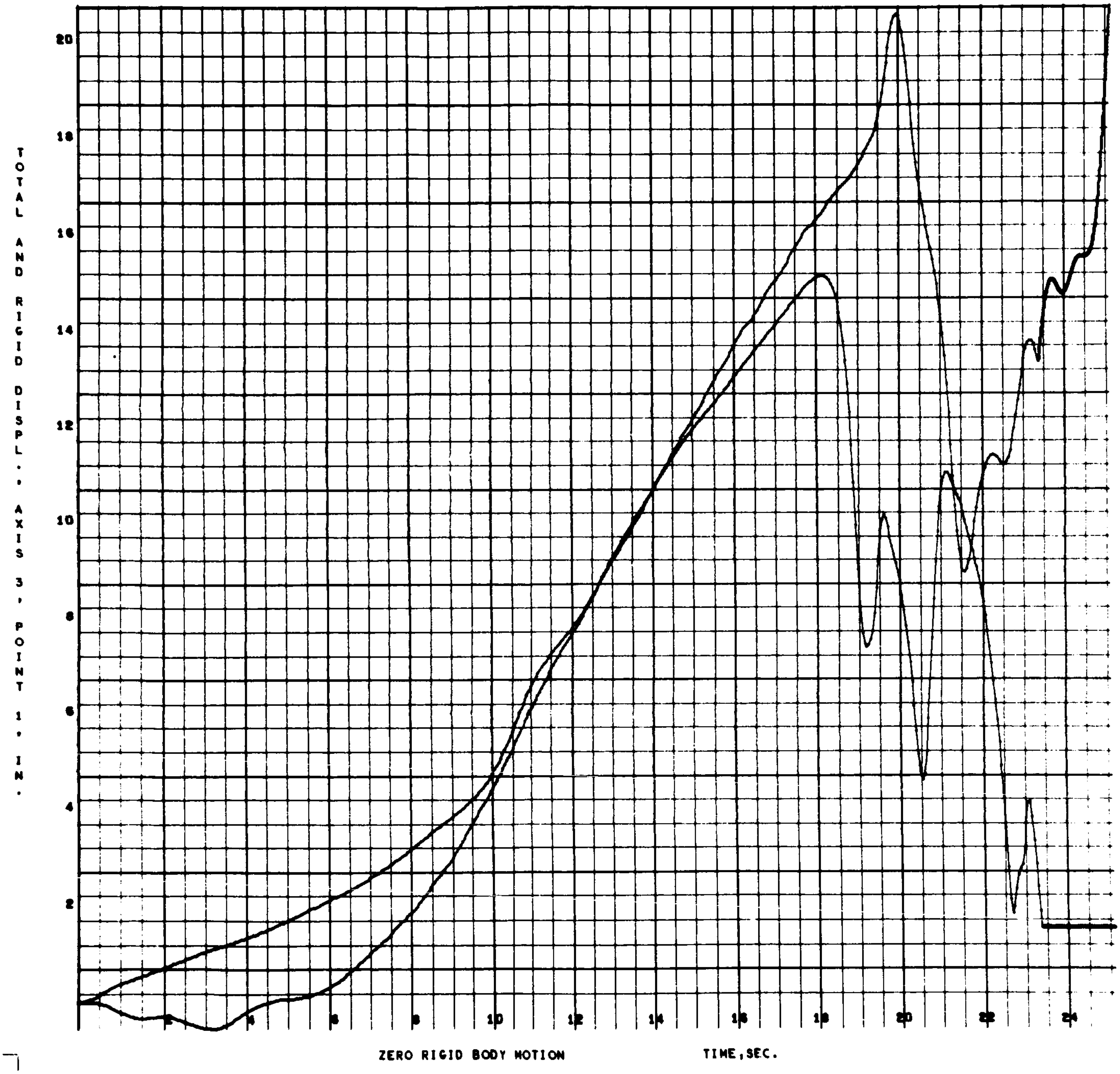

9828 47

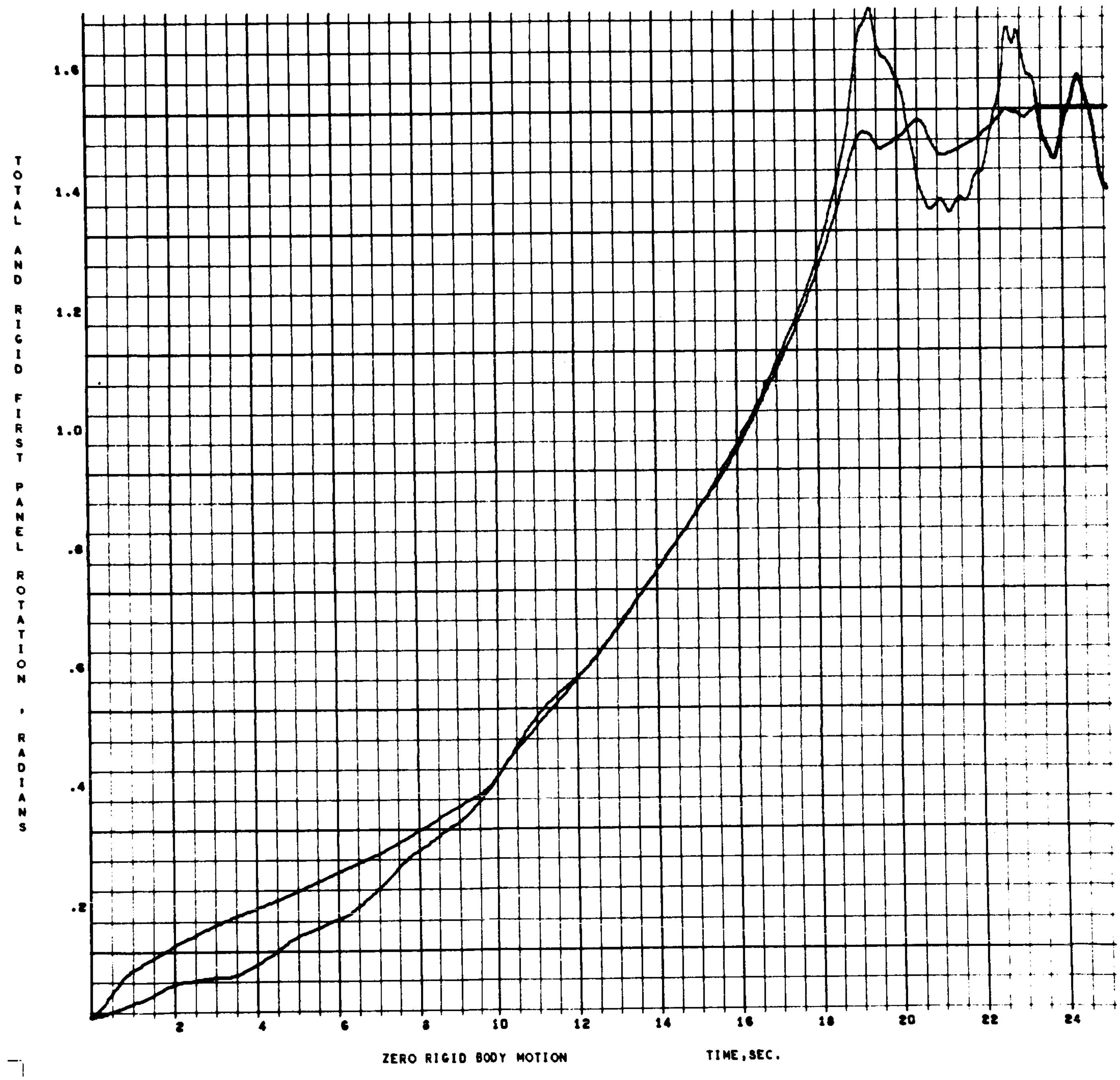
TOTAL AND RIGID FIRST PANEL ROTATION , RADIANS
1.6
1.4
1.2
1.0
.8
.6
.4
.2
2
4
6
8
10
12
14
16
18
20
22
24
ZERO RIGID BODY MOTION
TIME,SEC.

3828 48

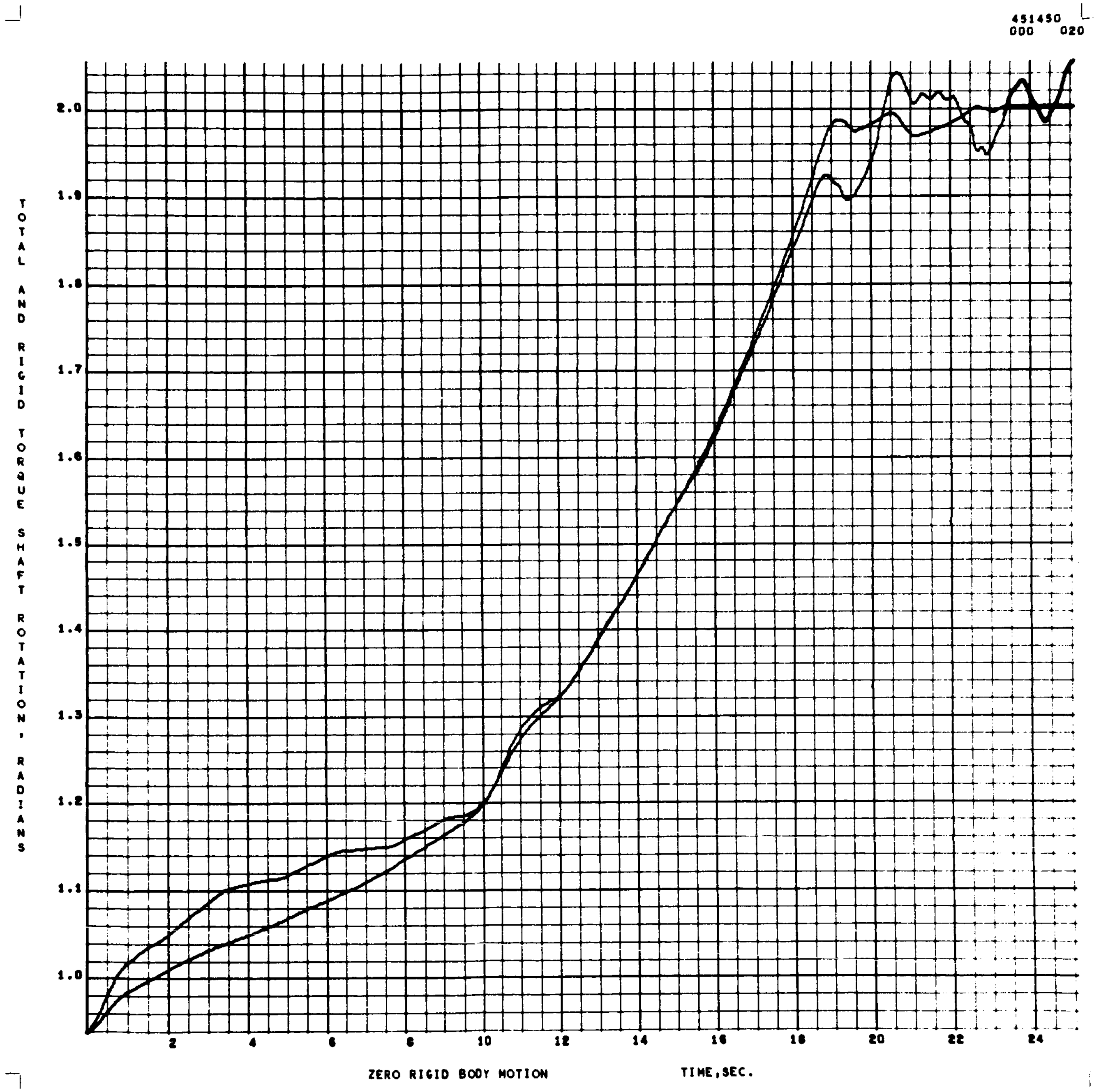
451450
000 020
TOTAL AND RIGID TORQUE SHAFT ROTATION, RADIANS
2.0
1.9
1.8
1.7
1.6
1.5
1.4
1.3
1.2
1.1
1.0
2
4
6
8
10
12
14
16
18
20
22
24
ZERO RIGID BODY MOTION
TIME, SEC.

9828 -1

451450
000 022

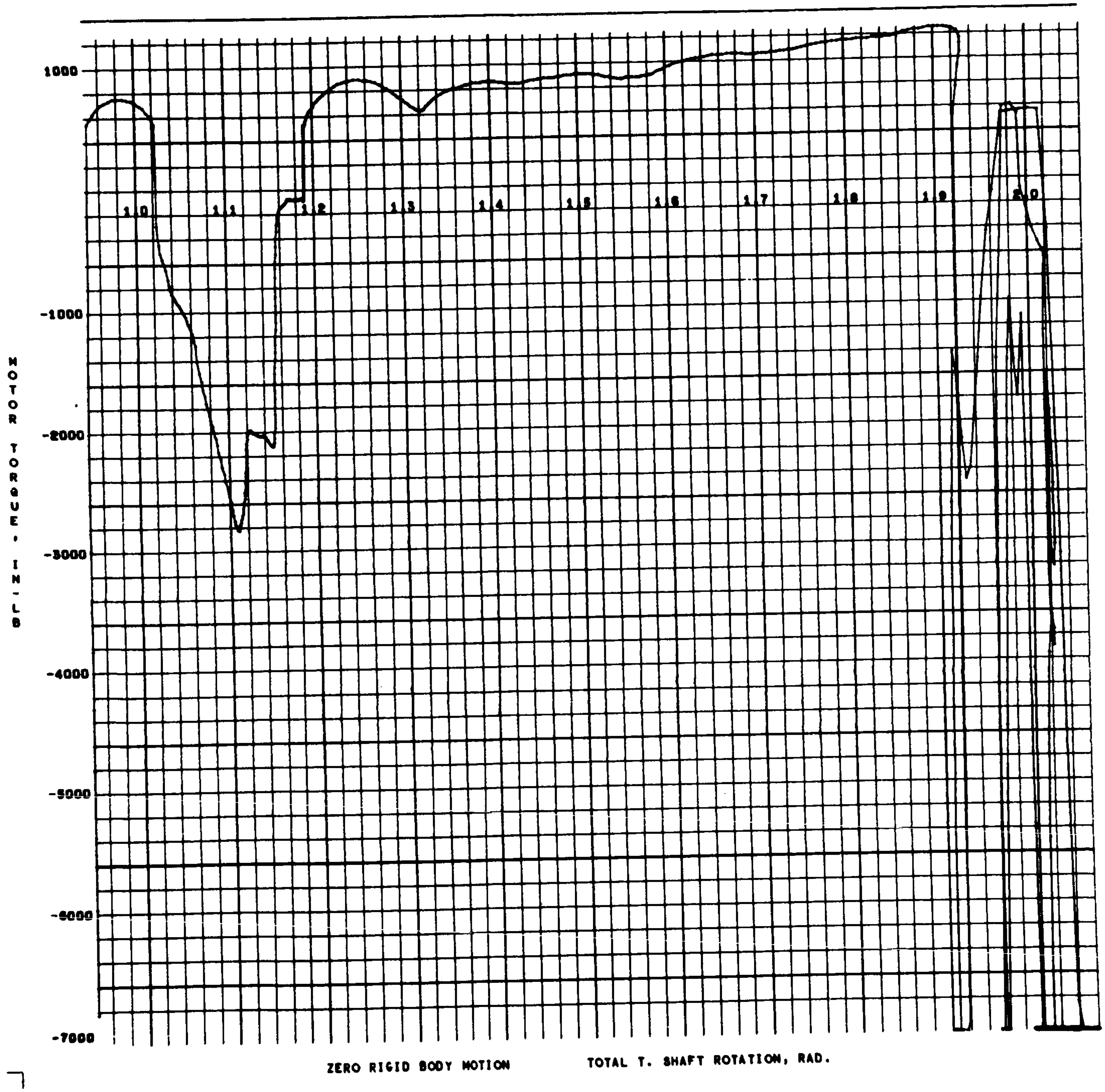

9828 50

451450
000 025

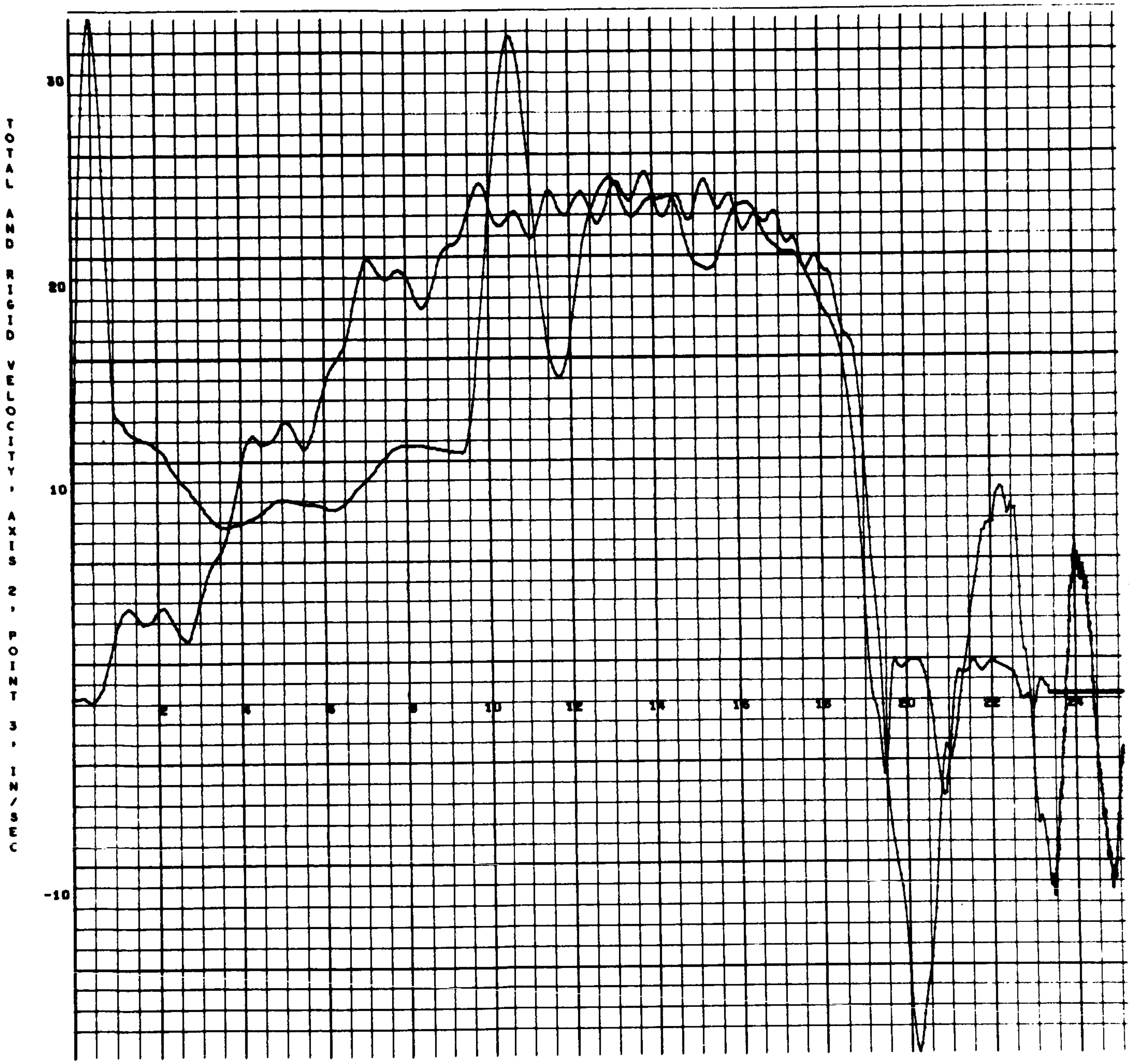

ZERO RIGID BODY MOTION TIME,SEC.

9828 51

451450
000 029

ZERO RIGID BODY MOTION TIME,SEC.

9828 52

451450
000 035

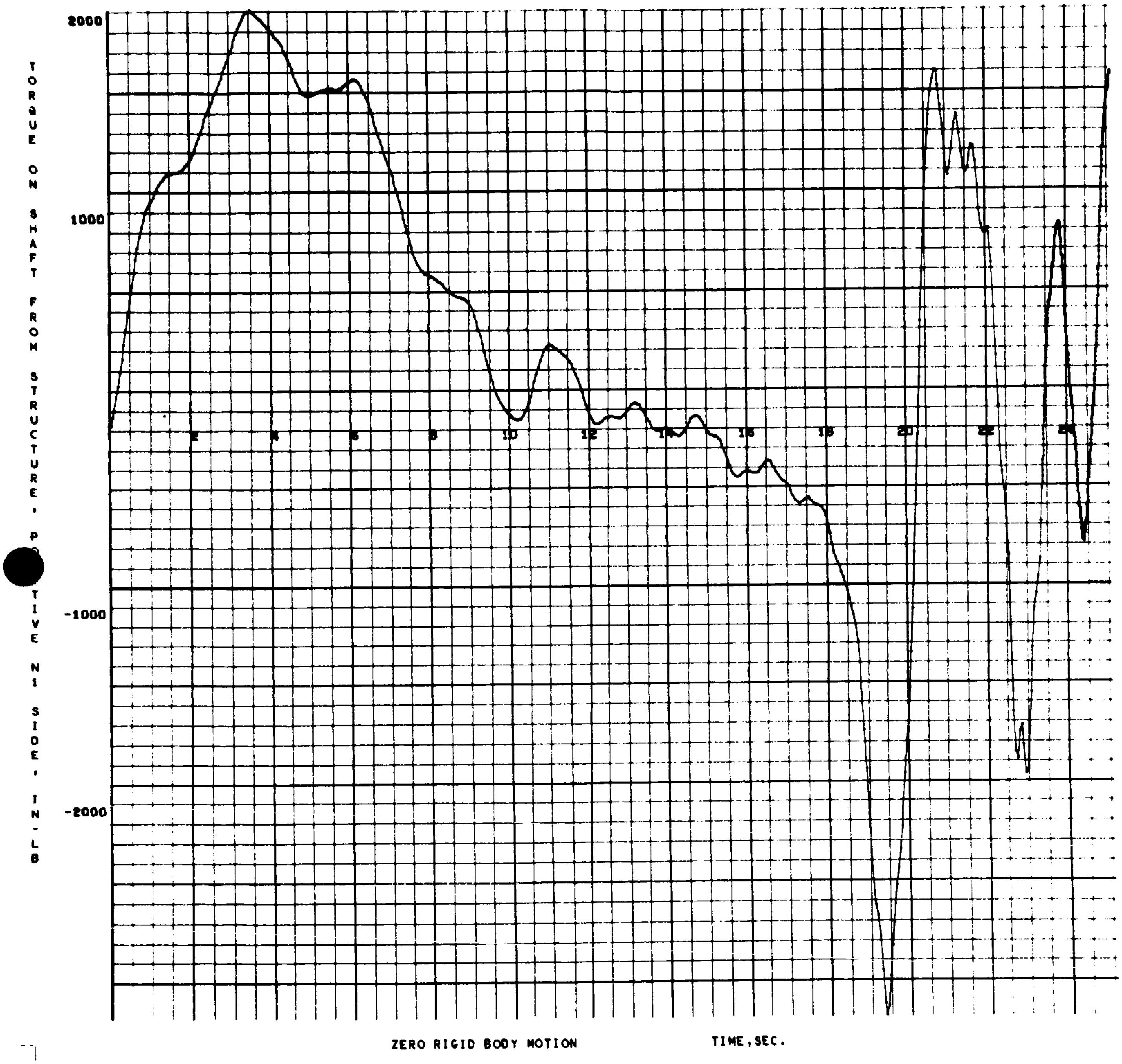

9828

451450
000 037

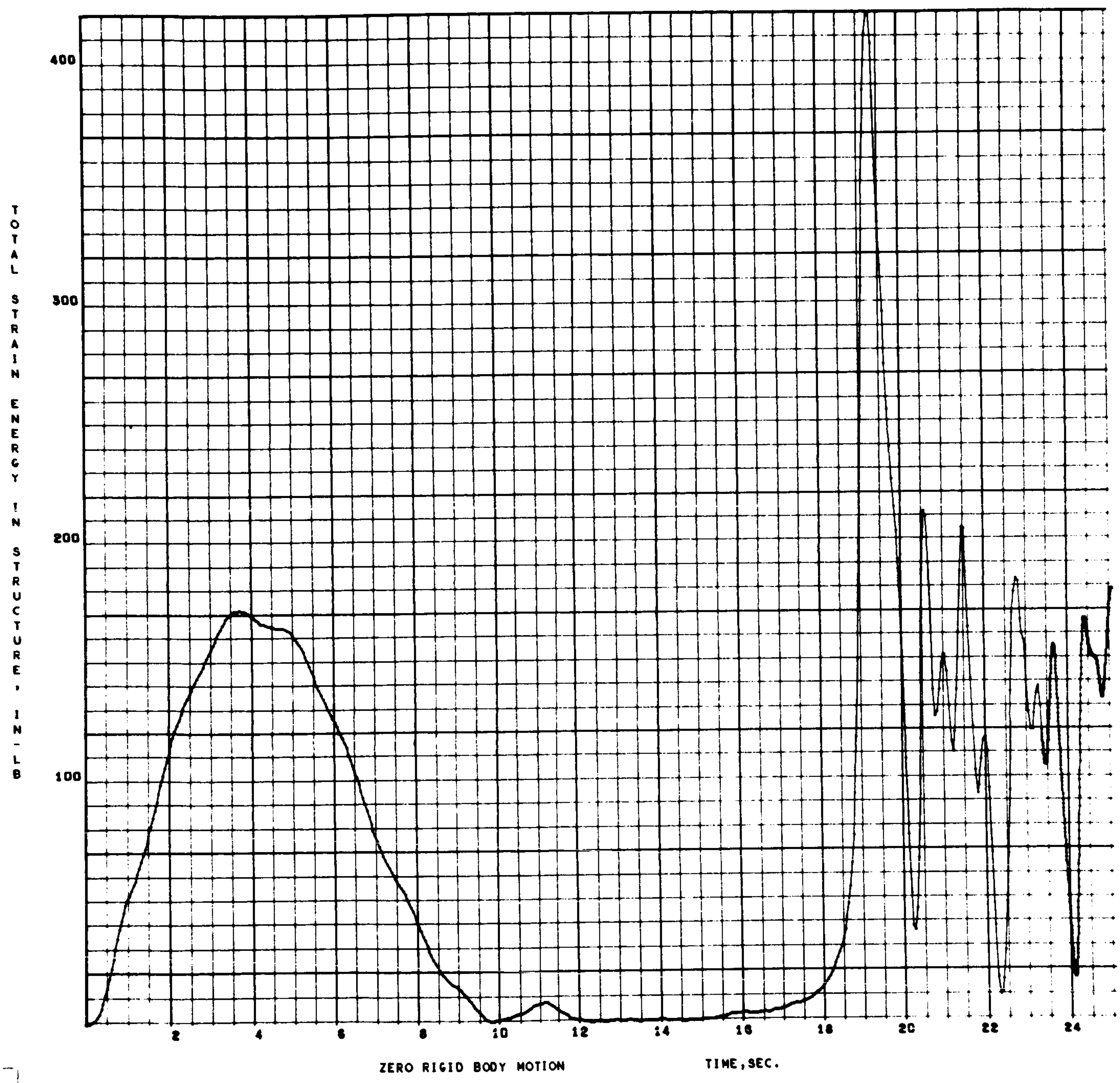

9828 54

451450
000 038

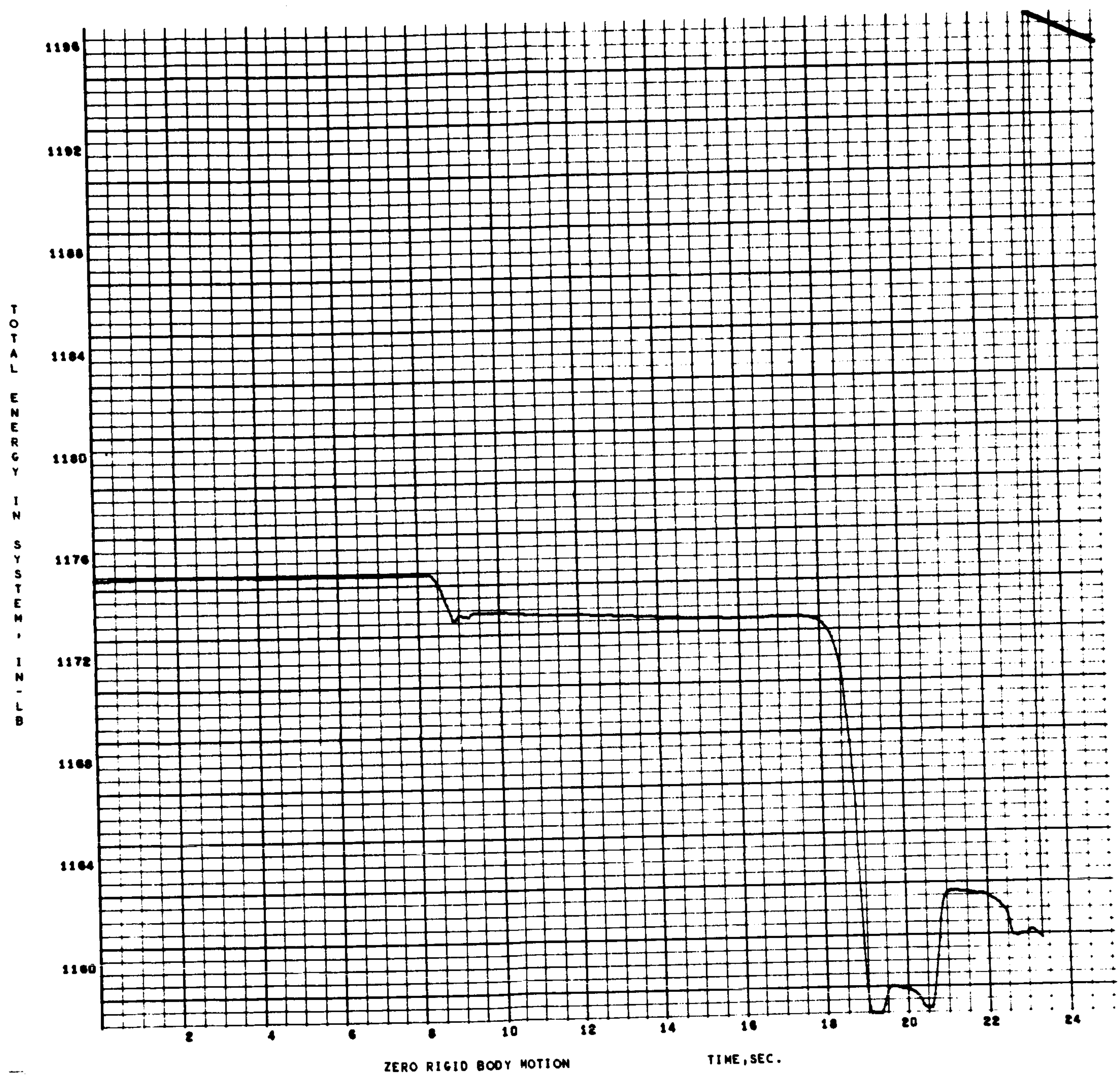

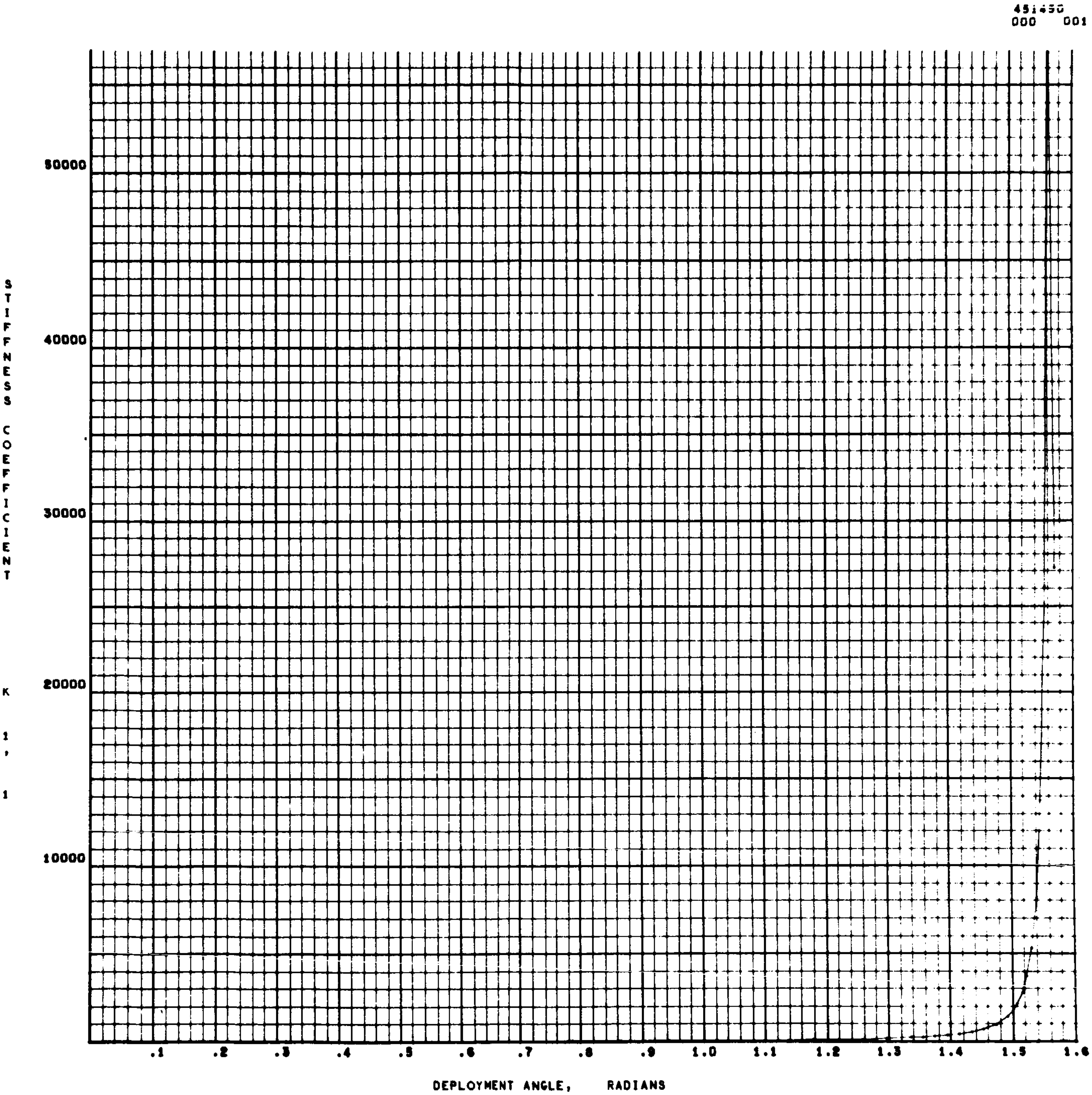
451450
000 001
50000
40000
30000
20000
10000
STIFFNESS COEFFICIENT K 1,1
.1 .2 .3 .4 .5 .6 .7 .8 .9 1.0 1.1 1.2 1.3 1.4 1.5 1.6
DEPLOYMENT ANGLE, RADIANS

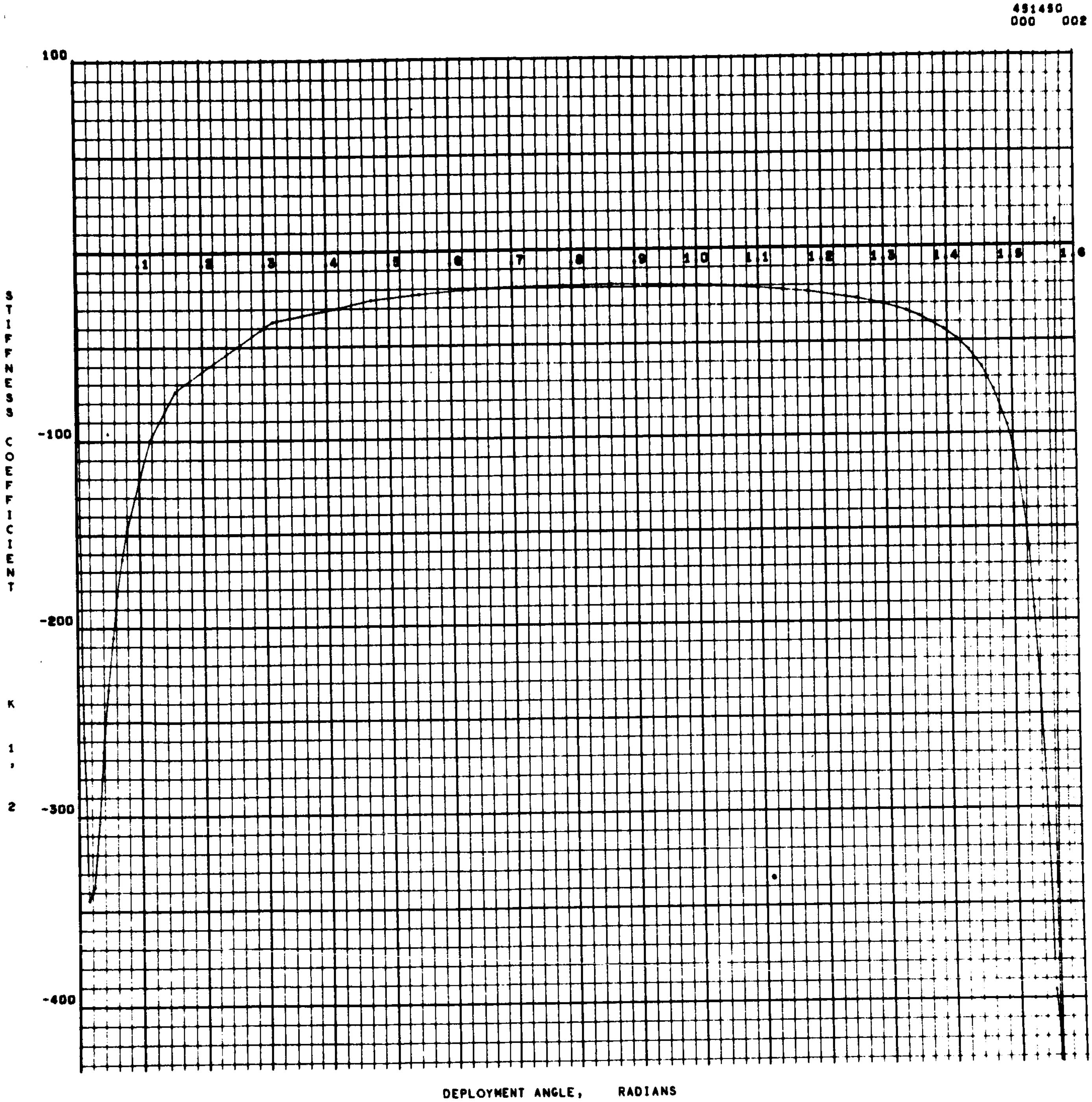
451450
000 002
100
-100
-200
-300
-400
.1
.2
.3
.4
.5
.6
.7
.8
.9
1.0
1.1
1.2
1.3
1.4
1.5
1.6
STIFFNESS COEFFICIENT K 1, 2
DEPLOYMENT ANGLE, RADIANS

451450
000 004

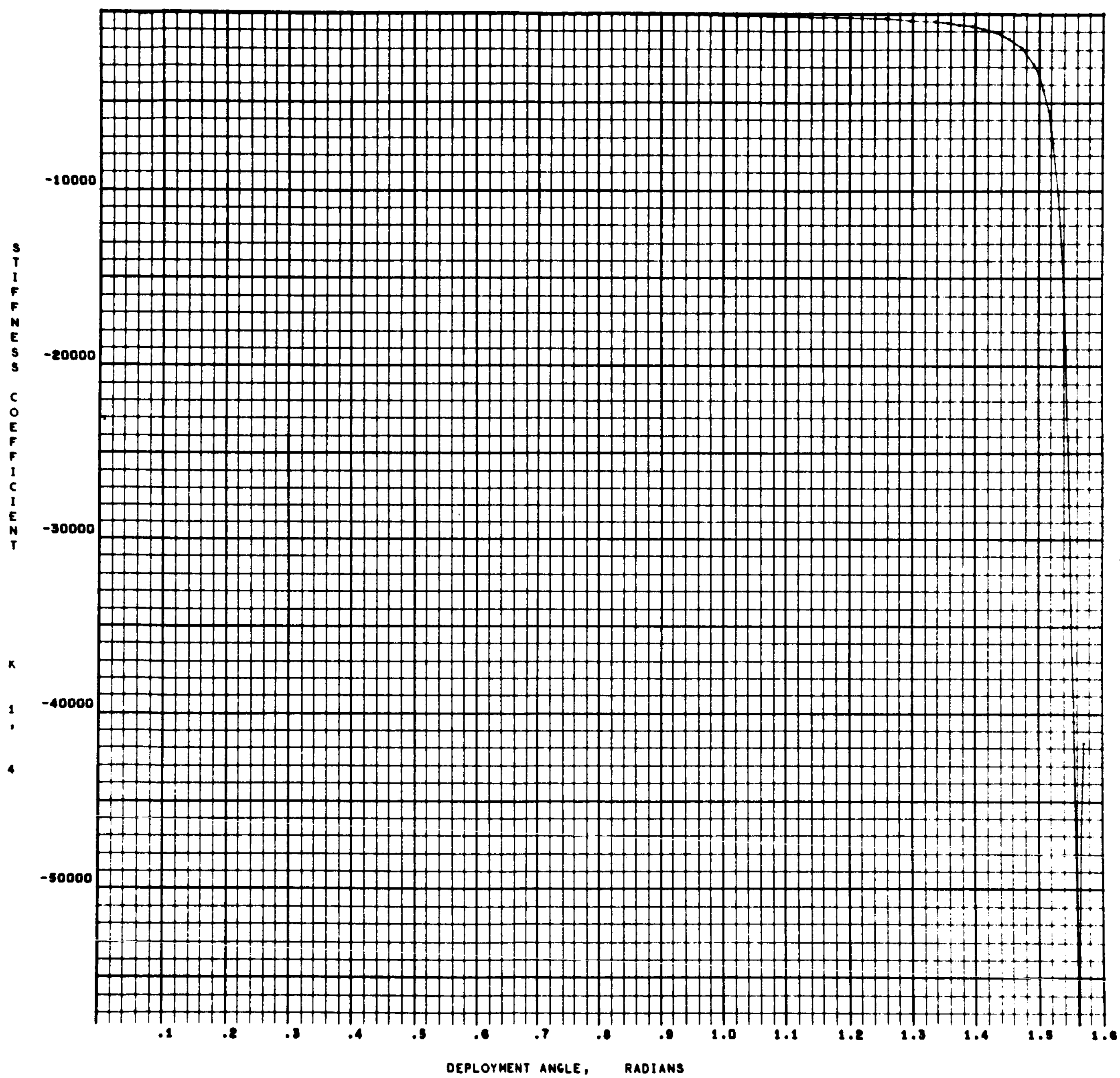

58

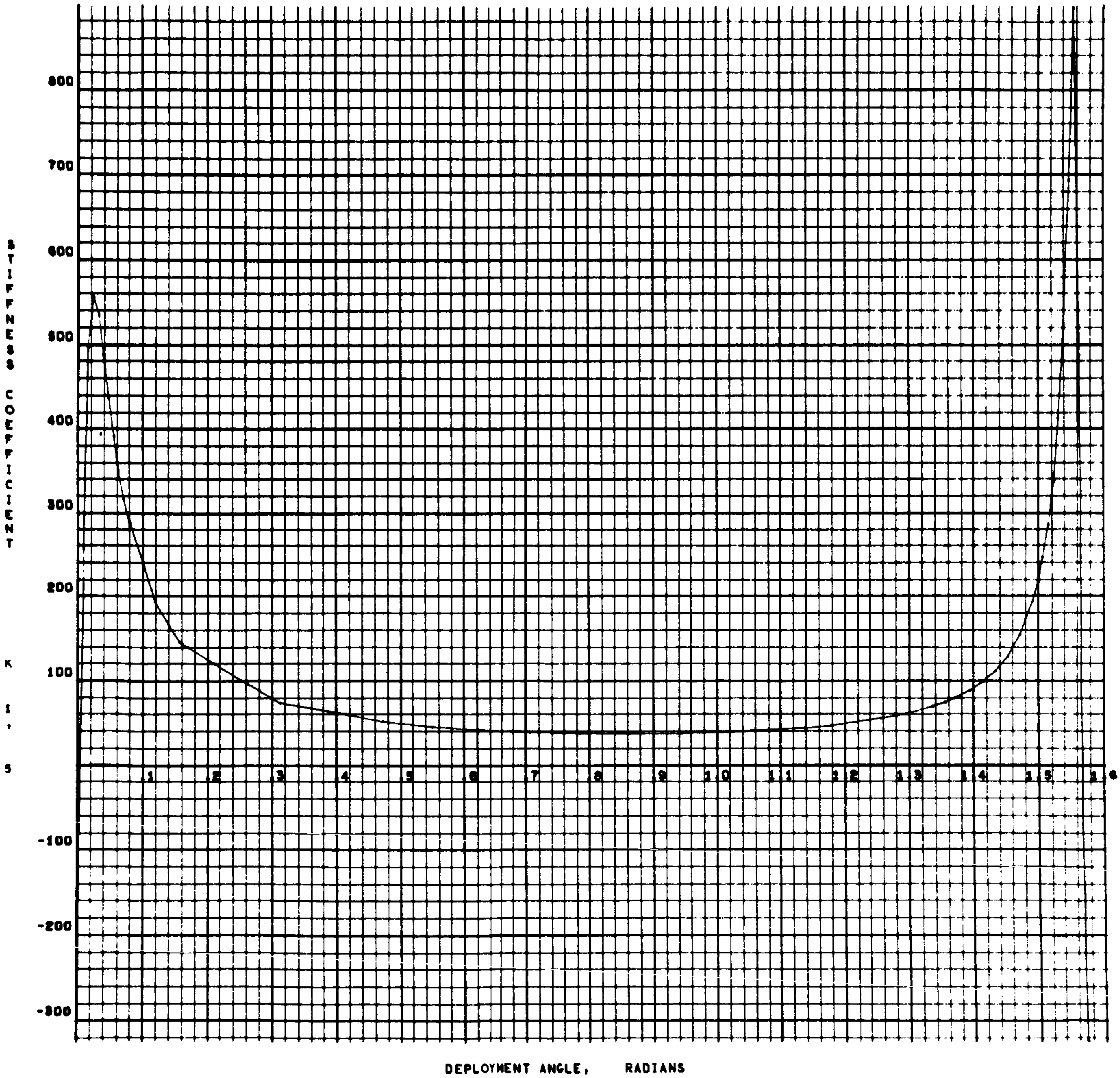
800
700
600
500
400
300
200
100
-100
-200
-300
STIFFNESS COEFFICIENT K 1, 5
.1
.2
.3
.4
.5
.6
.7
.8
.9
1.0
1.1
1.2
1.3
1.4
1.5
1.6
DEPLOYMENT ANGLE, RADIANS

451450
000 007

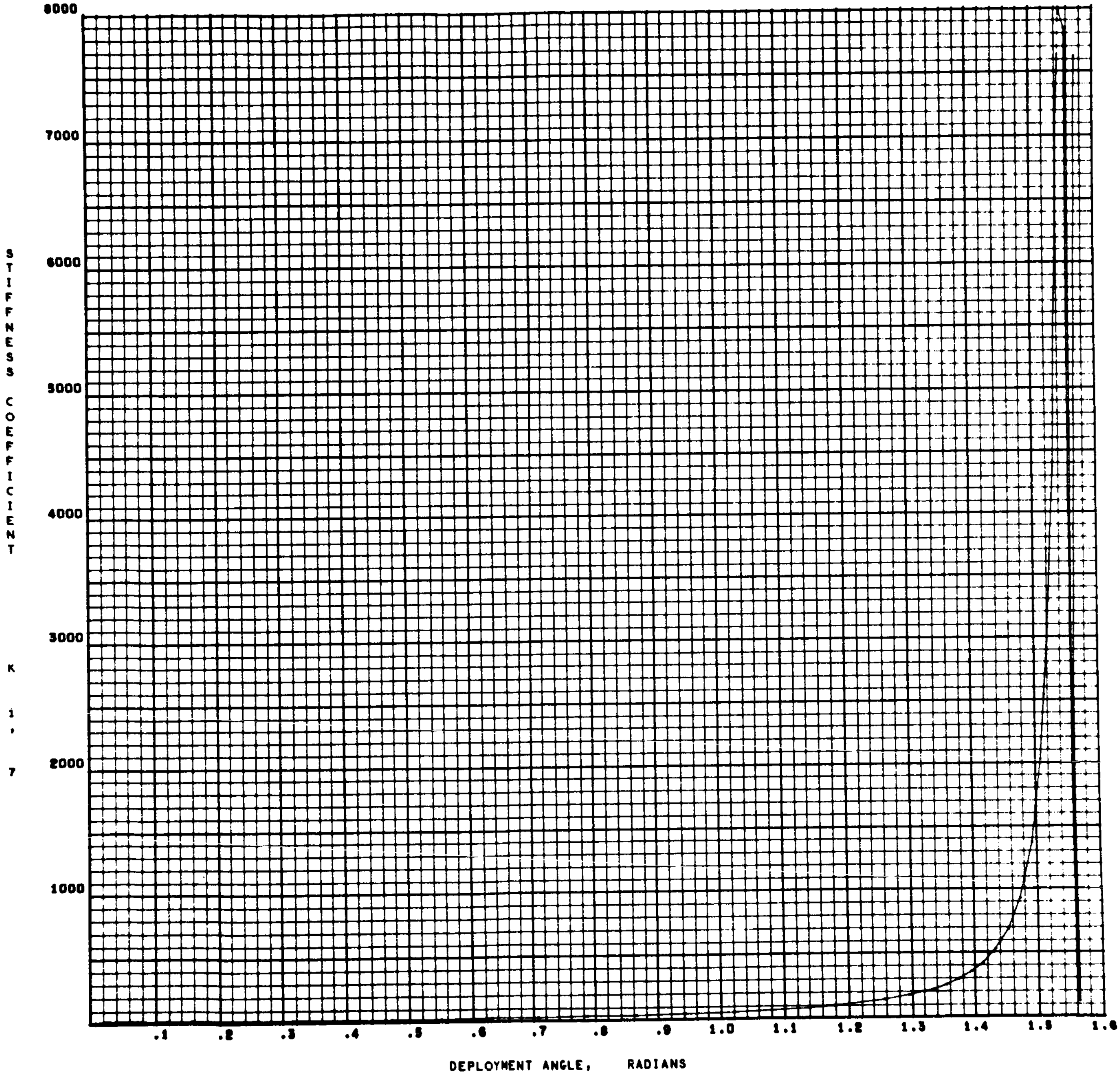

60

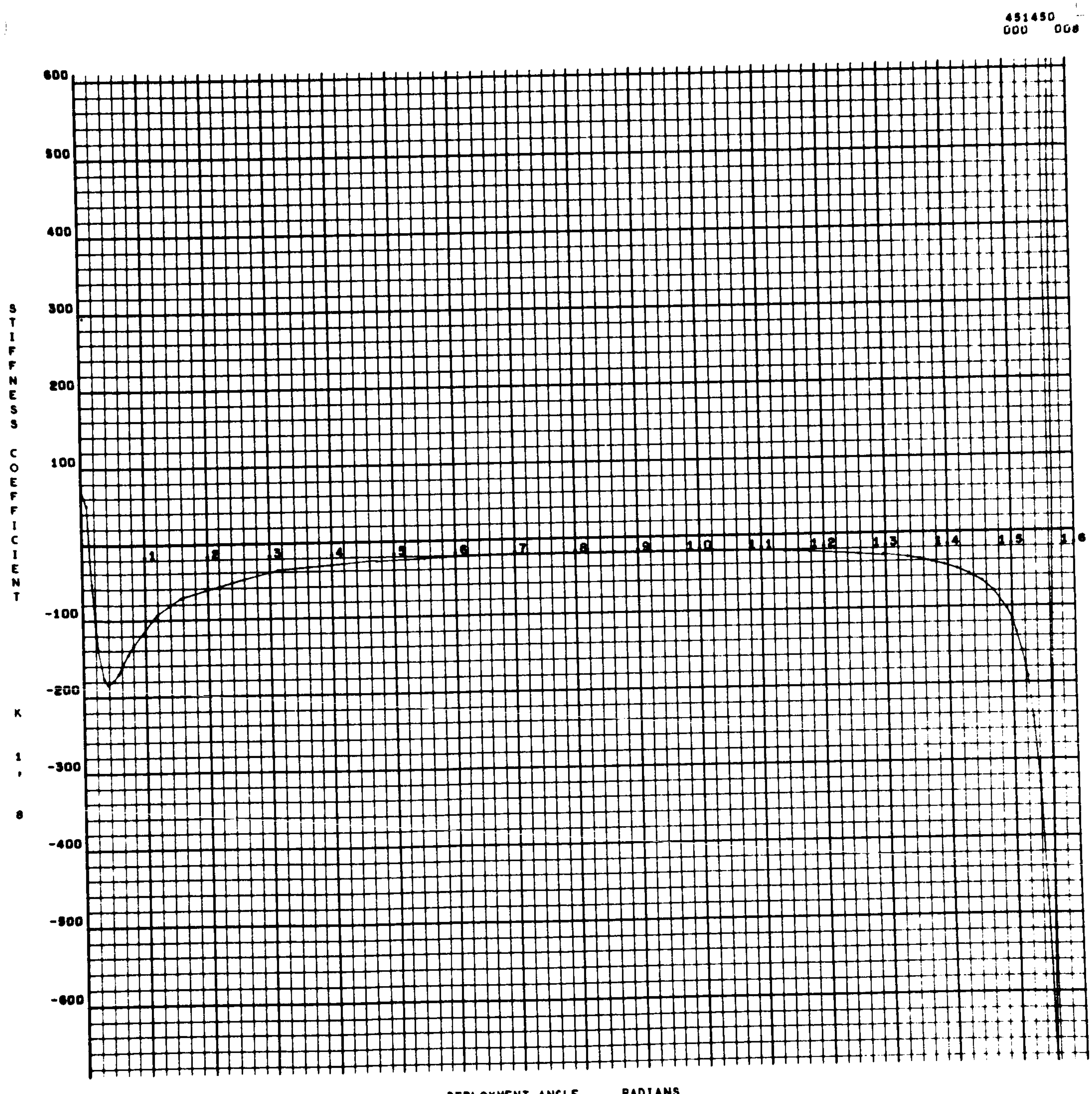

451450
000 008
600
500
400
300
200
100
-100
-200
-300
-400
-500
-600
STIFFNESS COEFFICIENT K 1,8
.1
.2
.3
.4
.5
.6
.7
.8
.9
1.0
1.1
1.2
1.3
1.4
1.5
1.6
DEPLOYMENT ANGLE, RADIANS

61

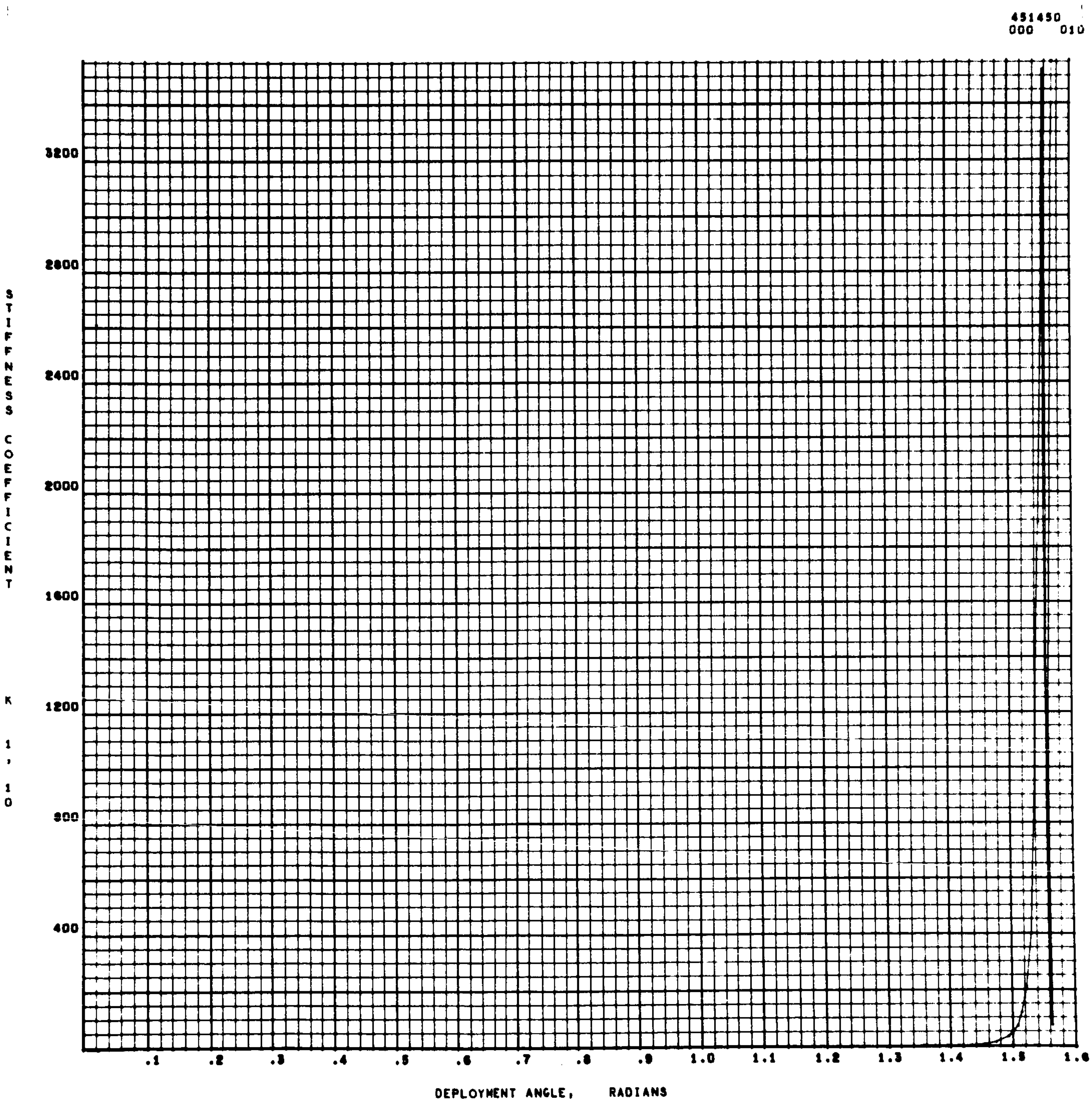
451450
000 010
3200
2800
2400
2000
1600
1200
800
400
STIFFNESS COEFFICIENT K 1,10
.1
.2
.3
.4
.5
.6
.7
.8
.9
1.0
1.1
1.2
1.3
1.4
1.5
1.6
DEPLOYMENT ANGLE, RADIANS

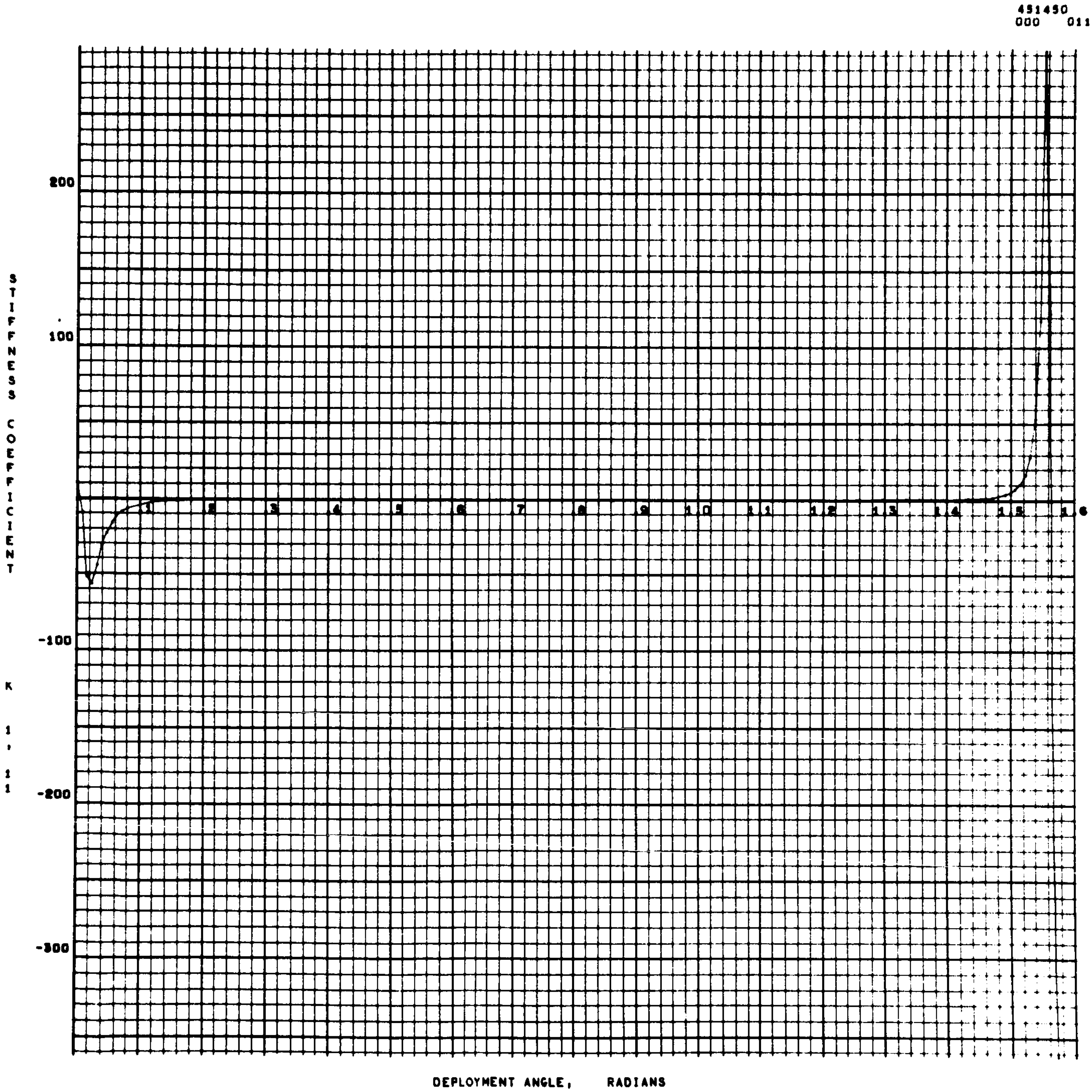

451450
000 011
200
100
-100
-200
-300
STIFFNESS COEFFICIENT K 1,11
.1
.2
.3
.4
.5
.6
.7
.8
.9
1.0
1.1
1.2
1.3
1.4
1.5
1.6
DEPLOYMENT ANGLE, RADIANS

451450
000 013

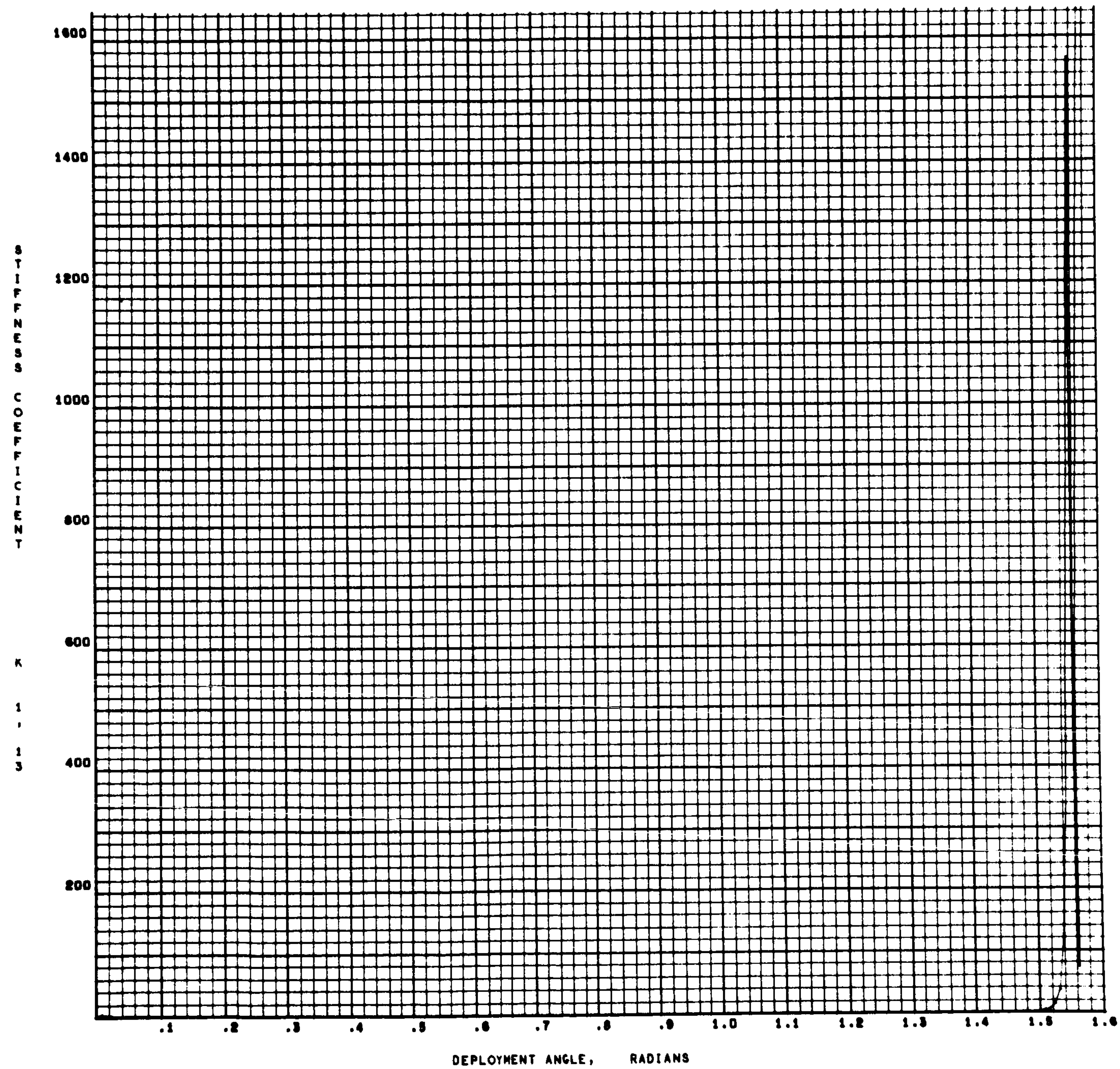

451450
000 014

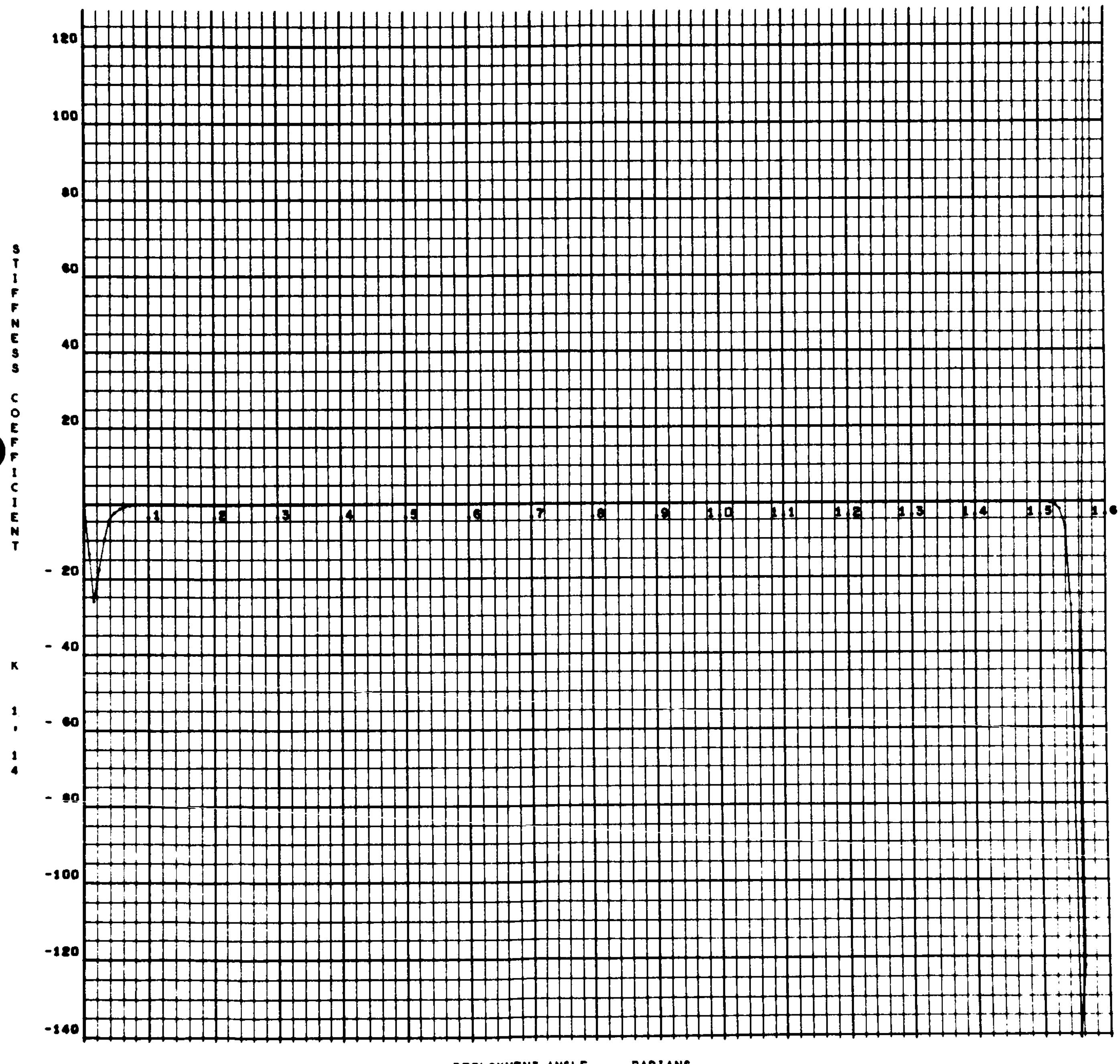

451450
000 016

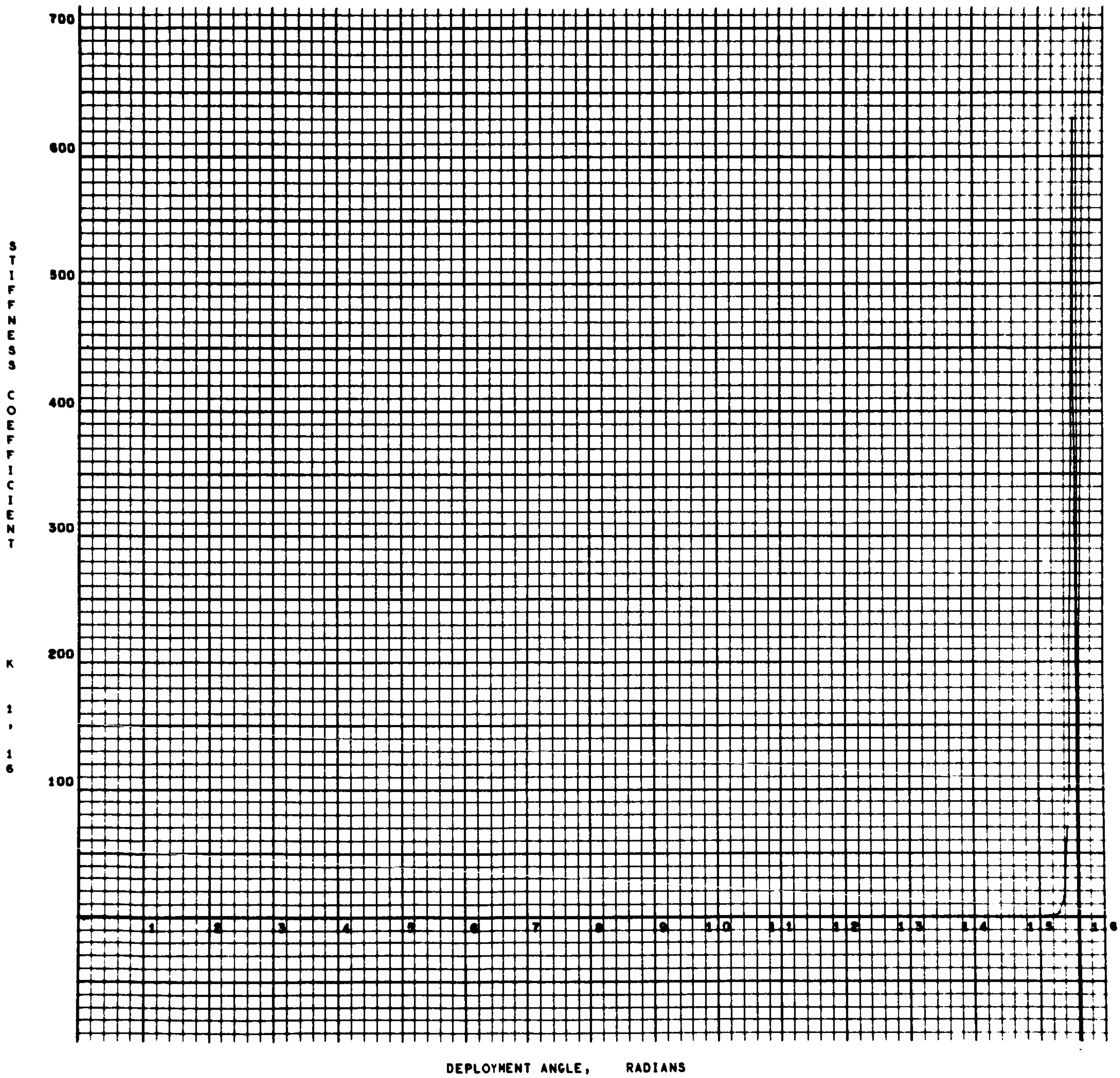

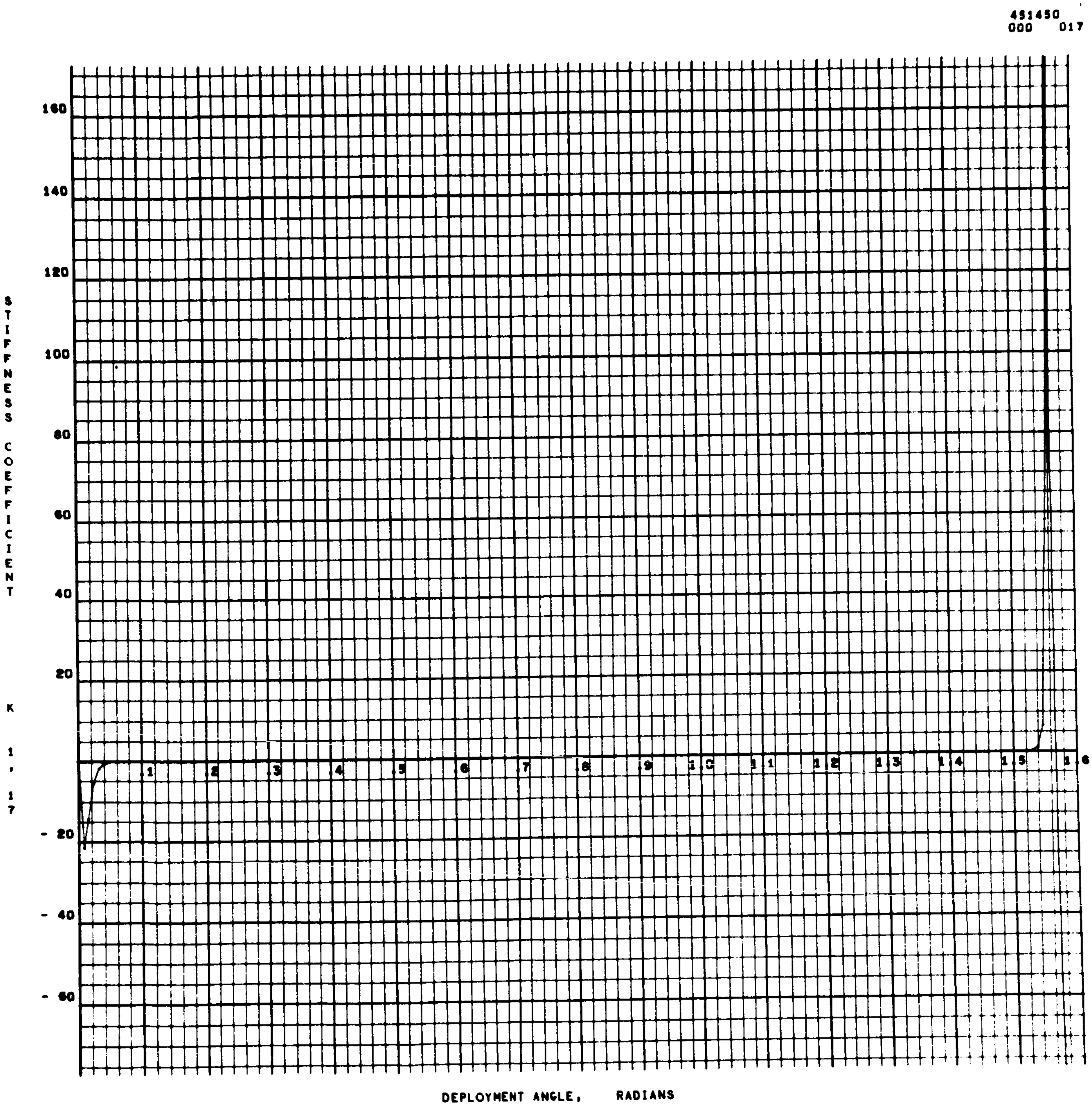

451450
000 017
STIFFNESS COEFFICIENT K 1, 17
160
140
120
100
80
60
40
20
- 20
- 40
- 60
.1
.2
.3
.4
.5
.6
.7
.8
.9
1.0
1.1
1.2
1.3
1.4
1.5
1.6
DEPLOYMENT ANGLE, RADIANS

451450
000 019

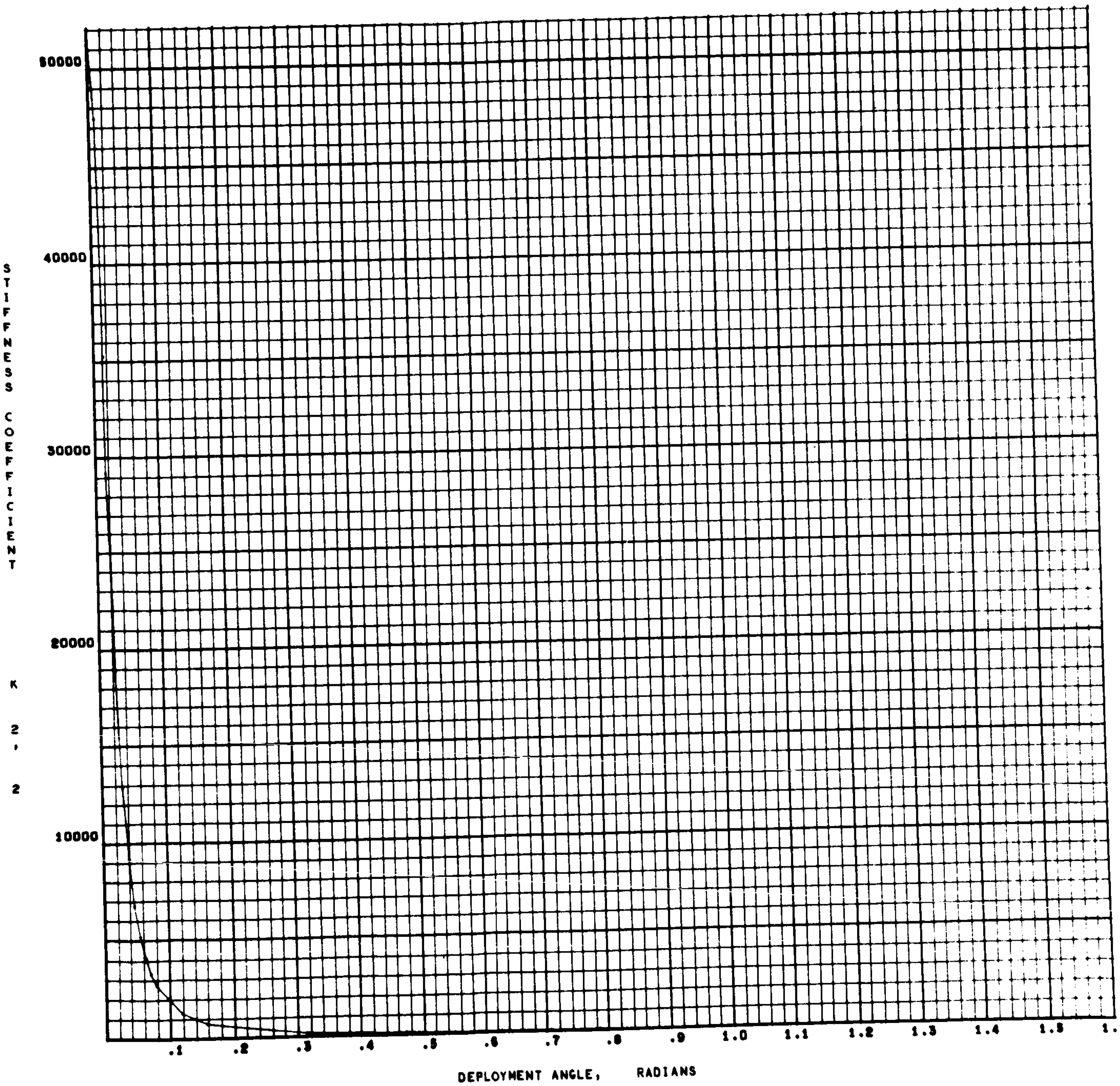

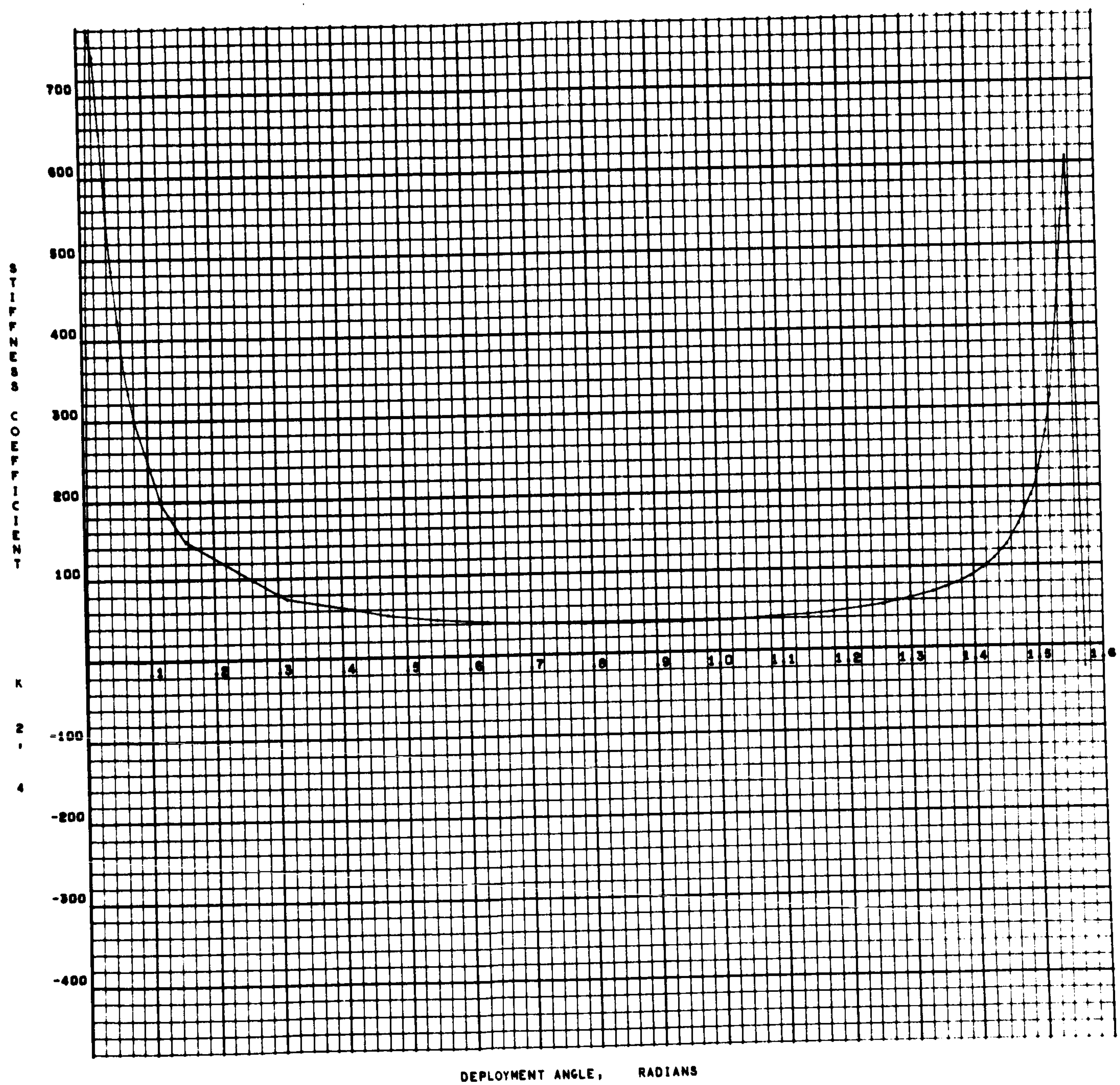
STIFFNESS COEFFICIENT K 2,4
700
600
500
400
300
200
100
-100
-200
-300
-400
.1
.2
.3
.4
.5
.6
.7
.8
.9
1.0
1.1
1.2
1.3
1.4
1.5
1.6
DEPLOYMENT ANGLE, RADIANS

451450
000 022

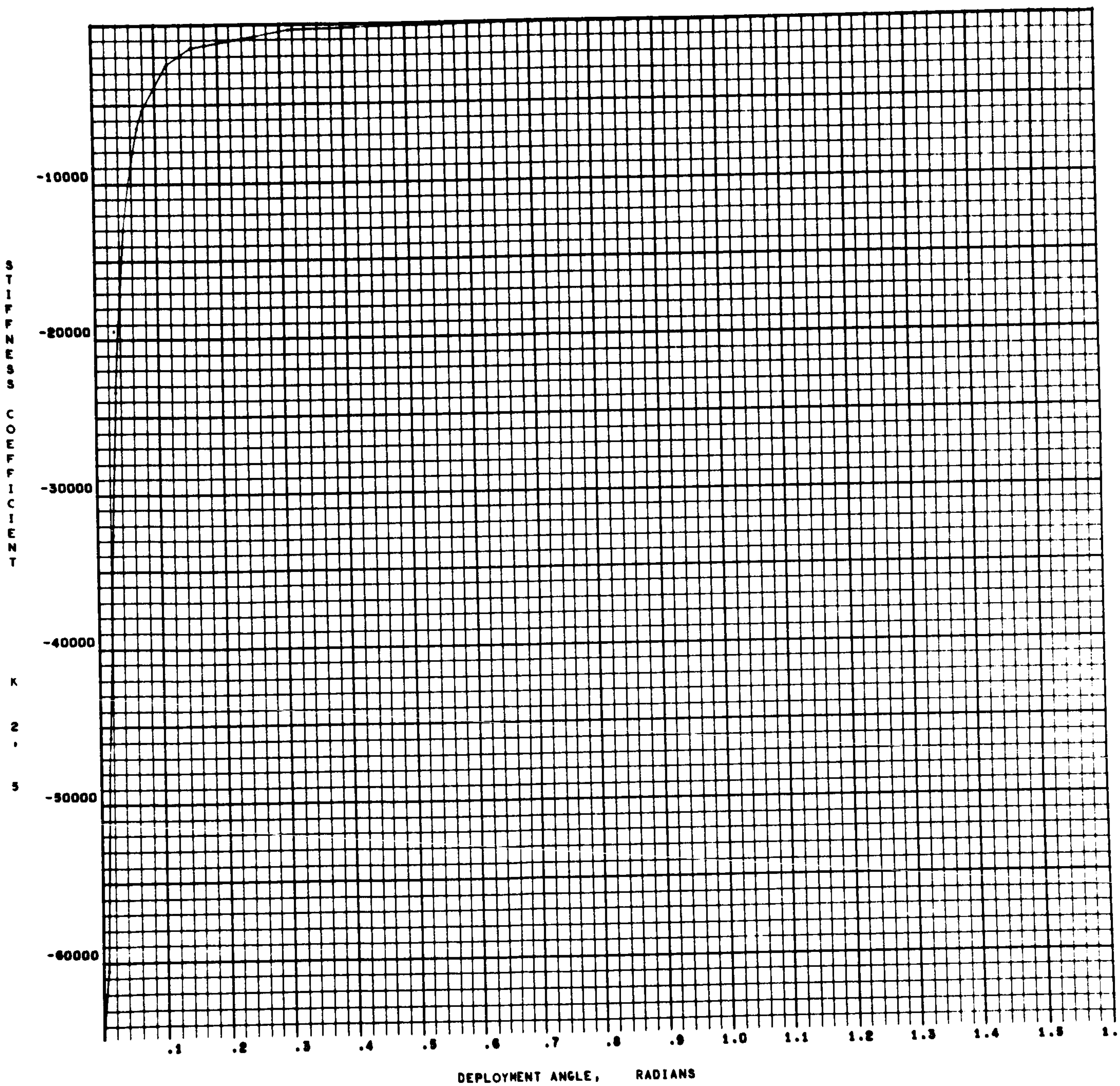

70

451450
000 024

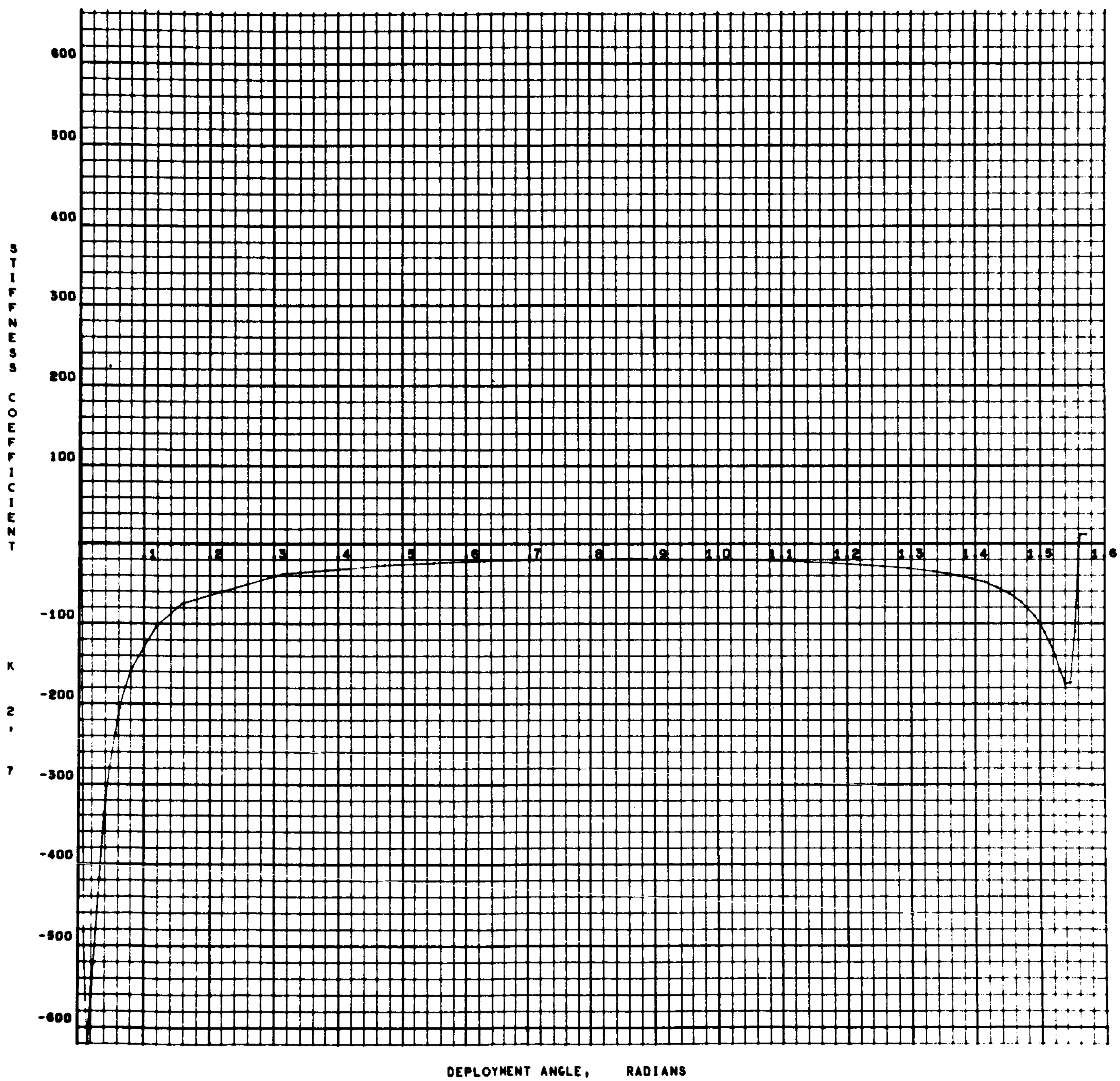

451450
000 025

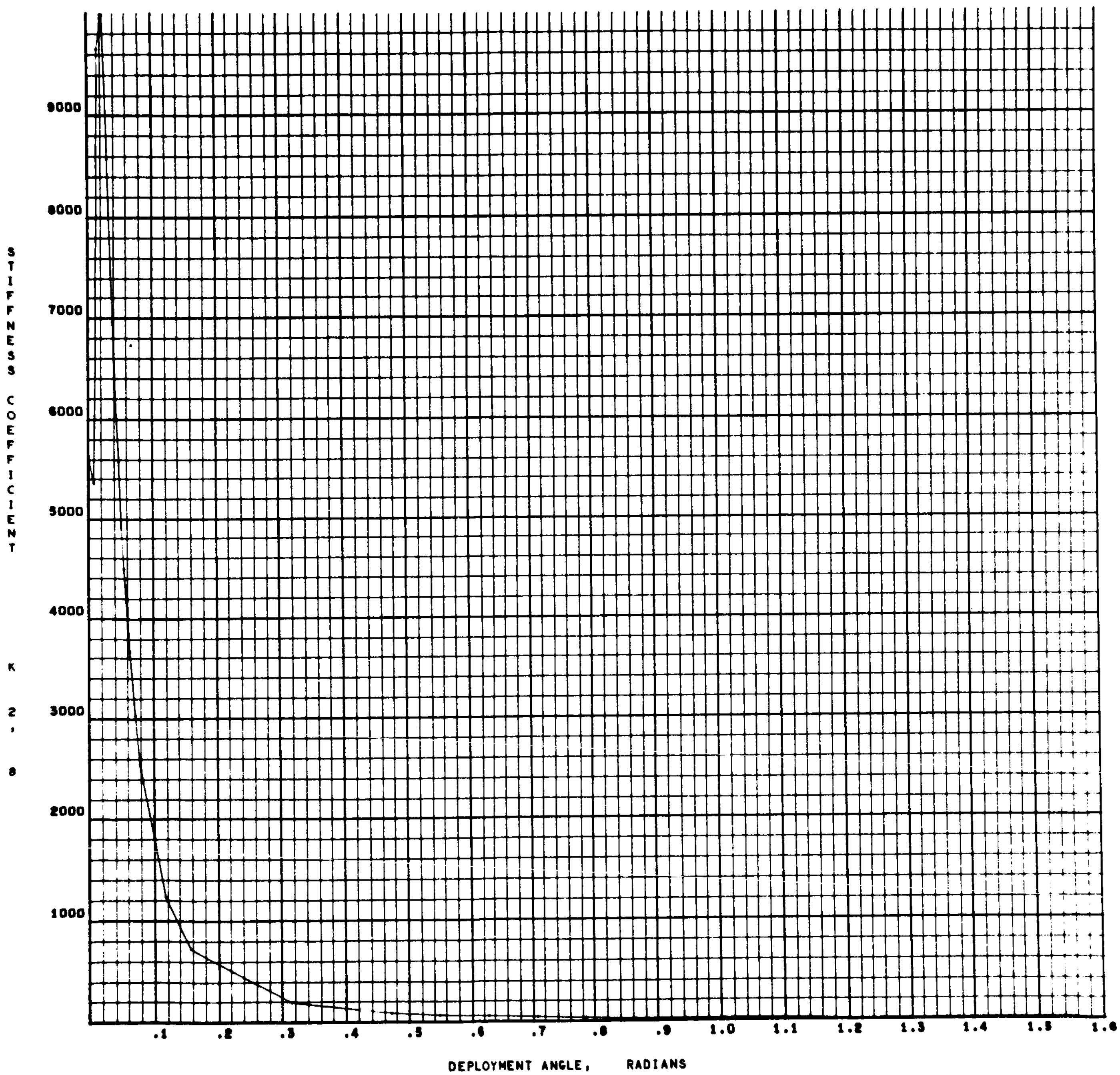

451450
000 027

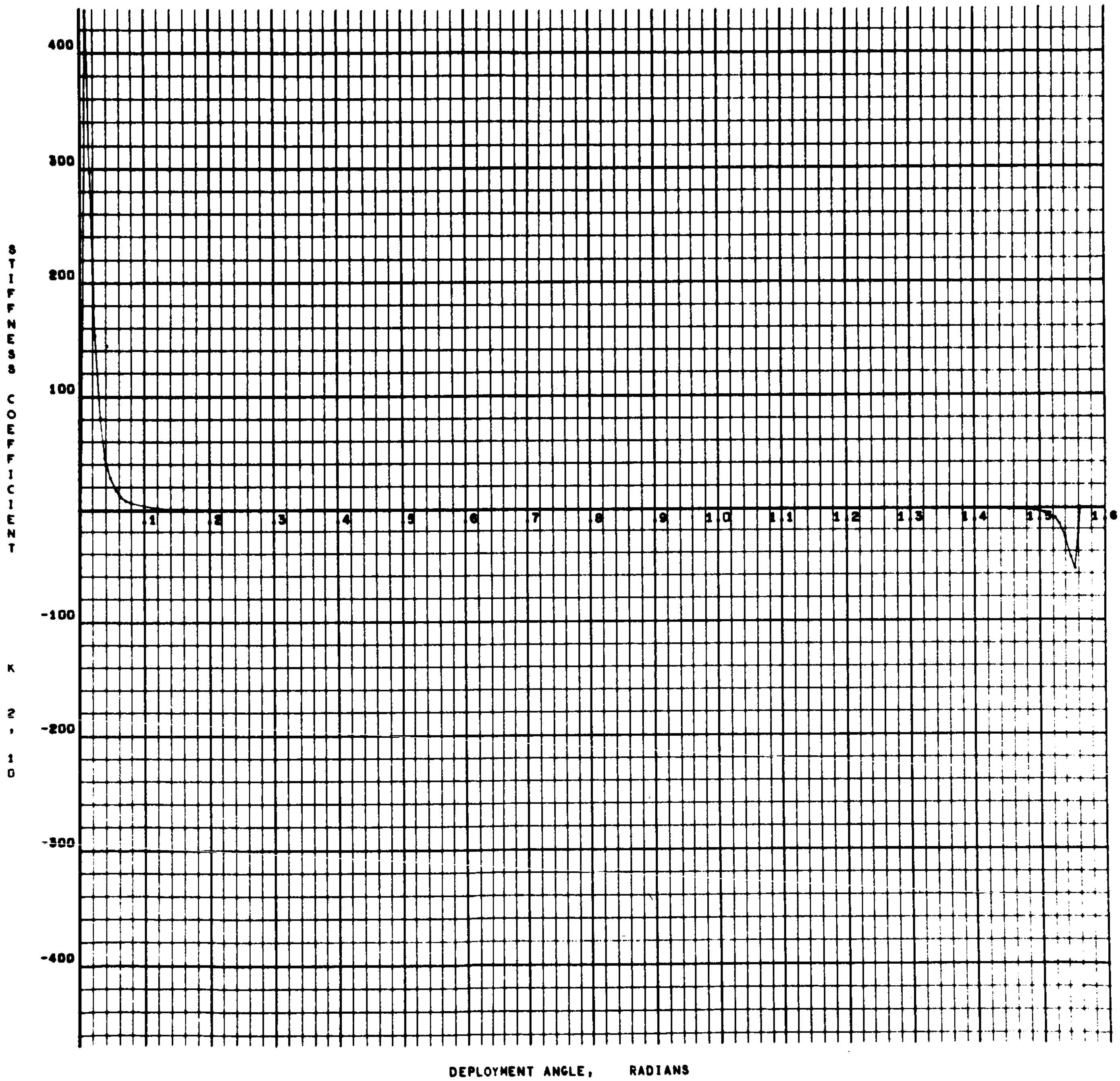

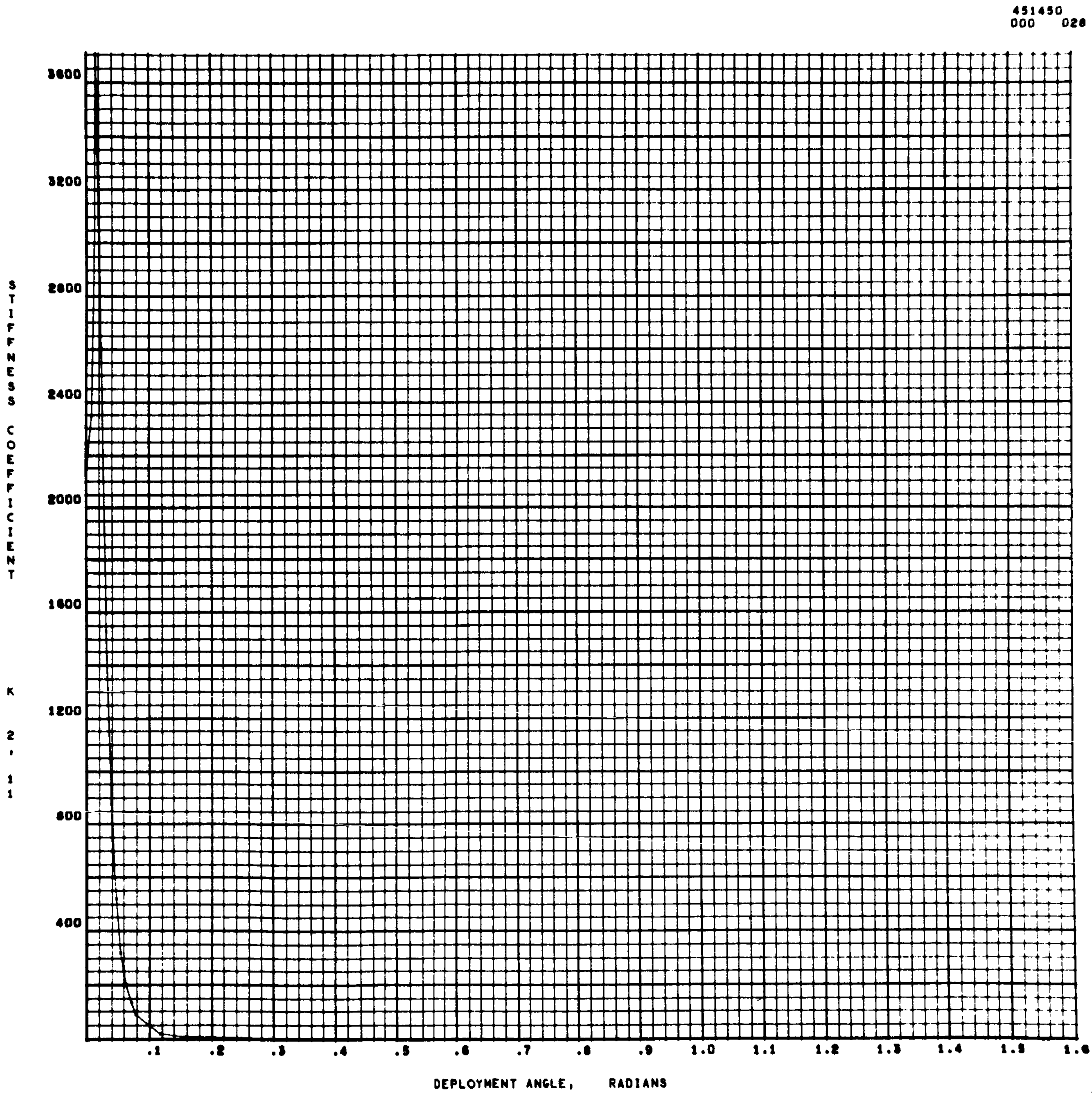
451450
000 028
3600
3200
2800
2400
2000
1600
1200
800
400
STIFFNESS COEFFICIENT K 2,11
.1
.2
.3
.4
.5
.6
.7
.8
.9
1.0
1.1
1.2
1.3
1.4
1.5
1.6
DEPLOYMENT ANGLE, RADIANS

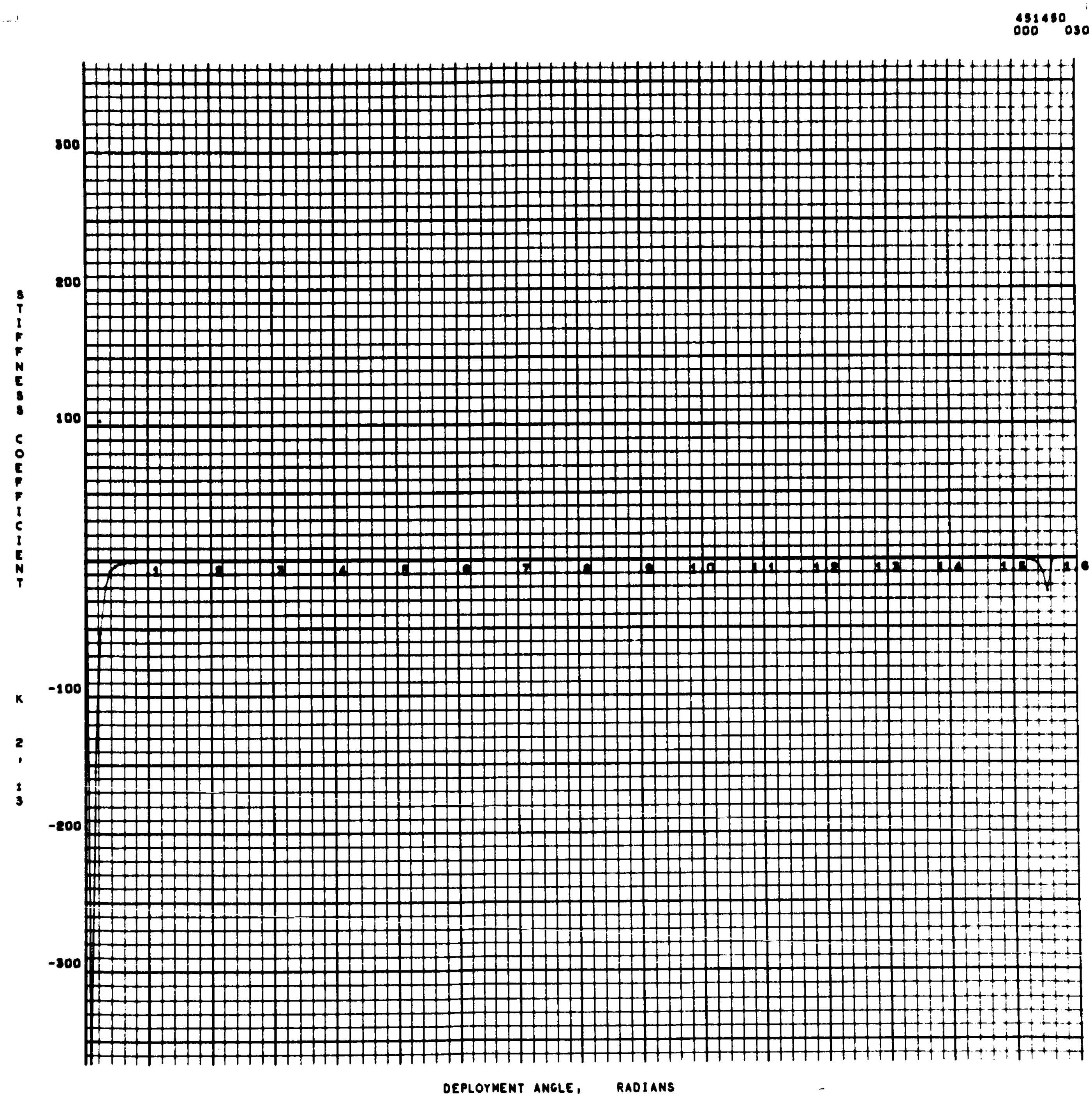

451450
000 030
300
200
100
-100
-200
-300
STIFFNESS COEFFICIENT K 2,13
.1
.2
.3
.4
.5
.6
.7
.8
.9
1.0
1.1
1.2
1.3
1.4
1.5
1.6
DEPLOYMENT ANGLE, RADIANS

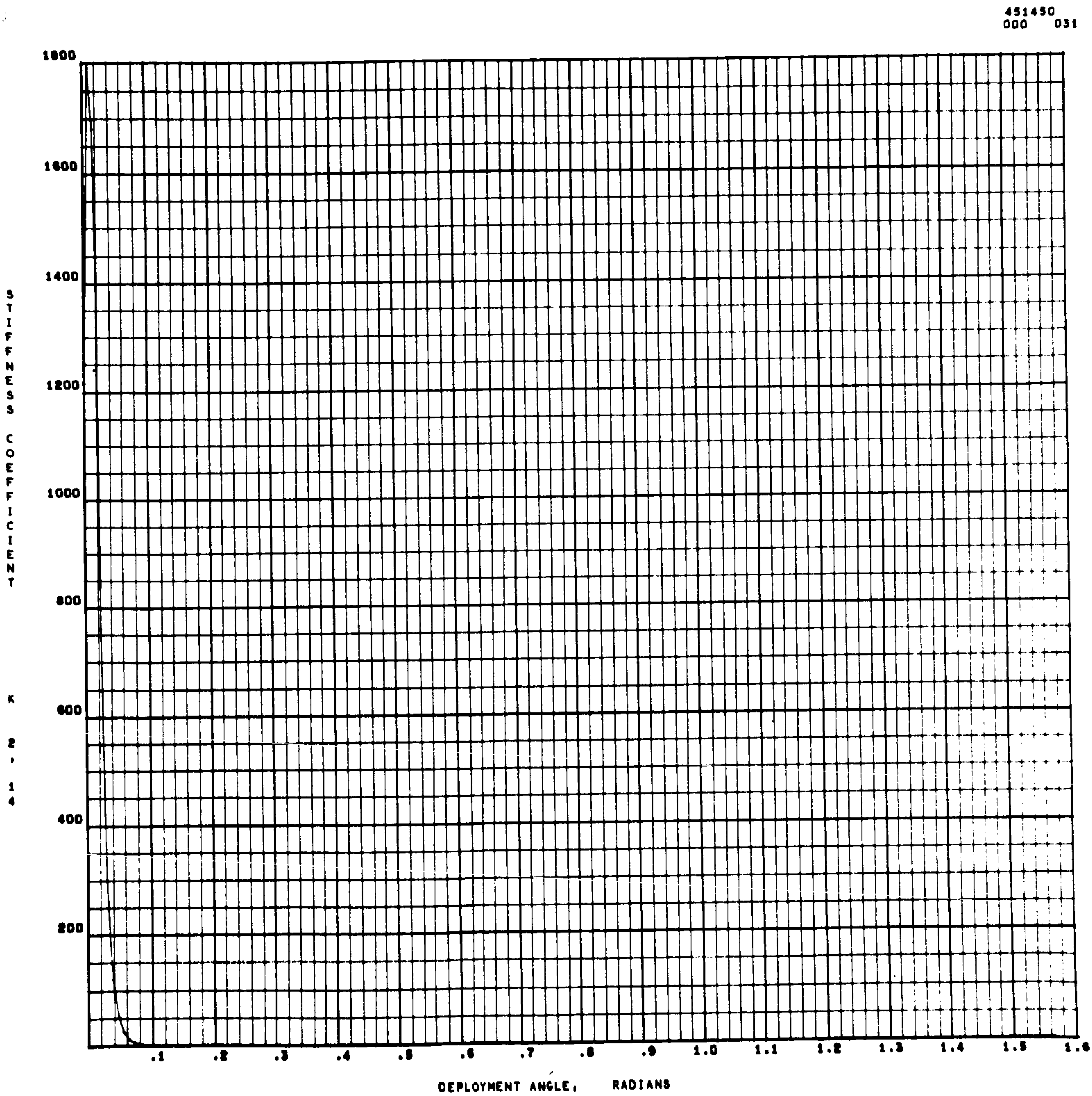
451450
000 031
1800
1600
1400
1200
1000
800
600
400
200
STIFFNESS COEFFICIENT K 2,14
.1
.2
.3
.4
.5
.6
.7
.8
.9
1.0
1.1
1.2
1.3
1.4
1.5
1.6
DEPLOYMENT ANGLE, RADIANS

451450
000 033

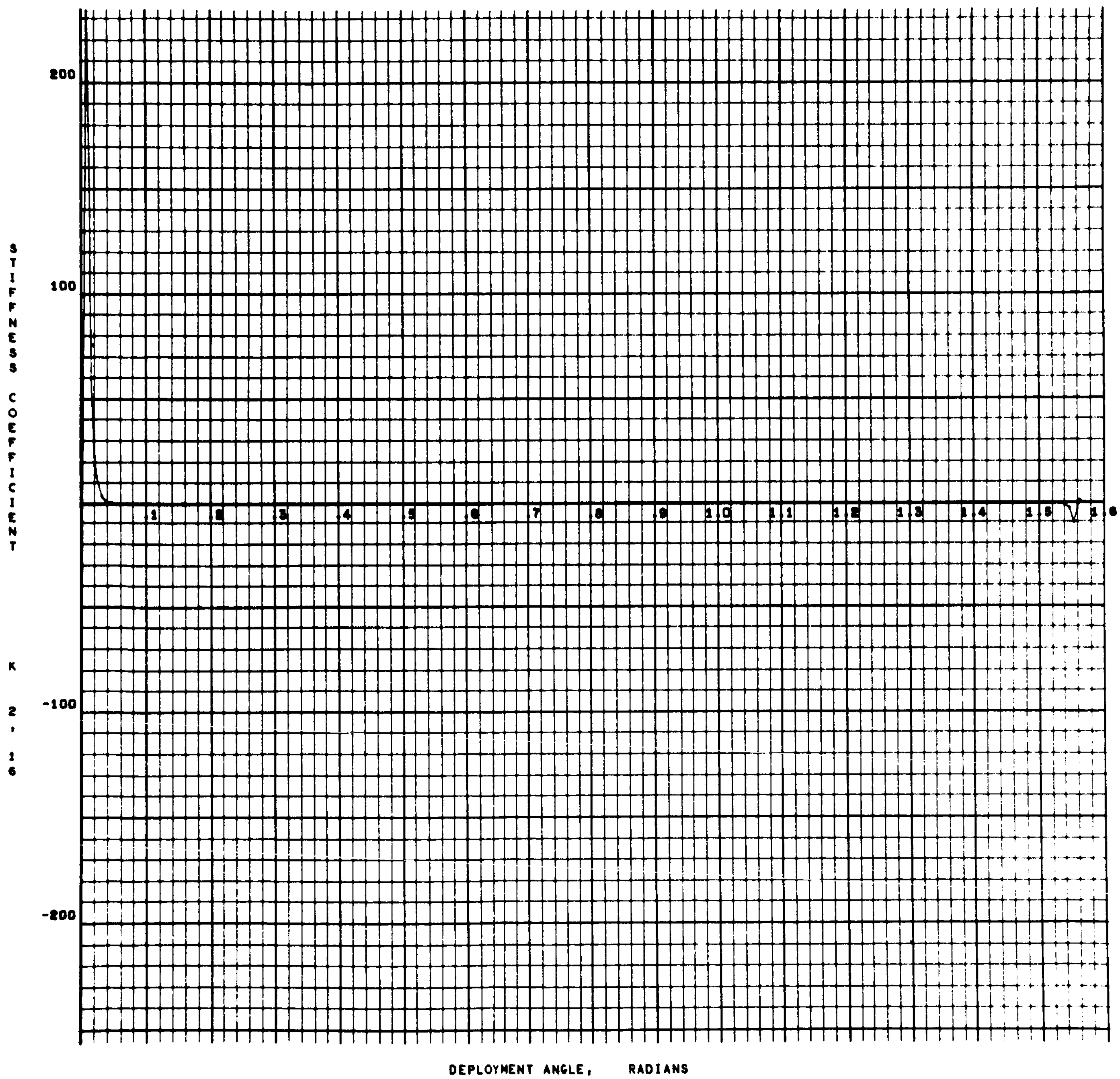

451450
000 034

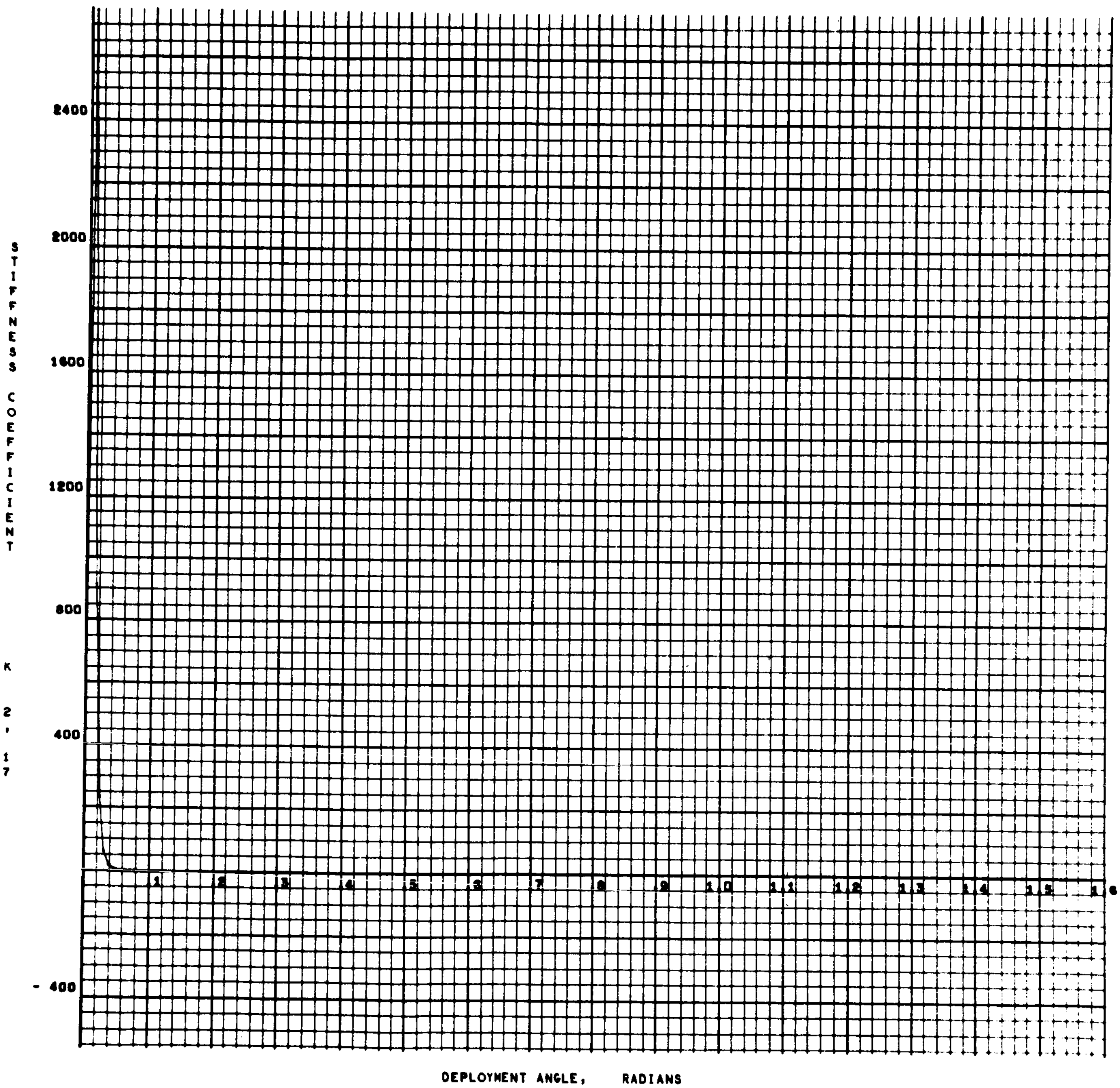

451450
000 036

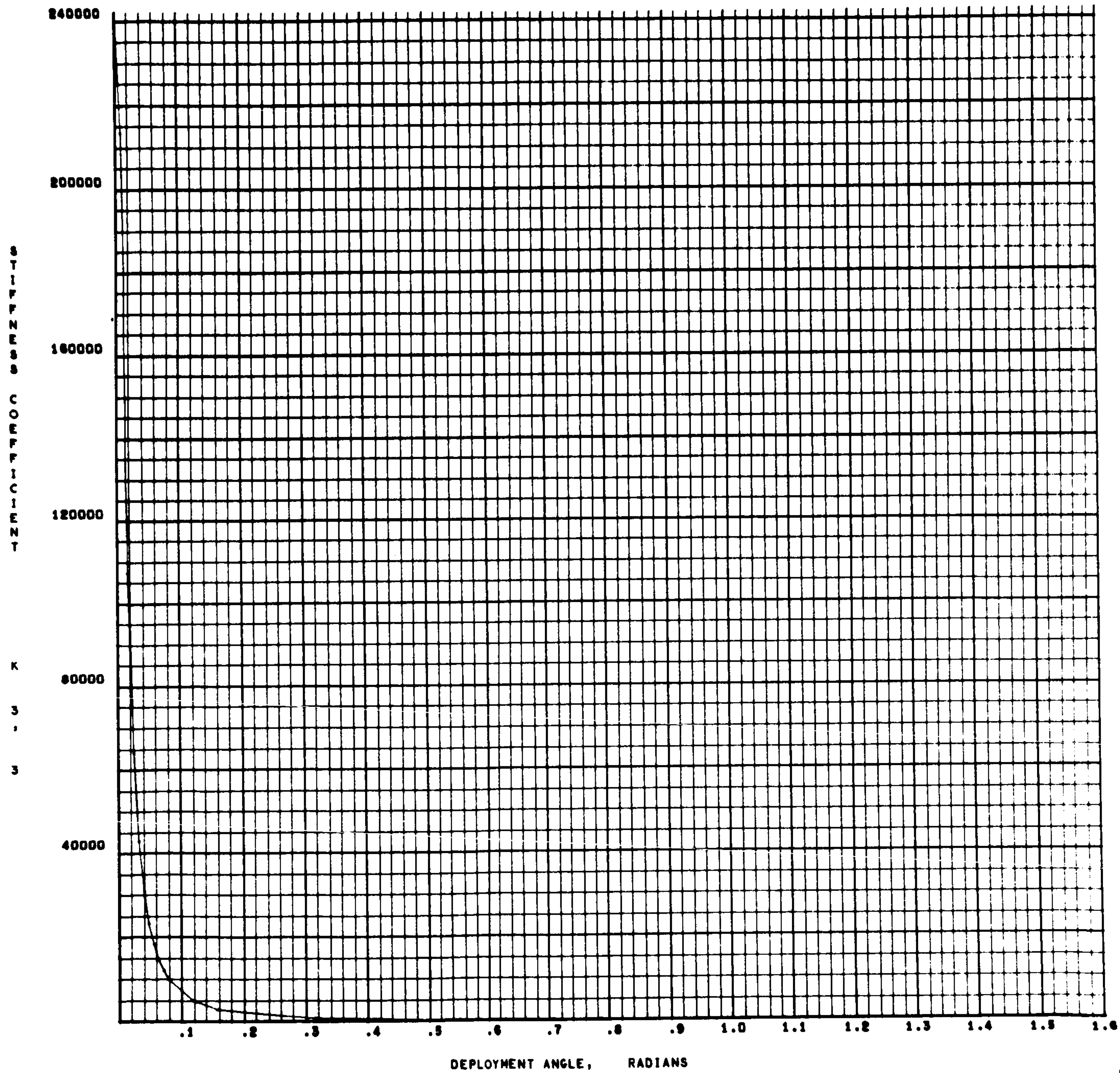

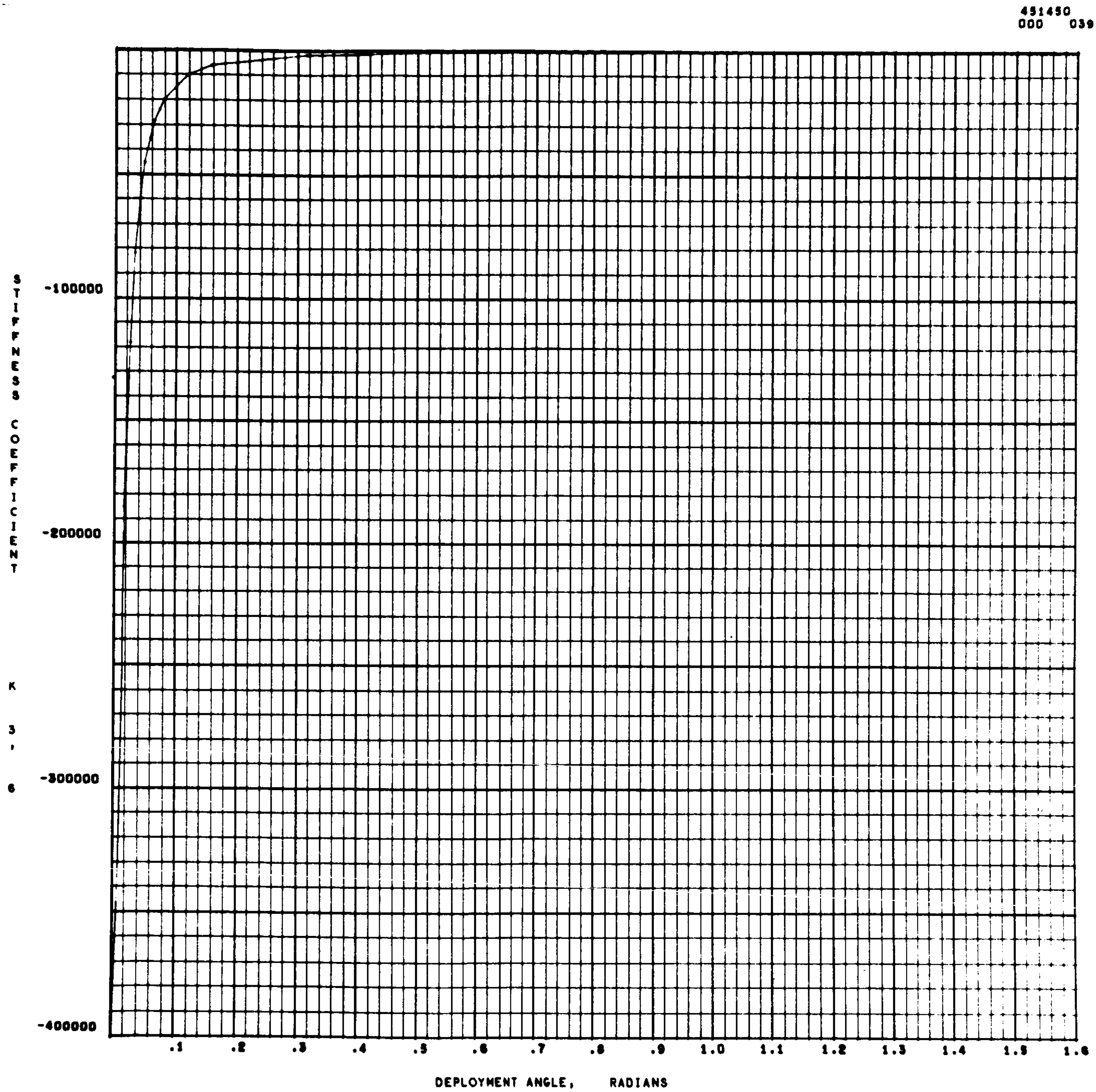
451450
000 039
STIFFNESS COEFFICIENT K 3, 6
-100000
-200000
-300000
-400000
.1
.2
.3
.4
.5
.6
.7
.8
.9
1.0
1.1
1.2
1.3
1.4
1.5
1.6
DEPLOYMENT ANGLE, RADIANS

451450
000 042

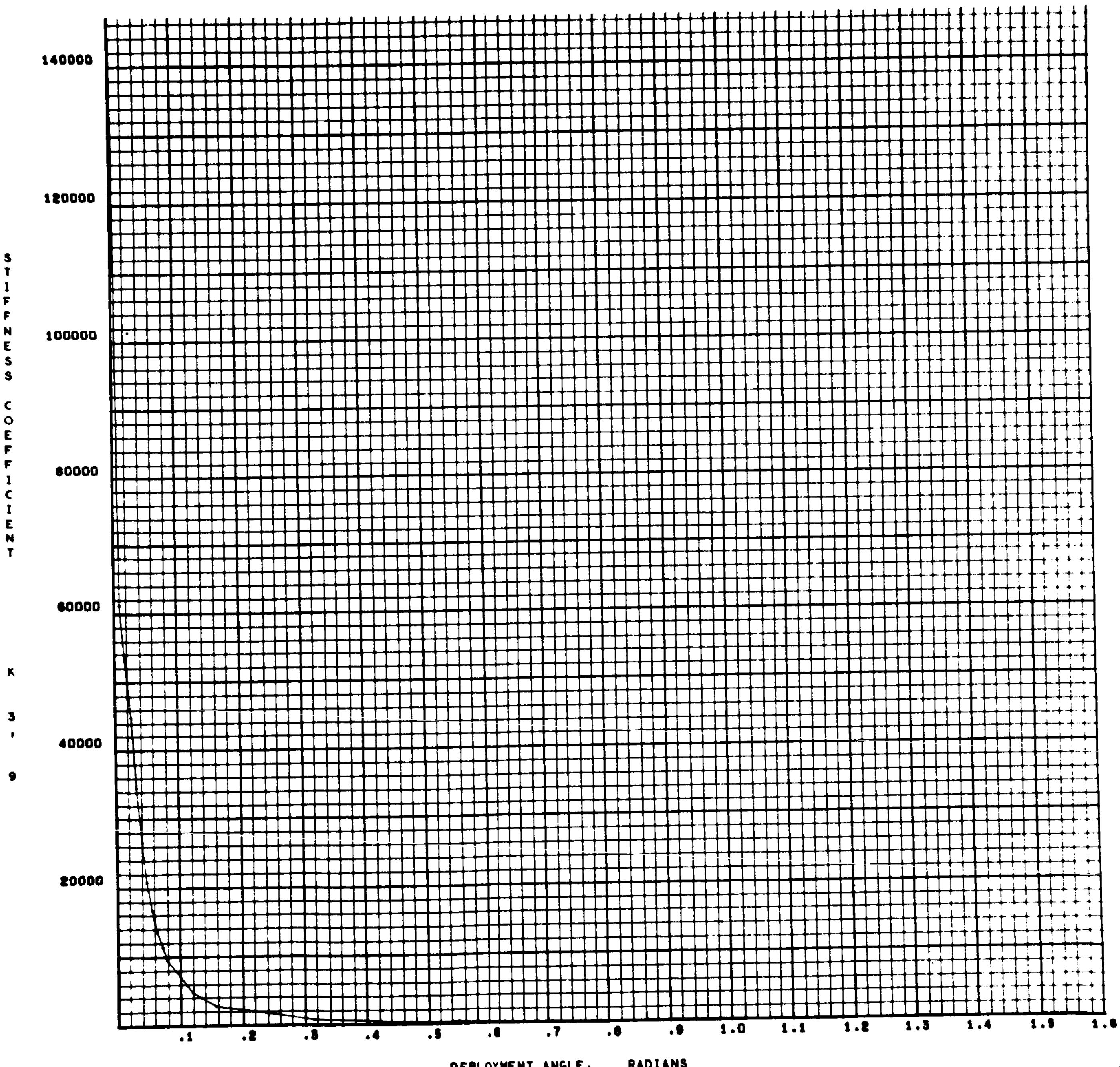

451450
000 045

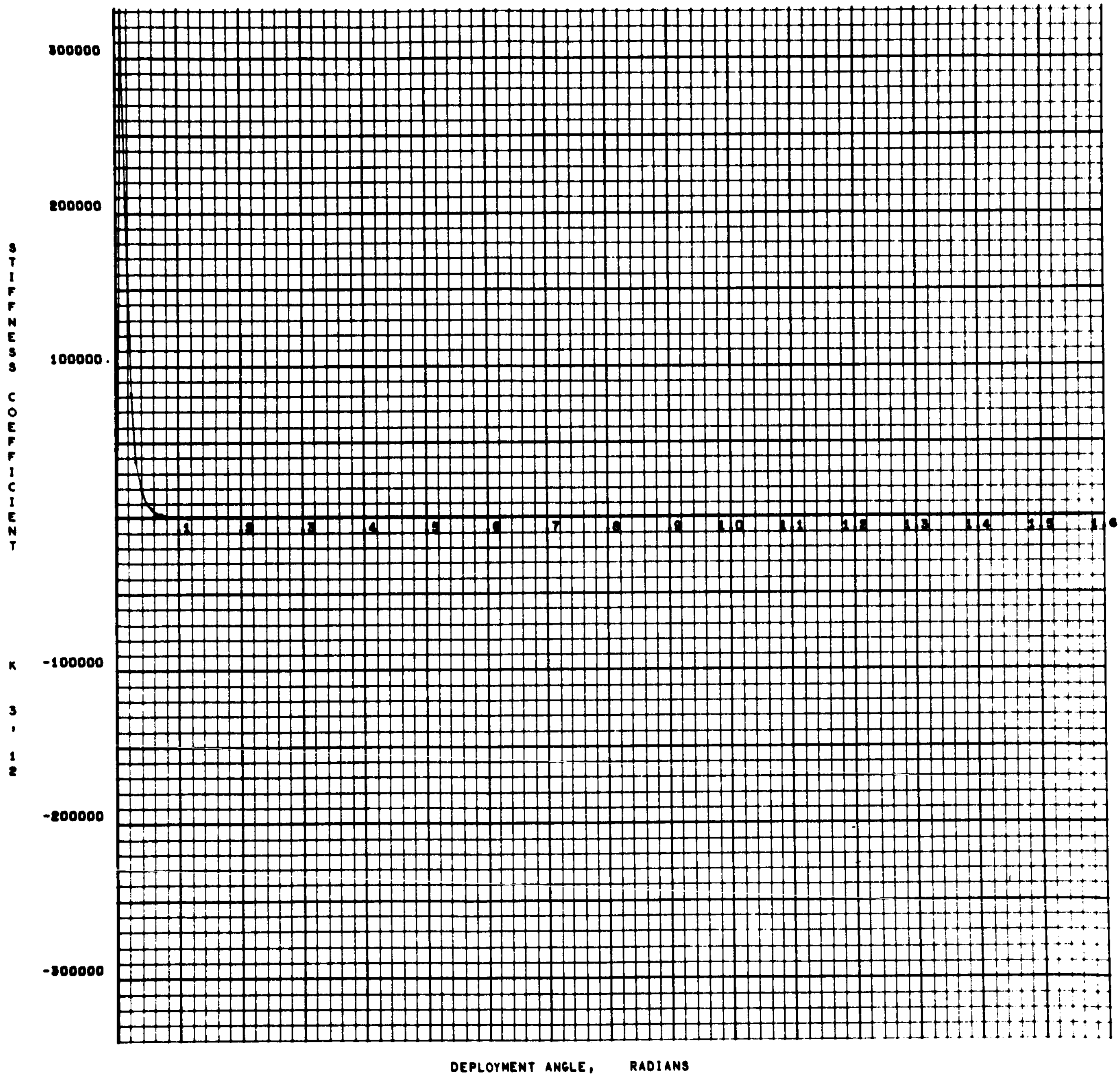

82

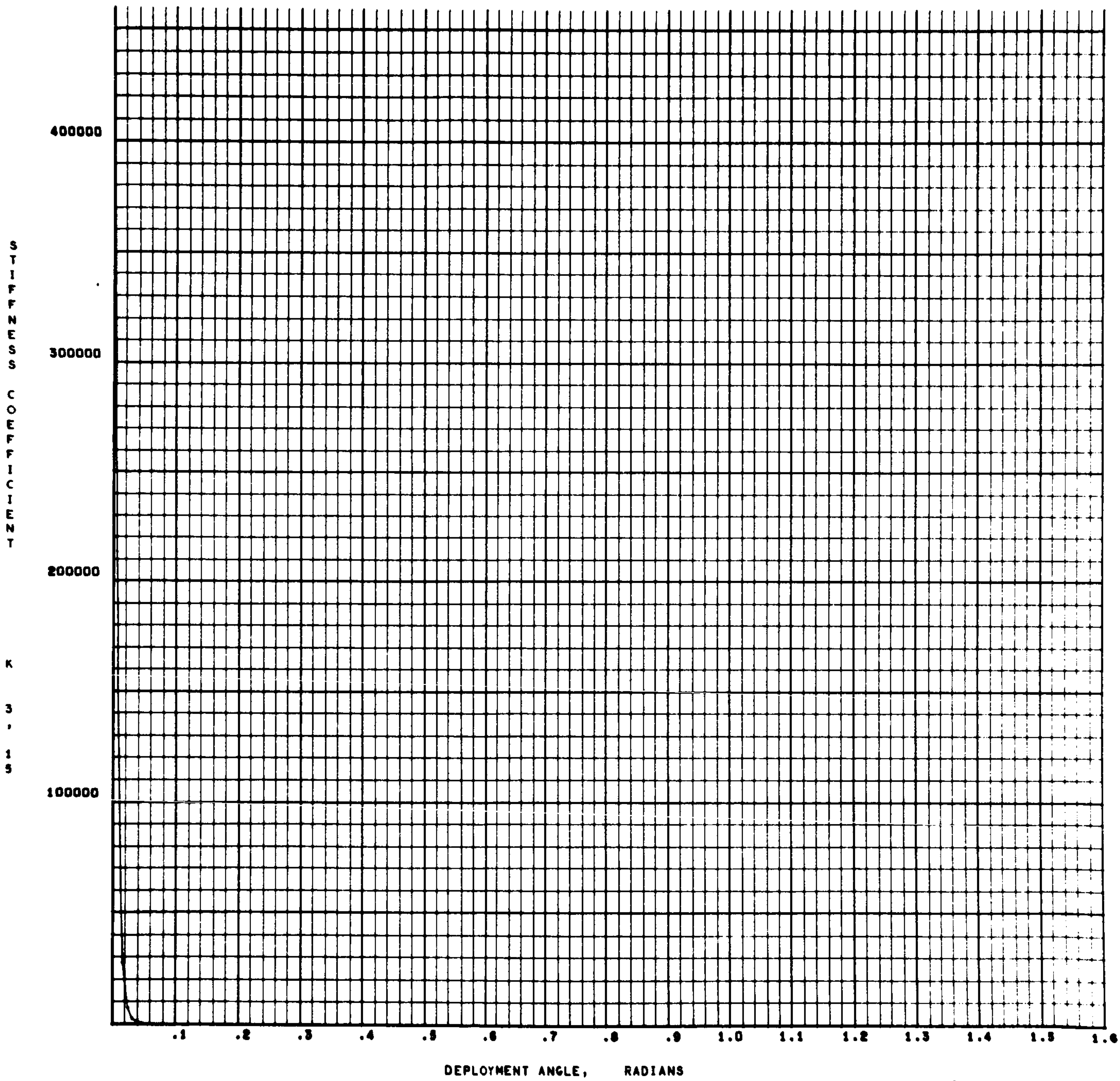
400000
300000
200000
100000
STIFFNESS COEFFICIENT K 3,15
.1
.2
.3
.4
.5
.6
.7
.8
.9
1.0
1.1
1.2
1.3
1.4
1.5
1.6
DEPLOYMENT ANGLE, RADIANS

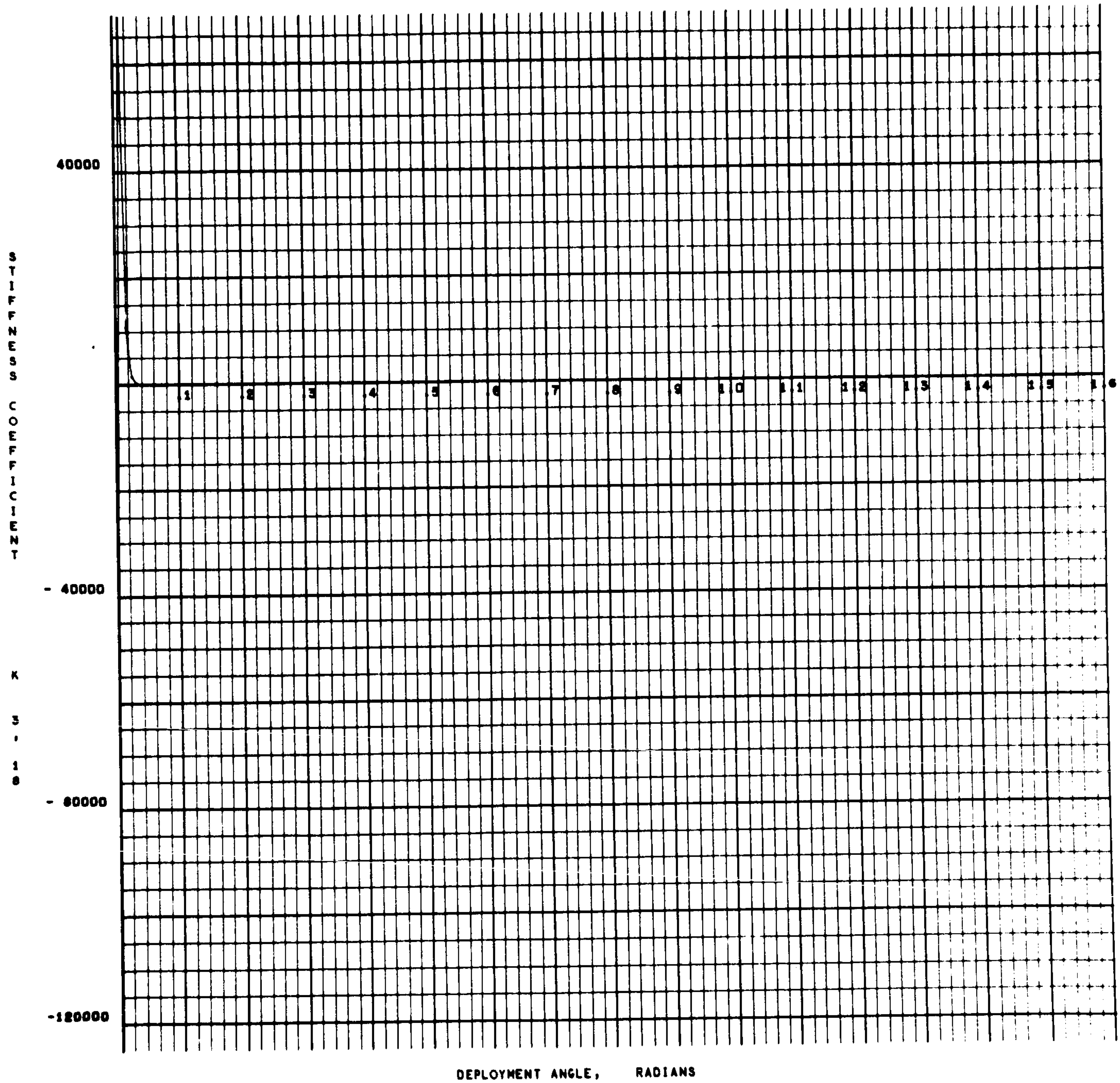
40000
- 40000
- 80000
-120000
STIFFNESS COEFFICIENT
K 3,18
.1
.2
.3
.4
.5
.6
.7
.8
.9
1.0
1.1
1.2
1.3
1.4
1.5
1.6
DEPLOYMENT ANGLE, RADIANS